

# Glass and jamming transition of simple liquids: static and dynamic theory

Hugo Jacquin

October 29, 2018

We study the glass and jamming transition of finite-dimensional models of simple liquids: hard-spheres, harmonic spheres and more generally bounded pair potentials that modelize frictionless spheres in interaction. At finite temperature, we study their glassy dynamics via field-theoretic methods by resorting to a mapping towards an effective quantum mechanical evolution, and show that such an approach resolves several technical problems encountered with previous attempts. We then study the static, mean-field version of their glass transition via replica theory, and set up an expansion in terms of the corresponding static order parameter. Thanks to this expansion, we are able to make a direct and exact comparison between historical Mode-Coupling results and replica theory. Finally we study these models at zero temperature within the hypotheses of the random-first-order-transition theory, and are able to derive a quantitative mean-field theory of the jamming transition.

The theoretic methods of field theory and liquid theory used in this work are presented in a mostly self-contained, and hopefully pedagogical, way. This manuscript is a corrected version of my PhD thesis, defended in June, 29th, under the advisorship of Frédéric van Wijland, and also contains the result of collaborations with Ludovic Berthier and Francesco Zamponi. The PhD work was funded by a CFM-JP Aguilar grant, and conducted in the Laboratory MSC at Université Denis Diderot –Paris 7, France.

<b>1</b>	<b>Introduction</b>	<b>3</b>	4.3	Expansion at third order . . . . .	87
1.1	Theory of amorphous solids . . . . .	3	4.4	Conclusion and discussion . . . . .	98
1.2	Current theoretical approaches . . . . .	10			
1.3	Questions discussed in this work . . . . .	14	<b>5</b>	<b>Jamming transition</b>	<b>101</b>
<b>2</b>	<b>Formalism of many-body systems</b>	<b>17</b>	5.1	Mean-field hypothesis . . . . .	101
2.1	Statistical field theories . . . . .	17	5.2	Thermodynamics of the glass . . . . .	113
2.2	Theory of liquids . . . . .	34	5.3	Jamming point of harmonic spheres	116
<b>3</b>	<b>Dynamics: a field theory approach</b>	<b>47</b>	5.4	The pair correlation function . . . . .	122
3.1	Field theory for supercooled liquids	47	5.5	Comparison with numerical data . . . . .	126
3.2	Quantum mechanical formulation . . . . .	54	5.6	Conclusions . . . . .	132
3.3	Fredrickson-Andersen model . . . . .	61	<b>6</b>	<b>Conclusion and perspectives</b>	<b>135</b>
3.4	Application to harmonic spheres . . . . .	68	6.1	Dynamics near the glass transition	135
<b>4</b>	<b>Statics: the replica method</b>	<b>75</b>	6.2	Statics vs. dynamics . . . . .	136
4.1	Focusing on the long time limit . . . . .	75	6.3	Theory of the jamming transition . . . . .	137
4.2	Replicated liquid theory . . . . .	80			
				<b>Bibliography</b>	<b>139</b>



# Chapter 1

## Introduction

### 1.1 Theory of amorphous solids

This thesis is devoted to the theoretical analysis of the properties of amorphous solids. Amorphous solids are ubiquitous in daily life: window glass, optical fibers, metallic glasses, plastics, ... all of those are amorphous solids, i.e. materials that have a disordered microscopic structure similar to that of dense liquids, while being solid on macroscopic scales. Despite many years of research efforts by theoreticians and experimentalists, the understanding of this kind of materials is still largely empirical, and no comprehensive physical theory has been devised yet. Many theoretical scenarios exist [15], but for the moment a coherent and quantitative theory of amorphous solids that would start from the microscopic scale, aiming at deriving the existence and properties of an amorphous solid phase, is still lacking.

This state of affairs poorly compares with the situation in liquid theory [77] or solid-state theory [7], where accurate quantitative theories allow for first-principles predictions for virtually any model. In liquid state theory, the validity of the ergodic hypothesis, i.e. the assumption that the system is able to visit all its possible configurations in a “short” time (when compared to the typical time of an experiment) allows for the use of equilibrium statistical mechanics, greatly reducing the theoretical difficulty. In the case of the solid state, the existence of a fixed lattice on which particles are attached allow for the treatment of quantum fluctuations thanks to invariance properties of the lattice, and to the localized classical trajectories of the particles.

In the case of amorphous solids, the disordered, liquid-like, positions of the particles require a description with the level of complexity of the liquid state theory, at least for what concerns static properties, but the ergodic hypothesis is not verified: amorphous materials are generically out of equilibrium, either because their relaxation time is comparable to the duration of an experiment or because microscopic configurations are forbidden due to mechanical constraints. Additionally, no underlying lattice symmetry is present to simplify the problem. As a consequence, the theoretical treatment of amorphous solids is mostly based on tools borrowed from liquid state theory, and a short introduction to its formalism is presented in the second part of chapter 2 of this thesis.

Many of the theoretical developments in the field of the glass transition have been concentrated on the study of idealized models [124], that aim at suppressing the complexity of the problem while keeping the essential ingredients needed to observe a phenomenology akin to that of amorphous solids. In this thesis we will systematically start from realistic finite-dimensional models, trying to derive from first-principles, and in a controlled way, the existence and properties of an amorphous phase, and to

understand the relations between different existing theoretical scenarios. Because of the difficulty of dealing with finite-dimensional, non-idealized systems, the range of questions addressed by such an approach is limited when compared to what can be learnt from numerical experiments or by heuristic arguments, but we believe that the quantitative implementation of the vast amount of theoretical ideas that emerged in the last decades in realistic models will give a firm basis for future developments of the field, and is complementary to other approaches.

### Glassy and jammed systems

Amorphous materials can be separated into two classes: the ones that are composed of molecules or atoms of size of the order of the Angström, and are formed at finite temperature, that are called structural glasses [25], and the ones composed of a large number of particles of sizes ranging from the micrometer to the centimeter, insensitive to thermal fluctuations [146].

Structural glasses can be formed starting from virtually any stable liquid, by many procedures [6], the most common one being the quench: the liquid has to be sufficiently rapidly cooled down below its melting temperature, avoiding the formation of crystalline states [36]. This is always possible thanks to the nature of the transition from liquid to solid: the formation of the crystalline structure requires the nucleation of a droplet of crystal inside the liquid, which is locally unfavorable when compared to the liquid structure, even though it is thermodynamically more stable. Thus cooling down at a sufficiently large rate will not open up the possibility of such nucleation, at least on experimental time scales. When the liquid has been placed below its melting temperature, it is said to be supercooled. The physical properties of supercooled liquids are at first indistinguishable from their liquid counterparts and can be deduced from the standard theory of liquids. However, when the system is further cooled down, its dynamics start to slow down very rapidly, and its viscosity increases by many orders of magnitude. The system then falls out of equilibrium and becomes an amorphous solid.

Athermal amorphous solids are formed by starting from a dilute assembly of particles in a box, and either pouring more and more objects in the box [13], inflating them [107] at constant rate while allowing the particles to move, or performing a sequence of inflations and minimization of the energy of the system [135], all procedures having the effect of increasing the density of objects, until mechanical rigidity is attained. These procedures are in essence non-equilibrium, free of thermal fluctuations that govern the behavior of glasses. As a consequence, the final states attained by these procedures, sometimes called jammed states, strongly depend on the followed protocol. The question of the maximal density that can be realized by such amorphous solids and the properties of the corresponding packings are largely open questions, and have deep connections in mathematics and computational sciences [46].

#### 1.1.1 Thermal systems: the glass transition

The very large increase of the viscosity upon cooling liquids below their melting point is called the glass transition, suggesting the idea that a proper thermodynamic phase transition exists from the liquid to the amorphous solid. However, experimentally no sharp transition can be detected: for example following the evolution of the viscosity, no proper divergence can be extracted from experiments, and the glass transition temperature  $T_g$  is often arbitrarily set to the temperature at which the viscosity  $\eta$  has reached  $10^{13}$  Poise. One can alternatively follow the evolution of the relaxation time of the system, that also increases drastically upon lowering the temperature. An early important remark is that structural glasses separate into two important classes: fragile and strong. This separation is

obvious when we represent the evolution of the viscosity on an Angell plot [5, 75], i.e. representing the logarithm of the viscosity against the temperature in units of  $T_g$ . An example of such plot, taken from [5], is given in Figure 1.1. By definition of  $T_g$ , all curves must meet at  $T/T_g = 1$  for which the logarithm of the viscosity (in base 10) must be equal to 13. We see that two tendencies arise: strong liquids for which the growth of the viscosity is essentially exponential, and fragile ones for which the growth is super-exponential upon approaching the transition. This dramatic increase of viscosity is

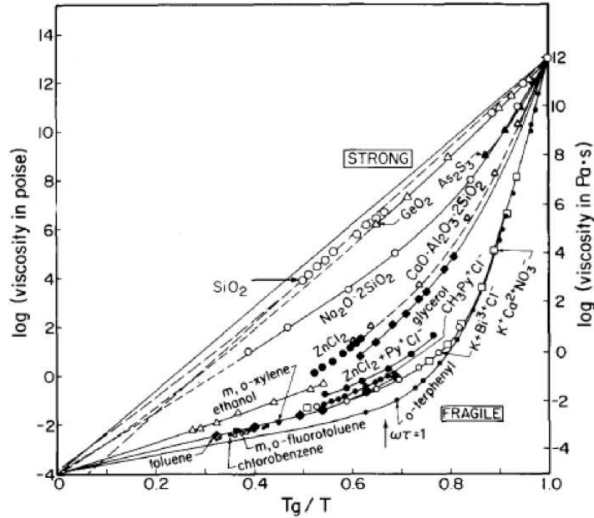


Figure 1.1: Viscosity against reduced temperature for various glass formers. A clear cut separation between two classes of glasses is observed, and corresponds to different behaviors of the activation energy required for relaxation. (from [5])

directly linked to the relaxation time  $\tau_\alpha$  of the system through a Maxwell model that gives  $\eta = G_\infty \tau_\alpha$ , where  $G_\infty$  is the instantaneous shear modulus. Relaxation processes in the system can schematically be imagined to be an accumulation of well-defined single events, such as the sudden escape of one particle from its local environment, that have an energy cost  $E$  (the “activation” energy). In that case the relaxation time will be described by an Arrhenius law:

$$\tau_\alpha = \tau_0 \exp\left(\frac{E}{k_B T}\right), \quad (1.1)$$

and the behavior of the viscosity in Fig. 1.1 allows us to identify the activation energy as the slope of the curves. For strong materials, such as Silica, the Arrhenius law is satisfied, but for fragile materials such as o-Terphenyl, the activation energy itself depends on temperature. This is consistent with the commonly observed Vogel-Fulcher-Tamman law which states that the relaxation time should diverge with inverse temperature as:

$$\tau_\alpha = \tau_0 \exp\left(\frac{DT_0}{T - T_0}\right), \quad (1.2)$$

and seems to be consistent with several sets of experimental data. This picture suggests that, for fragile liquids, the relaxation events in a supercooled liquid upon approaching its glass transition become more and more energetically costly, i.e. more and more cooperative, possibly associated with a divergence at finite temperature  $T_0$ , which should thus be identified with  $T_g$ , the glass transition. However the range of available data is not sufficient to provide an unambiguous fit, and other functional

forms can be chosen, that support a transition at zero temperature. The idea of a local “cage” formed by the neighbors of each particle is however appealing, and is thought to be the basic mechanism behind the physics of amorphous solids.

In dense liquids, a way to quantify the local environment of a single particle is to consider the radial distribution function  $g(r)$ , which is the probability of finding a particle at distance  $r$  of a given particle [77]. To compute it, we first define the microscopic density  $\hat{\rho}$  as:

$$\hat{\rho}(x, t) = \sum_{i=1}^N \delta(x - x_i(t)), \quad (1.3)$$

where  $x_i(t)$  is the position of particle  $i$  at time  $t$ . Obviously the average of this over many different experiments will give the average number of particles in the system  $\rho$ :

$$\rho(x, t) = \langle \hat{\rho}(x, t) \rangle. \quad (1.4)$$

Not much can be learnt from this quantity since it is expected to be constant in time and space if translational and time-translational invariance are respected, i.e. for homogeneous liquids at equilibrium. The radial distribution function is thus by definition related to the (normalized) equal time value of the second moment of this quantity:

$$g(x - y) = \frac{\left\langle \sum_{i \neq j} \delta(x - x_i(0)) \delta(y - x_j(0)) \right\rangle}{\rho^2} = 1 + \frac{\langle (\hat{\rho}(x, 0) - \rho)(\hat{\rho}(y, 0) - \rho) \rangle}{\rho^2} - \frac{1}{\rho} \delta(x - y), \quad (1.5)$$

where we made it obvious that for homogeneous systems,  $g$  only depends on one variable. The static structure factor  $S(k)$  is related to the Fourier transform of  $g$  by:

$$S(k) = 1 + \rho \int_x e^{ik \cdot x} [g(x) - 1] = \frac{1}{\rho} \int_x e^{ik \cdot (x-y)} \langle (\hat{\rho}(x, 0) - \rho)(\hat{\rho}(y, 0) - \rho) \rangle. \quad (1.6)$$

The function  $g$  has a characteristic shape in dense liquids, shown in the left frame of Fig. 1.2: it is

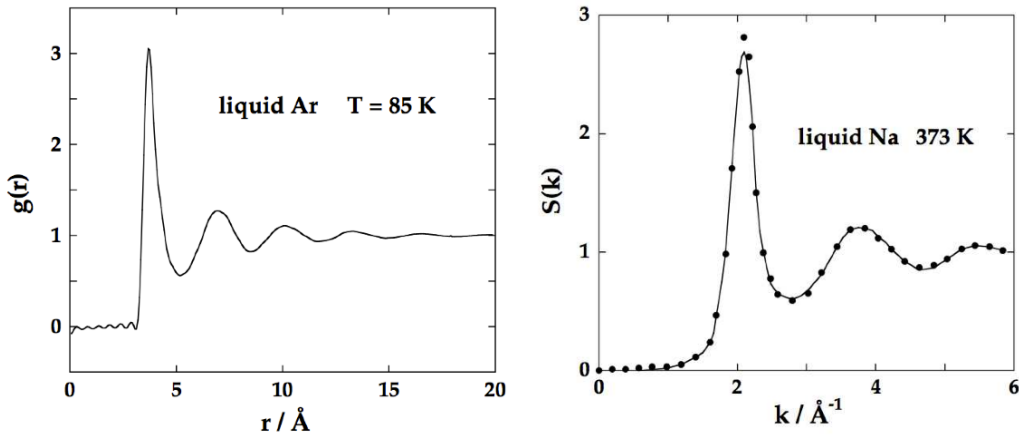


Figure 1.2: Left: Schematic form of the radial distribution function of a simple liquid.  $g(r)$  is equal to 0 for small distances, has marked peaks at  $\sigma, 2\sigma, \dots$ , and decays to 1 at large distances. Right: Corresponding schematic form of the structure factor of a simple liquid. From [77]

equal to zero for distances smaller than the particle diameters  $\sigma$ , reflecting the hard-core repulsion

between particles, has a very strong peak at  $r = \sigma$  reflecting the fact that a particle is surrounded by a spherical shell of neighbors, then has subsequent peaks at  $r = 2\sigma, 3\sigma, \dots$  of decreasing intensity, and finally decreases to 1 at long distances, reflecting the fact that no long range order exists in a liquid. The Fourier transform of  $g(r) - 1$ , shown in the right frame, is called the structure factor  $S(k)$ , and is directly accessible in neutron diffraction experiments, or light diffraction experiments in the case of colloids [14].

For liquid states, the knowledge of the pair distribution function, i.e. a static two-point function is enough to quantitatively deduce the thermodynamics and dynamics of the system. However such observable is essentially blind to the presence of the glass transition, since it is observed in the experiments that the glass is essentially an arrested liquid configuration. A better observable has to be found in order to discriminate between the supercooled liquid and the amorphous solid.

### Order parameters for the glass transition

This idea of a caging effect is better described by a dynamic correlation function: consider the time evolution of the position of one particle of the fluid. If a caging effect is present, the particle will spend most of its time vibrating around its initial position, until it will eventually be able to escape its cage. Instead of computing the density-density correlation function at equal times as in Eq.(1.6), we can compute the dynamic structure factor  $S(k, t)$  with:

$$S(k, t) = \frac{1}{\rho} \int_x e^{ik \cdot (x-y)} \langle (\hat{\rho}(x, t) - \rho)(\hat{\rho}(y, 0) - \rho) \rangle. \quad (1.7)$$

By definition this function reduces to the static structure factor at  $t = 0$ . The behavior of  $S(k, t)$  for

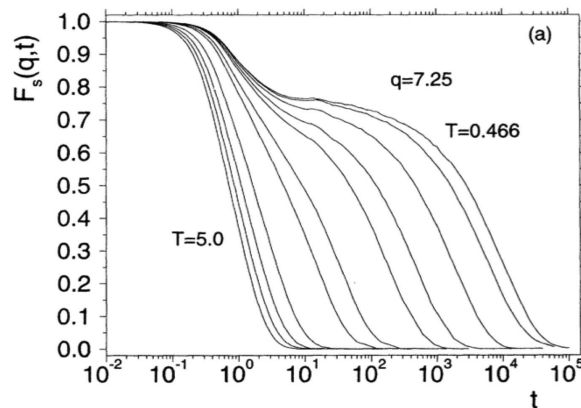


Figure 1.3: Time evolution of the self part (i.e. restricting to  $i = j$  in Eq. (1.5)) of the dynamical structure factor of a model glass-former, for wave vector  $2\pi/\sigma$ , for several temperatures above the glass transition. (from [99])

a typical glass former is shown in Fig. 1.3 for one given wave vector  $k \approx 2\pi/\sigma$ , which corresponds to a probe of the dynamics at the scale of one particle. At high enough temperatures, the relaxation is exponential just like in a liquid, particles are able to move freely in the fluid. However when the temperature is decreased, the function presents a two step relaxation: this is the signature of the cage effect discussed above. First a typical particle vibrates inside its cage, which corresponds to the initial relaxation, a process called  $\beta$  relaxation, then the relaxation saturates for a long time, while the particle is confined into its cage, finally the particle is able to escape its cage, and starts

to explore more of its phase space, which leads eventually to its final de-correlation, the so-called  $\alpha$  relaxation (which explains the  $\alpha$  subscript of the relaxation time of the system in Eq.(1.1)). Below the glass transition temperature, when the system falls out of equilibrium, the plateau developed by  $S(k, t)$  eventually extends to infinite times, which reflects the fact that  $\tau_\alpha \rightarrow \infty$ , which implies broken ergodicity. Thus this dynamical function appears as a good order parameter for the glass transition: defining the non-ergodicity factor  $f(k)$  as:

$$f(k) \equiv \lim_{t \rightarrow \infty} \frac{S(k, t)}{S(k)}, \quad (1.8)$$

$f$  jumps from 0 in a supercooled liquid, ergodic, phase, to non-zero values below the glass transition.

The correct order parameter for the glass transition is thus a two-point quantity, and the first task of a microscopic theory of glasses is to be able to derive from first-principles the existence of correlation functions that do not decay to zero at long times. This is a very different situation from that of the liquid-gas or the liquid-solid transitions: in both transitions the one-point density is enough to discriminate between different phases. In the liquid-gas transition the system will separate from a gas phase with uniform density to a coexistence between liquid and gas, where the density takes two different values. In the liquid-solid transition, the density switches from a uniform value in the system to a non-uniform value which presents modulations that reflect the lattice symmetry of the ordered phase. Thus accurate theories, such as the density functional theory [153] described below, can be built by looking at the free-energy of the system as a function of density, and comparing uniform density profiles to non-uniform profiles. For example the Ramakrishnan-Yussouf theory of freezing [144], which is the starting point of many theories of freezing, even in the context of glasses [154, 50, 93, 41], aims at finding non-uniform density profiles minima for a suitable free-energy. In this way amorphous glassy profiles can be obtained, as well as periodic density profiles that correspond to a crystal phase.

### 1.1.2 A-thermal systems: the jamming transition

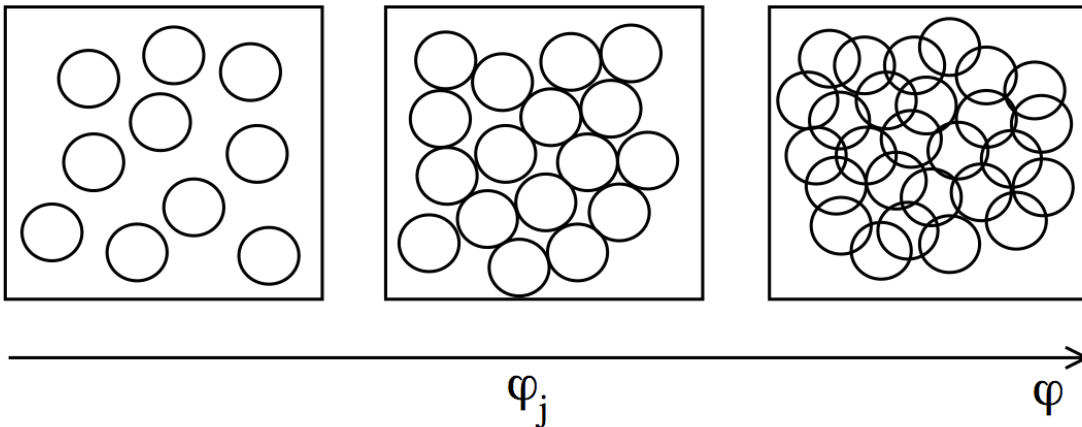


Figure 1.4: Schematic picture of the jamming transition. Upon increasing  $\varphi = \pi\rho\sigma^3/6$ , the fraction of the volume of space occupied by the spheres, a transition from zero contacts states to states with finite number of contacts is observed.

In the case of a-thermal systems such as heaps of grains, powders or foams, it has been observed experimentally and numerically that many physical quantities display critical scaling around the den-



sity at which the system acquires rigidity. A very large amount of numerical effort has been put since several years for the study of frictionless, spherical and deformable particles, that have a finite range interaction, and here we restrict the discussion to such systems for simplicity.

In commonly used algorithms [157, 135, 107], an assembly of such particles, initially randomly distributed, is gradually inflated, while minimizing its energy, or running microscopic dynamics, between each inflation step. Physical observables are then computed as averages over many realizations of one of the packing protocols described above. As long as the density is low, the lowest energy (amorphous) configuration is a state where there are no contacts between spheres. Of course this situation can not persist forever and a density exists above which no amorphous configuration without contacts can be found, and spheres begin to be deformed with finite energetic cost.

This situation is pictorially described in Figure 1.4. The density  $\varphi_J$  at which contacts begin to appear is called the Jamming point. At jamming, roughly situated around 0.64 for 3 dimensional frictionless spheres, the average number of contacts per particle  $z$  jumps from 0 to a finite value  $z_c$ , equal to  $2d$  for spherical frictionless particles [134], where  $d$  is the spatial dimension (2 or 3 for the systems of experimental interest). This value is precisely the minimal number of contacts required for a packing of spheres to be mechanically rigid: the packings are called isostatic [113]. When compressing the spheres further,  $z$  displays critical scaling with  $\varphi - \varphi_J$ , the distance to the jamming density, and so do thermodynamic quantities such as pressure and energy.

The radial distribution function defined above develops a diverging peak at  $r = \sigma$  upon approaching jamming, reflecting the fact that particles are found at contact with probability 1. Indeed the integral of this diverging peak counts the number of neighbors, and thus is equal to  $2d$  at jamming. Many more interesting scaling relations and critical behaviors, also concerning the rheology of these packings have been discovered, but the first-principles approach adopted in our work will be limited to the aforementioned properties, and the reader is advised to refer to specific reviews ([166], [86]).

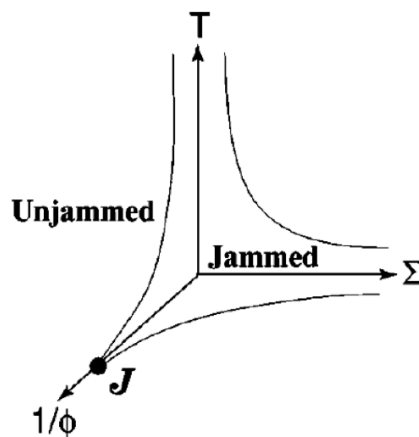


Figure 1.5: Jamming phase diagram, as proposed by Liu and Nagel. The inverse volume fraction, temperature and Stress imposed on the material are the three main control parameters involved in amorphous solids. The temperature–density plane contains the structural and colloidal glasses, while the plane stress–density concerns granular matter. The Jamming point is a point on the zero temperature and zero applied stress axis, and is postulated to influence its vicinity at  $T \neq 0$ . (from [135])

The jamming transition can be seen as the extreme case of the cage effect: at jamming the particles

do not have any space available to vibrate. It is thus tempting to associate the two phenomena by imagining that the jamming transition could be the real mechanism behind the glass transition. This hypothesis would support the idea of a true divergence of the relaxation time at zero temperature.

Following this line of thought, Liu and Nagel [104] proposed to gather all amorphous solids on a single phase diagram, shown in Fig. 1.5. In a diagram with inverse density, applied stress and temperatures as the axes, they identify a jammed phase for high density, low temperature and low applied stress. Indeed, an amorphous solid will always yield under a high enough stress, or start to flow at high enough temperature, or low enough density. The proper jamming point lies at a high density in the zero temperature, zero applied stress axis, and is postulated to control its vicinity. In particular the glass transition would be controlled by this zero-temperature fixed point. Although physically appealing, such relation between jamming and glass transition is mostly hypothetical, since the studies of the jamming transition almost exclusively focus on the zero temperature part of this phase diagram.

## 1.2 Current theoretical approaches

There are currently two analytical approaches that are able to predict the divergence of the viscosity for realistic models of glass formers by starting from a microscopic description and performing well-defined approximations (even if they are not *a priori* justified !): Mode-Coupling Theory (MCT) [155, 73], which is a theory that describes the dynamics of dense liquids in terms of the dynamical structure factor  $S(k, t)$ , and the Random First Order Transition theory (RFOT) [95, 96] which is a theory that focuses on the long time limit of the dynamical processes, working in a static framework only.

In the context of the jamming transition, no microscopic theory is able to predict the existence of jammed states and deduce the critical scalings of the different physical observables that are observed numerically or in the experiments. However, an adaptation of the RFOT to high-density states of hard spheres [138] has been able to identify glassy states of hard spheres with diverging pressure at a value close to the usual random close packing density 0.64 in three dimensions, and contact number very close to the isostatic value.

### 1.2.1 Dynamics: Mode-Coupling theory

Starting from Hamiltonian dynamics and focusing on slowly varying collective variables such as the density, one is able to formally derive, using the so-called Mori-Zwanzig projection operator formalism [180, 128], a closed equation for the dynamical structure factor  $S(k, t)$  defined in Eq.(1.7) that reads:

$$\frac{m}{k_B T} \frac{\partial^2 S(k, t)}{\partial t^2} + \frac{k^2}{S(k)} S(k, t) + \frac{\rho}{2} \int_0^t dt' K(k, t - t') \frac{\partial S(k, t')}{\partial t'} = 0. \quad (1.9)$$

All the complexity of the dynamics is now hidden in the calculation of the memory kernel  $K$ , which involves correlations between the density and all the other hydrodynamic variables in the system. The closure approximations made within Mode-Coupling Theory (MCT) lead to the following form for the memory kernel [12]:

$$K(k, t) = \int_q \left[ \frac{k \cdot q}{k} c(q) + \frac{k \cdot (k - q)}{k} c(k - q) + \rho c^{(3)}(k, -q) \right]^2 S(q, t) S(k - q, t) \quad (1.10)$$

The third-order direct correlation function that appears in the kernel is usually neglected by resorting to the factorization approximation whose effect is to simply eliminate it. Furthermore, it has been

shown to be negligible when compared to the term involving the second-order direct correlation function [10]. Eq.(1.9) combined with Eq.(1.10) constitutes a closed equation bearing on  $S(k, t)$  that can be solved given the equilibrium correlations of the liquid.

Letting the time go to infinity in these equations gives a self-consistent equation for the non-ergodicity parameter  $f(k)$  defined in Eq.(1.8):

$$\frac{f(k)}{1-f(k)} = \frac{\rho S(k)}{2} \int_q \left[ \frac{k \cdot q}{k^2} c(q) + \frac{k \cdot (k-q)}{k^2} c(k-q) + \rho c^{(3)}(q, k-q) \right]^2 S(q) S(k-q) f(q) f(k-q) \quad (1.11)$$

Numerically solving this self-consistent equation predicts the appearance, at constant density and below a critical temperature  $T_{\text{MCT}}$ , of a non-zero solution for  $f(k)$ , signaling ergodicity breaking and the appearance of a glass phase. Within MCT, the relaxation time is predicted to diverge at  $T_{\text{MCT}}$  with a power-law:

$$\tau_\alpha \sim \left( \frac{T - T_{\text{MCT}}}{T_{\text{MCT}}} \right)^{-\gamma}, \quad (1.12)$$

For  $T$  very close to the critical temperature,  $S(k, t)$  presents a two-step behavior such as the one showed in Fig. 1.3. The approach of  $S(k, t)$  to its plateau value (the  $\beta$ -relaxation) is given by:

$$\frac{S(k, t)}{S(k)} - f(k) \sim t^{-a}, \quad (1.13)$$

and the beginning of the  $\alpha$ -relaxation, i.e. the final de-correlation at long times in the ergodic phase is given by:

$$\frac{S(k, t)}{S(k)} - f(k) \sim -t^b \quad (1.14)$$

The three exponents  $a, b$  and  $\gamma$  are not independent, but verify scaling relations [12, 71]:

$$\lambda = \frac{\Gamma(1-a)^2}{\Gamma(1-2a)} = \frac{\Gamma(1-b)^2}{\Gamma(1-2b)}, \quad (1.15)$$

$$\gamma = \frac{1}{2a} + \frac{1}{2b}, \quad (1.16)$$

so that all exponents can be deduced from the knowledge of  $\lambda$ , which itself solely depends on the structure of the equation for the non-ergodicity factor Eq.(1.11) [71]. The predictions of MCT for the power-law scalings Eq.(1.13,1.14) are well verified experimentally [72], but the prediction for the critical temperature  $T_{\text{MCT}}$  is too high, predicted by MCT to be higher than  $T_g$ , the experimental glass transition, which is at worst an upper bound for the true transition, if it exists at all. Thus when comparing experiments with theoretical predictions, adjustments of  $\gamma$  and  $T_{\text{MCT}}$  are usually made to obtain the values of  $a$  and  $b$  for example. Given the difficulty to obtain accurate measurements for very long times, the ambiguities inherent to such adjustments can not be ignored.

Recently, several experiments [31, 64] have confirmed that the scalings predicted by MCT are only valid when the system is not too close to the transition, while closer to the transition the system enters another regime, where the power-law divergence of the relaxation time is strictly ruled out. The failure of MCT is commonly explained by the fact that MCT neglects activated events, i.e. temperature-induced escapes of local metastable states. MCT is thus seen as a ‘‘mean-field’’ theory, even though it has been shown recently to break down in high dimensions [38]. The approximations involved when expressing the kernel  $K$  in Eq.(1.9) are thus probably ill-behaved and call for improvement [29].

Careful inspection of equivalent dynamical theories have shown [4] under mild assumptions that the scaling predictions Eqs.(1.13–1.16) are in fact universal predictions for any dynamical theory

that predicts the existence of a critical temperature at which  $S(k, t)$  does not decay to zero at long times. Thus the quantitative failure of MCT must not hide the fact that it could provide an excellent starting point in order to find an accurate theory, able to predict the avoided singularity that seems to be observed numerically and experimentally. Recent extensions of MCT [49, 74] have claimed to predict this avoided singularity by including coupling to currents in the theory. However, the approximations performed to obtain this theory were later shown to violate a number of physical requirements [35], and have to be rejected for now. Moreover, such currents do not exist in colloidal systems, and another scenario must be built to deal with that case.

## 1.2.2 Random-First-Order Transition theory

Kauzmann noted very early that if one separates the total entropy of a glass former into a vibrational part, that accounts for the solid-like motions of the particles inside their cages, and a configurational part, that accounts for the liquid-like rearrangements that occur when cooperative movements allow the cages to reorganize, the latter is seen to decrease upon approaching the glass transition [89], as is shown in Fig. 1.6. The system then falls out of equilibrium and the configurational entropy saturates

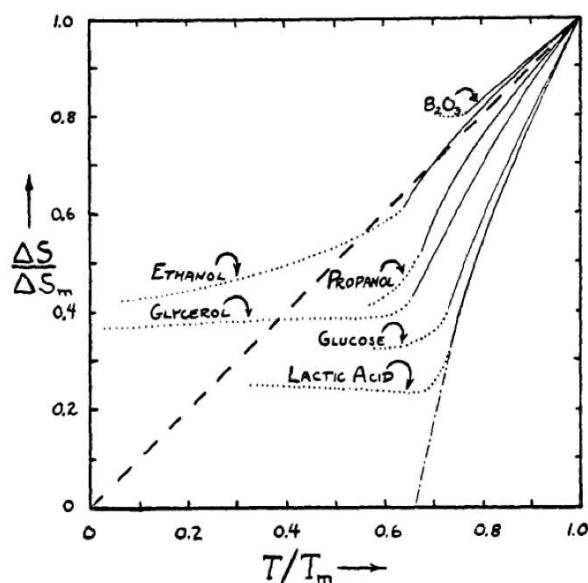


Figure 1.6: Configurational entropy of several glass formers as a function of temperature. For several components, the configurational entropy seems to extrapolate down to zero at a non-zero temperature: the Kauzmann temperature.

at a finite value. But Kauzmann noted that one could extrapolate the decrease of the configurational entropy all the way to zero, and that this canceling would then occur at a non-zero temperature  $T_K$ . Since an entropy cannot become negative, the system has to undergo a phase transition at this point. This hypothetical transition is commonly called the Kauzmann ideal glass transition.

Adam, Gibbs and Di Marzio [69, 1] have interpreted this in terms of cooperatively rearranging regions, the sizes of which increase upon lowering the temperature. As more and more particles need to be cooperatively moved in order to perform a structural relaxation of the system, the relaxation

time increases accordingly. The relaxation time would then obey:

$$\tau_\alpha = A \exp\left(\frac{C}{TS_c(T)}\right), \quad (1.17)$$

where  $S_c$  is the configurational entropy. An entropy crisis where  $S_c \rightarrow 0$  thus leads to a diverging relaxation time. In particular if the configurational entropy was found to vanish linearly, we would obtain the VFT law of Eq.(1.2).

This scenario has found a concrete application in the case of mean-field models of spin-glasses [124, 34], where it has been shown to hold exactly. The p-spin glass model [57, 76] is the paradigmatic model that has the phenomenology closest to that of structural glasses. In this model it is found that below a certain temperature  $T_d$ , a dynamical transition takes place because of the appearance of an extensive number of metastable states. One is led to define the complexity  $\Sigma$  as the extensive part of the number  $\mathcal{N}$  of metastable states:

$$\Sigma = \lim_{N \rightarrow \infty} \frac{1}{N} \ln \mathcal{N}, \quad (1.18)$$

where  $N$  is the number of particles in the system, and a finite  $\Sigma$  is found to appear for  $T < T_d$ .

Because these are mean-field models, the free-energy barriers between these states are infinite, and the system dynamically gets stuck for infinite times in one state, causing ergodicity breaking. However, thermodynamically, all these states are equivalent and no proper transition occurs at  $T_d$ . Upon decreasing the temperature, the number of relevant metastable states diminishes, until becoming sub-extensive. At that point, a thermodynamic phase transition occurs and there is only one state that dominates the partition function: the ideal glass. This critical temperature is thus naturally associated to the Kauzmann temperature  $T_K$ .

Beyond mean-field, activated events can allow for jumps between different metastable states, and one thus expects that the relaxation time will not diverge at  $T_d$  but only at  $T_K$  [95, 30]. Making the identification  $S_c \leftrightarrow \Sigma$ , the relaxation time should thus diverge at  $T_K$  as:

$$\tau_\alpha \sim \exp\left(\frac{C}{T\Sigma(T)}\right), \quad (1.19)$$

making contact with the Vogel-Fulcher-Tamman law and the conjecture of Kauzmann.

Furthermore, the divergence of the relaxation time was shown [95] to be described by equations similar to the Mode-Coupling ones at  $T_d$ . The hypothetical extension of this set of predictions made on mean-field disordered spin glasses to finite dimensional structural glasses has been named the Random-First-Order Transition theory. It is an elegant construction, but until recently, it was solely based on exact results found in models that can be argued to be quite far from the reality of structural glasses.

However, a series of works of Monasson [126], Mézard and Parisi [121, 122], and Cardenas, Franz and Parisi [33] have shown that this theoretical approach could be applied to models of structural glass formers, with qualitative success only.

## 1.3 Questions discussed in this work

### 1.3.1 Approach developed in this thesis

In this thesis, we have studied a model of harmonic spheres. This is a system of spherical and frictionless particles that interact via a pair potential

$$v(r) = \begin{cases} \varepsilon \left(1 - \frac{r}{\sigma}\right)^2 & \text{if } r < \sigma \\ 0 & \text{otherwise} \end{cases}, \quad (1.20)$$

where  $\varepsilon$  is an energy scale,  $r$  is the distance between two centers of spheres, and  $\sigma$  is the diameter of the spheres. This model has been introduced by Durian in the context of foam mechanics [61], and is now one of the paradigmatic models for studying the jamming transition [135].

Apart from being useful in the context of jamming, this pair potential can be seen as modelling the interaction between soft colloids in a dense regime [150, 65]. These colloids usually are polymer particles of poly (methylmethacrylate) (PMMA) [169, 64] or poly(N-isopropylacrylamide) (p-NIPAM) [151, 45] immersed in a solvent. Each polymer particle undergoes Brownian motion due to the presence of the solvent at finite temperature, and in the case where they are able to interpenetrate slightly, their mutual repulsion can be modeled by a simple harmonic repulsion like Eq.(1.20). Their Brownian nature introduces thermal fluctuations, which allows for a statistical treatment of the dynamics, contrary to Hamiltonian dynamics. They have been studied at finite temperature [21, 22, 178] and shown to reproduce the behavior of structural glass formers.

From the point of view of liquid theory, this potential has a well defined positive Fourier transform, which simplifies the computations. Furthermore, when the temperature decreases to zero, the finite repulsion between two particles cannot be overcome anymore, and the particles become exactly hard-spheres. Indeed, when the temperature goes to zero, the energy scale  $\varepsilon$  becomes infinite when compared to the thermal fluctuations (i.e.  $\varepsilon/k_B T \rightarrow \infty$ ) and the potential becomes equivalent to an infinite repulsion for  $r \leq \sigma$ , while still having zero repulsion for  $r > \sigma$ . This choice of model allows one to investigate both the athermal and the thermal amorphous solids, in a simplified way.

In this thesis, we attempt, without resorting to mean-field toy models and solely by focusing on the harmonic sphere model, to address several questions, which we summarize in the following.

### 1.3.2 What is the theoretical status of the Mode-Coupling transition ?

Can we find a theoretical framework where Mode-Coupling (or a corrected version of it) is well defined and easily generalizable, without resorting to unphysical approximations ? This question is the object of Chapter 3, where we propose a new framework that makes contact with the field of particle physics, and that solves several difficulties inherent to the treatment of the dynamics of glasses.

In view of the recent results and the RFOT scenario, the ideal result would be to obtain a theory where the dynamical transition is avoided, and a cross-over to a thermodynamic transition is observed.

### 1.3.3 Does the relation between MCT and the RFOT scenario hold beyond mean-field ?

For the moment, in non mean-field models, Mode-Coupling theory and the RFOT inspired calculations are intrinsically different and can not be compared. Can we make bridges between the two approaches ? This is the subject of Chapter 4, where we compute, from replica theory, a self-consistent equation

for the non-ergodicity factor similar to Eq.(1.11). We find that, in the two-mode approximation, that amounts to expanding the static free-energy at third order in the order parameter, replica theory and MCT can not be reconciled, although a three-body term, usually neglected within MCT, is recovered from replica theory.

As a valuable by-product, this calculation provides an expansion in powers of the static order parameter within replica theory. It allows to show that although the 1RSB transition found in replica theory is qualitatively stable against addition of further corrections, these corrections are nonetheless quantitatively relevant at the transition. Starting from our order-parameter expansion, one should be able to unify all approximation schemes of replica theory in order to obtain a theory that is quantitatively efficient.

### 1.3.4 What is the relation between jamming and the glass transition ?

Finally, is the jamming transition at  $T = 0$  related to the glass transition at finite temperature ? Krzakala and Kurchan [91] then Mari, Krzakala and Kurchan [110] have studied mean field models where it has been possible to prove, using replica theory or numerical simulations, that the dynamical arrest of the glass transition and the jamming transition are distinct mechanisms. Whether this situation persists in finite dimensional models is addressed in Chapter 5, where we show that replica theory allows us to properly disentangle the two phenomena, and show that they are indeed different.





## Chapter 2

# Formalism of many-body systems

We have seen that the proper order parameter for the glass transition is a dynamic two-point quantity. In chapter 4, we will see that, in the context of the random-first-order transition theory, the glass transition can also be characterized by a static two point quantity, via the introduction of replicas. In order to obtain theories that are able to capture a phase transition in terms of two-point quantities, it is convenient to resort to the so-called two-particle irreducible effective action, be it in the dynamic context or in a static context. In the dynamic case, this formalism is well documented in the context of quantum field theory, but less so in the context of classical statistical mechanics. Quantum field theory textbooks give only partial accounts, or do not mention it. In this chapter, we present an overview of the two-particle irreducible effective action, for a generic field theory, and in the special case of liquid theory.

### 2.1 Statistical field theories

We will generically denote by  $\varphi$  a microstate of the system, i.e. a set of variables or fields that completely determines its microscopic properties. In the case of equilibrium liquid theory,  $\varphi$  can be chosen to be the microscopic density of particles of the system. In the case of a dynamic theory, it can be for example the set of all time trajectories of density profiles. We will in the following denote the space and/or time variables, as well as internal indices (such as spin state for quantum mechanics, or replica indices in the last chapters of this manuscript), by a single number in subscript. Implicit summation over repeated indices is always assumed.

The macroscopic state of the system is supposed to be fully determined by a functional of  $\varphi$ , that we will denote by  $S$ . In a statistical field theory,  $S$  stands for the action, in the case of equilibrium theory,  $S$  would be replaced with the Hamiltonian of the system. The statistical weight of a particular configuration of the field,  $\mathcal{P}[\varphi]$ , is supposed to be of the form

$$\mathcal{P}[\varphi] = e^{-S[\varphi]} . \quad (2.1)$$

We will be interested in computing the statistical average of an observable  $\mathcal{O}$  that depends on the field. This average, denoted by  $\langle \cdot \rangle$  in the following, is obtained by summing over all possible realizations of the field, properly weighted by their statistical weights:

$$\langle \mathcal{O}[\varphi] \rangle = \frac{1}{Z} \text{Tr} \mathcal{O}[\varphi] e^{-S[\varphi]} , \quad (2.2)$$

where  $\text{Tr} \equiv \int \mathcal{D}\varphi$  and the normalization factor is  $Z$  the partition function:

$$Z = \text{Tr} e^{-S[\varphi]} . \quad (2.3)$$

Usually, one wants to compute averages of the field  $\varphi$  or powers of the field. A useful way to generate all averages of  $\varphi$  is to artificially introduce an external field  $J$  that is linearly coupled to  $\varphi$  in the action, and consider  $Z$  as a functional of the field  $J$ . Averages of  $\varphi$  will then be generated by successively differentiating  $Z$  with respect to  $J$ , and setting  $J$  to zero after the calculation to come back to the original theory:

$$\begin{aligned} \phi_1 \equiv \langle \varphi_1 \rangle &= \frac{1}{Z} \frac{\delta Z}{\delta J_1} \Big|_{J=0} , \\ \langle \varphi_1 \cdots \varphi_n \rangle &= \frac{1}{Z} \frac{\delta^n Z}{\delta J_1 \cdots \delta J_n} \Big|_{J=0} , \end{aligned} \quad (2.4)$$

where we defined the average field  $\phi$  in equation (2.4). Taking the logarithm of the partition function leads to a new functional  $W$

$$W = \ln Z, \quad (2.5)$$

that generates the set of all cumulants of  $\varphi$ :

$$\phi_1 = \frac{\delta W}{\delta J_1} = \frac{1}{Z} \frac{\delta Z}{\delta J_1} \Big|_{J=0} , \quad (2.6)$$

$$G_{12} \equiv \langle \varphi_1 \varphi_2 \rangle - \langle \varphi_1 \rangle \langle \varphi_2 \rangle = \frac{\delta^2 W}{\delta J_1 \delta J_2} \Big|_{J=0} , \quad (2.7)$$

$$W_{1,\dots,n}^{(n)} \equiv \frac{\delta^n W}{\delta J_1 \cdots \delta J_n} \Big|_{J=0} , \quad (2.8)$$

where we defined the propagator  $G$  in Eq.(2.7) because of its specific relevance with respect to higher-order members of the hierarchy. At each order, the  $n$ -th cumulant of  $\varphi$  is related to all averages of  $\varphi$  of order lesser or equal to  $n$ . To first order the average coincides with the cumulant. The relation at second order is shown in Eq.(2.7) . We show here for future use the relation for three-body functions:

$$\begin{aligned} W_{123}^{(3)} &= \langle \varphi_1 \varphi_2 \varphi_3 \rangle - \langle \varphi_1 \rangle \langle \varphi_2 \varphi_3 \rangle + 2 \langle \varphi_1 \rangle \langle \varphi_2 \rangle \langle \varphi_3 \rangle \\ &\quad - \langle \varphi_2 \rangle \langle \varphi_1 \varphi_3 \rangle \\ &\quad - \langle \varphi_3 \rangle \langle \varphi_1 \varphi_2 \rangle , \end{aligned} \quad (2.9)$$

which can be rewritten as:

$$\langle \varphi_1 \varphi_2 \varphi_3 \rangle = W_{123}^{(3)} + \phi_1 G_{23} + \phi_2 G_{13} + \phi_3 G_{12} + \phi_1 \phi_2 \phi_3 . \quad (2.10)$$

### 2.1.1 Expansion around a saddle-point

The action  $S$  is, in many-body problems such as the ones we will be interested in, usually too complex to be treated exactly, and one usually resorts to an expansion around a given approximation of the action, that is exactly solvable. In the case of quantum mechanics, the saddle point of the action corresponds to the classical trajectories, so that we can build semi-classical approximations by expanding the action around the saddle-point in inverse powers of Planck's constant. This starting point for expansions is not always justified, depending on the statistical theory that we are considering.

Following the example of quantum mechanics, we evaluate the partition function at its saddle point:

$$\left\{ \begin{array}{l} Z \approx Z^{(0)} \equiv e^{-S[\varphi^*]}, \\ \left. \frac{\delta S[\varphi]}{\delta \varphi_1} \right|_{\varphi^*} = 0, \end{array} \right. \quad (2.11)$$

Now we make a change of variables  $\varphi \rightarrow \varphi - \varphi^*$  in the trace defining the partition function:

$$\begin{aligned} Z &= \text{Tr} e^{-S[\varphi+\varphi^*]} \\ &= Z^{(0)} \text{Tr} \exp \left( -\frac{1}{2} \varphi_1 \left. \frac{\delta^2 S[\varphi]}{\delta \varphi_1 \delta \varphi_2} \right|_{\varphi^*} \varphi_2 - \sum_{N=3}^{\infty} \left. \frac{\delta^N S[\varphi]}{\delta \varphi_1 \cdots \delta \varphi_N} \right|_{\varphi^*} \varphi_1 \cdots \varphi_N \right), \end{aligned} \quad (2.12)$$

where we performed an expansion of the action around  $\varphi^*$  in powers of  $\varphi$ , and integration over repeated indices is assumed. The expansion around the saddle point has the effect to cancel the constant and linear terms in the action. We gather all the cubic and higher order terms in a functional  $S_{\text{ng}}[\varphi]$  and define  $V_{12}$  as the quadratic coefficient. We now artificially once again add an external source  $J$  coupled to  $\varphi$  to get the following expression of the partition function:

$$Z[J] = Z^{(0)} \text{Tr} e^{-\frac{1}{2} \varphi_1 V_{12} \varphi_2 - S_{\text{ng}}[\varphi] + J_1 \varphi_1}. \quad (2.13)$$

In an Ising model, the  $\varphi$  field could be the local magnetization, and the source  $J$  would in that case be an external magnetic field. In the case of liquid theory, the field  $\varphi$  is usually the local microscopic density in the liquid, and  $J$  is the chemical potential and a possible inhomogeneous external field. Now calculating the partition function can be done perturbatively around the quadratic part:

$$\begin{aligned} Z[J] &= Z^{(0)} \text{Tr} e^{-\frac{1}{2} \varphi_1 V_{12} \varphi_2 + J_1 \varphi_1} e^{-S_{\text{ng}}[\varphi]} \\ &= Z^{(0)} \sum_{N=0}^{\infty} \frac{(-1)^N}{N!} \text{Tr} S_{\text{ng}}[\varphi]^N e^{-\frac{1}{2} \varphi_1 V_{12} \varphi_2 + J_1 \varphi_1}. \end{aligned} \quad (2.14)$$

Expanding  $S_{\text{ng}}$  in powers of the field, the calculation of  $Z$  is reduced to an infinite sum of averages of  $\varphi$  with respect to a quadratic statistical weight. For example if  $S_{\text{ng}}$  was composed of a cubic term plus a quartic one:

$$S_{\text{ng}}[\varphi] = \frac{g_3}{3!} \varphi_1 \varphi_1 \varphi_1 + \frac{g_4}{4!} \varphi_1 \varphi_1 \varphi_1 \varphi_1 \quad (2.15)$$

the expansion of  $Z$  would then become:

$$Z[J] = Z^{(0)} Z_{\text{quad}}[J] \left( 1 + \sum_{N=1}^{\infty} \frac{(-1)^N}{N!} \frac{1}{Z_{\text{quad}}} \text{Tr} \left[ \frac{g_3}{3!} \varphi_1 \varphi_1 \varphi_1 + \frac{g_4}{4!} \varphi_1 \varphi_1 \varphi_1 \varphi_1 \right]^N e^{-\frac{1}{2} \varphi_1 V_{12} \varphi_2 + J_1 \varphi_1} \right), \quad (2.16)$$

where  $Z_{\text{quad}}$  is the partition function of the quadratic theory. This is indeed an infinite sum of averages of  $\varphi$ , under a quadratic weight. The quadratic weight is a generalization of a Gaussian distribution and thus integrals needed to compute averages of  $\varphi$  under such distribution are tractable, at least on a formal level. The average of a product of fields under quadratic weight is given by Wick's theorem [174], and simply expresses the fact that, for a quadratic weight, high-order averages of the field  $\varphi$  only depend on its two first cumulants, that we will call  $\phi^{(0)}$  and  $G^{(0)}$ . The calculation of these quantities is straightforward when looking at  $Z_{\text{quad}}$ :

$$Z_{\text{quad}}[J] = \text{Tr} e^{-\frac{1}{2} \varphi_1 V_{12} \varphi_2 + J_1 \varphi_1} = \text{Cte} e^{-\frac{1}{2} \int_{12} \ln V_{12} e^{\frac{1}{2} J_1 V_{12}^{-1} J_2}}, \quad (2.17)$$

hence

$$\phi_1^{(0)} = \frac{1}{Z} \frac{\delta Z}{\delta J_1} \Big|_{J=0} = 0, \quad (2.18)$$

$$G_{12}^{(0)} = \frac{\delta^2 W[J]}{\delta J_1 \delta J_2} \Big|_{J=0} = V_{12}^{-1}, \quad (2.19)$$

where we have set  $J = 0$  at the end of the calculations to come back to the original theory. Thus, the full expression of  $Z$  will be a sum of integrals that will contain only  $G^{(0)}$  functions (often called the “bare” propagator in field theory). This can pictorially be written, to second order in  $g_3$  and  $g_4$ , as (combinatorial factors have been omitted and can be dealt with by a proper definition of the diagrams):

$$Z = Z^{(0)} Z_{\text{quad}} \left( 1 - g_4 \text{diagram} + g_3^2 \text{diagram} + g_3^2 \text{diagram} + g_4^2 \text{diagram} + g_4^2 \text{diagram} + g_4^2 \text{diagram} + \dots \right). \quad (2.20)$$

The diagrams above are defined as follows: a black point is an integration point bearing an index, a line joining two black points of indices, say 1 and 2, is a bare propagator  $V_{12}^{-1}$ . Integration over repeated indices is understood, and numerical factors have been omitted for simplicity. Also, two diagrams standing side by side mean that the product of the two diagrams is carried out.

Eqs.(2.11–2.20) is only a textbook example of a starting point for expansion and its associated diagrammatic expansion Eq.(2.19). Of course the type of integrals, and thus diagrams that represent them, will depend on the particular theory considered, as well as the approximate starting point for the expansion. The diagrams of liquid theory (the Mayer diagrams [148, 70, 77]) do not have the same characteristics as usual diagrams in dynamical field theories used for glasses. However, we will not need in this chapter to know the particular form of the diagrammatic expansion nor the starting point of calculation, and wish to stay on a more generic level.

### 2.1.2 The free-energy and the linked cluster theorem

The free-energy  $W$  is defined as the logarithm of the partition function in Eq.(2.5). Taking the logarithm of the partition function has a dramatic effect on a diagrammatic expansion of the partition function: it systematically eliminates all diagrams that can be expressed as a product of other diagrams (they are usually called “connected” diagrams), and in a sense reduces the number of diagrams in the complete expression. As we saw in Eq.(2.7), the logarithm of the partition function is the generating functional of the cumulants of the field, that have the property of clustering: they are functions that decay to zero when two coordinates are infinitely far from each other. This property of clustering leads to the disappearance of the disconnected diagrams in the expansion of  $W$ . This is the “linked cluster theorem”, a physical demonstration of which can be found in [179], while a very elegant one in terms of replicas can be found in [132].

As an illustration, we show what Eq.(2.20) becomes upon taking its logarithm:

$$W = \ln Z = W^{(0)} + W_{\text{quad}} - g_4 \text{diagram} + g_3^2 \text{diagram} + g_3^2 \text{diagram} + g_4^2 \text{diagram} + g_4^2 \text{diagram} + \dots \quad (2.21)$$

The diagrams that were the product of two simpler diagrams have disappeared of the expression.

### 2.1.3 Reduction of diagrams: first Legendre transform

This procedure of diagrammatic reduction can be continued by performing a Legendre transformation of  $W$  with respect to the source field  $J$ . Define  $\Gamma_1$ , a functional of  $\phi$ , as:

$$\left\{ \begin{array}{l} \Gamma_1[\phi] = J_1^*[\phi]\phi_1 - W[J^*[\phi]] , \\ \text{with } J^*[\phi] \text{ such that } \left. \frac{\delta W[J]}{\delta J_1} \right|_{J^*} = \phi_1 . \end{array} \right. \quad (2.22)$$

We replaced one variable with its conjugate, here  $J$  with  $\phi$ . This operation will have a dramatic effect on the diagrammatic expansion of  $W$ , resumming whole classes of diagrams. By definition of the Legendre transform, we have:

$$e^{-\Gamma_1[\phi]} = \int \mathcal{D}\varphi e^{-S[\varphi] + J^*[\varphi](\varphi - \phi)} . \quad (2.23)$$

Under this form, we see why the  $\Gamma_1$  functional is often called the effective action: upon integrating the fluctuations (performing the path integral), the microscopic action  $S$  becomes a new “effective” action  $\Gamma_1$ . Expanding  $\Gamma_1$  and  $S$  in Taylor series, the coupling constants in  $S$  ( $g_3$  and  $g_4$  in our example) will be renormalized to give the corresponding effective couplings in  $\Gamma_1$ .

From the effective action, we obtain a new class of correlation functions, defined by the functional derivatives of the effective action:

$$\Gamma_{1\dots n}^{(N)}[\phi] \equiv \frac{\delta^N \Gamma_1[\phi]}{\delta \phi_1 \dots \delta \phi_N} . \quad (2.24)$$

The first of these derivatives is the source field, as we can see from the definition of  $\Gamma_1$ :

$$\frac{\delta \Gamma_1[\phi]}{\delta \phi_1} = \int_2 \frac{\delta J_2^*[\phi]}{\delta \phi_1} \phi_2 + J_1^*[\phi] - \int_2 \frac{\delta J_2^*[\phi]}{\delta \phi_1} \left. \frac{\delta W[J]}{\delta J_2} \right|_{J^*[\phi]} = J_1^*[\phi] . \quad (2.25)$$

The second derivative is the inverse of the propagator  $G[J]$  evaluated at the value of the source  $J^*[\phi]$ . This can be shown by noting that:

$$\begin{aligned} \delta_{12} &= \frac{\delta \phi_1}{\delta \phi_2} = \frac{\delta}{\delta \phi_2} \left( \left. \frac{\delta W[J]}{\delta J_1} \right|_{J^*[\phi]} \right) \\ &= \int_3 \frac{\delta J_3^*[\phi]}{\delta \phi_2} \left. \frac{\delta^2 W[J]}{\delta J_1 \delta J_3} \right|_{J^*[\phi]} . \end{aligned} \quad (2.26)$$

The second derivative of  $W$  is the propagator, while the derivative of  $J^*$  is the second derivative of  $\Gamma_1$ , we thus obtain:

$$\delta_{12} = \int_3 G_{13}[J^*[\phi]] \Gamma_{32}^{(2)}[\phi] . \quad (2.27)$$

Which shows that  $\Gamma^{(2)}$  is the functional inverse of  $G[J^*]$ :

$$\Gamma_{12}^{(2)}[\phi] = G_{12}[J^*[\phi]]^{-1} . \quad (2.28)$$

### Diagrammatic expansion of the effective action

Expanding the action around  $\phi$ , we get:

$$e^{-\Gamma_1[\phi]} = e^{-S[\phi]} \int \mathcal{D}\varphi \exp \left( -\frac{1}{2} S_{12}^{(2)}[\phi] \varphi_1 \varphi_2 - S_{\text{ng}}[\varphi, \phi] + \int_1 [J_1^*[\phi] - S_1^{(1)}[\phi]] \varphi_1 \right), \quad (2.29)$$

where  $S_{1\dots N}^{(N)}[\phi] = \left. \frac{\delta^N S[\varphi]}{\delta\varphi_1 \dots \delta\varphi_N} \right|_{\phi}$ , and  $S_{\text{ng}}$  gathers all derivatives of the action of order higher than three, evaluated at  $\phi$ :

$$S_{\text{ng}}[\varphi, \phi] \equiv \sum_{N=3}^{\infty} \frac{1}{N!} \int_{1,\dots,N} S_{1\dots N}^{(N)}[\phi] \varphi_1 \dots \varphi_n. \quad (2.30)$$

We get by taking the logarithm of Eq.(2.29):

$$\Gamma_1[\phi] = S[\phi] - \ln \left[ \int \mathcal{D}\varphi \exp \left( -\frac{1}{2} \int_{1,2} S_{12}^{(2)}[\phi] \varphi_1 \varphi_2 - S_{\text{ng}}[\varphi, \phi] + \int_1 [J_1^*[\phi] - S_1^{(1)}[\phi]] \varphi_1 \right) \right]. \quad (2.31)$$

As before, the evaluation of the path integral in Eq.(2.31) can be done by expanding around the quadratic part of the action. The second derivative of the action, which is the inverse of the propagator for the diagrams is now:

$$S_{12}^{(2)}[\phi] = \left( G_{12}^{(0)}[\phi] \right)^{-1} = \left. \frac{\delta^2 S[\varphi]}{\delta\varphi_1 \delta\varphi_2} \right|_{\phi}. \quad (2.32)$$

Before the Legendre transformation, the inverse propagator was the second derivative of the action, but evaluated at the saddle-point.

We explicitly extract the quadratic part of the action:

$$\Gamma_1[\phi] = S[\phi] - \ln \int \mathcal{D}\varphi \exp \left( -\frac{1}{2} \int_{1,2} S_{12}^{(2)}[\phi] \varphi_1 \varphi_2 \right) - \ln \left\langle e^{-S_{\text{ng}}[\phi, \varphi]} \right\rangle_{\text{1PI}}, \quad (2.33)$$

where the average is defined as:

$$\left\langle \bullet \right\rangle_{\text{1PI}} \equiv \frac{\int \mathcal{D}\varphi \left( \bullet \right) \exp \left( -\frac{1}{2} \int_{1,2} S_{12}^{(2)}[\phi] \varphi_1 \varphi_2 + \int_1 [J_1^*[\phi] - S_1^{(1)}[\phi]] \varphi_1 \right)}{\int \mathcal{D}\varphi \exp \left( -\frac{1}{2} \int_{1,2} S_{12}^{(2)}[\phi] \varphi_1 \varphi_2 \right)}. \quad (2.34)$$

### Average of the field

The linear term here in Eq.(2.31) exactly enforces that the average of  $\varphi$  is 0, a demonstration of which can be found in [83, 32], and we reproduce it below. We first rewrite the effective action with the change of variable  $\varphi \rightarrow \varphi + \phi$  to obtain:

$$\Gamma_1[\phi] = -\ln \int \mathcal{D}\varphi e^{-S[\phi+\varphi] + J_1^*[\phi] \varphi_1}. \quad (2.35)$$

From this expression we can take the derivative with respect to  $\phi_1$  to get:

$$\begin{aligned} \Gamma_1^{(1)}[\phi] &= \left\langle \frac{\delta S[\phi + \varphi]}{\delta\phi_1} - \frac{\delta J_1^*[\phi]}{\delta\phi_1} \varphi_1 \right\rangle_{\text{1PI}}, \\ &= \left\langle \frac{\delta S[\varphi + \phi]}{\delta\varphi_1} \right\rangle_{\text{1PI}} - \Gamma_{12}^{(2)}[\phi] \langle \varphi_1 \rangle_{\text{1PI}}. \end{aligned} \quad (2.36)$$

Now we also know that:

$$\begin{aligned} & \int \mathcal{D}\varphi \left[ -\frac{\delta S[\varphi + \phi]}{\delta \varphi_1} + J_1^*[\phi] \right] e^{-S[\varphi + \phi] + J_2^*[\phi]\varphi_2} = 0, \\ \Rightarrow & \left\langle \frac{\delta S[\phi + \phi]}{\delta \varphi_1} \right\rangle_{\text{1PI}} = \Gamma_1^{(1)}[\phi]. \end{aligned} \quad (2.37)$$

since the integral of a derivative is zero, up to boundary terms. Thus we get:

$$\begin{aligned} \Gamma_1^{(1)}[\phi] &= \Gamma_1^{(1)}[\phi] - \Gamma_{12}^{(2)}[\phi] \langle \varphi_1 \rangle_{\text{1PI}}, \\ \Rightarrow & \langle \varphi_1 \rangle_{\text{1PI}} = 0. \end{aligned} \quad (2.38)$$

The last equality is obtained because in order for the Legendre transform to be defined, the relation between  $J$  and  $\phi$  must be invertible, i.e.  $J^*[\phi]$  must be a monotonic function and thus  $\Gamma^{(2)}$  is invertible (in the functional sense). In practice this implies that we compute all diagrams with zero average field (“vacuum” diagrams).

### One-particle irreducibility

We can show that the diagrams that we must calculate in order to evaluate diagrammatically the effective action are all “one-particle irreducible” (1PI), which means that upon cutting one line of the diagram, they do not separate in disconnected parts. For example in Eq.(2.21), the second diagram is the only one that we pictured and that is one-particle reducible: it separates into two bubbles when cutting the central line.

A simple proof of the irreducibility of the diagrams of the effective action can be found in [179], and we reproduce it here. We start from the free energy without Legendre transformation, and add a perturbation to the action, defining:

$$W_\varepsilon[J] = \ln \int \mathcal{D}\varphi \exp \left( -S[\varphi] + J_1 \varphi_1 - \frac{\varepsilon}{2} \int_{1,2} \varphi_1 \varphi_2 \right). \quad (2.39)$$

This amounts to a shift in the inverse propagator:

$$\left( G_{12}^{(0)} \right)^{-1} \rightarrow \left( G_{12}^{(0)} \right)^{-1} + \varepsilon, \quad (2.40)$$

which gives a shift in the propagator (at first order in  $\varepsilon$ ):

$$G_{12}^{(0)} \rightarrow G_{12}^{(0)} - \varepsilon \int_{1'} G_{11'}^{(0)} \int_{2'} G_{22'}^{(0)} + \mathcal{O}(\varepsilon^2). \quad (2.41)$$

Now consider a diagram of the unperturbed free-energy. It is made of nodes and  $G_{12}^{(0)}$  lines. Now adding the perturbation doubles each line: either the line is untouched, either it is replaced by a  $\varepsilon \int G^{(0)} \int G^{(0)}$  line, which is disconnected. At first order in  $\varepsilon$ , we perform only one of these replacements, and this amounts to cut open one line of the diagram. If the resulting diagram is disconnected, this means that the original diagram was one-particle reducible. Proving one-particle irreducibility of a given quantity thus amounts to show that the first order in  $\varepsilon$  of the expansion of this quantity is a connected function.

Let us look at the first order in  $\varepsilon$  for the free-energy:

$$\begin{aligned} W_\varepsilon[J] &= W[J] + \varepsilon \left. \frac{dW_\varepsilon[J]}{d\varepsilon} \right|_{\varepsilon=0} + \mathcal{O}(\varepsilon^2) \\ &= W[J] - \frac{\varepsilon}{2} \int_{1,2} \langle \varphi_1 \varphi_2 \rangle + \mathcal{O}(\varepsilon^2) \\ &= W[J] - \frac{\varepsilon}{2} \int_{1,2} G_{12}[J] - \frac{\varepsilon}{2} \int_1 \phi_1[J] \int_2 \phi_2[J] + \mathcal{O}(\varepsilon^2), \end{aligned} \quad (2.42)$$

where we defined  $G_{12}[J]$  as the propagator in presence of a source  $J$ , and  $\phi[J]$  as the average of the field in presence of a source. The first order term obviously contains a disconnected part, and thus the diagrams in  $W[J]$  are not 1PI.

We turn now to the effective action, i.e. the Legendre transform of  $W_\varepsilon$ . Its derivative with respect to the external parameter  $\varepsilon$  is the same as that of  $W$  by the properties of the Legendre transformation:

$$\begin{aligned} \frac{d\Gamma_\varepsilon[\phi]}{d\varepsilon} &= \int_1 \frac{dJ_1^*[\phi]}{d\varepsilon} \phi_1 - \left. \frac{dW_\varepsilon[J]}{d\varepsilon} \right|_{J^*[\phi]} - \int_1 \frac{dJ_1^*[\phi]}{d\varepsilon} \left. \frac{\delta W[J]}{\delta J_1} \right|_{J^*[\phi]}, \\ &= - \left. \frac{dW_\varepsilon[J]}{d\varepsilon} \right|_{J^*[\phi]}. \end{aligned} \quad (2.43)$$

Thus we obtain:

$$\Gamma_\varepsilon[\phi] = \Gamma_1[\phi] + \frac{\varepsilon}{2} \int_{1,2} \phi_1 \phi_2 + \frac{\varepsilon}{2} \int_{1,2} G_{12}[\phi^*[\phi]] + \mathcal{O}(\varepsilon^2). \quad (2.44)$$

As it stands, the effective action is not 1PI either. However, the first of the  $\mathcal{O}(\varepsilon)$  terms is contained in the action evaluated at the average field. Indeed upon adding the perturbation, we made the change:

$$S[\varphi] \rightarrow S_\varepsilon[\varphi] = S[\varphi] + \frac{\varepsilon}{2} \int_{1,2} \varphi_1 \varphi_2. \quad (2.45)$$

Thus looking at the starting point of the diagrammatic expansion of  $\Gamma$ , Eq.(2.31), we see that the first term already contains this disconnected part. Thus we find:

$$\Gamma_\varepsilon[\phi] = S_\varepsilon[\phi] - \ln \int \mathcal{D}\varphi e^{-S_\varepsilon[\phi+\varphi] + S_\varepsilon[\phi] + J_1^*[\phi]\varphi}, \quad (2.46)$$

and we showed that the second term has an  $\mathcal{O}(\varepsilon)$  part that is connected. This proves that:

$$\Gamma_1[\phi] = S[\phi] + \Gamma_{1\text{PI}}[\phi], \quad (2.47)$$

where  $\Gamma_{1\text{PI}}$  is the sum of all “vacuum” (i.e. with zero average field) 1PI diagrams with propagator  $(S_{12}^{(2)})^{-1}$ . The microscopic action is thus a resummation of the one-particle reducible (1PR) diagrams, and this is why the effective action is sometimes also called “1PI effective action” or “1PI functional”.

### Gaussian approximation

The calculation at lowest order (when considering that  $S_{\text{ng}}$  is negligible with respect to the quadratic part), is formally the same than in the expansion of  $Z$  and we thus get:

$$- \ln \left[ \int \mathcal{D}\varphi \exp \left( -\frac{1}{2} \left. \frac{\delta^2 S[\varphi]}{\delta \varphi_1 \delta \varphi_2} \right|_\phi \varphi_1 \varphi_2 \right) \right] = \text{Cte} + \frac{1}{2} \int_{1,2} \ln \left( G_{12}^{(0)-1} \right). \quad (2.48)$$

Finally we obtain:

$$\Gamma_1[\phi] = \text{Cte} + S[\phi] + \frac{1}{2} \int_{1,2} \ln \left( G_{12}^{(0)-1} \right) + \{1\text{PI diagrams}\}. \quad (2.49)$$

For example, upon performing the Legendre transformation, Eq.(2.21) now becomes:

$$\Gamma_1[\phi] = S[\phi] + \int_{12} \ln \left( G_{12}^{(0)-1} \right) + g_4 \text{---} \text{---} \text{---} - g_3^2 \text{---} \text{---} \text{---} - g_4^2 \text{---} \text{---} \text{---} - g_4^2 \text{---} \text{---} \text{---} + \dots \quad (2.50)$$

Only a few diagrams are left here to this order in this expansion. The lines in the diagrams are  $G^{(0)}$ .



### Loop expansion of the effective action

In order to systematize the evaluation of the effective action, we can resort to the so-called loop expansion. We introduce a parameter  $\lambda$  in the definition of the partition function:

$$\begin{aligned} Z[J] &= \int \mathcal{D}\varphi e^{-\frac{1}{\lambda}[S[\varphi] - \int_1 J_1 \varphi_1]} , \\ W[J] &= \lambda \ln Z[J] . \end{aligned} \quad (2.51)$$

and expand  $W$  and  $\Gamma_1$ , its Legendre transform, around  $\lambda=0$ . The lowest order term is given by the saddle-point of the functional integral:

$$\left\{ \begin{array}{l} W[J] = -S[\varphi^*[J]] + \int_1 J_1 \varphi_1^*[J] + \mathcal{O}(\lambda) , \\ \varphi^*[J] \text{ such that } \left. \frac{\delta S[\varphi]}{\delta \varphi_1} \right|_{\varphi^*[J]} = J_1 . \end{array} \right. \quad (2.52)$$

We can now perform the Legendre transformation. The source  $J^*[\phi]$  that selects the correct average value of the field is defined by:

$$\left. \frac{\delta W_0[J]}{\delta J_1} \right|_{J^*[\phi]} = \phi_1 . \quad (2.53)$$

The saddle-point equation imposes that, for all values of  $J$ :

$$\frac{\delta W[J]}{\delta J_1} = \varphi_1^*[J] + \int_{1'} \frac{\delta \varphi_{1'}^*[J]}{\delta J_1} \left[ J_1 - \left. \frac{\delta S[\varphi]}{\delta \varphi} \right|_{\varphi^*[J]} \right] + \mathcal{O}(\lambda) = \varphi_1^*[J] + \mathcal{O}(\lambda) . \quad (2.54)$$

Thus we have that:

$$\varphi_1^*[J^*[\phi]] = \phi_1 + \mathcal{O}(\lambda) , \quad (2.55)$$

and thus:

$$\Gamma_1[\phi] = S[\phi] + \mathcal{O}(\lambda) . \quad (2.56)$$

We now turn to the first order term. Returning to Eq.(2.33), we have with the introduction of  $\lambda$ :

$$\begin{aligned} \Gamma_1[\phi] &= S[\phi] - \lambda \ln \int \mathcal{D}\varphi \exp \left( -\frac{1}{2} \int_{1,2} \frac{S_{12}^{(2)}[\phi]}{\lambda} \varphi_1 \varphi_2 \right) - \lambda \ln \left\langle e^{-\frac{1}{\lambda} S_{\text{ng}}[\phi, \varphi]} \right\rangle_{1PI} , \\ \left\langle \bullet \right\rangle_{1PI} &= \frac{\int \mathcal{D}\varphi \bullet e^{-\frac{1}{2} \int_{1,2} \frac{S_{12}^{(2)}[\phi]}{\lambda} \varphi_1 \varphi_2 + \int_1 \frac{J_1^*[\phi] - S_1^{(1)}[\phi]}{\lambda} \varphi_1}}{\int \mathcal{D}\varphi e^{-\frac{1}{2} \int_{1,2} \frac{S_{12}^{(2)}[\phi]}{\lambda} \varphi_1 \varphi_2}} \end{aligned} \quad (2.57)$$

We now perform the change of variables:

$$\varphi \rightarrow \sqrt{\lambda} \varphi \quad (2.58)$$

in the functional integrals to get:

$$\Gamma_1[\phi] = \text{Cte} + S[\phi] - \lambda \ln \int \mathcal{D}\varphi \exp \left( -\frac{1}{2} \int_{1,2} S_{12}^{(2)}[\phi] \varphi_1 \varphi_2 \right) - \lambda \ln \left\langle e^{-\frac{1}{\lambda} S_{\text{ng}}[\phi, \sqrt{\lambda} \varphi]} \right\rangle_{1PI} . \quad (2.59)$$

Note that an infinite normalization factor dependant on  $\lambda$  comes from this change of variables and is neglected here.

First we observe that we can neglect the contribution from the non-gaussian part of the action: its lowest order term is cubic in  $\varphi$  and thus gives a  $\lambda^{1/2}$  contribution. Thus the lowest order term

coming from this functional integral is  $\lambda^2$  because of the  $\lambda$  in front of the logarithm. We can also look at the linear term, that has a non-trivial  $\lambda$  dependence through the term  $\Gamma_1^{(1)}\varphi$ . But we see also that at lowest order,

$$J_1^*[\phi] \equiv \Gamma_1^{(1)}[\phi] = S_1^{(1)}[\phi] , \quad (2.60)$$

and the next order is  $\mathcal{O}(\lambda)$ , which means that the linear term is at least  $\mathcal{O}(\sqrt{\lambda})$ , and thus when evaluated diagrammatically, at least  $\mathcal{O}(\lambda)$ , and again  $\mathcal{O}(\lambda^2)$  because of the  $\lambda$  in factor of the logarithm.

Finally we end up with only the Gaussian integral to compute and thus:

$$\Gamma_1[\phi] = \text{Cte} + S[\phi] + \lambda \int_{1,2} \ln \left( S_{12}^{(2)}[\phi] \right) + \mathcal{O}(\lambda^2) . \quad (2.61)$$

We can also evaluate the next order in order to see the first non-trivial diagrams. We now have:

$$J_1^*[\phi] - S_1^{(1)}[\phi] = \frac{\lambda}{2} \int_{23} S_{123}^{(3)} G_{23}^{(0)} + \mathcal{O}(\lambda^2) . \quad (2.62)$$

An order 2 term comes from a  $\mathcal{O}(\lambda)$  term of the expansion of the exponential. The lowest order contribution come from the cubic and quartic terms:

$$\begin{aligned} & \int_{1\dots 6} S_{123}^{(3)} G_{14}^{(0)} G_{25}^{(0)} G_{36}^{(0)} S_{456}^{(3)} , \\ & \int_{1\dots 6} G_{12}^{(0)} S_{123}^{(3)} G_{34}^{(0)} S_{456}^{(3)} G_{56}^{(0)} , \\ & \int_{1\dots 4} G_{12}^{(0)} S_{1234}^{(4)} G_{34}^{(0)} . \end{aligned} \quad (2.63)$$

On the other hand the lowest order term coming from the source term is:

$$\int_{1\dots 6} G_{12}^{(0)} S_{123}^{(3)} G_{34}^{(0)} S_{456}^{(3)} G_{56}^{(0)} , \quad (2.64)$$

and it cancels exactly the corresponding diagram coming from the non-gaussian part of the action, which is 1PR. We obtain the second order expression written in Eq.(2.50). At the end of the calculation, we must send back  $\lambda$  to 1 to return to the original theory. In quantum field theory,  $\lambda$  is equal to Planck's constant  $\hbar$ , which is indeed small, and the loop expansion corresponds to a semi-classical expansion, and is thus justified.

### Variational principle and inverse Legendre transform

Finally, apart from simplifying computations in terms of diagrams, the Legendre transformation provides us with a variational principle to calculate both the average of the field and the free-energy. We recall Eq.(2.25) that the derivative of the effective action is the source field:

$$\frac{\delta \Gamma_1[\phi]}{\delta \phi_1} = J_1^*[\phi] . \quad (2.65)$$

Now starting from this equation, we can change again our viewpoint: instead of considering  $\phi$  as a variable, and  $J^*$  defined as the value of  $J$  that fixes this particular value of  $\langle \varphi \rangle$ , we can choose for  $\phi$  the physical average that corresponds to the initial value of  $J$  (which can be zero if it had been introduced by hand), let us call it  $\phi^*[J]$ . The derivative of the effective action, evaluated at  $\phi^*[J]$  is thus bound to be  $J$ :

$$\Gamma_1^{(1)}[\phi^*[J]] = J_1 . \quad (2.66)$$

If the physical case was  $J = 0$ , this amounts to say that  $\Gamma_1$  is extremal at the physical value of the average field.

At this particular value of  $\phi$ , we obtain the physical value of  $W$  as:

$$W[J] = \int_1 J_1 \phi_1^*[J] - \Gamma_1[\phi^*[J]]. \quad (2.67)$$

Mathematically, we have performed the inverse Legendre transform.

Eq.(2.66) is important in regards of the physical symmetries of the problem: it is used to obtain the consequences of the symmetries of the action on the effective action (sometimes called Ward-Takahashi identities), in order to obtain, when performing approximations, a theory that respects all physical requirements.

The program to perform approximations on the partition function is then the following:

- Choose an approximate starting point for the expansion of  $\ln Z$
- Write down the corresponding diagrammatic expansion
- Perform the Legendre transform to reduce diagrams
- Truncate the expansion by selecting a class of diagrams and obtain an approximate  $\Gamma_1[\phi]$
- Use the variational principle Eq.(2.66) to obtain the approximate  $\phi$
- Evaluate the approximate functional  $\Gamma_1$  at this particular value of  $\phi$  to get  $\ln Z$

This procedure is in fact much more than a reduction: one can show that keeping only one diagram in the expansion of  $\Gamma$  is equivalent to keeping an infinity of diagrams in  $\ln Z$ , thus providing better approximations.

### Higher-order correlation functions

Computing a functional derivative of Eq.(2.27) with respect to  $\phi_3$ , we get formally:

$$0 = \frac{\delta^3 \Gamma_1[\phi]}{\delta \phi_1 \delta \phi_3 \delta \phi_4} \frac{\delta^2 W[J]}{\delta J_2 \delta J_4} \Big|_{J^*} + \frac{\delta^2 \Gamma_1[\phi]}{\delta \phi_1 \delta \phi_4} \frac{\delta^2 \Gamma_1[\phi]}{\delta \phi_4 \delta \phi_5} \frac{\delta^3 W[J]}{\delta J_2 \delta J_4 \delta J_5} \Big|_{J^*}, \quad (2.68)$$

And multiplying through by a second derivative of  $\Gamma$  and using Eq.(2.27), we get:

$$\begin{aligned} \Gamma_{123}^{(3)} &= -\Gamma_{11'}^{(2)} \Gamma_{22'}^{(2)} \Gamma_{33'}^{(2)} W_{1'2'3'}^{(3)}, \\ \Leftrightarrow W_{123}^{(3)} &= -G_{11'} G_{22'} G_{33'} \Gamma_{1'2'3'}^{(3)}, \end{aligned} \quad (2.69)$$

where we dropped the functional dependances of the correlation functions for clarity. This is a standard equation that can be found in any textbook on field theory, for example in [179], that expresses the relation between the so-called vertex functions and the cumulants of the field. We can continue this procedure, and we can in this way express all cumulants of the field as a function of only the propagator and the derivatives of the effective action (sometimes called vertex functions, or proper vertexes in the context of field theory).

At each order, the  $n$ -th order functional  $\Gamma^{(n)}$  involves all functionals  $W^{(m)}$  of order lesser or equal to  $n$ . We will use such relations in Chapters 3 and 4. In the context of liquid theory, these functionals are related to the direct correlation functions. In the context of the dynamics of supercooled liquids, the second order functional  $\Gamma^{(2)}$  can be identified with the memory kernel of the Mori-Zwanzig formalism.

In the presence of phase transitions, the propagators of the theory often develop singularities or divergences at large wave-lengths, making the diagrams in the expansion of  $W$  singular. The vertex functionals  $\Gamma^{(2)}$  being the inverse (in Fourier space) of the propagator, they are often free of these divergences. For example, the direct correlation function of simple liquids develops no singularity near the liquid/gas transition [77]. If the order parameter of the transition is a one-point quantity (typically  $\phi$  itself), then due to the regularity of these functions, the phase transition can be detected with approximations of  $\Gamma_1$ , whereas performing approximations on  $W$  would lead to divergent integrals, making the analysis of the transition much harder.

Of course, when the order-parameter of the transition is a two-point quantity, which is the case in the glass transition, as explained in the introduction, it is necessary to go one step further in order to obtain approximations that are able to detect the transition. This is achieved by further Legendre transforming with respect to a two-point quantity, as explained in the following.

#### 2.1.4 Reduction of diagrams: second Legendre transform

As we saw in the introduction, the natural order parameter for the glass transition is a two-point correlation function. Thus, in order to be able to detect a possible transition in terms of this order parameter, it is important to be able to perform accurate approximations on two-point functions. This can be achieved by introducing another Legendre transformation [109, 53, 54, 47], with respect to a two-point quantity.

We now add to the original partition function a source  $K$  coupled to the square of the field, in addition to the linear source, and define:

$$W[J, K] = \ln \int \mathcal{D}\varphi e^{-S[\varphi] + J_1 \varphi_1 + \frac{1}{2} K_{12} \varphi_1 \varphi_2} , \quad (2.70)$$

The derivative of the free-energy with respect to the sources give:

$$\left\{ \begin{array}{l} \frac{\delta W[J, K]}{\delta J_1} = \langle \varphi_1 \rangle , \\ \frac{\delta W[J, K]}{\delta K_{12}} = \frac{1}{2} \langle \varphi_1 \varphi_2 \rangle = \frac{1}{2} \left( G_{12}[J] + \langle \varphi_1 \rangle \langle \varphi_2 \rangle \right) . \end{array} \right. \quad (2.71)$$

We can thus perform a double Legendre transform with respect to both  $J$  and  $K$ , which will give a functional of  $\phi$  and  $G$ , often called the 2PI effective action.

$$\left\{ \begin{array}{l} \Gamma_2[\phi, G] = \int_1 J_1^*[\phi, G] \phi_1 + \frac{1}{2} \int_{1,2} K_{12}^*[\phi, G] \left( \phi_1 \phi_2 + G_{12} \right) - W[J^*[\phi, G], K^*[\phi, G]] , \\ J^* \text{ such that } \left. \frac{\delta W[J, K]}{\delta J_1} \right|_{J^*, K^*} = \phi_1 \text{ and } K^* \text{ such that } \left. \frac{\delta W[J, K]}{\delta K_{12}} \right|_{J^*, K^*} = \frac{1}{2} \left( \phi_1 \phi_2 + G_{12} \right) . \end{array} \right. \quad (2.72)$$

We define the first derivative of the 2PI effective action as:

$$\left\{ \begin{array}{l} \Gamma_1^{(1,0)}[\phi, G] \equiv \frac{\delta \Gamma_2[\phi, G]}{\delta \phi_1} , \\ \Gamma_{12}^{(0,1)}[\phi, G] \equiv \frac{\delta \Gamma_2[\phi, G]}{\delta G_{12}} . \end{array} \right. \quad (2.73)$$

These derivatives are related to the sources by:

$$\begin{cases} \Gamma_1^{(1,0)}[\phi, G] = J_1^*[\phi, G] + \int_2 K_{12}^*[\phi, G]\phi_2, \\ \Gamma_{12}^{(0,1)}[\phi, G] = \frac{1}{2}K_{12}^*[\phi, G], \end{cases} \quad (2.74)$$

or equivalently, we obtain the expression of the sources in function of  $\phi$  and  $G$  only:

$$\begin{cases} J_1^*[\phi, G] = \Gamma_1^{(1,0)}[\phi, G] - 2 \int_2 \Gamma_{12}^{(0,1)}[\phi, G]\phi_2, \\ K_{12}^*[\phi, G] = 2\Gamma_{12}^{(0,1)}[\phi, G]. \end{cases} \quad (2.75)$$

Similarly as in the 1PI case, the second derivatives of the 2PI effective action is the inverse of a matrix of second derivatives of the free-energy. However its explicit expression is not very useful here (although we will need it in Chapter 4).

### Diagrammatic expansion of the 2PI effective action

Similarly as before, we rewrite the effective action as a functional integral:

$$\Gamma_2[\phi, G] = -\ln \int \mathcal{D}\varphi \exp \left( -S[\varphi] + \int_1 J_1^* (\varphi_1 - \phi_1) + \frac{1}{2} \int_{1,2} K_{12}^* (\varphi_1\varphi_2 - \phi_1\phi_2 - G_{12}) \right), \quad (2.76)$$

where we dropped the functional dependences of the sources. Replacing the sources by their expression in function of the derivatives of the effective action we get:

$$\Gamma_2[\phi, G] = -\ln \int \mathcal{D}\varphi \exp \left( -S[\varphi] + \int_1 \Gamma_1^{(1,0)} (\varphi_1 - \phi_1) + \int_{1,2} \Gamma_{12}^{(0,1)} [(\varphi_1 - \phi_1)(\varphi_2 - \phi_2) - G_{12}] \right). \quad (2.77)$$

Changing variables in the functional integral we get:

$$\Gamma_2[\phi, G] = -\ln \int \mathcal{D}\varphi \exp \left( -S[\phi + \varphi] + \int_1 \Gamma_1^{(1,0)} \varphi_1 + \int_{1,2} \Gamma_{12}^{(0,1)} [\varphi_1\varphi_2 - G_{12}] \right). \quad (2.78)$$

Again, this can be expanded around the quadratic part of the action to generate a diagrammatic expansion of the effective action. However the one-loop expression of the effective action is harder to extract.

### Average and correlations of the field

Intuitively, we see that the particular values of the sources will be here to enforce  $\langle \varphi \rangle = 0$  and  $\langle \varphi\varphi \rangle = G$ . We can prove this with a similar procedure than the 1PI case. We take a derivative of Eq.(2.78) with respect to  $\phi$  to get:

$$\Gamma_1^{(1,0)} = - \left\langle -\frac{\delta S[\phi + \varphi]}{\delta \phi_1} + \int_3 \Gamma_{13}^{(2,0)} \varphi_3 + \int_{3,4} \Gamma_{1,34}^{(1,1)} (\varphi_3\varphi_4 - G_{34}) \right\rangle. \quad (2.79)$$

Using the equation of movement again:

$$\left\langle -\frac{\delta S[\phi + \varphi]}{\delta \phi_1} + \Gamma^{(1,0)} + 2 \int_3 \Gamma_{13}^{(0,1)} \varphi_3 \right\rangle = 0, \quad (2.80)$$

to obtain:

$$\begin{aligned}\Gamma_1^{(1,0)} &= \left\langle \frac{\delta S[\phi + \varphi]}{\delta \phi_1} \right\rangle - \int_3 \Gamma_{13}^{(2,0)} \langle \varphi_3 \rangle - \int_{3,4} \Gamma_{1,34}^{(1,1)} \left( \langle \varphi_3 \varphi_4 \rangle - G_{34} \right), \\ &= \Gamma_1^{(1,0)} + 2 \int_{1'} \Gamma_{11'}^{(0,1)} \langle \varphi_{1'} \rangle - \int_3 \Gamma_{13}^{(2,0)} \langle \varphi_3 \rangle - \int_{3,4} \Gamma_{1,34}^{(1,1)} \left( \langle \varphi_3 \varphi_4 \rangle - G_{34} \right),\end{aligned}\quad (2.81)$$

and thus:

$$\int_3 \left[ \Gamma_{13}^{(2,0)} - 2\Gamma_{13}^{(0,1)} \right] \langle \varphi_3 \rangle + \int_{3,4} \Gamma_{1,34}^{(1,1)} \left( \langle \varphi_3 \varphi_4 \rangle - G_{34} \right) = 0. \quad (2.82)$$

We can also take a derivative of Eq.(2.78) to obtain:

$$\int_3 \Gamma_{3,12}^{(1,1)} \langle \varphi_3 \rangle + \int_{3,4} \Gamma_{12,34}^{(0,2)} \left( \langle \varphi_3 \varphi_4 \rangle - G_{34} \right) = 0. \quad (2.83)$$

We can combine these two last results in a matricial product:

$$\int_{3,4} \begin{pmatrix} \Gamma_{13}^{(2,0)} - 2\Gamma_{13}^{(0,1)} & \Gamma_{1,34}^{(1,1)} \\ \Gamma_{3,12}^{(1,1)} & \Gamma_{12,34}^{(0,2)} \end{pmatrix} \begin{pmatrix} \langle \varphi_3 \rangle \delta_{3,4} \\ \langle \varphi_3 \varphi_4 \rangle - G_{34} \end{pmatrix} = 0. \quad (2.84)$$

If the left hand matrix is non singular, the solution of this system is:

$$\begin{cases} \langle \varphi_1 \rangle = 0, \\ \langle \varphi_1 \varphi_2 \rangle = G_{12}. \end{cases} \quad (2.85)$$

To see that the left matrix is non-singular, we can re-express it in function of the sources to obtain:

$$\begin{pmatrix} \Gamma_{13}^{(2,0)} - 2\Gamma_{13}^{(0,1)} & \Gamma_{1,34}^{(1,1)} \\ \Gamma_{3,12}^{(1,1)} & \Gamma_{12,34}^{(0,2)} \end{pmatrix} = \begin{pmatrix} \frac{\delta J_1^*}{\delta \phi_3} + \int_{1'} \phi_{1'} \frac{\delta K_{11'}^*}{\delta \phi_2} & \frac{1}{2} \frac{\delta K_{34}^*}{\delta \phi_1} \\ \frac{1}{2} \frac{\delta K_{12}^*}{\delta \phi_3} & \frac{1}{2} \frac{\delta K_{12}^*}{\delta G_{34}} \end{pmatrix}. \quad (2.86)$$

In order for the double Legendre transform to exist, the relationship between  $(J^*, K^*)$  and  $(\phi, G)$  must be monotonous, thus the matrix above is positive definite, and thus invertible, which proves the result.

### Loop expansion of the 2PI effective action

Following the systematic expansion of the 1PI effective action, we again introduce an expansion parameter  $\lambda$ . We define thus:

$$\begin{aligned}Z[J, K] &= \int \mathcal{D}\varphi e^{-\frac{1}{\lambda} [S[\varphi] - \int_1 J_1 \varphi_1 - \frac{1}{2} \int_{12} K_{12} \varphi_1 \varphi_2]}, \\ W[J, K] &= \lambda \ln Z[J, K].\end{aligned}\quad (2.87)$$

Note that this modifies the definition of the propagator:

$$G_{12} \equiv \frac{\langle \varphi_1 \varphi_2 \rangle - \langle \varphi_1 \rangle \langle \varphi_2 \rangle}{\lambda}, \quad (2.88)$$

and thus that of the Legendre transform:

$$\left\{ \begin{array}{l} \Gamma_2[\phi, G] = \int_1 J_1^*[\phi, G] \phi_1 + \frac{1}{2} \int_{12} K_{12}^*[\phi, G] \left( \phi_1 \phi_2 + \lambda G_{12} \right) - W[J^*[\phi, G], K^*[\phi, G]] , \\ J^* \text{ and } K^* \text{ such that } \left. \frac{\delta W[J, K]}{\delta J_1} \right|_{J^*, K^*} = \phi_1 \text{ and } \left. \frac{\delta W[J, K]}{\delta K_{12}} \right|_{J^*, K^*} = \frac{1}{2} \left( \phi_1 \phi_2 + \lambda G_{12} \right) . \end{array} \right. \quad (2.89)$$

At lowest order in  $\lambda$ , we get again the saddle equation:

$$\left\{ \begin{array}{l} W[J, K] = -S[\varphi^*[J, K]] + \int_1 J_1 \varphi_1^*[J, K] + \frac{1}{2} \int_{12} \varphi_1^*[J, K] K_{12} \varphi_2^*[J, K] , \\ \varphi^*[J, K] \text{ such that } \left. \frac{\delta S[\varphi]}{\delta \varphi_1} \right|_{\varphi^*} = J_1 + \int_2 K_{12} \varphi_2^*[J, K] . \end{array} \right. \quad (2.90)$$

Performing the Legendre transformation lead us again to:

$$\Gamma_2[\phi, G] = S[\phi] + \mathcal{O}(\lambda) . \quad (2.91)$$

The lowest order functional is independant from the propagator, thus we are forced to explicitly evaluate the next order in order to get the lowest order dependance on  $G$ .

In order to do this we expand the free-energy around the saddle point (we omit the dependance of  $\varphi^*$  on the sources for compactness):

$$\begin{aligned} W[J, K] = & -S[\varphi^*] + \int_1 J_1 \varphi_1^* + \frac{1}{2} \int_{12} K_{12} \varphi_1^* \varphi_2^* \\ & + \lambda \ln \int \mathcal{D}\varphi \exp \left( -\frac{1}{2} \int_{12} \frac{S_{12}^{(2)}[\varphi^*] - K_{12}}{\lambda} \varphi_1 \varphi_2 - \frac{S_{\text{ng}}[\varphi^*; \varphi]}{\lambda} \right) \end{aligned} \quad (2.92)$$

We perform again the change of variables:

$$\varphi \rightarrow \sqrt{\lambda} \bar{\varphi} , \quad (2.93)$$

to get:

$$\begin{aligned} W[J, K] = & \text{Cte} - S[\varphi^*] + \int_1 J_1 \varphi_1^* + \frac{1}{2} \int_{12} K_{12} \varphi_1^* \varphi_2^* \\ & + \lambda \ln \int \mathcal{D}\varphi \exp \left( -\frac{1}{2} \int_{12} \left[ S_{12}^{(2)}[\varphi^*] - K_{12} \right] \varphi_1 \varphi_2 - \frac{S_{\text{ng}}[\varphi^*; \sqrt{\lambda} \varphi]}{\lambda} \right) . \end{aligned} \quad (2.94)$$

At first order we can neglect the contribution from the non-Gaussian part of the action and , and we end up with a Gaussian integral, which gives:

$$W[J, K] = \text{Cte} - S[\varphi^*] + \int_1 J_1 \varphi_1^* + \frac{1}{2} \int_{12} K_{12} \varphi_1^* \varphi_2^* - \frac{\lambda}{2} \int_{12} \ln \left( S_{12}^{(2)}[\varphi^*] - K_{12} \right) + \mathcal{O}(\lambda^2) . \quad (2.95)$$

The derivatives of  $W$  with respect to the sources are now:

$$\left\{ \begin{array}{l} \frac{\delta W[J, K]}{\delta J_1} = \varphi_1^* - \frac{\lambda}{2} \int_{345} \frac{\delta \varphi_5^*}{\delta J_1} S_{345}^{(3)}[\varphi^*] \left( S_{34}^{(2)}[\varphi^*] - K_{34} \right)^{-1} + \mathcal{O}(\lambda^2) , \\ \frac{\delta W[J, K]}{\delta K_{12}} = \frac{1}{2} \varphi_1^* \varphi_2^* + \frac{\lambda}{2} \left( S_{12}^{(2)}[\varphi^*] - K_{12} \right)^{-1} \\ \qquad \qquad \qquad - \frac{\lambda}{2} \int_{345} \frac{\delta \varphi_5^*}{\delta K_{12}} S_{345}^{(3)}[\varphi^*] \left( S_{34}^{(2)}[\varphi^*] - K_{34} \right)^{-1} + \mathcal{O}(\lambda^2) . \end{array} \right. \quad (2.96)$$

We also have the equation defining  $\varphi^*$ :

$$S_1^{(1)}[\varphi^*[J, K]] = J_1 + \int_2 K_{12} \varphi_2^*[J, K], \quad (2.97)$$

which lead us to equations on the derivatives of  $\varphi^*$ :

$$\left\{ \begin{array}{l} \frac{\delta \varphi_1^*[J, K]}{\delta K_{23}} = \frac{\left( S_{13}^{(2)}[\varphi^*[J, K]] - K_{13} \right)^{-1} \varphi_2^*[J, K] + \left( S_{12}^{(2)}[\varphi^*[J, K]] - K_{12} \right)^{-1} \varphi_3^*[J, K]}{2}, \\ \frac{\delta \varphi_1^*[J, K]}{\delta J_2} = \left( S_{12}^{(2)}[\varphi^*[J, K]] - K_{12} \right)^{-1}. \end{array} \right. \quad (2.98)$$

We can reinsert these into the derivatives of the free-energy in Eq.(2.96) to get their final expressions, that are entirely parametrized by  $J, K$  and  $\varphi^*$  (we omit the dependance of  $\varphi^*$  on  $J^*[\phi, G]$  and  $K^*[\phi, G]$  for compactness):

$$\left\{ \begin{array}{l} \frac{\delta W[J, K]}{\delta J_1} = \varphi^* - \frac{\lambda}{2} \int_{345} \left( S_{15}^{(2)}[\varphi^*] - K_{15} \right)^{-1} S_{345}^{(3)}[\varphi^*] \left( S_{34}^{(2)}[\varphi^*] - K_{34} \right)^{-1}, \\ \frac{\delta W[J, K]}{\delta K_{12}} = \frac{1}{2} \varphi_1^* \varphi_2^* + \frac{\lambda}{2} \left( S_{12}^{(2)}[\varphi^*] - K_{12} \right)^{-1} \\ \quad - \frac{\lambda}{4} \int_{345} \left( S_{34}^{(2)}[\varphi^*] - K_{34} \right)^{-1} S_{345}^{(3)}[\varphi^*] \left[ \varphi_2^* \left( S_{15}^{(2)}[\varphi^*] - K_{15} \right)^{-1} + \varphi_1^* \left( S_{25}^{(2)}[\varphi^*] - K_{25} \right)^{-1} \right]. \end{array} \right. \quad (2.99)$$

We can now evaluate these two equations at  $J^*[\phi, G]$  and  $K^*[\phi, G]$ . We know that at lowest order  $\varphi^*$  coincides with  $\phi$ . Thus in all first order terms, we can replace  $\varphi^*[J^*, K^*]$  by  $\phi$ . By definition of  $J^*$ , the left hand side of the first equation of Eq.(2.99) is  $\phi$ . This leads to the first order correction to the relation between  $\varphi^*$  and  $\phi$ :

$$\varphi_1^*[J^*, K^*] = \phi_1 + \frac{\lambda}{2} \int_{345} \left( S_{25}^{(2)}[\phi] - K_{25}^* \right)^{-1} S_{345}^{(3)}[\phi] \left( S_{34}^{(2)}[\phi] - K_{34}^* \right)^{-1} + \mathcal{O}(\lambda^2). \quad (2.100)$$

The second equation of Eq.(2.99), when evaluated at  $J^*$  and  $K^*$  must give

$$\frac{1}{2} \left( \phi_1 \phi_2 + \lambda G_{12} \right) \quad (2.101)$$

by definition. Replacing  $\varphi^*$  by its estimation at first order in  $\lambda$ , we see that the complex terms cancels and we get a simple equation on  $K^*$  alone, which finally gives the desired value of  $K^*$  at lowest order:

$$K_{12}^*[\phi, G] = S_{12}^{(2)}[\phi] - G_{12}^{-1} + \mathcal{O}(\lambda). \quad (2.102)$$

We evaluate now effective action:

$$\begin{aligned} \Gamma_2[\phi, G] &= \text{Cte} + S[\varphi^*] + \int_1 J_1^* (\phi_1 - \varphi_1^*) + \frac{1}{2} \int_{12} K_{12}^* (\phi_1 \phi_2 + \lambda G_{12} - \varphi_1^* \varphi_2^*) \\ &\quad + \frac{\lambda}{2} \int_{12} \ln(G_{12}^{-1}) + \mathcal{O}(\lambda^2). \end{aligned} \quad (2.103)$$

Expanding the action around  $\phi$ , and using the fact that  $\varphi^* - \phi$  is  $\mathcal{O}(\lambda)$ , we obtain:

$$\begin{aligned} \Gamma_2[\phi, G] &= \text{Cte} + S[\phi] + \int_1 \left( S_1^{(1)}[\phi] - J_1^* \right) (\varphi_1^* - \phi_1) - \int_{12} K_{12}^* (\varphi_1^* - \phi_1) \phi_2 \\ &\quad + \frac{\lambda}{2} \int_{12} \ln(G_{12}^{-1}) + \frac{\lambda}{2} \int_{12} K_{12}^* G_{12} + \mathcal{O}(\lambda^2). \end{aligned} \quad (2.104)$$



We know that:

$$J_1^*[\phi, G] = \frac{\delta \Gamma_2[\phi, G]}{\delta \phi_1} - \int_2 K_{12}^*[\phi, G] \phi_2 . \quad (2.105)$$

Thus at lowest order we have:

$$J_1^*[\phi, G] = S_1^{(1)}[\phi] - \int_2 K_{12}^* \phi_2 + \mathcal{O}(\lambda) . \quad (2.106)$$

Reinserting this in Eq.(2.103), along with the lowest order values of  $J^*$  and  $K^*$ , we obtain the final result:

$$\Gamma_2[\phi, G] = \text{Cte} + S[\phi] + \frac{\lambda}{2} \int_{12} \left( S_{12}^{(2)}[\phi] - G_{12}^{-1} \right) G_{12} + \frac{\lambda}{2} \int_{1,2} \ln(G_{12}^{-1}) + \mathcal{O}(\lambda^2) . \quad (2.107)$$

Evaluating at  $\lambda = 1$  we obtain the standard expression of the 2PI functional:

$$\Gamma_2[\phi, G] = \text{Cte} + S[\phi] + \frac{1}{2} \int_{12} \left( S_{12}^{(2)}[\phi] - G_{12}^{-1} \right) G_{12} + \frac{1}{2} \int_{1,2} \ln(G_{12}^{-1}) + \Phi[\phi, G] , \quad (2.108)$$

where  $\Phi$  is a sum of diagrams, with propagators  $G$ , average field 0, vertices  $S^{(N)}[\phi]$ , and that are two-particle irreducible, meaning that they do not become disconnected when we cut two of their  $G$  lines. They are thus called 2PI diagrams. The  $\Phi$  functional is sometimes called the Luttinger-Ward functional [109, 143]. The proof that the diagrams are 2PI is much more tedious than in the 1PI case, and can be found in [47]. Note that the term  $G^{-1}G$  has zero derivative with respect to  $G$ , and thus must be considered as a constant for all practical means. For translationally invariant systems it is the integral over the reciprocal space of 1:

$$\int_{12} G_{12}^{-1} G_{12} = V \int_r G(r) G^{-1}(r) = V \int_k G(k) G^{-1}(k) = V \int_k 1 . \quad (2.109)$$

We can evaluate the lowest order values of the two sources (we have already found the value of  $K^*$  but not that of  $J^*$ ):

$$\left\{ \begin{array}{l} K_{12}^*[\phi, G] = S_{12}^{(2)}[\phi] - G_{12}^{-1} + \mathcal{O}(\lambda) , \\ J_1^*[\phi, G] = S_1^{(1)}[\phi] - \int_2 G_{12}^{-1} \phi_2 + \mathcal{O}(\lambda) . \end{array} \right. \quad (2.110)$$

This can be used to evaluate the diagrams contributing to the next order. This clearly shows the role of the source terms:  $K$  replaces the bare propagator by the full one, while  $J$  gets rid of the 2PR diagrams.

To continue with our example, after this Legendre transformation, Eq.(2.111) becomes:

$$\begin{aligned} \Gamma_2[\phi, G] = & \text{Cte} + S[\phi] + \frac{1}{2} \int_{12} \left( S_{12}^{(2)}[\phi] - G_{12}^{-1} \right) G_{12} + \frac{1}{2} \int_{1,2} \ln(G_{12}^{-1}) \\ & + g_4 \text{ (diagram)} + g_3^2 \text{ (diagram)} - g_4^2 \text{ (diagram)} + \dots , \end{aligned} \quad (2.111)$$

The lines of these diagrams are now the full propagators  $G$ .

### Variational principle and inverse Legendre transformation

Equivalently to Eq.(2.66) we have as a consequence of the Legendre transformation:

$$\frac{\delta \Gamma_2[\phi, G]}{\delta G_{12}} = \frac{1}{2} K_{12}^*[\phi, G] \quad (2.112)$$

As in the 1PI case, this equation can be seen as a variational principle that we can use to obtain self-consistent equations on the propagator. Performing the inverse Legendre transformation is done by setting the source to its original value, i.e. 0, which means that the physical propagator extremalizes the 2PI functional.

Now the variational principle in Eq.(2.112) becomes:

$$0 = S_{12}^{(2)}[\phi] - G_{12}^{-1} + 2 \frac{\delta\Phi[\phi, G]}{\delta G_{12}} . \quad (2.113)$$

Thus we obtain an equation for the self-energy, under the form of a self-consistent equation:

$$\Sigma_{12}[\phi, G] \equiv \left( G_{12}^{(0)}[\phi, G] \right)^{-1} - G_{12}^{-1} = 2 \frac{\delta\Phi[\phi, G]}{\delta G_{12}} . \quad (2.114)$$

In order to perform approximations on the correlation function, the program is then:

- Choose an approximate starting point for the expansion of  $\ln Z$ .
- Write down the corresponding diagrammatic expansion.
- Perform the double Legendre transform to reduce diagrams.
- Truncate the expansion by selecting a class of diagrams and obtain an approximation of  $\Gamma_2[\phi, G]$ .
- Use the variational principles Eq.(2.112) to obtain a self consistent equation on  $G$ .
- Evaluate the approximate functional  $\Gamma_2$  at these particular values of  $\phi$  and  $G$  to get  $\ln Z$ .

A crucial property of these truncation schemes is that if the Gaussian part and the non-Gaussian part of the action are separately invariant under a linear symmetry, then the deduced self-consistent equations for the propagator will also possess this symmetry [3]. If the non-Gaussian action is invariant, and if the diagrams are evaluated at the physical propagator, which respects this invariance, then automatically all the 2PI diagrams will also be invariant, and so will be  $\Sigma$ , whatever the chosen truncation of the diagrammatic series. This is true only for a linear symmetry, for which the consequences on the propagators are simply relations between them, that can be enforced when evaluating the diagrams, whereas for a non-linear symmetry, the propagators must satisfy relations that involve higher-order correlation functions, and building a consistent expansion would then require to keep a possibly infinite number of terms in the expansion.

We will exploit this property of the 2PI expansions in Chapter 3 in order to build self-consistent equations for the non-ergodicity parameter that preserves the time-reversal.

## 2.2 Theory of liquids

We review here the equivalent of the discussion above for the case of equilibrium liquid theory. In that case, the starting point for systematic expansions is chosen to be the ideal gas, and thus the diagrammatic formulation is different from that presented above. However, the idea is still to perform a double Legendre transform to obtain a functional of both mean-field and propagator. This leads to the standard hyper-netted chain approximation, which we will use in the following chapters of this manuscript, and provides the basis for the replica formulation of Chapter 4.

We consider spherical particles of diameter  $\sigma$ , the center of which is located at position  $x_i$  in a 3-dimensional space. The particles interact via a pair potential  $v$ , have a chemical potential  $\mu$  and are

placed in an external field  $\Psi$ . Finally the system is in contact with a thermal bath at temperature  $T$ , and can exchange particles with a particle reservoir, so that the probability  $P_N$  of observing  $N$  particles located at  $x_1, \dots, x_N$  is given by the following Boltzmann weight:

$$P_N[x_1, \dots, x_N] = e^{-\beta \sum_{i < j} v(x_i - x_j) + \sum_{j=1}^N (\beta\mu - \beta\Psi(x_j))}, \quad (2.115)$$

where  $\beta$  is the inverse temperature  $1/k_B T$ ,  $k_B$  is the Boltzmann constant. We will be interested in computing the microscopic density defined in Eq.(1.4) and its cumulants. For simplicity in the following, three-dimensional space coordinates will be replaced by numerical subscripts, we gather the chemical potential and external field in a single field  $\nu$ , and we define a dimensionless potential  $w$ :

$$\nu_1 = \beta\mu - \beta\Psi_1, \quad (2.116)$$

$$w_1 = -\beta v_1. \quad (2.117)$$

Note that we will most of the time stick to the notation  $w$  in the rest of the manuscript.

The probability  $P_N$  can be rewritten in terms of these quantities as:

$$P_N[\hat{\rho}, \nu] = e^{\frac{1}{2} w_{12} (\hat{\rho}_1 \hat{\rho}_2 - \hat{\rho}_1 \delta_{12}) + \nu_1 \hat{\rho}_1}, \quad (2.118)$$

so that the equivalent of the action  $S$  in the previous section is the potential term  $\frac{1}{2} w_{12} (\hat{\rho}_1 \hat{\rho}_2 - \hat{\rho}_1 \delta_{12})$ , the field  $\varphi$  is replaced by  $\hat{\rho}$  and the field  $J$  is replaced by  $\nu$ .

Finally the partition function is obtained by summing over all possible configurations, i.e. summing over the number of particles  $N$  and integrating over all variables  $x_i$ :

$$\begin{aligned} Z[\nu, w] &= \text{Tr} e^{\frac{1}{2} w_{12} (\hat{\rho}_1 \hat{\rho}_2 - \hat{\rho}_1 \delta_{12}) + \nu_1 \hat{\rho}_1}, \\ W[\nu, w] &= \ln Z[\nu, w]. \end{aligned} \quad (2.119)$$

where  $\text{Tr}$  must now be understood as  $\sum_{N=0}^{\infty} \frac{1}{N!} \int dx_1 \dots dx_N$ .

Although it may seem redundant, it will prove useful in the following to consider that the Boltzmann weight is a functional of two fields,  $\hat{\rho}$  and  $\hat{\rho}^{(2)}$ , with  $\hat{\rho}^{(2)}$  defined as:

$$\hat{\rho}^{(2)} = \hat{\rho}_1 \hat{\rho}_2 - \hat{\rho}_1 \delta_{12}. \quad (2.120)$$

This gives:

$$Z[\nu, w] = \text{Tr} e^{\frac{1}{2} w_{12} \hat{\rho}_1^{(2)} + \nu_1 \hat{\rho}_1}. \quad (2.121)$$

Since  $\nu$  is the field conjugated to  $\hat{\rho}$ ,  $W[\nu]$  is the generating functional of the cumulants of the density, defined in the same way as in Eqs.(2.6–2.10):

$$\rho_1 \equiv \frac{\delta W[\nu, w]}{\delta \nu_1}, \quad (2.122)$$

and the propagator and third order cumulant are defined as in the previous section. More interestingly,  $w$  is coupled to the function  $\hat{\rho}^{(2)}$ :

$$\frac{\delta W[\nu, w]}{\delta w_{12}} = \frac{1}{2} \rho_{12}^{(2)} \equiv \frac{1}{2} \langle \hat{\rho}_{12}^{(2)} \rangle. \quad (2.123)$$

The correlation function  $\rho^{(2)}$  is called the two-point density. From this correlation function we simply recover the radial distribution function  $g$  and the pair correlation function  $h$ :

$$g_{12} = \frac{\rho_{12}^{(2)}}{\rho_1 \rho_2}, \quad (2.124)$$

$$h_{12} = g_{12} - 1. \quad (2.125)$$

The advantage of the pair correlation function  $h$  over  $g$  is that it is a clustering function: it decays to zero at large separation between 1 and 2. Since  $\hat{\rho}^{(2)} = \hat{\rho}_1 \hat{\rho}_2 - \hat{\rho}_1 \delta_{12}$ , the three functions are related to the propagator  $G$  of the theory:

$$G_{12} = \langle \hat{\rho}_1 \hat{\rho}_2 \rangle - \rho_1 \rho_2, \quad (2.126)$$

$$\rho_{12}^{(2)} = G_{12} + \rho_1 \rho_2 - \rho_1 \delta_{12}, \quad (2.127)$$

$$g_{12} = \frac{G_{12}}{\rho_1 \rho_2} - \frac{1}{\rho_1} \delta_{12} + 1, \quad (2.128)$$

$$h_{12} = \frac{G_{12}}{\rho_1 \rho_2} - \frac{1}{\rho_1} \delta_{12}. \quad (2.129)$$

Finally, for homogeneous liquids, the structure factor of Eq.(1.6) is related to the Fourier transform of  $h$  by:

$$S_k = 1 + \rho h_k = \frac{1}{\rho} G_k. \quad (2.130)$$

Note that the structure factor is sometimes defined as  $1 + \rho g_k$ , the difference between the two definitions being a delta function at  $k = 0$ . This term represents the unscattered light in a light diffusion experiment, and is most of the times eliminated by looking at the transmitted light under a small angle.

In the same way than in the field-theoretic case, we also define the first Legendre transform of the free-energy (note the difference in the choice of sign):

$$\left\{ \begin{array}{l} \Gamma_1[\rho, w] = \ln Z[\nu^*[\rho], w] - \int_1 \nu_1^*[\rho] \rho_1, \\ \nu^*[\rho] \text{ such that } \left. \frac{\delta \ln Z[\nu, w]}{\delta \nu_1} \right|_{\nu^*} = \rho_1, \end{array} \right. \quad (2.131)$$

As well as the second Legendre transform:

$$\left\{ \begin{array}{l} \Gamma_2[\rho, \rho^{(2)}] = \Gamma_1[\rho, w^*[\rho, \rho^{(2)}]] - \frac{1}{2} \int_{12} w_{12}^*[\rho, \rho^{(2)}] \rho_{12}^{(2)}, \\ w^*[\rho, \rho^{(2)}] \text{ such that } \left. \frac{\delta \ln Z[\nu, w]}{\delta w_{12}} \right|_{w^*} = \frac{1}{2} \rho_{12}^{(2)}. \end{array} \right. \quad (2.132)$$

Although it is fully equivalent, we will see that in the case of liquid theory, it is simpler to perform the two Legendre transformations successively.

### 2.2.1 The case of the ideal gas

In the case  $v = 0$ , the partition function simplifies into:

$$\begin{aligned} Z[\nu, w = 0] &= \sum_{N=0}^{\infty} \frac{1}{N!} \int_{1, \dots, N} e^{\sum_{i=1}^N \nu_i} = \sum_{N=0}^{\infty} \frac{1}{N!} \left( \int_1 e^{\nu_1} \right)^N \\ &= \exp \left( \int_1 e^{\nu_1} \right). \end{aligned} \quad (2.133)$$

Note that we have thus  $Z[\nu = 0, w = 0] = e^V$ , which is a diverging normalization constant in the thermodynamic limit. Which leads to:

$$W[\nu, w = 0] = \int_1 e^{\nu_1}. \quad (2.134)$$

We can thus calculate the density at fixed chemical potential and external field:

$$\rho_1[\nu, w = 0] = e^{\nu_1}, \quad (2.135)$$

and inverting this relation we find that the value of  $\nu$  that fixes  $\rho_1$  as density is:

$$\nu_1^*[\rho] = \ln \rho_1. \quad (2.136)$$

This allows to perform the Legendre transform of  $W[\nu, w = 0]$  with respect to  $\nu$  to get:

$$\begin{aligned} \Gamma_1[\rho, w = 0] &= W[\nu^*[\rho]] - \int_1 \rho_1 \nu_1^*[\rho] = \int_1 e^{\ln \rho_1} - \int_1 \rho_1 \ln \rho_1 \\ &= \int_1 \rho_1 [1 - \ln \rho_1], \end{aligned} \quad (2.137)$$

which is the expected ideal gas term in the free-energy. We can also calculate the different two-point functions defined above:

$$G_{12}[\nu, w = 0] = e^{\nu_1} \delta_{12}, \quad (2.138)$$

$$\rho_{12}^{(2)}[\nu, w = 0] = e^{\nu_1} e^{\nu_2}, \quad (2.139)$$

$$g_{12}[\nu, w = 0] = 1, \quad (2.140)$$

$$h_{12}[\nu, w = 0] = 0, \quad (2.141)$$

and the derivatives of the functional  $\Gamma$  to get:

$$\Gamma_1^{(1)}[\rho, w = 0] = -\ln \rho_1, \quad (2.142)$$

$$\Gamma_{1\dots n}^{(n)}[\rho, w = 0] = -\frac{(-1)^n}{(n-1)\rho_1^{n-1}} \prod_{i=2}^n \delta_{1i}. \quad (2.143)$$

We also see that the correlation functions defined by successive functional differentiation with respect to  $\rho$  are non-zero at every order, which leads to define the non-ideal gas part of these correlation functions, that are called the direct correlation functions in liquid theory:

$$c_{1\dots n}^{(n)}[\rho, w] \equiv \frac{\delta [\Gamma[\rho, w] - \Gamma[\rho, w = 0]]}{\delta \rho_1 \cdots \delta \rho_n} = \Gamma_{1\dots n}^{(n)}[\rho, w] + \frac{(-1)^n}{(n-1)\rho_1^{n-1}} \prod_{i=2}^n \delta_{1i} \quad (2.144)$$

In the same way, we can compute the higher-order correlation functions of the density by successive differentiation, and we obtain:

$$W_{1\dots n}^{(n)}[\nu, w = 0] = e^{\nu_1} \prod_{i=2}^n \delta_{1i} \quad (2.145)$$

This shows that the ideal gas, as simple as it may appear, is a highly non-gaussian theory: it has non-vanishing cumulants at all order. An expansion around the ideal gas is thus bound to have a very different structure than an expansion around a Gaussian theory, as we did in the previous section, and we can not blindly use this approach. However, the procedure of diagrammatic reduction by successive Legendre transformation is still useful in order to obtain a microscopic theory in terms of the order parameter of the transition that we are interested in: in our case it is the correlations of the density.



The ideal gas partition function is reduced to the single dot at the beginning of the expansion. For the moment,  $\ln Z$  is a functional of both  $\nu$  and  $w$ , though only indirectly via  $z = e^\nu$  and  $f = e^w - 1$ .

### First Legendre transform via an expansion in powers of $f$

To perform the first Legendre transform defined in Eq.(2.131), we will use the  $f$  lines as an organizing device for the diagrammatic series we will be using. We will show the result to first orders, then generalize the result to all orders in  $f$ . At third order in  $f$  we have:

$$\ln Z = \bullet + \bullet\text{---}\bullet + \begin{array}{c} \bullet \\ / \quad \backslash \\ \bullet \quad \bullet \end{array} + \begin{array}{c} \bullet \\ / \quad \backslash \\ \bullet \quad \bullet \\ / \quad \backslash \\ \bullet \quad \bullet \end{array} + \begin{array}{c} \bullet\text{---}\bullet \\ | \quad | \\ \bullet\text{---}\bullet \end{array} + \begin{array}{c} \bullet\text{---}\bullet \\ / \quad \backslash \\ \bullet \quad \bullet \\ | \quad | \\ \bullet \quad \bullet \end{array} + \mathcal{O}(f^4). \quad (2.150)$$

We can evaluate the density by differentiating with respect to  $\nu$ , or in a simpler way with respect to  $z$ :

$$\rho_1 = \frac{\delta \ln Z}{\delta \nu_1} = \int_3 \frac{\delta z_3}{\delta \nu_1} \frac{\delta \ln Z}{\delta z_3} = z_1 \frac{\delta \ln Z}{\delta z_1}. \quad (2.151)$$

Diagrammatically differentiating with respect to  $z_1$  amounts to replace one black dot by a white dot labeled by 1 (which is just an unintegrated constant weight equal to 1). We thus find:

$$\frac{\rho_1}{z_1} = 1 + \begin{array}{c} \circ\text{---}\bullet \\ 1 \end{array} + \begin{array}{c} \bullet \\ / \quad \backslash \\ \circ \quad \bullet \\ 1 \end{array} + \begin{array}{c} \bullet \\ / \quad \backslash \\ \circ \quad \bullet \\ 1 \end{array} + \begin{array}{c} \bullet \\ / \quad \backslash \\ \circ \quad \bullet \\ 1 \end{array} + \begin{array}{c} \bullet\text{---}\bullet \\ | \quad | \\ \circ\text{---}\bullet \\ 1 \end{array} + \begin{array}{c} \bullet\text{---}\bullet \\ / \quad \backslash \\ \circ \quad \bullet \\ | \quad | \\ \bullet \quad \bullet \\ 1 \end{array} + \begin{array}{c} \bullet\text{---}\bullet \\ / \quad \backslash \\ \circ \quad \bullet \\ | \quad | \\ \bullet \quad \bullet \\ 1 \end{array} + \begin{array}{c} \bullet\text{---}\bullet \\ / \quad \backslash \\ \circ \quad \bullet \\ | \quad | \\ \bullet \quad \bullet \\ 1 \end{array} + \mathcal{O}(f^4). \quad (2.152)$$

Our strategy to compute the Legendre transform will be to find a diagrammatic expression of  $\nu^*[\rho]$ , which we know is by definition (minus) the first derivative of the  $\Gamma_1$  functional, then integrate this expression with respect to density to obtain the result.

In order to obtain an expression for  $\nu$ , we have to take the logarithm of  $z$ . Taking the logarithm of Eq.(2.152) will suppress the diagrams in which the white circle is an articulation circle, since such diagrams are product of simpler subdiagrams. We will thus obtain:

$$\ln\left(\frac{\rho_1}{z_1}\right) = \begin{array}{c} \circ\text{---}\bullet \\ 1 \end{array} + \begin{array}{c} \bullet \\ / \quad \backslash \\ \circ \quad \bullet \\ 1 \end{array} + \begin{array}{c} \bullet \\ / \quad \backslash \\ \circ \quad \bullet \\ 1 \end{array} + \begin{array}{c} \bullet\text{---}\bullet \\ | \quad | \\ \circ\text{---}\bullet \\ 1 \end{array} + \begin{array}{c} \bullet\text{---}\bullet \\ / \quad \backslash \\ \circ \quad \bullet \\ | \quad | \\ \bullet \quad \bullet \\ 1 \end{array} + \mathcal{O}(f^4). \quad (2.153)$$

We put together the two results:

$$\left\{ \begin{array}{l} \nu_1 = \ln \rho_1[\nu] - \begin{array}{c} \circ\text{---}\bullet \\ 1 \end{array} - \begin{array}{c} \bullet \\ / \quad \backslash \\ \circ \quad \bullet \\ 1 \end{array} - \begin{array}{c} \bullet \\ / \quad \backslash \\ \circ \quad \bullet \\ 1 \end{array} - \begin{array}{c} \bullet\text{---}\bullet \\ | \quad | \\ \circ\text{---}\bullet \\ 1 \end{array} - \begin{array}{c} \bullet\text{---}\bullet \\ / \quad \backslash \\ \circ \quad \bullet \\ | \quad | \\ \bullet \quad \bullet \\ 1 \end{array} + \mathcal{O}(f^4), \\ z_1 = \rho_1 - \begin{array}{c} \circ\text{---}\bullet \\ 1 \end{array} - \begin{array}{c} \bullet \\ / \quad \backslash \\ \circ \quad \bullet \\ 1 \end{array} - \begin{array}{c} \bullet \\ / \quad \backslash \\ \circ \quad \bullet \\ 1 \end{array} - \begin{array}{c} \bullet\text{---}\bullet \\ | \quad | \\ \circ\text{---}\bullet \\ 1 \end{array} - \begin{array}{c} \bullet\text{---}\bullet \\ / \quad \backslash \\ \circ \quad \bullet \\ | \quad | \\ \bullet \quad \bullet \\ 1 \end{array} - \begin{array}{c} \bullet\text{---}\bullet \\ / \quad \backslash \\ \circ \quad \bullet \\ | \quad | \\ \bullet \quad \bullet \\ 1 \end{array} - \begin{array}{c} \bullet\text{---}\bullet \\ / \quad \backslash \\ \circ \quad \bullet \\ | \quad | \\ \bullet \quad \bullet \\ 1 \end{array} + \mathcal{O}(f^4). \end{array} \right. \quad (2.154)$$

Note that in the second line, white circles are weighted by  $z$ , while in the first one they are not weighted at all. We can now solve iteratively the second line in order to obtain the expression of  $z$  as a function only of density, then reinsert this expression in the expression of  $\nu$  to obtain:

$$\nu_1 = \ln \rho_1[\nu] - \begin{array}{c} \circ\text{---}\bullet \\ 1 \end{array} - \begin{array}{c} \bullet \\ / \quad \backslash \\ \circ \quad \bullet \\ 1 \end{array} + \mathcal{O}(f^4), \quad (2.155)$$

where the black dots are now  $\rho[\nu]$  functions, lines are still  $f$  functions, and white dots are constant (equal to 1) functions. We can now evaluate this equation at  $\nu^*[\rho]$ , which will have the effect to replace the black  $\rho[\nu]$  dots by  $\rho$  dots, which gives:

$$\nu_1^*[\rho] = -\frac{\delta\Gamma_1[\rho]}{\delta\rho_1} = \ln\rho_1 - \underset{1}{\circ} \bullet - \underset{1}{\circ} \triangle \bullet + \mathcal{O}(f^4) . \quad (2.156)$$

Finally integrating this with respect to density leads to the final expression of  $\Gamma_1$  (the integration constant is strictly zero as can be checked by evaluating in the ideal-gaz):

$$\Gamma_1[\rho] = \int_1 \rho_1 [1 - \ln\rho_1] + \bullet \text{---} \bullet + \underset{1}{\circ} \triangle \bullet + \mathcal{O}(f^4) . \quad (2.157)$$

This procedure can be continued at all orders in  $f$ , and one can show [115, 131] that the full Legendre transform  $\Gamma_1$  is represented by the sum of all unlabeled, connected diagrams with  $\rho$  nodes and  $f$  lines, that are free of articulation circles, i.e. circles that cut the diagrams in two separate parts when removed. This can easily be checked order by order, or by iteration, but the complete proof is more tedious. Thus we obtain the result:

$$\Gamma_1[\rho] = \int_1 \rho_1 [1 - \ln\rho_1] + \bullet \text{---} \bullet + \underset{1}{\circ} \triangle \bullet + \begin{array}{c} \bullet \text{---} \bullet \\ | \quad | \\ \bullet \text{---} \bullet \end{array} + \begin{array}{c} \bullet \text{---} \bullet \\ / \quad \backslash \\ \bullet \text{---} \bullet \end{array} + \begin{array}{c} \bullet \text{---} \bullet \\ / \quad \backslash \\ \bullet \text{---} \bullet \\ / \quad \backslash \\ \bullet \text{---} \bullet \end{array} + \dots \quad (2.158)$$

This is the so-called virial expansion of liquid theory. The diagrams carry  $\rho$  nodes and  $f$  lines. They are all the connected 1-irreducible diagrams, i.e. that do not disconnect upon removal of a node.

In the same way than the previous section, if we want to obtain approximations for two-point functions, we would have to perform another Legendre transform, this time with respect to  $w$ .

### 2.2.3 Second Legendre transform: Morita & Hiroike functional

We now want to perform another Legendre transformation, this time with respect to  $w$ . Before turning to this, we will define a new functional, the excess free-energy, defined as the non-ideal gaz part of  $\Gamma_1$ :

$$\Gamma_{\text{ex}}[\rho, w] = \Gamma_1[\rho, w] - \int_1 \rho_1 [1 - \ln\rho_1] . \quad (2.159)$$

Inserting the diagrammatic expression of  $\Gamma_1$  we get:

$$\Gamma_{\text{ex}}[\rho, w] = \bullet \text{---} \bullet + \underset{1}{\circ} \triangle \bullet + \begin{array}{c} \bullet \text{---} \bullet \\ | \quad | \\ \bullet \text{---} \bullet \end{array} + \begin{array}{c} \bullet \text{---} \bullet \\ / \quad \backslash \\ \bullet \text{---} \bullet \end{array} + \begin{array}{c} \bullet \text{---} \bullet \\ / \quad \backslash \\ \bullet \text{---} \bullet \\ / \quad \backslash \\ \bullet \text{---} \bullet \end{array} + \dots . \quad (2.160)$$

The Legendre transform of  $\Gamma_{\text{ex}}$  with respect to  $w$  is the same as that of  $\Gamma_1$  since they differ only by a term independant of  $f$ .

We can no longer use the  $f$  lines as an organizing device for the diagrammatic expansions, since we want to Legendre transform with respect to  $w$ , but we can now use the density as an organizing device. We will thus compute everything at order 4 in density, and then present the result generalized at all orders in density.

We note first again that the dependance of  $\Gamma_{\text{ex}}$  on  $w$  is only through  $f = e^w - 1$ . We already know with Eq.(2.123) that  $w$  is coupled to the two-point density  $\rho^{(2)}$ , so if we perform a differentiation of  $\Gamma_{\text{ex}}$  with respect to  $f$  we will obtain:

$$\begin{aligned} \frac{\delta\Gamma_{\text{ex}}}{\delta f_{12}} &= \int_{34} \frac{\delta w_{34}}{\delta f_{12}} \frac{\delta\Gamma_1}{\delta w_{34}} = \int_{34} \frac{\delta \ln(1 + f_{34})}{\delta f_{12}} \frac{\delta \ln Z[\nu]}{\delta w_{34}} \Big|_{\nu^*} \\ \Leftrightarrow (1 + f_{12}) \frac{\delta\Gamma_{\text{ex}}}{\delta f_{12}} &= \frac{1}{2} \rho_{12}^{(2)} . \end{aligned} \quad (2.161)$$



Differentiating a diagram of Eq.(2.158) with respect to  $f_{12}$  amounts to erasing a line and labeling 1 and 2 the two points that were joined by this line. In every diagram, the two densities attached to the nodes 1 and 2 will factor out and give an overall factor  $\rho_1\rho_2$ . In the following an open point will be a point without a density weight whose coordinates are not integrated over. The definition of the two point density gives then [114]:

$$g_{12}[w] = \frac{\rho_{12}^{(2)}[w]}{\rho_1\rho_2} = e^{w_{12}} \left( 1 + \begin{array}{c} \bullet \\ / \quad \backslash \\ \circ_1 \quad \circ_2 \end{array} + \begin{array}{c} \bullet \quad \bullet \\ | \quad | \\ \circ_1 \quad \circ_2 \end{array} + \begin{array}{c} \bullet \quad \bullet \\ / \quad \backslash \\ \circ_1 \quad \circ_2 \end{array} + \begin{array}{c} \bullet \quad \bullet \\ \backslash \quad / \\ \circ_1 \quad \circ_2 \end{array} + \begin{array}{c} \bullet \quad \bullet \\ \backslash \quad / \\ \circ_1 \quad \circ_2 \end{array} + \begin{array}{c} \bullet \quad \bullet \\ / \quad \backslash \\ \circ_1 \quad \circ_2 \end{array} + \begin{array}{c} \bullet \quad \bullet \\ / \quad \backslash \\ \circ_1 \quad \circ_2 \end{array} \right) + \mathcal{O}(\rho^3), \quad (2.162)$$

which means that the function  $h$  behaves like  $e^w - 1 = f$  to lowest order in density. This is also an *a-posteriori* justification for the choice of  $f$  as links in the diagrammatic expansion: Legendre transforming with respect to  $w$  will have the effect of replacing  $f$  links by  $h$  functions [118], which have the good behavior for us: it cancels in the ideal gas limit and decays to zero at large separations in all cases, giving rise to well-behaved integrals.

We can now obtain a diagrammatic expression of  $w$  by taking the logarithm of Eq.(2.162). As can be seen order by order, and as expected, taking the logarithm will cancel diagrams that are the product of subdiagrams, and we obtain:

$$w_{12} = \ln(1 + h_{12}[w]) - \begin{array}{c} \bullet \\ / \quad \backslash \\ \circ_1 \quad \circ_2 \end{array} - \begin{array}{c} \bullet \quad \bullet \\ | \quad | \\ \circ_1 \quad \circ_2 \end{array} - \begin{array}{c} \bullet \quad \bullet \\ / \quad \backslash \\ \circ_1 \quad \circ_2 \end{array} - \begin{array}{c} \bullet \quad \bullet \\ \backslash \quad / \\ \circ_1 \quad \circ_2 \end{array} - \begin{array}{c} \bullet \quad \bullet \\ / \quad \backslash \\ \circ_1 \quad \circ_2 \end{array} + \mathcal{O}(\rho^3). \quad (2.163)$$

In order to replace all  $f$  lines in this expression by  $h$  lines, which will allow for the Legendre transformation, we also need the corresponding diagrammatic expansion of  $f$  as a function of  $h$ . This is obtained by iteration of Eq.(2.162), rewritten in a slightly different way:

$$f_{12} = h_{12}[w] - (1 + f_{12}) \left( \begin{array}{c} \bullet \\ / \quad \backslash \\ \circ_1 \quad \circ_2 \end{array} + \begin{array}{c} \bullet \quad \bullet \\ | \quad | \\ \circ_1 \quad \circ_2 \end{array} + \begin{array}{c} \bullet \quad \bullet \\ / \quad \backslash \\ \circ_1 \quad \circ_2 \end{array} + \begin{array}{c} \bullet \quad \bullet \\ \backslash \quad / \\ \circ_1 \quad \circ_2 \end{array} + \begin{array}{c} \bullet \quad \bullet \\ / \quad \backslash \\ \circ_1 \quad \circ_2 \end{array} + \begin{array}{c} \bullet \quad \bullet \\ \backslash \quad / \\ \circ_1 \quad \circ_2 \end{array} \right) + \mathcal{O}(\rho^3) \quad (2.164)$$

We can solve this iteratively in order to obtain  $f$  as a function of  $h$  only, then reinject this in the expression of  $w$  to obtain  $w$  as a function of  $h$ . Since  $f$  lines are always accompanied by at least one  $\rho$  weight, we only have to compute the first order expansion of  $f$  in order to obtain the second order expansion of  $w$ . We simply find:

$$f_{12} = h_{12}[w] - \begin{array}{c} \bullet \\ / \quad \backslash \\ \circ_1 \quad \circ_2 \end{array} - \begin{array}{c} \bullet \\ / \quad \backslash \\ \circ_1 \quad \circ_2 \end{array} + \mathcal{O}(\rho^2), \quad (2.165)$$

where the lines on the diagrams are now  $h[w]$  lines. Reinserting in the expression of  $w$ , we find:

$$w_{12} = \ln(1 + h_{12}[w]) - \begin{array}{c} \bullet \\ / \quad \backslash \\ \circ_1 \quad \circ_2 \end{array} + \begin{array}{c} \bullet \quad \bullet \\ | \quad | \\ \circ_1 \quad \circ_2 \end{array} - \begin{array}{c} \bullet \quad \bullet \\ / \quad \backslash \\ \circ_1 \quad \circ_2 \end{array} + \mathcal{O}(\rho^3). \quad (2.166)$$

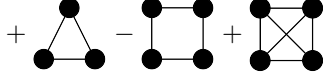
The lines on the diagrams are of course again  $h[w]$  lines. We can now evaluate this safely at  $w^*[\rho^{(2)}]$ , which will simply amount to replace the  $h[w]$  nodes by  $h$  nodes:

$$w_{12}^*[\rho^{(2)}] = \ln(1 + h_{12}) - \begin{array}{c} \bullet \\ / \quad \backslash \\ \circ_1 \quad \circ_2 \end{array} + \begin{array}{c} \bullet \quad \bullet \\ | \quad | \\ \circ_1 \quad \circ_2 \end{array} - \begin{array}{c} \bullet \quad \bullet \\ / \quad \backslash \\ \circ_1 \quad \circ_2 \end{array} + \mathcal{O}(\rho^3). \quad (2.167)$$

The lines are now  $h$  lines. To come back to the expression of the free-energy, we notice that:

$$-\frac{1}{2}w_{12}^*[\rho^{(2)}] = \frac{\delta\Gamma_2[\rho, \rho^{(2)}]}{\delta\rho_{12}^{(2)}} = \int_{34} \frac{\delta h_{34}}{\delta\rho_{12}^{(2)}} \frac{\delta\Gamma_2[\rho, \rho^{(2)}]}{\delta h_{34}} = \frac{1}{\rho_1\rho_2} \frac{\delta\Gamma_2[\rho, \rho^{(2)}]}{\delta h_{12}}. \quad (2.168)$$

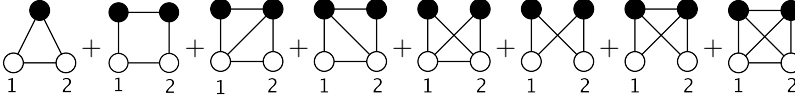
We can thus multiply Eq.(2.167) by  $\rho_1\rho_2/2$  and integrate with respect to  $h_{12}$  to get  $\Gamma_2$ :

$$\Gamma_2[\rho, \rho^{(2)}] = \int_1 \rho_1 [1 - \ln \rho_1] + \frac{1}{2} \int_{12} \rho_1\rho_2 \left[ h_{12} - (1 + h_{12}) \ln(1 + h_{12}) \right] + \text{diagrams} + \mathcal{O}(\rho^2). \quad (2.169)$$


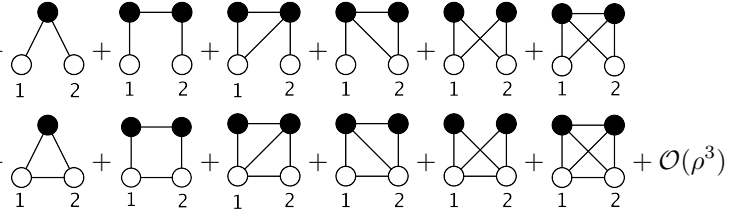
We have fixed the normalization constant by the ideal-gas case, where we must have  $\Gamma_2[\rho, h = 0]$  that coincides with the ideal gas result. Here we see that the Legendre transformation does not give rise to usual 2PI diagrams, meaning diagrams that do not separate in several parts when differentiated twice with respect to their lines: there seems to remain “ring diagrams” in addition to 2PI diagrams. This is again a consequence of the fact that we did not perform an expansion around a Gaussian theory, but around a Poissonian one. We can nonetheless get a generalization of this result to all orders in density.

### Generalization to all orders: Morita & Hiroike functional

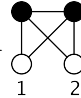
Before doing the second Legendre transformation, we can obtain the expression of the second derivative of  $\Gamma_1$  with respect to  $\rho$ , which is  $c_{12}$  by definition. It reads:

$$c_{12}[w] = f_{12} + \text{diagrams} + \mathcal{O}(\rho^3) \quad (2.170)$$


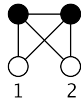
We can go back to the expression of  $h$  as a function of  $f$  to compare the two:

$$h_{12}[w] = f_{12} + \text{diagrams} + \mathcal{O}(\rho^3). \quad (2.171)$$


We see that in the expression of  $w$  in Eq.(2.163) we can recognize exactly, at this order in density, the diagrammatic expansion of  $h - c$ , with the exception of one diagram:

$$w_{12} = \ln(1 + h_{12}[w]) - h_{12}[w] + c_{12}[w] - \text{diagram} + \mathcal{O}(\rho^3). \quad (2.172)$$


Since  $f$  is  $h + \mathcal{O}(\rho)$ , we can at lowest order replace again the  $f$  lines in the diagram above by  $h$  lines, and we obtain upon evaluating at  $w^*[\rho^{(2)}]$  the expression:

$$w_{12}^*[\rho^{(2)}] = \ln(1 + h_{12}) - h_{12} + c_{12}[w^*[\rho^{(2)}]] - \text{diagram} + \mathcal{O}(\rho^3). \quad (2.173)$$


The lines in the diagram above are now  $h$  lines. Morita & Hiroike [131] have shown that to all orders in density, this property is still true, i.e. that we have:

$$w_{12}^*[\rho^{(2)}] = \ln(1 + h_{12}) - h_{12} + c_{12} + \{ \text{a class of diagrams} \}. \quad (2.174)$$

The diagrams contributing to  $w_{12}^*$  are diagrams that have two white circles labelled 1 and 2,  $\rho$  nodes,  $h$  lines, and that do not disconnect upon removal of a line and the pair of circles that it connects.

What is the expression of  $c$  in function of  $h$ ? we know that the propagator and the two-point vertex function  $\Gamma^{(2)}$  are inverse of each other by properties of the Legendre transform. Eq.(2.27) reads, in the notations of liquid state theory:

$$\begin{aligned} \int_3 G_{13} \Gamma_{32}^{(2)} &= \delta_{12}, \\ \Leftrightarrow c_{12} &= h_{12} - \int_3 h_{13} \rho_3 c_{32}. \end{aligned} \quad (2.175)$$

This equation can be solved iteratively in powers of  $h$  to get:

$$c_{12} = h_{12} + \sum_{n'=1}^{\infty} (-1)^{n'} \int_{1', \dots, n'} h_{11'} \rho_{1'} h_{1'2'} \rho_{2'} \cdots \rho_{n'} h_{n'2}, \quad (2.176)$$

Or diagrammatically:

$$c_{12} = h_{12} - \text{Diagram 1} + \text{Diagram 2} - \text{Diagram 3} + \dots, \quad (2.177)$$

where the lines of the diagrams are  $h$  lines. Thus  $c$  is a sum of chain diagrams. Eq.(2.175) is called the Ornstein-Zernike equation [137, 147] and was introduced independently of its interpretation in terms of Legendre transformations. Note that this equation is valid for any choice of potential  $w$ , including  $w^*[\rho^{(2)}]$ , and thus is valid also after the second Legendre transformation.

Now if we integrate  $h - c$  with respect to  $h$ , we see that we get an alternate sum of ring diagrams, the first two terms of which we already obtained when we calculated the Legendre transform at order  $\rho^4$ . The final expression of the full Legendre transform is thus:

$$\begin{aligned} \Gamma_2[\rho, \rho^{(2)}] &= \int_1 \rho_1 [1 - \ln \rho_1] + \frac{1}{2} \int_{12} \rho_1 \rho_2 \left[ h_{12} - (1 + h_{12}) \ln(1 + h_{12}) \right] \\ &+ \text{Diagram 1} - \text{Diagram 2} + \text{Diagram 3} + \dots \end{aligned} \quad (2.178)$$

$$- \{2\text{PI diagrams}\} \quad (2.179)$$

Although this result was present in Morita's work, a clearer presentation in terms of Legendre transforms is found in [51, 11]. The diagrams above have  $\rho$  on the nodes and  $h$  links, are connected, and more importantly, are 2-irreducible: they do not disconnect upon two differentiations with respect to  $\rho^{(2)}$ .

Note that even though the natural parameter entering the diagrammatic expressions is  $h$ , we emphasize that  $\Gamma_2$  is a functional of  $\rho$  and  $\rho^{(2)}$ : these are the two independent variables. For example  $h$  depends on  $\rho$  even when  $\rho^{(2)}$  is kept constant since we have  $\rho_{12}^{(2)}/(\rho_1 \rho_2) - 1 = h_{12}$ . The diagrams above have  $\rho$  on the nodes and  $h$  links, and they do not separate in several parts if one or two  $h$  links are removed.

### Variational principle and inverse Legendre transform

Thus to get the variational principle that will give a self-consistent equation on  $h$ , we perform the functional differentiation with respect to  $h_{12}$  and use Eq.(2.112) to come back again to:

$$w_{12} = \ln(1 + h_{12}) - h_{12} + c_{12} + \frac{2}{\rho_1 \rho_2} \frac{\delta}{\delta h_{12}} \{2\text{PI diagrams}\}. \quad (2.180)$$

Since the 2PI diagrams are functionals of  $\rho$  and  $h$ , to perform approximations, one way is to select a class of 2PI diagrams and discard the others, then perform the differentiation, to finally obtain a self-consistent equation bearing on  $h$  alone. Taking the exponential of this equation, we obtain:

$$h_{12} = e^{w_{12}} e^{h_{12} - c_{12} - \frac{2}{\rho_1 \rho_2} \frac{\delta}{\delta h_{12}} \{2\text{PI diagrams}\}} - 1, \quad (2.181)$$

Under this form, this equation is applicable to the hard sphere case since the singular hard-sphere potential only appears through  $e^w$ , which is a Heaviside function. We see that this kind of approximations will naturally enforce the condition that the pair correlation function is zero for distance smaller than the particle diameter: two hard-spheres cannot overlap ! The functional derivative of the 2PI diagrams appears under the terminology of “bridge function”.

Eq.(2.181) is an exact equation which was derived originally by the Percus method [140]. The Percus method uses the following property of the partition function of the liquid: consider a fluid of  $N$  particles subject to the influence of a  $(N + 1)$ th particle at a fixed position. The effect of this additional particle can be treated in perturbation. But a crucial property for homogeneous systems is that when one computes the one-particle distribution function of the perturbed liquid, it is in fact equal to the two-particle distribution function of the unperturbed liquid. Thus performing a perturbation expansion in powers of the density will give integral equations in terms of the pair correlation function of the unperturbed liquid. By this mean, one can show that the bridge function, usually noted  $b$ , is equal to the sum of all third and higher order direct correlation functions:

$$b_{12} = -\frac{2}{\rho_1 \rho_2} \frac{\delta}{\delta h_{12}} \{2\text{PI diagrams}\} = \sum_{n=2}^{\infty} \frac{1}{n!} \int_{1', \dots, n'} c_{11' \dots n'}^{(n+1)} \rho_{1'} h_{1'2} \dots \rho_{n'} h_{n'2}. \quad (2.182)$$

## 2.2.4 Hyper-Netted-Chain approximation

The Hyper-Netted-Chain (HNC) approximation, which was derived independently by Morita & Hiroike [130] and Van Leeuwen, Groeneveld and De Boer [168], simply consists in discarding all the 2PI diagrams in Eq.(2.179). By looking at Eq.(2.182), we see that it is equivalent to setting all the  $c^{(n)}$ 's with  $n \geq 3$  to zero. Since a large use of this approximation will be made in the rest of the manuscript, a brief overview of the results within HNC approximation is presented here.

Note again that the approximation we perform keeps the higher-order correlations of the fluid equal to their ideal-gas values, since it is only the  $c^{(n)}$  that are approximated to zero. This is a natural consequence of the fact that Mayer diagrams perform an expansion around the ideal-gas ground state, and not around a Gaussian theory.

Discarding the 2PI diagrams in Eq.(2.180), we obtain a self consistent equation on  $h$ , which involves the direct correlation function  $c$ , which is related to  $h$  by Eq.(2.175). In the homogeneous case, two-point functions depend only on  $r = |1 - 2|$ , the modulus of the difference between the two points, and the HNC approximation thus reads in terms of the 1-dimensional functions  $h$  and  $c$ :

$$\begin{cases} c(r) &= e^{w(r)} e^{h(r) - c(r)} - 1 - [h(r) - c(r)] \\ h(k) &= \frac{\rho c(k)}{1 - \rho c(k)} \end{cases} \quad (2.183)$$

These equations are more easily solved in terms of the function  $kc(k)$  since, for isotropic functions, the three-dimensional Fourier transform reads:

$$kc(k) = 4\pi \int_0^{\infty} dr \, rc(r) \sin(kr), \quad (2.184)$$

$$rc(r) = \frac{1}{2\pi^2} \int_0^{\infty} dk \, kc(k) \sin(kr). \quad (2.185)$$

We will need to solve these equations in the next three chapters: either in the dynamical context to solve the equations obtained for the non-ergodicity factor, which needs as an input the liquid structure, or in the context of replica theory where a replicated version of HNC is used, or when computing the thermodynamics of the jammed states of harmonic spheres. The scheme that we used for solving the HNC equations is an adaptation of a Picard iterative scheme:

- Start from a good guess for  $kc(k)$
- Deduce the corresponding  $kh(k)$  and thus  $k[h(k) - c(k)]$
- Inverse Fourier transform to obtain  $r[h(r) - c(r)]$
- Plug into the HNC equation to obtain a new estimate of  $rc(r)$
- Fourier transform and mix the new solution with the old one to get the new estimate for  $kc(k)$
- Iterate the procedure until the absolute value of the maximum of the difference between old and new solution is smaller than some prescribed accuracy

This kind of iterative scheme can be very sensitive to variations of  $c(k)$ . Indeed if an abrupt change in  $c(k)$  occurs, the denominator in the Ornstein-Zernike equation Eq.(2.175) can reach zero, and make the calculation diverge. This is why at each step, the new solution is incorporated gradually within the old one, to avoid unphysical values of the functions. Also, the starting guess in the calculation is important, since the calculation can become unstable if we stand far away from the physical solution. Thus, we systematically started our calculations at high temperatures and/or low density, where the virial expansion is valid, and where the function  $g$  is equal approximately to  $e^w$ . Then when convergence is achieved at this high temperature/low density, we gradually increased the density or lowered the temperature to attain the  $\rho, T$  point of interest.

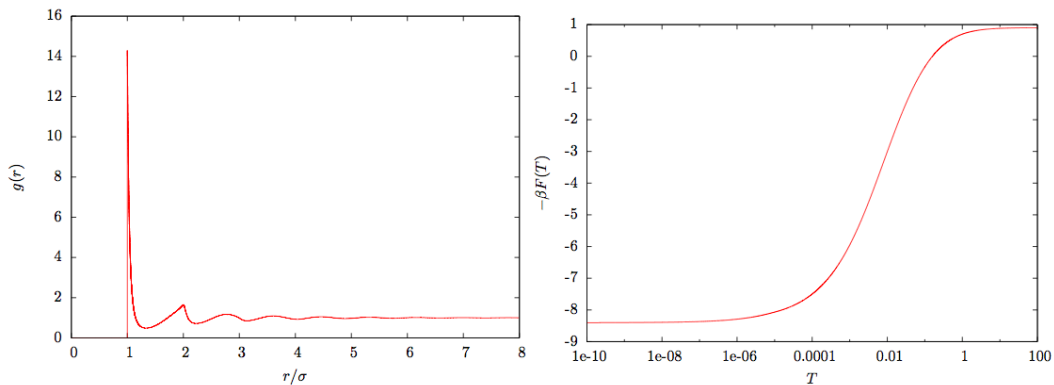


Figure 2.1: Left panel: pair correlation function  $g$  as a function of  $r/\sigma$  in the HNC approximation at density  $\rho\sigma^3 = 1.1$  and temperature  $k_B T/\epsilon = 3.58 \times 10^{-4}$ . Right panel: free energy  $-\beta F$  as a function of temperature, at fixed density  $\rho\sigma^3 = 1.1$ .

We show in the left frame of Figure 2.1 the result for the pair correlation function of harmonic spheres at high density  $\rho = 1.2$  and very low  $a$ -dimensional temperature  $k_B T/\epsilon = 3.58 \times 10^{-4}$ . This pair correlation function satisfies all the physical requirements: it decays to 1 at large  $r$ , is almost equal to zero for  $r < \sigma$ , since at very low temperature, harmonic spheres behave like hard spheres, and thus no overlaps are authorized for  $r < 1$ , except on a very narrow regime close to 1. It presents

a very pronounced first peak at  $r = \sigma$ , and secondary peaks at  $r = 2\sigma, 3\sigma, \dots$ , reflecting the shells of neighbors that develop in very dense liquids.

Inserting this result into the approximate functional  $\Gamma_2$  obtained by discarding the 2PI diagrams, we obtain the approximate equation of state of the liquid. We can notice that, in the isotropic and homogeneous case, a Fourier transform of one ring diagram reads, for example:

$$\begin{array}{c} \bullet \\ \diagup \quad \diagdown \\ \bullet \quad \bullet \end{array} = \frac{1}{3!} \int_{123} \rho_1 h_{12} \rho_2 h_{23} \rho_3 h_{31} = \frac{V}{2} \frac{1}{3} \rho^3 \int_k h(k)^3, \quad (2.186)$$

so that the sum of all diagrams is a logarithm function in Fourier space, which leads to the following analytic expression:

$$\begin{aligned} \Gamma_2^{\text{HNC}}[\rho, h] = & V\rho [1 - \ln \rho] - \frac{V}{2} \rho^2 \int_r \left( [1 + h(r)] \ln[1 + h(r)] - h(r) \right) \\ & + \frac{V}{2} \int_k \left( \ln[1 + \rho h(k)] - \rho h(k) + \frac{1}{2} \rho^2 h(k)^2 \right). \end{aligned} \quad (2.187)$$

When this functional is evaluated at  $h^*$ , the solution of the variational equation, and the inverse Legendre transformation is performed, we obtain the  $\Gamma_1$  functional, which is related to the free-energy of the liquid by:

$$\beta F = -\ln Z = -\Gamma_1[\rho] = -\Gamma_2[\rho, h^*] - \frac{1}{2} w_{12} \rho_1 \rho_2 (1 + h_{12}^*), \quad (2.188)$$

$$\begin{aligned} \Rightarrow \beta F^{\text{HNC}} = & V\rho [\ln \rho - 1] + \frac{V}{2} \rho^2 \int_r \left( [1 + h(r)] (\ln[1 + h(r)] - w(r)) - h(r) \right) \\ & - \frac{V}{2} \int_k \left( \ln[1 + \rho h(k)] - \rho h(k) + \frac{1}{2} \rho^2 h(k)^2 \right). \end{aligned} \quad (2.189)$$

We show in the right frame of Fig.(2.1) the resulting free-energy as a function of temperature, at fixed density  $\rho\sigma^3 = 1.1$ . When  $T \rightarrow 0^+$ , it converges to the entropy of hard spheres, while increasing towards an ideal gas value for large temperatures.

## Chapter 3

# Dynamics: a field theory approach

Independently from an active community that attempts to improve Mode-Coupling Theory, it is believed that a convenient way to formulate the dynamics of colloids is by resorting to field theory, i.e. finding a diagrammatic approach inspired from quantum field theory. This step forward would allow us to use all the powerful diagrammatic tools developed in this context, such as those described in Chapter 2.

The search for a good field theory for studying the dynamics near the glass transition has a long history by now, and was pioneered by Das and Mazenko for coarse grained models [49]. However application to realistic models such as colloidal glasses has been delayed until a Langevin equation for the time-dependent density was derived by Dean [55]. This provided a starting point to formulate field theories for colloidal glasses, but they were soon shown by Miyazaki and Reichman [125] to be inconsistent with the time-reversibility of the dynamics. A first attempt by Andreatov, Biroli and Lefèvre to go beyond that problem gave unsatisfactory results [3], due to the difficulty to correctly deal with the entropic  $\rho \ln \rho$  term inherent to the description of the ideal gas. Finally Kawasaki and Kim [91] managed to settle this last issue, but at the cost of a very heavy formalism, leaving little hope to extend their approach to higher orders.

In this chapter we briefly review the field-theoretic methods described above, and introduce an original way to formulate a field theory, that allows us to overcome some of their limitations, and more importantly provide a compact formalism.

### 3.1 Field theory for supercooled liquids

A system of  $N$  harmonic spheres is placed in a solvent at temperature  $T$ , that plays the role of a thermal bath. Each particle of our system is therefore a Brownian particle, that moves according to Brownian dynamics, more easily written in terms of Langevin equations. The space position of particle  $i$  at time  $t$ , will be denoted by  $x_i(t)$ , and we suppose that each trajectory satisfies the following over-damped Langevin equation:

$$\left\{ \begin{array}{l} \frac{dx_i(t)}{dt} = F_i(t) + \zeta_i(t), \\ F_i(t) = -\nabla_{x_i} \sum_{j \neq i} v(x_i(t) - x_j(t)), \\ \langle \zeta_i(t) \zeta_j(t) \rangle = 2T \delta_{ij} \delta(t - t). \end{array} \right. \quad (3.1)$$

The field  $\zeta$  is a three-dimensional Gaussian white noise of variance  $2T$ , as indicated in Eq.(3.1). This particular value of the variance ensures that the system converges towards equilibrium at long times, as given by the Boltzmann weight of Eq.(2.115), i.e.  $\exp\left(-\beta \sum_{i<j} v(x_i - x_j)\right)$ .

This type of Brownian dynamics are much simpler to analyze than the usual Hamiltonian dynamics since no velocities are involved, and the presence of a fluctuating noise allows us for more direct statistical descriptions. However, apart from differences between the short time evolutions of Hamiltonian and Brownian dynamics, the glassy features at long times are largely independent of the choice of dynamics [162].

### 3.1.1 Formulation in terms of the density and field-theoretic formulation

We are not interested in being able to follow the trajectory of each individual particle of the system, but rather in being able to accurately predict collective quantities, such as correlation functions of the fluctuations of density, as described in the introduction. In analogy with the equilibrium theory of liquids, we can define the time-dependent microscopic density of the system as:

$$\hat{\rho}(x, t) = \sum_{i=1}^N \delta(x - x_i(t)), \quad (3.2)$$

and seek for an evolution equation for  $\hat{\rho}$  rather than for all the  $x_i$ 's. Dean [55] showed that the  $N$  Langevin equations written in Eq.(3.1) exactly give the following equation of evolution for  $\hat{\rho}$ :

$$\left\{ \begin{array}{l} \partial_t \hat{\rho}(x, t) = \nabla_x \cdot \left( \hat{\rho}(x, t) \int_y \hat{\rho}(y, t) \nabla_x v(x - y) \right) + T \nabla_x^2 \hat{\rho}(x, t) + \nabla_x \cdot \left( \sqrt{\hat{\rho}(x, t)} \eta(x, t) \right), \\ \langle \eta(x, t) \eta(y, t) \rangle = 2T \delta(x - y) \delta(t - t). \end{array} \right. \quad (3.3)$$

Of course these dynamics conserves the number of particles, since they can be written as:

$$\left\{ \begin{array}{l} \partial_t \hat{\rho}(x, t) + \nabla_x j_L(x, t) = 0, \\ j_L(x, t) = -\hat{\rho}(x, t) \int_y \hat{\rho}(y, t) \nabla_x v(x - y) - T \nabla_x \hat{\rho}(x, t) - \sqrt{\hat{\rho}(x, t)} \eta(x, t). \end{array} \right. \quad (3.4)$$

The  $-T \nabla_x \hat{\rho}(x, t)$  term expresses Fick's law of diffusion, while each particle is additionally driven by the force field  $-\int_y \nabla_x v(x - y) \hat{\rho}(y, t)$  created by the others particles. The current  $j_L$  can alternatively be put under the form:

$$\left\{ \begin{array}{l} j_L(x, t) = -\hat{\rho}(x, t) \nabla_x \frac{\delta \mathcal{F}[\hat{\rho}]}{\delta \hat{\rho}(x, t)}, \\ \mathcal{F}[\hat{\rho}] = T \int_x \hat{\rho}(x, t) \left[ \ln \left( \frac{\hat{\rho}(x, t)}{\rho_0} \right) - 1 \right] + \frac{1}{2} \int_{x, y} \hat{\rho}(x, t) v(x - y) \hat{\rho}(y, t). \end{array} \right. \quad (3.5)$$

By insisting on working with a collective field, we turned the equations on  $x_i$  with additive noise into an equation for  $\hat{\rho}$  with a multiplicative noise. This equation must thus be understood in the Itô sense [167]: at each new time step, the new value of the multiplicative noise is computed with the values of the density at the previous time step. Note that this expression superficially seems to coincide with a phenomenological equation derived by Kawasaki [90], where the pair potential has to be replaced by the two-body direct correlation function of the liquid. It was later shown by



Kawasaki and Kim [92] that the use of Eq.(3.3) provides a correct treatment of the static quantities in a dynamical calculation, whereas using of a phenomenological equation does not.

Another difficulty is in the evaluation of the density profile at the beginning of the dynamics, that requires an input at time  $t = 0$ . To clarify this, the experiment that we have in mind is the following: at time  $t = -\infty$ , we prepare a system of harmonic spheres in a bath at temperature  $T$ , then let them evolve freely towards equilibrium. At  $t = 0$ , equilibrium is achieved, and we start monitoring the dynamics, which are modeled by our equation (3.3). In this interpretation, the initial value of  $\hat{\rho}(x, t)$  must be obtained from an equilibrium distribution. This distribution is known, at least formally, from the discussion in the previous section. Indeed, exactly at  $t = 0$ , there will be fluctuations of the space dependent field  $\hat{\rho}(x, t = 0)$  around its equilibrium value  $\rho_0$ , which is constant in time and space because of translational and time-translational invariance. Defining the density fluctuation field  $\delta\rho$  as:

$$\delta\rho(x, t) = \hat{\rho}(x, t) - \rho_0, \quad (3.6)$$

we thus have to know the probability distribution of  $\delta\rho(x, 0)$ . It is given by the  $\Gamma_1$  functional of the liquid state theory described in the previous subsection. Indeed, expanding  $\Gamma_1$  around a flat profile of density, we get:

$$\begin{aligned} \Gamma_1[\delta\rho] &= \Gamma_1[\rho_0] + \sum_{N=1}^{\infty} \int_{x_1, \dots, x_N} \frac{\delta\Gamma_1[\rho]}{\delta\rho(x_1) \cdots \delta\rho(x_N)} \delta\rho(x_1) \cdots \delta\rho(x_N) \\ &= \Gamma_1[\rho_0] + \int_x (\rho_0 + \delta\rho(x)) \left[ \ln \left( 1 + \frac{\delta\rho(x)}{\rho_0} \right) - 1 \right] \\ &\quad - \sum_{N=1}^{\infty} \int_{x_1, \dots, x_N} c^{(N)}(x_1, \dots, x_N) \delta\rho(x_1) \cdots \delta\rho(x_N). \end{aligned} \quad (3.7)$$

Now performing the inverse Legendre transformation to come back to the free-energy of the liquid simply cancels the  $c^{(1)}$  term, in order to obtain the following probability of observing a density profile at equilibrium:

$$P[\delta\rho(x, t = 0)] \propto \exp \left( \begin{array}{l} - \int_x (\rho_0 + \delta\rho(x)) \left[ \ln \left( 1 + \frac{\delta\rho(x)}{\rho_0} \right) - 1 \right] \\ + \sum_{N=2}^{\infty} \int_{x_1, \dots, x_N} c^{(N)}(x_1, \dots, x_N) \delta\rho(x_1) \cdots \delta\rho(x_N) \end{array} \right). \quad (3.8)$$

By evaluating this functional in the HNC approximation, where all  $c^{(N)}$ 's are set to zero for  $N \geq 3$ , we get the Ramakrishnan-Yussouf [144] expression for the probability of observing a density profile.

We show now for future use a standard procedure to turn the dynamical equation Eq.(3.3) into a diagrammatic computational scheme similar to the one described in the first section of this chapter. In order to obtain a particular density profile between time 0 and time  $t_f$ , we first have to draw an initial density profile out of the distribution in Eq.(3.8), then we have at each time step to draw a value of the noise out of its distribution  $P[\eta]$ , which is Gaussian, and finally we must find the correct value of the density profile that satisfies the Langevin equation given the value of the noise that was chosen. Grouping all these contributions together, we can write down the probability of observing

any density profile between time 0 and  $t_f$  (probability which is equal to one by definition !) as:

$$1 = Z = \int \mathcal{D}\rho_0 P[\rho_0] \int \mathcal{D}\eta P[\eta] \int \mathcal{D}\rho \prod_{t=0^+}^{t_f} \prod_x \delta(\text{Langevin equation at time } t \text{ and point } x) \quad (3.9)$$

$$= \int \mathcal{D}\rho \mathcal{D}\bar{\rho} \mathcal{D}\eta \mathcal{D}\rho_0 P[\rho_0] P[\eta] \exp\left(-\int_{t=0}^{t_f} \int_x \bar{\rho}(x, t) \times \text{Langevin equation at time } t\right) \quad (3.10)$$

$$= \int \mathcal{D}\rho_0 P[\rho_0] \int \mathcal{D}\rho \mathcal{D}\bar{\rho} \exp\left(-\int_{t,x} \left[ \begin{array}{l} \bar{\rho}(x, t) \partial_t \rho(x, t) - T \bar{\rho}(x, t) \nabla_x^2 \rho(x, t) \\ -\bar{\rho}(x, t) \nabla_x \cdot \left( \rho(x, t) \int_y \rho(y, t) \nabla_x v(x-y) \right) \end{array} \right]\right) \\ \int \mathcal{D}\eta \exp\left(-\frac{1}{4T} \int_{t,x} \left[ \eta^2(x, t) - 4T \bar{\rho}(x, t) \nabla_x \cdot \left( \sqrt{\rho(x, t)} \eta(x, t) \right) \right]\right). \quad (3.11)$$

In order to go from the first to the second line, we used the integral representation of the delta function, as well as a change of variables in the delta function, which has determinant 1 when the equation is understood in the Itô sense. After an integration by parts, the integral over the noise is Gaussian, and we obtain :

$$\left\{ \begin{array}{l} Z = \int \mathcal{D}\rho_0 e^{-\beta \mathcal{F}_{\text{equ}}[\rho_0]} \int \mathcal{D}\rho \mathcal{D}\bar{\rho} e^{-S[\rho, \bar{\rho}]} \\ S[\rho, \bar{\rho}] = \int_{t=0}^{t_f} \int_x \left[ \bar{\rho}(x, t) \partial_t \rho(x, t) - \bar{\rho}(x, t) \nabla_x \cdot \left( \rho(x, t) \nabla_x \frac{\delta \beta \mathcal{F}[\rho]}{\delta \rho(x, t)} \right) - T \rho(x, t) (\nabla_x \bar{\rho}(x, t))^2 \right], \\ \beta \mathcal{F}_{\text{equ}}[\rho] = \int_x \rho(x) \left[ \ln \frac{\rho(x)}{\rho} - 1 \right] + \sum_{N=2}^{\infty} \frac{1}{N!} \int_{x_1, \dots, x_N} c^{(N)}(x_1, \dots, x_N) \rho(x_1) \cdots \rho(x_N), \\ \beta \mathcal{F}[\rho] = \int_x \rho(x, t) \left[ \ln \frac{\rho(x, t)}{\rho} - 1 \right] + \frac{1}{2} \int_{x,y} \rho(x, t) \beta v(x-y) \rho(y, t). \end{array} \right. \quad (3.12)$$

This formalism was first formulated by Martin, Siggia, and Rose [111], and put to work by De Dominicis [52] and Janssen [87, 88]. Now we find ourselves in the position of formulating a statistical field theory in the form described in the first chapter.

### 3.1.2 Diagrammatic structure of the theory

Following the line described in the first section, we look at the saddle point of the functional integral, defined as:

$$\left\{ \begin{array}{l} 0 = (-\partial_t - \nabla_x^2) \bar{\rho}(x, t) - \nabla_x \cdot \left( \rho(x, t) \frac{\delta \beta \mathcal{F}[\rho]}{\delta \rho(x, t)} \right) - T (\nabla_x \bar{\rho})^2 \\ 0 = (\partial_t - \nabla_x^2) \rho(x, t) - \nabla_x \cdot \frac{\delta \mathcal{F}[\rho]}{\delta \rho(x, t)} \cdot \nabla_x \bar{\rho}(x, t) - \int_y \bar{\rho}(y, t) \partial_y \rho(y, t) \cdot \partial_y \frac{\delta^2 \mathcal{F}[\rho]}{\delta \rho(x, t) \delta \rho(y, t)}. \end{array} \right. \quad (3.13)$$

Time translation invariance, isotropy and translation invariance enforce, if they are not spontaneously broken, that averages of one point quantities are constant, therefore leaving us with only  $\rho(x, t) = \rho_0$  and  $\bar{\rho}(x, t) = 0$ . Now we gather the two fluctuations of the fields around their mean values into a vector  $\varphi$  defined by:

$$\varphi(x, t) = \begin{pmatrix} \delta \bar{\rho}(x, t) \\ \delta \rho(x, t) \end{pmatrix} \quad (3.14)$$

and obtain a field theory described by:

$$S[\varphi] = \frac{1}{2} \int_{k,t} \varphi(k,t) G_0^{-1}(k,t) \varphi(-k,t) + S_{\text{ng}}[\varphi], \quad (3.15)$$

$$G_0^{-1}(k,t) = \begin{pmatrix} -2T\rho_0 k^2 & \partial_t + k^2(1 + \beta\rho_0 v(k)) \\ -\partial_t + k^2(1 + \beta\rho_0 v(k)) & 0 \end{pmatrix}, \quad (3.16)$$

$$S_{\text{ng}}[\varphi] = \int_{k_1, k_2, k_3} \delta_{k_1+k_2+k_3} \begin{pmatrix} Tk_2 \cdot k_3 \delta\rho(k_1, t) \delta\bar{\rho}(k_2, t) \delta\bar{\rho}(k_3, t) \\ + \frac{1}{2} [k_1 \cdot k_3 \beta v(k_1) + k_2 \cdot k_3 \beta v(k_2)] \delta\rho(k_1, t) \rho(k_2, t) \delta\bar{\rho}(k_3, t) \end{pmatrix} \quad (3.17)$$

### 3.1.3 Structure of the perturbative expansion

In a perturbative expansion as described in the first section of this chapter, the main quantity to compute is the bare propagator  $G^{(0)}$ , which is the inverse of the quadratic term in the action. In our case, we find:

$$G^{(0)}(k,t) = \begin{pmatrix} 0 & \theta(-t) \\ \theta(t) & T\rho_0 k^2 \end{pmatrix} e^{-k^2(1-\rho_0 w(k))|t|} \quad (3.18)$$

This form of propagator is crucial to obtain a causal structure, as was pointed out by De Dominicis. Indeed, if we look now at the diagrammatic structure of our theory, we see that we will have two kind of vertices to build diagrams, pictured as follows:

$$\delta\bar{\rho}(k, t_1) \equiv \leftarrow \bigcirc \quad (3.19)$$

$$\delta\rho(k, t_1) \equiv \bigcirc \rightarrow \quad (3.20)$$

$$\int_{k_1, k_2, k_3} \delta_{k_1+k_2+k_3} Tk_2 \cdot k_3 \delta\rho(k_1, t) \delta\bar{\rho}(k_2, t) \delta\bar{\rho}(k_3, t) \equiv \text{---} \bullet \begin{array}{c} \curvearrowright \\ \curvearrowleft \end{array} \quad (3.21)$$

$$- \int_{k_1, k_2, k_3} \delta_{k_1+k_2+k_3} \frac{1}{2} [k_1 \cdot k_3 w(k_1) + k_2 \cdot k_3 w(k_2)] \rho(k_1, t) \rho(k_2, t) \delta\bar{\rho}(k_3, t) \equiv \begin{array}{c} \curvearrowright \\ \bullet \rightarrow \end{array} \quad (3.22)$$

$$G_{11}(k, t) \equiv 0 \equiv \bigcirc \rightarrow \leftarrow \bigcirc \quad (3.23)$$

$$G_{12}(k, t) \equiv \theta(t_1 - t_2) e^{-k^2(1-\rho_0 w(k))|t_2-t_1|} \equiv \bigcirc \rightarrow \bigcirc \quad (3.24)$$

$$G_{22}(k, t) \equiv T\rho_0 k^2 e^{-k^2(1-\rho_0 w(k))|t_2-t_1|} \equiv \bigcirc \text{---} \bigcirc \quad (3.25)$$

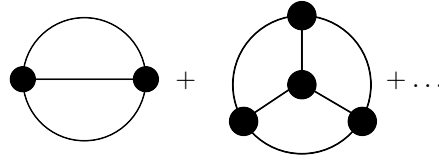
Given the value of the bare propagator, we see that joining one  $\delta\rho$  line with a  $\delta\bar{\rho}$  line gives a causal step function. Thus the arrows of the lines indicate the arrow of time, and if a diagram contains two arrows that run in opposite directions, or make a loop, the diagram is equal to zero.

Inevitably, diagrams of the free-energy are then all equal to zero, because by definition they are closed, and we recover the fact that  $Z = 1$  in this dynamical theory.

We also see that the causal structure of the propagators is conserved when we add diagrams to the Gaussian estimate  $G^{(0)}$ : indeed a diagram that contributes to renormalize  $G_{11}$  has conflicting arrow of times and is therefore equal to zero, hence the property  $G_{11} = 0$  holds non perturbatively. And a diagram that contributes to  $G_{12}(k, t_2 - t_1)$  forces  $t_2$  to be greater than  $t_1$ , and thus  $G_{12}$  is always proportional to a Heaviside function.

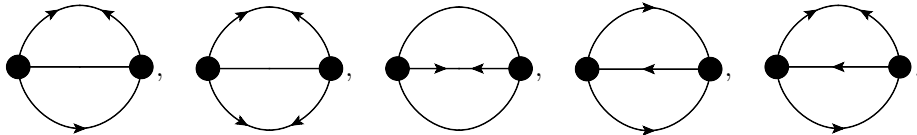
### 3.1.4 Symmetries and approximations

Now that we have a field-theoretic formulation, we can come back to the prescription of Chapter 2, and build up self consistent equations for the correlation functions. We use the variational principle in Eq.(2.114) to obtain the two-point vertex function  $\Sigma$  as the derivative of the sum of all 2PI diagrams of the theory. Since our formulation contains only cubic interactions, the first terms in this sum of diagrams will be of the form:



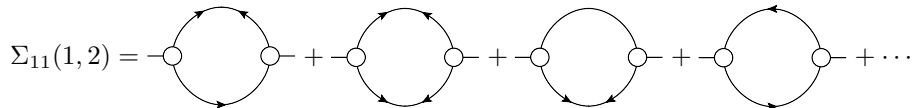
$$(3.26)$$

where the double lines represent the full propagators. We show here all the diagrams corresponding to the first term of Eq.(3.26):



$$(3.27)$$

Note that since we have performed the second Legendre transform, the propagators on the lines of these diagrams are arbitrary functions; they are not necessarily causal. To obtain a self consistent equation on the propagators, we have to differentiate with respect to  $G$ , which leads to an expression for the  $\Sigma$  functional described in Chapter 2 via Eq.(2.114). In our case, we have two fields, so that the propagator and two-point vertex functions  $\Sigma$  are  $2 \times 2$  matrices. Differentiating the diagrams in Eq.(3.27) with respect to  $G_{11}$  for example leads to:



$$(3.28)$$

Note that it is customary to represent the vertex functions with external lines to recall which vertex function is considered, but these lines must be omitted when the diagram is computed. These are called amputated diagrams in the field-theoretic language.

When evaluated at the physical propagators, which have been proved to be causal, we see that all these contributions will disappear. We can see that this property is conserved whatever the number of diagrams we keep in our expansion is, so that  $\Sigma_{11} = 0$  non-perturbatively as a consequence of causality. In the same way we will find that  $\Sigma_{12}$  is non-zero but is proportional to a step function of the difference between its two time arguments, and  $\Sigma_{22}$  is generically non zero. These causality properties for  $G$  and  $\Sigma$  are non-perturbative features, and have to be conserved by a truncation of the  $\Gamma_2$  functional in order to obtain a consistent approximation for the propagators.

Another important physical constraint imposed on dynamical theories is the time-reversal invariance: i.e. the invariance of the dynamical equations with respect to a change  $t \rightarrow -t$ . It has been shown by Janssen[88] to correspond, in the formalism that we present here, to a non-linear symmetry

relating the density field and the response field:

$$\left\{ \begin{array}{l} t \rightarrow -t \\ \delta\rho(x, t) \rightarrow \delta\rho^R(x, t) = \delta\rho(x, -t), \\ \delta\bar{\rho}(x, t) \rightarrow \delta\bar{\rho}^R(x, t) = -\delta\bar{\rho}(x, -t) + \frac{\delta\beta\mathcal{F}[\rho]}{\delta\rho(x, -t)} \end{array} \right. \quad (3.29)$$

Because of the purely entropic ideal gas term in  $\mathcal{F}[\rho]$ , this symmetry is non-linear in the sense that it relates the fields to their higher order cumulants. While a truncation of the 2PI functional  $\Gamma_2$  can easily be shown to automatically conserve linear symmetries of the action (if evaluated at propagators that verify themselves these symmetries), this is not the case automatically for non-linear symmetries. Thus an arbitrary truncation will surely violate micro reversibility [125], which is a crucial symmetry in our case: indeed we want to obtain an approximation that is able to predict a transition from an ergodic phase to a non-ergodic one. If we use an approximation that explicitly breaks time-reversal symmetry, a possible transition may be an artifact of this approximation. To be sure that we find (or do not find !) *spontaneous* symmetry breaking, we have to make sure time-reversal is properly enforced, as well as causality.

### 3.1.5 Linearizing the time-reversal

There are currently two different ways to linearize the time-reversal symmetry. Within the MSR formalism, the original idea was introduced by Andrianov Biroli and Lefèvre in [3], but was properly implemented later by Kawasaki and Kim in [92]. One introduces a Lagrange multiplier  $\theta$  in the path integral, which will constrain all the non-linear contributions coming from  $\frac{\delta\mathcal{F}[\rho]}{\delta\rho}$  to be equal to  $\theta$ :

$$Z = \int \mathcal{D}\rho \mathcal{D}\bar{\rho} \delta\left(\theta - \frac{\delta\beta\mathcal{F}[\rho]}{\delta\rho} + \frac{\delta\rho}{\rho_0}\right) e^{-S[\rho, \bar{\rho}]}, \quad (3.30)$$

$$= \int \mathcal{D}\rho \mathcal{D}\bar{\rho} \mathcal{D}\theta \mathcal{D}\bar{\theta} e^{-S_{\text{KK}}[\rho, \bar{\rho}, \theta, \bar{\theta}]}, \quad (3.31)$$

$$S_{\text{KK}}[\varphi] = \frac{1}{2} \int_{k, t} \varphi(k, t) G_0^{-1}(k, t) \varphi(-k, t) + S_{\text{ng}}[\varphi], \quad (3.32)$$

$$G_0^{-1}(k, t) = \begin{pmatrix} 0 & -i\partial_t + k^2(1 - \rho_0 w(k)) & 0 & 0 \\ i\partial_t + k^2(1 - \rho_0 w(k)) & 2\rho_0 k^2 & \rho_0 k^2 & 0 \\ 0 & \rho_0 k^2 & 0 & -1 \\ 0 & 0 & -1 & 0 \end{pmatrix}, \quad (3.33)$$

$$S_{\text{ng}}[\varphi] = - \int_{x, t} \left[ \begin{array}{l} \delta\bar{\rho}(x, t) \nabla_x \cdot \left( \delta\rho(x, t) \nabla_x \left[ \theta(x, t) + \frac{\delta\rho(x, t)}{\rho_0} - (w \otimes \delta\rho)(x, t) \right] \right) \\ -\delta\rho(x, t) (\nabla_x \delta\bar{\rho}(x, t))^2 + \bar{\theta}(x, t) \left( \sum_{n=2}^{\infty} \frac{(-1)^n}{(n-1)} \frac{\delta\rho(x, t)^n}{\rho_0^{n-1}} \right) \end{array} \right], \quad (3.34)$$

where  $\otimes$  denotes space convolution. The time reversal is now a linear transformation of the fields:

$$\left\{ \begin{array}{l} t \rightarrow -t \\ \rho(x, t) \rightarrow \rho^R(x, t) = \rho(x, -t) \\ \bar{\rho}(x, t) \rightarrow \rho^R(x, t) = -\bar{\rho}(x, -t) + \frac{1}{\rho_0} \delta\rho(x, -t) - (w \otimes \delta\rho)(x, -t) + \theta(x, -t) \\ \theta(x, t) \rightarrow \theta^R(x, t) = \theta(x, -t) \\ \bar{\theta}(x, t) \rightarrow \bar{\theta}^R(x, t) = \bar{\theta}(x, -t) - i\partial_t \rho(x, -t) \end{array} \right. \quad (3.35)$$

and will therefore automatically be conserved by a truncation of the 2PI functional  $\Gamma_2$ . However the cost has been to introduce an infinite number of interaction vertices in the action, that are all related to the non-interacting system. Thus, to each order of the calculation, one has to calculate an infinite number of diagrams in order to be able to fully describe the correct non-interacting system.

Note that these symmetry considerations on the time-reversal do not apply if one works with the Itô discretization, but only in the Stratonovich discretization [167]. Luckily, for the precise Langevin equation under scrutiny, the two discretizations are identical !

By cleverly taking into account the ideal gas contributions non-perturbatively, Kawasaki and Kim [92] were able to derive back the MCT equation. The same analysis were later performed by Nishino and Hayakawa [133] for the fluctuating non-linear hydrodynamics. However, the cost of taking correctly into account the ideal gas is a very heavy formalism, leaving little hope to extend the calculation to next orders properly. It would be better to have a theory that directly starts from non-interacting particles and treats the interactions as a perturbation. In the following sections of this chapter we present a first step towards such a theory, that is provided by a mapping of the particles onto effective bosons.

## 3.2 Quantum mechanical formulation

### 3.2.1 Master equation and Doi-Peliti formalism

Coming back to a discretized version of the dynamics of our system, we now consider that our  $N$  particles are dispatched on an infinite, 3D, square lattice with mesh size  $a$ . The possible positions of the spheres are denoted  $x_i = a(pe_1 + qe_2 + re_3)$ , where  $\{p, q, r\}$  are positive or negative numbers and  $e_1, e_2, e_3$  are unitary vectors which form an orthonormal basis. The ensemble of vectors belonging to the lattice is called  $\mathcal{L}$  in the following.

The equivalent of the microscopic density that we are interested in is now the set of occupation numbers of the lattice sites. We call  $n_x$  the occupation number of the site located at  $x$ . A microscopic configuration of the system  $\mathcal{C}$  is then the set of all numbers of occupations :

$$\mathcal{C} = \{n_x, x \in \mathcal{L}\} \quad (3.36)$$

We call  $E_p(\mathcal{C})$  the total potential energy of a given configuration  $\mathcal{C}$ , defined by :

$$E_p(\mathcal{C}) = \frac{1}{2} \sum_{y \neq z} n_y v(y-z) n_z, \quad (3.37)$$

where  $v$  is still the pair potential of our system, that can be for example the pair potential of harmonic spheres given in Eq.(1.20). We choose the following dynamic rules : within a time interval  $dt$ , a particle can jump from a site  $x$  to another site  $y$  (changing the microscopic configuration from  $\mathcal{C}$  to  $\mathcal{C}'$ ) with probability  $\exp\left(-\frac{\beta}{2}[E_p(\mathcal{C}') - E_p(\mathcal{C})]\right) n_x dt$ . We consider the evolution with time of the probability of observing a particular configuration  $\mathcal{C}$  at time  $t$ :  $P(\mathcal{C}, t)$ . We call  $\mathcal{C}'$  the configuration that differs from  $\mathcal{C}$  only by a jump of one particle to a closest neighbor :

$$\begin{aligned} \mathcal{C} &= \{\dots, n_x, \dots, n_{x+e}, \dots\}, \\ \mathcal{C}' &= \{\dots, n_x - 1, \dots, n_{x+e} + 1, \dots\}, \\ &\text{with } e = \pm a e_i, i \in \{1, 2, 3\} \end{aligned} \quad (3.38)$$

Note that this type of dynamics is compatible with the hard-sphere case, where  $e^{-\beta v}$  is equal to 0 or 1 depending whether the configuration has overlaps or not. The only restriction is that the initial configuration must be an authorized one. In that case, the rate to go from the current configuration to a forbidden one is always 0, and the hard-sphere constraint is always satisfied.

These dynamics obviously satisfy detailed balance, and thus lead to a unique stationary distribution, which is the Boltzmann one:

$$P(\mathcal{C}, t) \underset{t \rightarrow \infty}{\sim} P_{\text{eq}}(\mathcal{C}) = e^{-\beta E_p(\mathcal{C})} \quad (3.39)$$

The continuum limit (letting  $a$  go to 0 while properly rescaling the physical quantities of interest) of these dynamics can be shown to be equivalent to the Langevin approach presented above [2]. However, we are interested in finding an alternative formulation, in which the non-interacting particles are exactly treated and time-reversal invariance is linear.

The microscopic dynamics described here corresponds to an evolution equation for  $P(\mathcal{C}, t)$  that reads:

$$\left\{ \begin{array}{l} \partial_t P(\mathcal{C}, t) = WP(\mathcal{C}, t) \\ W = \sum_{x \in \mathcal{L}} \sum_e \left[ (n_{x+e} + 1) e^{-\frac{\beta}{2}(E_p(\mathcal{C}) - E_p(\mathcal{C}'))} P(\mathcal{C}', t) - n_x e^{\frac{\beta}{2}(E_p(\mathcal{C}') - E_p(\mathcal{C}))} P(\mathcal{C}, t) \right], \end{array} \right. \quad (3.40)$$

We follow now the work of Doi [58], popularized in the context of reaction-diffusion processes by Peliti [139]. It consists in introducing a Fock space corresponding to the states  $\mathcal{C}$  and making use of the ladder operators of quantum mechanics to obtain the evolution of our system in a second quantized form, i.e. in terms of occupation numbers, which are the discrete versions of the microscopic densities defined in Eq.(3.2). We introduce the lowering and raising operators  $\hat{a}_x$  and  $\hat{a}_x^+$ , which satisfy bosonic commutation relations:

$$\begin{aligned} [\hat{a}_x, \hat{a}_y] &= 0 \\ [\hat{a}_x^+, \hat{a}_y^+] &= 0 \\ [\hat{a}_x, \hat{a}_y^+] &= \delta_{x,y} \end{aligned} \quad (3.41)$$

Defining  $\hat{n}_x = \hat{a}_x^+ \hat{a}_x$ , and choosing convenient normalizations we then construct the Fock space of states from the vacuum state  $|0\rangle$  with no particles in it:

$$\hat{a}_x |0\rangle = 0 \quad \forall x. \quad (3.42)$$

Starting from the vacuum state  $|0\rangle$ , the creation operators  $\hat{a}_x^+$  generate all the microscopic states  $\mathcal{C}$ , that have their corresponding kets  $|\mathcal{C}\rangle$ :

$$|\mathcal{C}\rangle \equiv |\dots, n_x, \dots\rangle = \prod_x (\hat{a}_x^+)^{n_x} |0\rangle. \quad (3.43)$$

Application of the operators  $\hat{a}, \hat{a}^+$  and  $\hat{n}$  on these states, and on their corresponding bra's are given by the following relations (note that the normalizations are different from usual conventions for the

quantum harmonic oscillator):

$$\begin{aligned}
\hat{n}_x |\dots, n_x, \dots\rangle &= n_x |\dots, n_x, \dots\rangle \\
\hat{a}_x^+ |\dots, n_x, \dots\rangle &= |\dots, n_x + 1, \dots\rangle \\
\hat{a}_x |\dots, n_x, \dots\rangle &= n_x |\dots, n_x - 1, \dots\rangle \\
\langle \dots, n_x, \dots | \hat{a}_x &= \langle \dots, n_x + 1, \dots | (n_x + 1) \\
\langle \dots, n_x, \dots | \hat{a}_x^+ &= \langle \dots, n_x - 1, \dots | \\
\langle 0 | \hat{a}_x^+ &= 0 \quad \forall x.
\end{aligned} \tag{3.44}$$

In this way, the states are normalized so that:

$$\langle \mathcal{C} | \mathcal{C}' \rangle = \delta_{\mathcal{C}, \mathcal{C}'} = \prod_x \delta_{n_x, n'_x} \tag{3.45}$$

We can now re-write the master equation Eq.(3.40) in the Fock space, by defining a wave function  $|\Psi\rangle$  that contains all the information on the statistical state of the system:

$$|\Psi\rangle_t = \sum_{\mathcal{C}} P(\mathcal{C}, t) |\mathcal{C}\rangle \tag{3.46}$$

We can then rewrite the master equation as:

$$\partial_t |\Psi\rangle_t = \hat{W} |\Psi\rangle_t, \tag{3.47}$$

$$\hat{W} = \sum_{x \in \mathcal{L}} \sum_e e^{\frac{\beta V(e)}{2}} \left[ \hat{a}_x^+ \hat{a}_{x+e} e^{\frac{\beta}{2} \Delta \hat{E}_p} - \hat{a}_x^+ \hat{a}_x e^{-\frac{\beta}{2} \Delta \hat{E}_p} \right], \tag{3.48}$$

$$\Delta \hat{E}_p = \sum_{y \neq x} (\hat{n}_{y+e} - \hat{n}_y) v(x - y), \tag{3.49}$$

which is functionally solved in time as:

$$|\Psi\rangle_t = e^{\hat{W}t} |\Psi\rangle_{t=0}. \tag{3.50}$$

The average of an observable  $A(\mathcal{C})$  that depends on occupation numbers, such as  $E_p$  in Eq.(3.37) is defined as:

$$\langle A \rangle_t = \sum_{\mathcal{C}} A(\mathcal{C}) P(\mathcal{C}, t). \tag{3.51}$$

To compute this kind of object, we introduce the projection state:

$$\langle P | = \sum_{\mathcal{C}} \langle \mathcal{C} | = \langle 0 | \prod_x e^{a_x}, \tag{3.52}$$

which has the following properties:

$$\langle P | \hat{a}_x^+ = \langle P |, \tag{3.53}$$

$$\langle P | (\hat{a}_x^+ - 1) = 0, \tag{3.54}$$

$$\langle P | \Psi \rangle_t = \sum_{\mathcal{C}, \mathcal{C}'} P(\mathcal{C}', t) \langle \mathcal{C} | \mathcal{C}' \rangle = \sum_{\mathcal{C}} P(\mathcal{C}, t) = 1 \quad \forall t, \tag{3.55}$$

$$\langle P | \mathcal{C} \rangle = 1 \quad \forall \mathcal{C}, \tag{3.56}$$

and thus compute the average of an observable, as:

$$\langle A \rangle_t = \langle P | \hat{A} | \Psi \rangle_t, \tag{3.57}$$

where  $\hat{A}$  is the canonically quantized operator obtained by replacing all  $n_x$  in  $A$  by  $\hat{n}_x$ .



### 3.2.2 Passage to a field theory

Given a set of states  $|\phi\rangle$  that form a representation of the identity,

$$\text{Id} = \sum_{\phi} |\phi\rangle\langle\phi|, \quad (3.58)$$

we can construct a path integral similar to the Feynman path integral by splitting the time interval  $[0, t]$  into  $N$  slices of size  $\Delta t = t/N$  and write:

$$\begin{aligned} \langle A \rangle_t &= \langle P | \hat{A} e^{\hat{H}\Delta t} \dots e^{\hat{H}\Delta t} | \Psi \rangle_{t=0} \\ &= \sum_{\phi_0, \dots, \phi_N} \langle P | \hat{A} | \phi_N \rangle \langle \phi_N | e^{\hat{H}\Delta t} | \phi_{N-1} \rangle \dots \langle \phi_1 | e^{\hat{H}\Delta t} | \phi_0 \rangle \langle \phi_0 | \Psi \rangle_{t=0} \\ &= \sum_{\phi_0, \dots, \phi_N} \langle P | \hat{A} | \phi_N \rangle \prod_{i=1}^N \langle \phi_i | \phi_{i-1} \rangle \langle \phi_0 | \Psi \rangle_{t=0} e^{\Delta t \sum_{i=1}^N \frac{\langle \phi_i | \hat{H} | \phi_{i-1} \rangle}{\langle \phi_i | \phi_{i-1} \rangle}} \end{aligned} \quad (3.59)$$

We specify now the complete set of states that we use to construct the path integral. We construct coherent states:

$$|a\rangle = |\dots, a_x, \dots\rangle = e^{-\frac{1}{2} \sum_x |a_x|^2} e^{\sum_x a_x \hat{a}_x^+} |0\rangle, \quad (3.60)$$

$$\langle a| = \langle \dots, a_x, \dots| = e^{-\frac{1}{2} \sum_x |a_x|^2} \langle 0| e^{\sum_x \bar{a}_x \hat{a}_x}. \quad (3.61)$$

The action of  $\hat{a}$  and  $\hat{a}^+$  on these states are:

$$\begin{aligned} \hat{a}_x |a\rangle &= e^{-\frac{1}{2} \sum_x |a_x|^2} \prod_{y \neq x} e^{a_y \hat{a}_y^+} \hat{a}_x e^{a_x \hat{a}_x^+} |0\rangle \\ &= e^{-\frac{1}{2} \sum_x |a_x|^2} \prod_x e^{a_x \hat{a}_x^+} (a_x + \hat{a}_x) |0\rangle \\ &= a_x |a\rangle. \end{aligned} \quad (3.62)$$

$$\begin{aligned} \langle a | \hat{a}_x^+ &= e^{-\frac{1}{2} \sum_x |a_x|^2} \langle 0 | (\bar{a}_x + \hat{a}_x^+) \prod_x e^{\bar{a}_x \hat{a}_x} \\ &= \langle a | \bar{a}_x. \end{aligned} \quad (3.63)$$

The normalisation is given by:

$$\langle a | a \rangle = 1, \quad (3.64)$$

$$\langle a' | a \rangle = \exp\left(-\frac{1}{2} \sum_x [|a'_x|^2 + |a_x|^2]\right) \exp\left(\sum_x \bar{a}'_x a_x\right), \quad (3.65)$$

$$= \exp\left(\frac{1}{2} \sum_x [|a'_x|^2 - |a_x|^2]\right) \exp\left(\sum_x \bar{a}'_x [a_x - a'_x]\right). \quad (3.66)$$

Finally these states form a complete set of the space, as we wanted. To show it, first we remark that (defining  $a = u + iv$ ):

$$\begin{aligned} \int \frac{dudv}{\pi} \bar{a}^n a^m e^{-|a|^2} &= \frac{1}{\pi} \int_{r=0}^{\infty} \int_{\theta=0}^{2\pi} dr d\theta r e^{-r^2} r^{n+m} e^{i(n-m)\theta} \\ &= 2\delta_{n,m} \int_0^{\infty} r^{2n+1} e^{-r^2} dr = n! \delta_{n,m}. \end{aligned} \quad (3.67)$$

It is easy to verify, by resorting to Eq. (3.67), that we have the unity representation:

$$\text{Id} = \int \prod_x \left( \frac{d\text{Re}z_x d\text{Im}z_x}{\pi} \right) |a\rangle\langle a|. \quad (3.68)$$

An important remark is that:

$$\langle P| = e^{\frac{M}{2}} \langle a = 1|, \quad (3.69)$$

where  $M$  is the number of lattice sites.

Coming back to Eq. (3.59), we define  $t_i = i\Delta t$  and we use those coherent states to get:

$$\langle A \rangle_t = \int \prod_{i,x} \frac{d\Re a_{x,t_i} d\Im a_{x,t_i}}{\pi} \left[ \langle P|\hat{A}|a_t\rangle \langle a_0|\Psi\rangle_{t=0} \prod_{i=1}^N \langle a_{t_i}|a_{t_{i-1}}\rangle \right] e^{\Delta t \sum_{i=1}^N \frac{\langle a_{t_i}|\hat{W}|a_{t_{i-1}}\rangle}{\langle a_{t_i}|a_{t_{i-1}}\rangle}} \quad (3.70)$$

We have:

$$\begin{aligned} \prod_{i=1}^N \langle a_{t_i}|a_{t_{i-1}}\rangle &= \prod_{i=1}^N e^{\frac{1}{2} \sum_x (|a_{x,t_i}|^2 - |a_{x,t_{i-1}}|^2)} e^{\sum_{i=1}^N \sum_x \bar{a}_{x,t_i} (a_{x,t_i} - a_{x,t_{i-1}})} \\ &= \exp\left(\frac{1}{2} \sum_x [|a_{x,t}|^2 - |a_{x,0}|^2]\right) \exp\left(\sum_{i=1}^N \sum_x \bar{a}_{x,t_i} (a_{x,t_i} - a_{x,t_{i-1}})\right) \end{aligned} \quad (3.71)$$

There is still the term  $\langle P|\hat{A}|a_t\rangle$  to calculate. The properties of our coherent states and of the projection state are such that, if in  $\hat{A}$ , all  $\hat{a}^+$  operators are placed on the left and all  $\hat{a}$  operators on the right, this average will be easy to calculate. The operation of putting  $\hat{a}^+$  on the left and  $\hat{a}$  on the right is called normal ordering [28]. Defining as  $\tilde{A}$  the normal ordered form of  $\hat{A}$ , we will have:

$$\begin{aligned} \langle P|\hat{A}|a_t\rangle &= e^{\frac{N}{2}} \langle 1|\hat{A}|a_t\rangle \\ &= e^{\frac{N}{2}} \tilde{A}(1, a_t) e^{\frac{1}{2} \sum_x (1 - |a_{x,t}|^2)} e^{\sum_x (a_{x,t} - 1)} \\ &= \tilde{A}(1, a_t) \exp\left(\sum_x \left[ a_{x,t} - \frac{1}{2} |a_{x,t}|^2 \right]\right), \end{aligned} \quad (3.72)$$

where  $\tilde{A}(1, a_t)$  is a short-hand notation for the function of the  $\bar{a}$ 's and the  $a$ 's obtained by replacing all  $\hat{a}^+$  operators by their corresponding eigenvalues  $\bar{a}$  and all  $\hat{a}$  operators by their eigenvalues  $a$ , and finally setting all  $\bar{a}$  to unity. Finally, after taking the continuum limit, we arrive at:

$$\langle A \rangle_T = \int \mathcal{D}\bar{a} \mathcal{D}a \tilde{A}(1, a(x, T)) \langle a(x, 0)|\Psi\rangle_{t=0} e^{-S[\bar{a}, a]}, \quad (3.73)$$

$$S[\bar{a}, a] = \int_x (|a(x, 0)|^2 - a(x, T)) + \int_0^T \int_x (\bar{a}(x, t) \partial_t a(x, t) - \tilde{W}(\bar{a}(x, t), a(x, t))). \quad (3.74)$$

We thus have found a field theory representation of our stochastic process. In the same way as above, we have had to normal order the operator  $\hat{W}$  to be able to easily calculate the matrix elements  $\langle a_{t_i}|\hat{W}|a_{t_{i-1}}\rangle$ , and we denoted the resulting function of  $\bar{a}$  and  $a$  by  $\tilde{W}(\bar{a}(x, t), a(x, t))$ . Note that the  $\bar{a}$ 's always have to be calculated at an earlier time than the  $a$ 's, a distinction which has disappeared when taking the continuum limit, but has to be remembered when calculating functions at equal times in this formalism. This is the equivalent of the Itô's interpretation of the Langevin equation.

### 3.2.3 Cole-Hopf transformation

Since the representation in terms of a master equation is fully equivalent to the Langevin equation in Eq.(3.3), all this procedure is for now only a complicated way to reformulate an existing theory. A Cole-Hopf change of variables (first introduced to deal with the Burgers equation in fluid mechanics [44, 78]) defined by:

$$\begin{cases} \bar{a}(x, t) & \rightarrow \exp(\bar{\rho}(x, t)) \\ a(x, t) & \rightarrow \rho(x, t) \exp(-\bar{\rho}(x, t)) \end{cases} \quad (3.75)$$

will lead exactly to the action Eq.(3.17). The terms involving the pair potential that come from the evolution operator  $\hat{W}$  will be obvious since they will depend only on  $\bar{a}a$  which becomes  $\rho$  in this change of variables. Let us look at the other bulk terms. We see that they transform exactly into the ideal gas part of the action in Eq.(3.17):

$$\int_0^T \int_x \bar{a}(x, t) (\partial_t - \nabla_x^2) a(x, t) \rightarrow \int_0^T \int_x [\bar{\rho}(x, t) (\partial_t - \nabla_x^2) \rho(x, t) - \rho(x, t) (\nabla_x \bar{\rho}(x, t))^2] \quad (3.76)$$

up to boundary terms. This change of formulation, although mathematically equivalent to the Langevin formulation is very convenient since we see that the ideal gas part of the problem is now represented by a quadratic action, which is trivially solvable, whereas in the Langevin representation, an analysis in terms of causality of the diagrams must be performed. What about the time reversal?

The transformation Eq.(3.29) when considered for the case of non-interacting particles simply becomes:

$$\begin{cases} a(x, -t) & \rightarrow \bar{a}(x, t) \\ \bar{a}(x, -t) & \rightarrow a(x, t) \end{cases}, \quad (3.77)$$

which is a linear transformation. However the interacting part of the free-energy involved in the transformation makes the symmetry look more complicated, giving:

$$\begin{cases} a(x, -t) & \rightarrow \bar{a}(x, t) \\ \bar{a}(x, -t) & \rightarrow a(x, t) \exp\left(\int_y \beta v(x-y) \bar{a}(y, t) a(y, t)\right) \end{cases} \quad (3.78)$$

We see that in this new formulation, all the difficulty of conserving the time-reversal is now contained in the interacting part of the problem. In a sense this second quantized form has solved one of our problems, the ideal gas contribution, but not yet the other one: the non-linear expression of the time-reversal.

### 3.2.4 An alternative linearization of the time-reversal

In order to render time-reversal a linear invariance, we can make use of the well-known similarity transformation [167], that corresponds in our formalism to a rotation in the Fock space:

$$|\Psi\rangle \rightarrow \hat{P}_{\text{eq}}^{1/2} |\Psi\rangle, \quad (3.79)$$

where  $\hat{P}_{\text{eq}}$  is the canonical quantized form of  $P_{\text{eq}}(\mathcal{C})$ , i.e.:

$$\hat{P}_{\text{eq}} = \exp\left(\frac{1}{2} \sum_{x \neq y} \hat{n}_x w(x-y) \hat{n}_y\right). \quad (3.80)$$

This has the effect of modifying the evolution operator as follows:

$$\hat{W} \rightarrow \hat{W}_{\text{sym}} \equiv \hat{P}_{\text{eq}}^{-1/2} \hat{W} \hat{P}_{\text{eq}}^{1/2}, \quad (3.81)$$

$$\hat{W}_{\text{sym}} = \sum_{x \in \mathcal{L}} \sum_e \left[ \hat{a}_x^+ \hat{a}_{x+e} - \hat{a}_x^+ \hat{a}_x e^{-\frac{\beta V(e)}{2}} e^{-\frac{\beta}{2} \Delta \hat{E}_p} \right]. \quad (3.82)$$

Taking the continuum limit, which we define as:

$$\left\{ \begin{array}{ll} \hat{a}_x & \rightarrow \hat{a}(x) a^{3/2} \\ \hat{a}_x^+ & \rightarrow \hat{a}^+(x) a^{3/2} \\ \hat{n}_x & \rightarrow \hat{n}(x) a^3 \\ \sum_{y \neq x} a^3 & \rightarrow \int_y \end{array} \right. \quad (3.83)$$

and expanding the exponentials to second order in the lattice spacing leads to the following evolution equation:

$$\left\{ \begin{array}{l} \partial_t |\Psi\rangle = \hat{W}_{\text{sym}} |\Psi\rangle \\ \hat{W}_{\text{sym}} = e^2 \int_x (\hat{a}^+(x, t) \partial_x^2 \hat{a}(x, t) - U_{\text{eff}}[\hat{n}](x, t)) \\ U_{\text{eff}}[\hat{n}](x, t) = \frac{1}{4} \hat{n}(x, t) \int_{y, z} \partial_y \hat{n}(y, t) \cdot \partial_z \hat{n}(z, t) w(x-y) w(x-z) - \frac{1}{2} \hat{n}(x, t) \int_y \partial_y^2 \hat{n}(y) w(x-y) \end{array} \right. \quad (3.84)$$

The appearance of the effective potential  $U_{\text{eff}}$  is at this stage very satisfying. Indeed this quantity can be seen as the local rate of escaping from a state, and therefore seems to be a good dynamical quantity in terms of which formulating our dynamical theory. Following the procedure described earlier, Eq.(3.82) leads to a field theory in the continuum in terms of the two fields  $\bar{a}$  and  $a$  that read:

$$Z = \int \mathcal{D}\bar{a} \mathcal{D}a e^{-S[\bar{a}, a]}, \quad (3.85)$$

$$S[\bar{a}, a] = \int_{x, t} [\bar{a}(x, t) (\partial_t - \nabla_x^2) a(x, t) + U_{\text{eff}}[\bar{a}(x, t) a(x, t)]]. \quad (3.86)$$

A drawback of this formulation is that the density  $\bar{a}a$  is not the physical density, unless we place ourselves in the bulk of time: it is easily seen from Eq.(3.71) that the only modification due to the rotation that we performed is in the initial and final terms in the time discretization. The averages in the functional integral will thus correspond to the physical averages only if we send the initial time in the far past and the final observation time in the far future.

What has time-reversal become in this formalism ? Now, thanks to the symmetrization of the evolution operator, the dynamics can fully be interpreted as a quantum mechanical evolution (albeit in imaginary time), and time reversal is simply guaranteed by the symmetry of the action upon exchange of  $\bar{a}$  and  $a$ , i.e. we are back to the much simpler symmetry:

$$\left\{ \begin{array}{ll} \bar{a}(x, -t) & \rightarrow a(x, t) \\ a(x, -t) & \rightarrow \bar{a}(x, t) \end{array} \right. , \quad (3.87)$$

which is finally a linear symmetry. Thus the second of our problems is settled, and we can now safely perform a diagrammatic analysis of our theory. The strength of the interactions will be taken as an

expansion parameter, and since all the non-quadratic parts of the action depend only on  $\bar{a}a$  through the effective potential  $U_{\text{eff}}$ , we are guaranteed never to break the time-reversal symmetry.

A last problem that has to be dealt with is the fact that we want to compute a density-density correlation function, which in our formalism is a four-point function. We dealt with that by constraining  $\bar{a}a$  to be equal to  $\rho$  by a Lagrange multiplier  $\lambda(x, t)$ :

$$Z = \int \mathcal{D}\bar{a}\mathcal{D}a e^{-\int_{x,t} \bar{a}(x,t)(\partial_t - \nabla_x^2)a(x,t)} \int \mathcal{D}\rho \delta(\rho - \bar{a}a) e^{-\int_{x,t} U_{\text{eff}}[\rho(x,t)]} \quad (3.88)$$

$$= \int \mathcal{D}\bar{a}\mathcal{D}a\mathcal{D}\rho\mathcal{D}\lambda e^{-S[\bar{a},a,\rho,\lambda]}, \quad (3.89)$$

$$S[\bar{a}, a, \rho, \lambda] = \int_{x,t} \left( \bar{a}(x,t) (\partial_t - \nabla_x^2) a(x,t) + \lambda(x,t) [\rho(x,t) - \bar{a}(x,t)a(x,t)] + U_{\text{eff}}[\rho(x,t)] \right) \quad (3.90)$$

Introducing by hand the density has had the effect of adding a new cubic vertex in the action. Finally we are left with a four-field theory that contains two cubic interaction vertices, which is a much simpler situation than in the case of the Langevin representation, since in that case there is an infinity of interacting vertices in the action, that must be manipulated with care in order to take properly into account the non-interacting particles. The advantages of our formulation are two-fold:

- The ideal gas case is the natural starting point of the perturbative expansion, thus will be correct at all order of approximation, and the strength of the interactions will serve as an organizing device for the diagrammatic expansion
- The time-reversal is a ‘‘rapidity’’ symmetry between  $\bar{a}$  and  $a$ , and the introduction of the density  $\rho = \bar{a}a$  ensures that these two fields will always play a symmetric role when truncations will be performed

### 3.3 Fredrickson-Andersen model

The Fredrickson-Andersen (FA) model [67, 68] is a model of independent spins on a lattice that have two states, up and down, or zero and one, whose dynamics is constrained by a dynamical rule saying that a spin can flip only if one of its neighbors is in the up state. This model represents a coarse grained version of structural glasses. If one considers that the glass transition is a purely dynamical phenomenon, it must have a finite static correlation length. One then separates the system into cells of size of the order of this length, and consider these cells as independent at equilibrium. However, dynamically, one supposes that for a rearrangement to occur in one given cell (for a spin to flip), at least one of the neighboring cells must be in a mobile state (spin up). It is the idea of dynamical facilitation [145].

These models are called a kinetically constrained model, and although they usually have trivial thermodynamics, as a consequence of the kinetic constraints, their dynamics can reproduce various aspects of the glassy dynamics.

We study the FA model only as a toy model, in which the statics are trivial, and the dynamics present glassy features. We will see that in terms of field theory it will correspond to a simplification of the interaction terms when compared to the complicated case of interacting particles in Eq.(3.90). We will thus use this model as a benchmark for our method. The following is yet unpublished material.

### 3.3.1 The model: dynamics without the statics

We start from the standard action in the Doi-Peliti formalism for the FA model [172], and symmetrize it using the similarity transformation described in the previous section. We obtain as a starting point the following field theory:

$$S[\bar{a}, a] = \int_{x,t} \left[ \bar{a} (\partial_t - \Delta) a + \zeta \bar{a} a + \bar{a}^2 a^2 - \sqrt{\zeta} \bar{a} a (\bar{a} + a) \right]. \quad (3.91)$$

Introducing the density, we get:

$$S[\bar{a}, a, \lambda, \rho] = \int_{x,t} \left[ \bar{a} (\partial_t - \Delta) a + \zeta \bar{a} a + \rho^2 - \sqrt{\zeta} \rho (\bar{a} + a) + \lambda (\bar{a} a - \rho) \right]. \quad (3.92)$$

In the following, we will group the four fields in a vector  $\varphi_i(1)$ , defined by:

$$\varphi(1) \equiv \begin{pmatrix} a(x, t) \\ \bar{a}(x, t) \\ \lambda(x, t) \\ \rho(x, t) \end{pmatrix} \quad (3.93)$$

The propagators are defined as  $G_{ij}(1, 2) \equiv \langle \varphi_i(1) \varphi_j(2) \rangle - \langle \varphi_i(1) \rangle \langle \varphi_j(2) \rangle$ .

#### Consequences of time-reversal

As described in the previous section, the time-reversal symmetry of the action reads:

$$\begin{cases} a(x, t) \rightarrow \bar{a}(x, -t) \\ \bar{a}(x, t) \rightarrow a(x, -t) \\ \lambda(x, t) \rightarrow \lambda(x, -t) \\ \rho(x, t) \rightarrow \rho(x, -t) \end{cases} \quad (3.94)$$

This symmetry has consequences on the propagators, expressed in the Fourier space for space directions and real space for the time direction:

$$\begin{cases} G_{11}(k, \tau) = G_{22}(k, \tau) \\ G_{13}(k, \tau) = G_{23}(k, -\tau) \\ G_{14}(k, \tau) = G_{24}(k, -\tau) \\ G_{34}(k, \tau) = G_{34}(k, -\tau) \end{cases}, \quad (3.95)$$

We introduce a source term  $J$  for the fields, and define as in Chapter 2 the functional  $\Gamma$ , the Legendre transform of the logarithm of the partition function with respect to  $J$ . Defining as  $\phi$  the means of the fields, the functional derivatives of  $\Gamma$  with respect to  $\phi$  are defined as:

$$\Gamma_i^{(1)}(1) \equiv \frac{\delta \Gamma[\phi]}{\delta \phi_i(1)}, \quad (3.96)$$

$$\Gamma_{ij}^{(2)}(1, 2) \equiv \frac{\delta^2 \Gamma[\phi]}{\delta \phi_i(1) \delta \phi_j(2)}. \quad (3.97)$$

The time reversal has the same consequences on the two-point functions  $\Gamma^{(2)}$  than on  $G$ :

$$\begin{cases} \Gamma_{11}^{(2)}(k, \tau) = \Gamma_{22}^{(2)}(k, \tau) \\ \Gamma_{13}^{(2)}(k, \tau) = \Gamma_{23}^{(2)}(k, -\tau) \\ \Gamma_{14}^{(2)}(k, \tau) = \Gamma_{24}^{(2)}(k, -\tau) \\ \Gamma_{34}^{(2)}(k, \tau) = \Gamma_{34}^{(2)}(k, -\tau) \end{cases}, \quad (3.98)$$

### Averages of the field and mean-field approximation

The derivative of the action is:

$$\frac{\delta S[\varphi]}{\delta \varphi(1)} = \begin{pmatrix} [-\partial_t - \Delta_x + \zeta + \lambda(1)] \bar{a}(1) - \sqrt{\zeta} \rho(1) \\ [-\partial_t - \Delta_x + \zeta + \lambda(1)] a(1) - \sqrt{\zeta} \rho(1) \\ \bar{a}(1) a(1) - \rho(1) \\ 2\rho(1) - \sqrt{\zeta} [\bar{a}(1) + a(1)] - \lambda(1) \end{pmatrix} \quad (3.99)$$

The saddle-point is defined by the value of  $\varphi$  where this derivative is zero. We assume translational invariance, so that means of fields are independent of space and time, to obtain:

$$\begin{cases} a = \bar{a} = \sqrt{\zeta} \\ \lambda = 0 \\ \rho = \zeta \end{cases} \quad (3.100)$$

Shifting the fields by their mean field values, we find that the propagator of the theory is:

$$G_0(k, \omega) = \frac{1}{\omega^2 + \Omega^2} \begin{pmatrix} 0 & -i\omega + \Omega & \sqrt{\zeta}(-i\omega + \Omega) & \sqrt{\zeta}(-i\omega + \Omega) \\ i\omega + \Omega & 0 & \sqrt{\zeta}(i\omega + \Omega) & \sqrt{\zeta}(i\omega + \Omega) \\ \sqrt{\zeta}(i\omega + \Omega) & \sqrt{\zeta}(-i\omega + \Omega) & -2(\omega^2 + \Omega^2) + 2\zeta\Omega & -(\omega^2 + \Omega^2) + 2\zeta\Omega \\ \sqrt{\zeta}(i\omega + \Omega) & \sqrt{\zeta}(-i\omega + \Omega) & -(\omega^2 + \Omega^2) + 2\zeta\Omega & 2\zeta\Omega \end{pmatrix}, \quad (3.101)$$

which reads, in the real time domain:

$$G_0(k, \tau) = \begin{pmatrix} 0 & \theta(\tau) & \sqrt{\zeta}\theta(\tau) & \sqrt{\zeta}\theta(\tau) \\ \theta(-\tau) & 0 & \sqrt{\zeta}\theta(-\tau) & \sqrt{\zeta}\theta(-\tau) \\ \sqrt{\zeta}\theta(-\tau) & \sqrt{\zeta}\theta(\tau) & -2e^{\Omega|\tau|} + \zeta & -e^{\Omega|\tau|} + \zeta \\ \sqrt{\zeta}\theta(-\tau) & \sqrt{\zeta}\theta(\tau) & -e^{\Omega|\tau|} + \zeta & \zeta \end{pmatrix} e^{-\Omega|\tau|} \quad (3.102)$$

We see that, concerning the fields  $a$ ,  $\bar{a}$  and  $\lambda$ , we have a causal structure of the bare propagator. In the very same way than the analysis performed in the case of the MSR formalism, an analysis of the diagrams that may renormalize  $G_{13}$  at all order of perturbation shows that all corrections to  $G_{13}(k, \tau)$  remain proportional to  $\theta(\tau)$ . By symmetry, it is the same for  $G_{23}$ , and the analysis can be carried for  $G_{12}$  also, leading to the same result.

Since, for the Doi-Peliti construction we used, the action Eq. (3.92) must be understood in Itô's sense, we must conclude that  $G_{12}$ ,  $G_{13}$  and  $G_{23}$  must be zero when evaluated at equal times.

We can compute evolution equations for the average fields by exploiting the fact that, when the source  $J$  is set to zero, we have:

$$\left\langle \frac{\delta S[\varphi]}{\delta \varphi(1)} \right\rangle = 0, \quad (3.103)$$

which gives four evolution equations:

$$\begin{cases} \sqrt{\zeta} \rho = (\zeta + \lambda) \bar{a} + G_{23}(1, 1) \\ \sqrt{\zeta} \rho = (\zeta + \lambda) a + G_{13}(1, 1) \\ \rho = \bar{a} a + G_{12}(1, 1) \\ \lambda = 2\rho - \sqrt{\zeta} (\bar{a} + a) \end{cases} \quad (3.104)$$

The rapidity symmetry imposes that  $\bar{a} = a$  and  $G_{13}(1, 1) = G_{23}(1, 1) = G_{12}(1, 1) = 0$  by causality so we are left with:

$$\begin{cases} a = \bar{a} = \sqrt{\zeta} \\ \lambda = 0 \\ \rho = \zeta \end{cases}, \quad (3.105)$$

i.e. the mean-field averages are exact at all order of perturbation.

### Interaction vertices

Defining  $\varphi = (a - \sqrt{\zeta}, \bar{a} - \sqrt{\zeta}, \lambda, \rho - \zeta)$ , the field theory reads:

$$Z = \int \mathcal{D}\varphi e^{-\frac{1}{2} \int_{1,2} \varphi(1) G_0^{-1}(1,2) \varphi(2) - S_{\text{ng}}[\varphi]}, \quad (3.106)$$

$$G_0^{-1}(k, \tau) \equiv \begin{pmatrix} 0 & [-\partial_\tau + k^2 + \zeta] & \sqrt{\zeta} & -\sqrt{\zeta} \\ [\partial_\tau + k^2 + \zeta] & 0 & \sqrt{\zeta} & -\sqrt{\zeta} \\ \sqrt{\zeta} & \sqrt{\zeta} & 0 & -1 \\ -\sqrt{\zeta} & -\sqrt{\zeta} & -1 & 2 \end{pmatrix}, \quad (3.107)$$

$$S_{\text{ng}}[\varphi] = \int_{x,t} \varphi_3(x,t) \varphi_1(x,t) \varphi_2(x,t). \quad (3.108)$$

We see now that this model has the very same structure than the interacting particles, but without the interaction term coming from the pair potential, which involves the density field  $\varphi_4$ . Here the absence of this term will greatly simplify the formalism. However, this suppresses the possibility of organizing the diagrammatic expansion in powers of the pair potential.

### 3.3.2 Building self-consistent equations for correlation functions

Following the prescription of Chapter 2, we will write self-consistent equations on the two-point functions by performing the double Legendre transformation. We define the vertex functions  $\Sigma$ :

$$\Sigma \equiv \begin{pmatrix} \Sigma_{11} & \Sigma_{12} & \Sigma_{13} & \Sigma_{14} \\ \Sigma_{21} & \Sigma_{22} & \Sigma_{23} & \Sigma_{24} \\ \Sigma_{31} & \Sigma_{32} & \Sigma_{33} & \Sigma_{34} \\ \Sigma_{41} & \Sigma_{42} & \Sigma_{43} & \Sigma_{44} \end{pmatrix} \quad (3.109)$$

By definition  $G_0^{-1} - \Sigma$  is the inverse of the full (unknown) propagator  $G$  of the system. A self consistent equation for  $G$  is obtained by resorting to the stationary condition of the Legendre transform Eq.(2.114), which gives an expression of  $\Sigma$  as a function of  $G$ , and then inserting this expression in the Dyson equation:

$$(G_0^{-1} - \Sigma)G = 1 \quad (3.110)$$

$\Sigma$  is bound to respect the symmetries of the action, so that it simplifies its matrix composition:

$$\Sigma \equiv \begin{pmatrix} \Sigma_{11} & \Sigma_{12} & \Sigma_{13} & \Sigma_{14} \\ \Sigma_{12}^+ & \Sigma_{11} & \Sigma_{13}^+ & \Sigma_{14}^+ \\ \Sigma_{13}^+ & \Sigma_{13} & \Sigma_{33} & \Sigma_{34} \\ \Sigma_{14}^+ & \Sigma_{14} & \Sigma_{34} & \Sigma_{44} \end{pmatrix}, \quad (3.111)$$

where the superscript  $\cdot^+$  denotes time-reversed quantities.



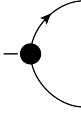


The diagrams above must be understood with the following convention:

$$\bar{a}(k, t_1) - \sqrt{\zeta} \equiv \leftarrow \bigcirc \quad (3.123)$$

$$a(k, t_1) - \sqrt{\zeta} \equiv \text{---} \bigcirc \quad (3.124)$$

$$l(k, t_1) \equiv - - \bigcirc \quad (3.125)$$

$$\int_{k_1, k_2, k_3} \delta_{k_1+k_2+k_3} \lambda(k_1, t) (\bar{a}(k, t_1) - \sqrt{\zeta}) (a(k, t_1) - \sqrt{\zeta}) \equiv - \bullet \quad (3.126)$$


$$G_{11}(k, t) \equiv \bigcirc \text{---} \bigcirc \quad (3.127)$$

$$G_{12}(k, t) \equiv \bigcirc \leftarrow \bigcirc \quad (3.128)$$

$$G_{13}(k, t) \equiv \bigcirc \text{---} - \bigcirc \quad (3.129)$$

$$G_{22}(k, t) \equiv \bigcirc \rightarrow \leftarrow \bigcirc \quad (3.130)$$

$$G_{23}(k, t) \equiv \bigcirc \rightarrow - \bigcirc \quad (3.131)$$

$$G_{33}(k, t) \equiv \bigcirc - - - \bigcirc \quad (3.132)$$

The natural thing to do in a field-theoretic context would be then to compute the first correction to mean-field in terms of all the propagators and look at the result for  $G_{44}$ . However, in order to understand the structure of the Mode-Coupling theory, we are interested in obtaining an equation solely on  $G_{44}$ , that leads us to perform another approximation allowing us to replace all the  $G_{ij}$ s with  $(i, j) \neq (4, 4)$  in terms of  $G_{44}$ . This step is rather arbitrary in the context on the FA model, but will take its sense in the context of particle systems.

At the level of mean-field, all propagators are proportional to  $G_{44}$ , as can be seen in Eq.(3.102), and we will use these relations in order to eliminate them in favor of  $G_{44}$ :

$$G_{11}(k, \tau) = G_{22}(k, \tau) = 0, \quad (3.133)$$

$$G_{13}(k, \tau) = \frac{1}{2\sqrt{\zeta}\Omega(k)} [-\partial_\tau + \Omega(k)] G_{44}(k, \tau), \quad (3.134)$$

$$G_{23}(k, \tau) = \frac{1}{2\sqrt{\zeta}\Omega(k)} [\partial_\tau + \Omega(k)] G_{44}(k, \tau), \quad (3.135)$$

$$G_{12}(k, \tau) = \frac{1}{2\zeta\Omega(k)} [-\partial_\tau + \Omega(k)] G_{44}(k, \tau), \quad (3.136)$$

$$G_{33}(k, \tau) = -2\delta(\tau) + G_{44}(k, \tau), \quad (3.137)$$

$$G_{14}(k, \tau) = \frac{1}{2\sqrt{\zeta}\Omega(k)} [-\partial_\tau + \Omega(k)] G_{44}(k, \tau) \quad (3.138)$$

Furthermore, we observe that, when neglecting all vertex functions, we have the following relations:

$$G_{44}(k, \tau) = \zeta e^{-\Omega(k)|\tau|}, \quad (3.139)$$

$$\Rightarrow \begin{cases} G_{44}(k, \tau) = -\frac{1}{\Omega(k)} s(\tau) \partial_\tau G_{44}(k, \tau) \\ [\partial_\tau + \Omega(k)] G_{44}(k, \tau) = 2\theta(-\tau)\Omega(k)G_{44}(k, \tau) \\ [-\partial_\tau + \Omega(k)] G_{44}(k, \tau) = 2\theta(\tau)\Omega(k)G_{44}(k, \tau) \end{cases} \quad (3.140)$$

Which induce:

$$\begin{cases} G_{11}(k, \tau) = G_{22}(k, \tau) = 0, \\ G_{13}(k, \tau) = \frac{1}{\sqrt{\zeta}}\theta(\tau)G_{44}(k, \tau), \\ G_{23}(k, \tau) = \frac{1}{\sqrt{\zeta}}\theta(-\tau)G_{44}(k, \tau), \\ G_{12}(k, \tau) = \frac{1}{\zeta}\theta(\tau)G_{44}(k, \tau), \\ G_{33}(k, \tau) = -2\delta(\tau) + G_{44}(k, \tau), \\ G_{14}(k, \tau) = -\frac{1}{\sqrt{\zeta}\Omega(k)}\theta(\tau)G_{44}(k, \tau) \end{cases} \quad (3.141)$$

Replacing these relations in the diagrammatic expressions of the  $\Sigma_{ij}$ s, we obtain:

$$\begin{cases} \Sigma_{12}(k, \tau) = \frac{2}{\zeta}\theta(-\tau) \int_q G_{44}(k-q, \tau)G_{44}(q, \tau) \\ \Sigma_{ij}(k, \tau) = 0 \quad \text{if } (i, j) \neq (1, 2) \end{cases} \quad (3.142)$$

We thus see that:

$$\begin{aligned} [ ]_{14} &= \int_{t'} \Sigma_{12}(k, t')G_{14}^+(k, t-t') \\ &= \frac{2}{\zeta^{3/2}} \int_{t'} \theta(-t')\theta(t'-t) \int_q G_{44}(k-q, t')G_{44}(q, t')G_{44}(k, t-t') \\ &= 0 \end{aligned} \quad (3.143)$$

$$\begin{aligned} [ ]_{24} &= \int_{t'} \Sigma_{12}^+(k, t')G_{14}(k, t-t') \\ &= \frac{2}{\zeta^{3/2}} \int_{t'} \theta(t')\theta(t-t') \int_q G_{44}(k-q, t')G_{44}(q, t')G_{44}(k, t-t') \end{aligned} \quad (3.144)$$

$$= \frac{2}{\zeta^{3/2}} \int_0^t dt' \int_q G_{44}(k-q, t')G_{44}(q, t')G_{44}(k, t-t') \quad (3.145)$$

$$[ ]_{ij} = 0 \quad \text{otherwise} \quad (3.146)$$

Inserting these relations in Eq. (3.116), we get:

$$2\zeta\Omega(k)\delta(\tau) = [-\partial_\tau^2 + \Omega(k)^2] G_{44}(k, \tau) + \frac{4}{\zeta} \int_0^t dt' \int_q G_{44}(k-q, t-t')G_{44}(q, t-t')\partial_{t'} G_{44}(k, t'), \quad (3.147)$$

which has the structure of a Mode-Coupling equation, albeit with a trivial kernel, which is due to the trivial statics of this particular model.

Suppose that the two-point correlation function can have a non-zero value at  $t \rightarrow \infty$ , which would signal a loss of ergodicity. Then we can obtain an equation on the non-ergodicity factor by Laplace transform. Defining:

$$G_{44}(k, t) = f(k)G_{44}(k, t=0) + g(k, t), \quad (3.148)$$

with  $g$  a function that decreases to 0 for  $t \rightarrow \infty$ , for all  $k$ . We get in that case:

$$\frac{f(k)}{1-f(k)} = \frac{4}{\zeta\Omega(k)^2} \int_q G_{44}(q, t=0)G_{44}(k-q, t=0)f(q)f(k-q). \quad (3.149)$$

At  $t=0$ , the correlation function takes its equilibrium value, which is:

$$G_{44}(k, t=0) = \zeta. \quad (3.150)$$

We obtain an equation for  $f^* = f(k=0)$ :

$$\frac{f^*}{1-f^*} = \frac{4}{\zeta} f^{*2}, \quad (3.151)$$

which has a trivial solution  $f^* = 0$ , but also, for  $\zeta \leq 1$ , two solutions:

$$f^* = \frac{1 \pm \sqrt{1-\zeta}}{2} \quad (3.152)$$

This analysis shows that by a well defined set of approximations, a Mode-Coupling like equation can be found. This procedure is directly applicable to the case of interacting particles, as we show below, but provides a very compact formalism when compared to the only existing field-theory approach, that of Kawasaki and Kim [91].

It was shown in [173, 158] that the slow dynamics of the FA model are governed by a zero-temperature fixed point, whereas the initial predictions of Fredrickson and Andersen [68] was a divergence at finite temperature of the relaxation time of the system.

The transition predicted by our theory is thus spurious. Indeed, this is a consequence of the absence of small parameter in the theory, that made our approximations quite unjustified. However, this encourages us to apply now this method to the case of particle systems, where the strength of the interaction can be used as an organizing device for the perturbation expansion.

## 3.4 Application to harmonic spheres

Now that we presented the approximation method in a simplified model, we present here its application in the case of the dynamics of harmonic spheres, or any equivalent pair potential that has a repulsive finite-range interaction. The steps of the derivation are essentially the same, but complicated by the appearance of a second interaction vertex that depends on the pair potential, and with a modification of the bare action. A conceptual difference with the derivation above is that the pair potential naturally serves as an expansion parameter around the ideal-gas contribution.

### 3.4.1 Diagrammatic structure and time-reversal

The time-reversal transformation is unchanged when compared to the FA case, so that Eqs.(3.95) and (3.98) hold. The mean values of the fields are now constrained, since the density is a conserved quantity, so that we have at all times:

$$\langle a(x, t) \rangle = \langle \bar{a}(x, t) \rangle = \sqrt{\rho_0}, \quad (3.153)$$

$$\langle \rho(x, t) \rangle = \rho_0, \quad (3.154)$$

$$\langle \lambda(x, t) \rangle = \langle \bar{\rho}(x, t) \rangle = 0. \quad (3.155)$$

Expanding the action Eq.(3.90) around these saddle point solutions, we get the expression of the inverse bare propagator for our system of particles:

$$G_0^{-1}(k, \tau) = \begin{pmatrix} 0 & \partial_\tau + k^2 & -\sqrt{\rho_0} & 0 \\ -\partial_\tau + k^2 & 0 & -\sqrt{\rho_0} & 0 \\ -\sqrt{\rho_0} & -\sqrt{\rho_0} & 0 & 1 \\ 0 & 0 & 1 & u(k) \end{pmatrix}, \quad (3.156)$$

with

$$u(k) = \frac{k^2}{2\rho_0} \left[ (1 + \beta\rho_0 v(k))^2 - 1 \right]. \quad (3.157)$$

There is now an additional vertex in the theory, that contains the pair potential. Diagrammatically, the fields are defined as:

$$\bar{a}(k, t_1) - \sqrt{\rho_0} \equiv \leftarrow \bigcirc \quad (3.158)$$

$$a(k, t_1) - \sqrt{\rho_0} \equiv \bigcirc \quad (3.159)$$

$$\lambda(k, t_1) \equiv - - \bigcirc \quad (3.160)$$

$$\rho(k, t) - \rho_0 \equiv \text{wavy} \bigcirc, \quad (3.161)$$

the interaction vertices as:

$$\int_{k_1, k_2, k_3} \delta_{k_1+k_2+k_3} \lambda(k_1, t) (\bar{a}(k, t_1) - \sqrt{\zeta}) (a(k, t_1) - \sqrt{\zeta}) \equiv - - \bullet \quad (3.162)$$

$$\int_{k_1, k_2, k_3} \delta_{k_1+k_2+k_3} (\rho(k_1, t) - \rho_0) (\rho(k_2, t_1) - \sqrt{\rho_0}) (a(k_3, t_1) - \sqrt{\rho_0}) \equiv \text{wavy} \bullet \quad (3.163)$$

and the propagators as:

$$G_{11}(k, t) \equiv \bigcirc \text{---} \bigcirc \quad (3.164)$$

$$G_{12}(k, t) \equiv \bigcirc \leftarrow \bigcirc \quad (3.165)$$

$$G_{13}(k, t) \equiv \bigcirc \text{---} - \bigcirc \quad (3.166)$$

$$G_{14}(k, t) \equiv \bigcirc \text{---} \text{wavy} \bigcirc \quad (3.167)$$

$$G_{22}(k, t) \equiv \bigcirc \rightarrow \bigcirc \quad (3.168)$$

$$G_{23}(k, t) \equiv \bigcirc \rightarrow - \bigcirc \quad (3.169)$$

$$G_{24}(k, t) \equiv \bigcirc \rightarrow \text{wavy} \bigcirc \quad (3.170)$$

$$G_{33}(k, t) \equiv \bigcirc - - \bigcirc \quad (3.171)$$

$$G_{34}(k, t) \equiv \bigcirc - - \text{wavy} \bigcirc \quad (3.172)$$

$$G_{44}(k, t) \equiv \bigcirc \text{wavy} \bigcirc. \quad (3.173)$$

### 3.4.2 Mori-Zwanzig equation

Now we can write the equivalent of Eq.(3.116), i.e. the Mori-Zwanzig equation for the density density correlation function by the very same procedure to obtain:

$$\delta(\tau) = \frac{1}{2\rho_0 k^2} (-\partial_\tau^2 + \Omega(k)^2) G_{44}(k, \tau) - [ ]_{44} - \frac{-\partial_\tau^2 + k^4}{2\rho_0 k^2} [ ]_{34} - \frac{\partial_\tau + k^2}{2\sqrt{\rho_0} k^2} [ ]_{24} - \frac{-\partial_\tau + k^2}{2\sqrt{\rho_0} k^2} [ ]_{14}, \quad (3.174)$$



All propagators verify a Mori-Zwanzig equation such as Eq.(3.175) that relates them to  $G_{44}$  at lowest order, with loop corrections that depend on  $\Sigma$ , in the same way as in the case of the FA model. The expression of the inverse propagator is rather complicated, but we will only need it at the lowest order in  $\varepsilon$ . Setting  $\varepsilon = 0$  gives:

$$G_0(k, \tau) = \frac{1}{\rho_0} \begin{pmatrix} 0 & \theta(-\tau) & 0 & \sqrt{\rho_0}\theta(-\tau) \\ \theta(\tau) & 0 & 0 & \sqrt{\rho_0}\theta(\tau) \\ 0 & 0 & 0 & 0 \\ \sqrt{\rho_0}\theta(\tau) & \sqrt{\rho_0}\theta(-\tau) & 0 & 1 \end{pmatrix} G_{44}(k, \tau) \quad (3.183)$$

Using the lowest order diagrams combined with the lowest order expressions of the propagators in function of  $G_{44}$ , we get that all vertex corrections can be expressed as integrals of memory kernels multiplied by density-density correlation functions:

$$\Sigma_{ij}(k, \tau) = \int_q \mathcal{M}_{ij}(k, q, \tau) G_{44}(q, \tau) G_{44}(k - q, \tau), \quad (3.184)$$

with the memory kernels given by:

$$\mathcal{M}_{11}(k, q, \tau) = -\frac{\varepsilon(q)\varepsilon(k-q)}{4\rho_0^3} [q^4\varepsilon(q) + (k-q)^4\varepsilon(k-q)], \quad (3.185)$$

$$\mathcal{M}_{12}(k, q, \tau) = \frac{\theta(\tau)}{2\rho_0^3} [q^2\varepsilon(q) + (k-q)^2\varepsilon(k-q)]^2, \quad (3.186)$$

$$\mathcal{M}_{13}(k, q, \tau) = \frac{\theta(\tau)}{4\rho_0^{5/2}} [\varepsilon(k-q) - \varepsilon(q)] [q^2\varepsilon(q) - (k-q)^2\varepsilon(k-q)], \quad (3.187)$$

$$\mathcal{M}_{14}(k, q, \tau) = \frac{\theta(\tau)}{4\rho_0^{3/2}} [k \cdot q\varepsilon(k)\varepsilon(q) + k \cdot (k-q)\varepsilon(k)\varepsilon(k-q) - q \cdot (k-q)\varepsilon(q)\varepsilon(k-q)] \quad (3.188)$$

$$[q^2\varepsilon(q) + (k-q)^2\varepsilon(k-q)]. \quad (3.189)$$

$$\mathcal{M}_{33}(k, q, \tau) = \frac{1}{8\rho_0^2} [\varepsilon(q) + \varepsilon(k-q)]^2, \quad (3.190)$$

$$\mathcal{M}_{34}(k, q, \tau) = \frac{1}{4\rho_0} [k \cdot q\varepsilon(k)\varepsilon(q) + k \cdot (k-q)\varepsilon(k)\varepsilon(k-q) - q \cdot (k-q)\varepsilon(q)\varepsilon(k-q)] [\varepsilon(q) + \varepsilon(k-q)], \quad (3.191)$$

$$\mathcal{M}_{44}(k, q, \tau) = \frac{1}{2} [k \cdot q\varepsilon(k)\varepsilon(q) + k \cdot (k-q)\varepsilon(k)\varepsilon(k-q) - q \cdot (k-q)\varepsilon(q)\varepsilon(k-q)]^2, \quad (3.192)$$

$$(3.193)$$

We see that all vertex functions are proportional at least to  $\varepsilon^2$ , even when evaluating the propagators at zero order in the potential. Therefore the relations between propagators that we used are correct to  $\mathcal{O}(\varepsilon)$ .

Finally, we see that we can drop, at order  $\mathcal{O}(\varepsilon^2)$ , all contributions except  $\Sigma_{12}, \Sigma_{13}$  and  $\Sigma_{33}$ . Upon substituting their expressions in Eq.(3.175), we also see that we can neglect the contribution from  $\Sigma_{33}$  since it is convoluted with  $G_{34}$ , which is  $\mathcal{O}(\varepsilon)$ . Only the two first lines of the loop corrections in Eq.(3.175) survive at this order, and we can also replace  $G_{14}$  and  $G_{14}^+$  by expressions at the lowest order in the potential in function of  $G_{44}$ :

$$(\partial_\tau + k^2)G_{14}(k, \tau) = 2\sqrt{\rho_0}\theta(-\tau)\partial_\tau G_{44}(k, \tau), \quad (3.194)$$

$$(-\partial_\tau + k^2)G_{14}^+(k, \tau) = -2\sqrt{\rho_0}\theta(\tau)\partial_\tau G_{44}(k, \tau). \quad (3.195)$$

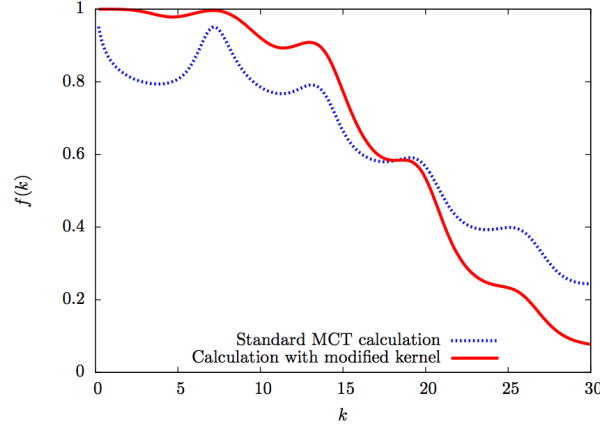


Figure 3.1: Non-ergodicity factor of harmonic spheres obtained by numerically solving Eq.(3.199) (solid line) and the original mode-coupling result Eq.(1.11) (dashed line), for density  $\rho_0 = 1.01$  and reduced temperature  $\beta\varepsilon = 10^{-4}$ .

If  $\tau > 0$  the Heaviside functions restrict the time interval to  $[0, \tau]$  for the term containing  $\Sigma_{12}G_{14}^+$  and cancels the term containing  $\Sigma_{12}^+G_{14}$ , and we finally obtain:

$$0 = (-\partial_\tau^2 + \Omega(k)^2) G_{44}(k, \tau) + \frac{k^2}{2\Omega(k)\rho_0^3} \int_0^\tau dt \int_q [q^2\varepsilon(q) + (k-q)^2\varepsilon(k-q)]^2 G_{44}(q, \tau-t) G_{44}(k-q, \tau-t) \partial_t G_{44}(k, t) \quad (3.196)$$

We note that  $G_{44}$  is equal to  $\rho S(k, t)$ , where  $S(k, t)$  is the dynamical structure factor. By Laplace transforming Eq.(3.196) and focusing on the long-time limit, we get an equation for the non-ergodicity parameter:

$$\frac{f(k)}{1-f(k)} = \frac{\rho_0 k^2}{2\Omega(k)^3} \int_q [q^2\beta v(q) + (k-q)^2\beta v(k-q)]^2 S(q)S(k-q)f(q)f(k-q). \quad (3.197)$$

This equation has a flavor of the Mode-Coupling equation (1.11), but because we insisted on staying at the lowest order in the potential, we have that the direct correlation function is approximated by  $c(k) = -\beta v(k)$ , which is equivalent to setting  $S(k) = 1/(1 + \beta\rho_0 v(k)) \Leftrightarrow \Omega(k) = k^2/S(k)$ . This is the RPA approximation of liquid theory [77]. Restoring the renormalized values of the static quantities we end up with:

$$\frac{f(k)}{1-f(k)} = \frac{\rho S(k)}{2k^4} \int_q [q^2 c(q) + (k-q)^2 c(k-q)]^2 S(q)S(k-q)f(q)f(k-q). \quad (3.198)$$

Put under this form, the only difference with the true MCT equation is that in the kernel we have  $q^2$  instead of  $k \cdot q$  and  $(k-q)^2$  instead of  $k \cdot (k-q)$ . We can simplify the integral by switching to bi-polar coordinates, i.e. defining  $u = |q|, v = |k-q|$  and making the change of variables  $q \rightarrow (u, v, \theta)$ , where  $\theta$  is the angle between  $k$  and  $q$ . The Jacobian of this transformation is  $uv/k$ , and we thus obtain:

$$\frac{f(k)}{1-f(k)} = \frac{\rho S(k)}{2k^5} \int_0^\infty du \int_{|k-u|}^{k+u} dv uv [u^2 c(u) + v^2 c(v)]^2 S(u)f(u)S(v)f(v) \quad (3.199)$$

Numerically solving this equation for harmonic spheres gives the result shown in Fig. 3.1. We see that  $f$  goes to one when  $k$  is small, which seems to constrain the form of the result in the vicinity



of  $k = 0$ . Indeed, it is a direct mathematical consequence of the form of the kernel: because of the replacement  $k \cdot q \rightarrow q^2$ , the small  $k$  behavior of the right hand side of Eq.(3.199) is singular, which forces the left hand side to be singular too, which means that  $f(k = 0)$  must be equal to 1.

### 3.4.4 A new symmetry

This small  $k$  divergence is related to the appearance in the formalism of a new symmetry. Upon the transformation:

$$\begin{cases} \bar{a}(x, t) & \rightarrow \bar{a}(x, t)e^{i\theta} \\ a(x, t) & \rightarrow a(x, t)e^{i\theta} \end{cases}, \quad (3.200)$$

the original action is invariant. This gauge symmetry naturally enforces that  $\langle \bar{a} \rangle = \langle a \rangle = 0$ , a condition that we break in the beginning of our calculation. Even if this symmetry is not as crucial as time-reversal, and we could obtain reasonable results while breaking it, it is obvious that in order to have a consistent formalism, we need to find a way to properly include it in the formalism. The search for a 2PI action that would be operational in the symmetry-broken phase of Bose-Einstein condensate is of current interest in condensed matter, see in particular [97, 98], and we hope that such extension of the existing tools will be developed in the next years.

### 3.4.5 Discussion

The approach presented here has three main advantages:

- it takes into account the ideal gas part of the dynamics without having to resort to complicated non-perturbative manipulations as in [91]
- it possesses a small parameter when the pair potential of the liquid under scrutiny has an energy scale
- and it gives an operational result with few calculations when staying at the lowest order in the potential

It shows in a transparent way what kind of approximations are made in order to obtain a mode-coupling like equation. In particular it emphasizes the role of projection onto the density-density correlation functions, also present in the formulation of [91]: a more natural thing to do would be to keep all correlators and solve their self-consistent equations all at once, without performing substitutions. In the case of an expansion at the lowest order in the potential this procedure is well defined, however in most cases in the study of glasses, such expansion would not be possible, for example for hard-spheres an expansion in powers of the potential would clearly break down. Also the glass transition happens at quite low temperature, so that the parameter  $\varepsilon$  of the theory, which is  $\beta v(k)$ , is rarely small ! A possible exception could be provided by the Gaussian core model when studied at very high densities, where MCT has been found to be quite accurate [79, 81, 80].

In the case of the FA model, we have found that when solving the whole set of Dyson equations without focusing on the density-density sector, the ergodic phase with  $f(k) = 0$  is always stable at finite temperature. Whether the situation is the same for the particles is much harder to analyse.

Another intriguing aspect is that it has been proved, when studying a schematic version of the Mode-Coupling equations, where space indices are dropped, that upon including successively higher order corrections, the transition is gradually shifted to larger and larger densities, and eventually

disappears when the whole series is re-summed [116], while the MCT fits still provide a good representation of the exact result for a limited time-interval. This is exactly the current experimental and numerical situation, and extending such results to the full dynamics of the system would be particularly satisfying.

There are two main drawbacks to the present theory:

- first the use of the similarity transformation forces one to consider a calculation in the bulk of time, therefore losing track of the initial conditions, which are ordinarily used to recover the full static correlations of the system [3, 91].
- secondly, a  $U(1)$  symmetry has been added in the problem, which is broken by hand by our approximation scheme, and is speculated to deteriorate the results at large wave-length.

The first drawback is easily dealt with thanks to the accumulation of knowledge in the field theory formulation of glassy dynamics, since we know on independent grounds how the static correlations get renormalized, but the second issue is more serious and prevents an attempt to go to next order in the calculation.

## Chapter 4

# Statics: the replica method

After focusing on the treatment of the glass transition by dynamical approaches, this chapter is devoted to the presentation of results obtained by using the replica method in the vicinity of the glass transition. Starting from assumptions on the structure of the system in the glass phase inspired by the RFOT scenario, and working in a static framework, one is able to derive self-consistent equations for the non-ergodicity factor [138], a quantity which is originally defined in terms of dynamical quantities.

The link between such equations in dynamical and static theories is still unclear, in particular because the assumptions made by RFOT on the metastable states of the system are not explicitly *a priori* related to a dynamical calculation, except in some mean-field disordered models [95, 48, 27]. A first attempt to relate the two approaches by Szamel [161], by characterizing metastable states by a vanishing current condition, is promising, but suffers from the same short-comings than MCT itself, in the sense that the truncation procedure is again rather arbitrary.

We adopt here a complementary approach, by staying in the hypotheses of RFOT, and setting up an expansion of the free-energy in powers of the static order parameter defined within replica-theory. The replicated version of the Hyper-Netted-Chain approximation of liquid theory discussed at the end of Chapter 2 provides us with the correct starting point for this expansion, and we calculated the lowest order (in powers of the static order parameter) correction to this approximation. This lowest order correction corresponds to a quadratic term in the self-consistent equation for the non-ergodicity parameter, and thus we find the *exact* quadratic part of this equation within replica theory: this should be equivalent to the two-mode approximation made within dynamical formulations.

Surprisingly, we show that a part of the MCT kernel is recovered, while the other and most important can not be recovered within statics, thus disentangling its static and dynamic parts. We found that the qualitative picture of dynamical glass transition is stable against inclusion of the lowest order correction to the Hyper-Netted-Chain result, but that these corrections are quantitatively relevant at and away from the transition. Our expansion provides a starting point in order to take correctly these corrections into account, and possibly offer a unified picture with the results presented in Chapter 5.

### 4.1 Focusing on the long time limit

Motivated by the observations from dynamical calculations such as Mode-Coupling theory, or the calculation presented in Chapter 3, we will now make the assumption that there exists a well-defined transition from an ergodic liquid to a non-ergodic one, at a density  $\rho_d(T)$ . Above this density, adopting

the point of view of the RFOT, the system is supposed to be stuck in one of many metastable states, and is not able to visit its whole phase-space anymore. The partition function is thus postulated to be separated in many pure states, parts of the phase space that are disconnected from one another. This picture is of course inspired from mean-field models, where it is exactly realized [124]. In finite dimension, the time needed in order to jump from one state to the other will be finite. A phenomenological theory of nucleation [94, 62, 30, 26] has been devised in order to correct the mean-field vision that we describe here. However, until now, no theoretic calculation on realistic models such as harmonic spheres or hard spheres have been able to put quantitative background on these ideas, and we will stay at the level of these mean-field concepts.

### 4.1.1 Ergodicity breaking and complexity

By definition, ergodicity breaking, if it takes place, separates the phase space into “pure” states, i.e. states that can not be connected by any dynamical process in the thermodynamic limit, even in the  $t \rightarrow \infty$  limit. Thus, we index these states by  $\alpha$  that runs from 1 to  $\mathcal{N}$ , and we calculate the average of an observable  $A$  as follows:

$$\langle A \rangle = \frac{1}{Z} \sum_{\mathcal{C}} e^{-\beta H(\mathcal{C})} A(\mathcal{C}) = \sum_{\alpha=1}^{\mathcal{N}} \frac{\sum_{\mathcal{C} \in \alpha} e^{-\beta H(\mathcal{C})}}{Z} \frac{1}{\sum_{\mathcal{C} \in \alpha} e^{-\beta H(\mathcal{C})}} \sum_{\mathcal{C} \in \alpha} e^{-\beta H(\mathcal{C})} A(\mathcal{C}), \quad (4.1)$$

where  $\mathcal{C}$  is a microscopic state of the system (here the set of positions of the particles). Defining

$$Z_{\alpha} = \sum_{\mathcal{C} \in \alpha} e^{-\beta H(\mathcal{C})}, \quad (4.2)$$

$$w_{\alpha} = \frac{1}{Z} \sum_{\mathcal{C} \in \alpha} e^{-\beta H(\mathcal{C})}, \quad (4.3)$$

We thus define the average inside a state  $\alpha$ :

$$\langle A \rangle_{\alpha} \equiv \frac{1}{Z_{\alpha}} \sum_{\mathcal{C} \in \alpha} A(\mathcal{C}) e^{-\beta H(\mathcal{C})}, \quad (4.4)$$

and an average over all states:

$$\overline{A_{\alpha}} \equiv \sum_{\alpha=1}^{\mathcal{N}} w_{\alpha} A_{\alpha}. \quad (4.5)$$

Finally any average will be denoted by  $\overline{\langle \cdot \rangle_{\alpha}}$ .

Defining  $f_{\alpha}$ , the effective free-energy of state  $\alpha$ , by:

$$f_{\alpha} = -\frac{k_B T}{N} \ln Z_{\alpha}, \quad (4.6)$$

where  $N$  is the number of particles in the system, and inserting this definition in the partition function we get:

$$Z = \sum_{\alpha=1}^{\mathcal{N}} e^{-N\beta f_{\alpha}}. \quad (4.7)$$

We define now the complexity as the extensive component of the number of metastable states. For a given free-energy level  $f$ , supposing that there are  $\mathcal{N}(f)$  metastable states that have this precise free-energy, we introduce  $\Sigma(f)$  as:

$$\Sigma(f) = \frac{1}{N} \ln \mathcal{N}(f). \quad (4.8)$$

By introducing a delta function in the partition function, we obtain:

$$Z = \sum_{\alpha=1}^{\mathcal{N}} \sum_f \delta(f - f_\alpha) e^{-N\beta f} \quad (4.9)$$

$$= \sum_f e^{-N\beta f} \underbrace{\sum_{\alpha=1}^{\mathcal{N}} \delta(f - f_\alpha)}_{=\mathcal{N}(f)} \quad (4.10)$$

$$= \sum_f e^{-N\beta[f - T\Sigma(f)]}. \quad (4.11)$$

In the thermodynamic limit, the free-energy  $F$  of the system will be dominated by the free-energy that minimizes the argument of the exponential:

$$F \equiv \lim_{N \rightarrow \infty} -\frac{k_B T}{N} \ln Z \quad (4.12)$$

$$\Rightarrow \begin{cases} F = f^* - T\Sigma(f^*) \\ f^* \text{ defined as } \left. \frac{\partial \Sigma(f)}{\partial f} \right|_{f^*} = \frac{1}{T} \end{cases} \quad (4.13)$$

If the number of metastable states is sub-exponential, we will have  $\Sigma = 0$ , and the partition function will be dominated by the true free-energy minimum. But if we have  $\Sigma \neq 0$ , the free-energy of the glass in Eq.(4.13) will be smaller than the free energy of this isolated free-energy minimum, and thus the glass phase will be preferred thermodynamically.

We have now reduced the problem of detecting the glass transition to checking whether there exists or not a finite complexity. It is worth noting that, if there exists a transition from zero to non-zero complexity, this won't be associated to a true thermodynamic phase transition: indeed the entropic term  $-T\Sigma(f^*)$  will act, thermodynamically, as a driving force that allows the system to visit all metastable states, thus restoring ergodicity.

However, dynamically, and in the thermodynamic limit, the time needed to perform these jump goes to infinity at the transition  $\rho_d(T)$ , and the system is effectively stuck forever in this particular state.

Of course Eq.(4.13) is useless since we still do not know the free-energy of the states  $f^*$  and the complexity  $\Sigma(f^*)$ , and we need a tool to go further. An adaptation of the replica method used in the study of mean-field models provides such a tool, as was realized by Monasson [126].

### 4.1.2 Order parameter for the glass transition

In analogy with the ferromagnet-paramagnet transition, detecting the transition in that case with thermodynamical methods is easy, since we know exactly the structure of the two equivalent ordered states: all spins up or all spins down. Thus, we add a small external field which is coupled to the magnetization to explicitly break the symmetry between the two states, calculate the free-energy with this small symmetry breaking field, then let the strength of the field go to zero. If the system is in the disordered phase, letting go of the external field averages the magnetization to zero. However, if the system is in the ordered (ferromagnetic) state, the total magnetization will be equal to a non-zero value even in the limit of zero external field. This provides a scalar order parameter for the ferromagnet-paramagnet transition: the magnetization.

In the case of the glass transition, we do not know the possible final states after the transition: they are infinitely numerous, and are frozen liquid configurations. Thus it is much harder to pin the system towards one of these states. However, one possible way is to introduce exact copies of the system, say for example  $m$  copies. The copies are indexed by  $a = 1, \dots, m$ . If the copies are uncorrelated, then the partition function of the replicated liquid is just  $Z^m$ . Now consider introducing a small attractive coupling between the copies. More precisely, particle  $i$  in copy  $a$  will interact with particle  $j$  in copy  $b$  (if  $a \neq b$ ) via an attractive pair potential  $\tilde{w}(x_i^a - x_j^b)$ , that has a small amplitude  $\varepsilon$ .

Exactly as in liquid theory, we are interested in global quantities such as the density, and we can generalize the definitions of the density and correlation functions to the case of the replicated liquid, defining:

$$\hat{\rho}_a(x) = \sum_{i=1}^N \delta(x - x_i^a), \quad (4.14)$$

$$\rho_a(x) = \langle \hat{\rho}_a(x) \rangle. \quad (4.15)$$

Of course by translational invariance and because all copies are identical, in the vanishing coupling limit,  $\rho_a(x) = \rho$ . We have to look at a two-point quantity, as in the dynamical framework. We now search for a quantity playing the role of an order parameter for the glass transition, and we expect it to be a two-point quantity. We naturally turn to the generalization for copies of the pair correlation function defined in Eq.(2.125) for copies:

$$h_{ab}(x, y) \equiv \frac{\langle \hat{\rho}_a(x) \hat{\rho}_b(y) \rangle}{\rho^2} - 1 - \delta_{ab} \frac{1}{\rho} \delta(x - y), \quad (4.16)$$

and we show below that this is indeed the correct order parameter. Note that, for  $a \neq b$ , the coinciding point term is absent, because particle  $i$  of copy  $a$  interacts with all particles of copy  $b$ , including particle  $i$ , whereas within copy  $a$ , particle  $i$  does not interact with itself. At finite  $N$ , ergodicity is guaranteed and the small attraction will ensure that the two copies will be in the same state. Now perform the large system size limit  $N \rightarrow \infty$ :

- if  $\rho < \rho_d$ , ergodicity is maintained, and letting  $\varepsilon$  to zero will lead the two copies to de-correlate, i.e.  $h_{ab} = 0$ ;
- if  $\rho > \rho_d$ , the two copies will be trapped into a metastable state  $\alpha$ . Finally letting  $\varepsilon$  go to zero, the two copies will remain correlated and  $h_{ab} \neq 0$ .

We see that the  $h_{ab}$  function, provided it is calculated with vanishingly small attractive coupling, is a good order parameter for the glass transition.

The average in Eq.(4.16) is, in our static interpretation, first an average inside a state  $\alpha$ , then an average over all states. The presence of the attractive coupling between the copies will force them into the same pure state  $\alpha$ , leading to:

$$h_{ab}(x, y) = \frac{\langle \hat{\rho}_a(x) \hat{\rho}_b(y) \rangle_\alpha}{\rho^2} - 1 \quad \text{for } a \neq b. \quad (4.17)$$

Letting the interaction go to zero will allow them to de-correlate inside the state, leading to:

$$\lim_{\varepsilon \rightarrow 0} h_{ab}(x, y) = \frac{\langle \hat{\rho}(x) \rangle_\alpha \langle \hat{\rho}(y) \rangle_\alpha}{\rho^2} - 1 \quad (4.18)$$

Note that the average density inside a state is the same for all copies, but needs not be constant, since translational invariance is restored only after summation over all the states.

Independently, the time-dependent density-density correlation, which serves as a dynamic order parameter for the glass transition is defined in real-space by:

$$S(x, y, t) = \langle (\hat{\rho}(x, t) - \rho)(\hat{\rho}(y, 0) - \rho) \rangle. \quad (4.19)$$

The RFOT interpretation is that, at a volume fraction above the glass transition volume fraction, and in the long time limit, the system is stuck in a pure state  $\alpha$ , and we have:

$$S(x, y, t) \xrightarrow{t \rightarrow \infty} \overline{\langle \hat{\rho}(x, t) \hat{\rho}(y, 0) \rangle_\alpha} - \rho^2 \quad (4.20)$$

But the system is at least able to de-correlate inside the state, giving:

$$S(x, y, t) \xrightarrow{t \rightarrow \infty} \overline{\langle \hat{\rho}(x) \rangle_\alpha \langle \hat{\rho}(y) \rangle_\alpha} - \rho^2 = \rho^2 h_{ab}(x, y). \quad (4.21)$$

Now we get in Fourier space:

$$S(k, t) \xrightarrow{t \rightarrow \infty} \rho^2 h_{ab}(k). \quad (4.22)$$

Finally we see that  $h_{ab}$  is directly proportional to the non-ergodicity parameter [138] defined in Eq.(1.8) of Chapter 1:

$$f(k) = \frac{\rho h_{ab}(k)}{S(k)} \text{ with } a \neq b \quad (4.23)$$

We see that the static order parameter that we defined with the introduction of copies is the same physical observable as the one defined by dynamical means. It is thus interesting to investigate the degree of relevance of the set of approximations made to obtain this static description (separation of the partition function into pure states, form of the spectrum of free-energies, number of metastable states, ...), in order to sort out what is purely static from what is purely dynamic in the glass transition.

### 4.1.3 Computing the complexity with replicas

We have seen that introducing copies attracted to each other allows one to define an order parameter, but it also gives a way to compute the complexity and free energy of the system. Consider  $m$  identical copies of the original system. If copies are attracted to each other, they fall in the same state. Then in the limit of vanishing coupling, they de-correlate inside this state. Moreover, the free-energy landscape felt by all copies is the same as that of the original one when the coupling is sent to zero, such that for the partition function  $Z_m$  of the replicated liquid can now be written, in the same way as in Eq.(4.13) as:

$$Z_m = \sum_f e^{-N\beta(mf - T\Sigma(f))}, \quad (4.24)$$

$$\Rightarrow \left\{ \begin{array}{l} F_m = f^*(m) - T\Sigma(f^*(m)), \\ \left. \frac{\partial \Sigma}{\partial f} \right|_{f^*(m)} = \frac{m}{T} \end{array} \right. \quad (4.25)$$

Performing now an analytic continuation for arbitrary values of  $m$ , the free energy and complexity can be calculated as [126]:

$$\left\{ \begin{array}{l} f^*(m) = \left. \frac{\partial F_m}{\partial m} \right|_{m=1}, \\ \Sigma(f^*(m)) = \left. \frac{m^2}{T} \frac{\partial F_m/m}{\partial m} \right|_{m=1}. \end{array} \right. \quad (4.26)$$

The program is now clear:

- compute the free-energy of an  $m$ -time replicated liquid in the presence of an attractive coupling
- take the large system size limit
- let the coupling go to zero
- make the free-energy analytic in  $m$
- take a derivative with respect to  $m$  to get  $\Sigma(f^*(m))$
- take the limit  $m \rightarrow 1$

If the resulting complexity is non zero, the glass transition has been detected and we can compute the corresponding structure factor by computing the correlation function between two copies.

## 4.2 Replicated liquid theory

To realize our program, we only need tools issued from liquid theory, as described in chapter 2, since a replicated liquid can be seen as a mixture of  $m$  different species of particles. All results from chapter 2 have straightforward generalizations to multi-component systems. The partition function of the replicated system is:

$$Z_m = \text{Tr} e^{\frac{1}{2} \sum'_{i,j,a,b} w_{ab}(x_i^a - x_j^b) + \sum_{i,a} \nu_a(x_i^a)} , \quad (4.27)$$

where  $w_{ab}$  is equal to  $w$  for  $a = b$ , and  $w_{ab}$  is a small attractive coupling when  $a \neq b$ . The prime on the summation sign  $\sum'$  means that when  $a = b$ , the summation must exclude the case  $i = j$ , and the trace operation is now defined as:  $\text{Tr} \bullet = \sum_{N=0}^{\infty} \frac{1}{N!^m} \int \prod_{a=1}^m \prod_{i=1}^N dx_i^a \bullet$ . For the sake of simplicity,  $\boldsymbol{\nu}$  in the following will denote the set of  $m$  chemical potentials  $\{\nu_a\}_{a=1\dots m}$ , and  $\mathbf{w}$  will denote the set of  $m^2$  pair potentials  $\{w_{ab}\}_{a,b=1\dots m}$ . Equivalently the family of  $m$  average densities  $\{\rho_a\}_{a=1\dots m}$  defined in Eq. (4.15) will be denoted by  $\boldsymbol{\rho}$  and the family of  $m^2$  correlation functions  $\{h_{ab}\}_{a,b=1\dots m}$  will be denoted by  $\mathbf{h}$ . The replicated two-point density and pair potential are defined as [121]:

$$\hat{\rho}_{ab}^{(2)}(x, y) = \hat{\rho}_a(x) \hat{\rho}_b(y) - \delta_{ab} \delta(x - y) \hat{\rho}_a(x) , \quad (4.28)$$

$$w_{ab}(x, y) = w(x, y) \delta_{ab} + \tilde{w}(x, y) (1 - \delta_{ab}) . \quad (4.29)$$

We see at that point that a replica index always appears with a space index, so that, depending on the context, we may group them in one subscript for simplicity. As in the non-replicated case, the chemical potentials  $\boldsymbol{\nu}$  is coupled to the replicated one-point density defined in Eqs. (4.15–4.14):

$$\frac{\delta \ln Z_m[\boldsymbol{\nu}, \mathbf{w}]}{\delta \nu_a(x)} = \rho_a(x) , \quad (4.30)$$

and the pair potentials  $\mathbf{w}$  are coupled to the replicated two-point density:

$$\frac{\delta \ln Z_m[\boldsymbol{\nu}, \mathbf{w}]}{\delta w_{ab}(x, y)} = \frac{1}{2} \rho_{ab}^{(2)}(x, y) . \quad (4.31)$$

The two-point density is trivially related to the pair correlation function defined in Eq. (4.16):

$$h_{ab}(x, y) = \frac{\rho_{ab}^{(2)}(x, y)}{\rho_a(x) \rho_b(y)} - 1 . \quad (4.32)$$

The static order parameter of the glass transition is thus the two-point density. We saw that in order to obtain accurate and consistent approximations on the free-energy (that is needed to access



the complexity) and pair correlation function (that we need to compute the non-ergodicity factor), it is better to start from the double Legendre transform of the partition function with respect to the chemical potential and the pair potential (note the different choice of sign when compared to Chap. 2) :

$$\left\{ \begin{array}{l} \Gamma_m[\boldsymbol{\rho}, \mathbf{h}] = \sum_a \int_x \rho_a(x) \nu_a^*(x) + \frac{1}{2} \sum_{a,b} \int_{x,y} \rho_{ab}^{(2)}(x,y) w_{ab}^*(x,y) - \ln Z_m[\boldsymbol{\nu}^*, \mathbf{w}^*] \\ \frac{\delta \ln Z_m[\boldsymbol{\nu}, \mathbf{w}]}{\delta \nu_a(x)} \Big|_{\boldsymbol{\nu}^*, \mathbf{w}^*} = \rho_a(x) \quad \text{and} \quad \frac{\delta \ln Z_m[\boldsymbol{\nu}, \mathbf{w}]}{\delta w_{ab}(x,y)} \Big|_{\boldsymbol{\nu}^*, \mathbf{w}^*} = \frac{1}{2} \rho_{ab}^{(2)}(x,y) . \end{array} \right. \quad (4.33)$$

As in the non-replicated case, this double Legendre transform was found by Morita [129] to be given by:

$$\begin{aligned} \Gamma_m[\boldsymbol{\rho}, \mathbf{h}] &= \Gamma_{\text{IG}}[\boldsymbol{\rho}, \mathbf{h}] + \Gamma_{\text{ring}}[\boldsymbol{\rho}, \mathbf{h}] + \Gamma_{2\text{PI}}[\boldsymbol{\rho}, \mathbf{h}] , \\ \Gamma_{\text{IG}}[\boldsymbol{\rho}, \mathbf{h}] &= \sum_a \int_x \rho_a(x) \left[ \ln \rho_a(x) - 1 \right] \\ &\quad + \frac{1}{2} \sum_{a,b} \int_{x,y} \rho_a(x) \rho_b(y) \left( [1 + h_{ab}(x,y)] \ln[1 + h_{ab}(x,y)] - h_{ab}(x,y) \right) , \\ \Gamma_{\text{ring}}[\boldsymbol{\rho}, \mathbf{h}] &= \frac{1}{2} \sum_{n \geq 3} \frac{(-1)^n}{n} \text{Tr} \rho_{a_1}(x_1) h_{a_1 a_2}(x_1, x_2) \cdots \rho_{a_n}(x_n) h_{a_n a_1}(x_n, x_1) , \end{aligned} \quad (4.34)$$

and  $\Gamma_{2\text{PI}}$  is the sum of all 2-irreducible diagrams composed of black nodes  $\rho_a(x)$  and links  $h_{ab}(x,y)$ . They are such that when two links are removed from a diagram, it doesn't disconnect in two separate parts. As in the one-component case,  $\Gamma_{\text{ring}}$  in Eq.(4.34) is the sum of all ring diagrams, with appropriate weighting. Note that we use  $\mathbf{h}$  as a variable, but the natural pair of variables is  $\boldsymbol{\rho}$  and  $\rho^{(2)}$ , and differentiations with respect to  $\rho_a$  must be done at  $\rho_{ab}^{(2)}$  fixed instead of  $h_{ab}$  fixed: this can be important since  $h_{ab}$  is a function of both  $\rho^{(2)}$  and  $\rho$ !

We define for convenience the propagator and self-energy of the replicated system:

$$\begin{aligned} G_{ab}(x,y) &= \langle \rho_a(x) \rho_b(y) \rangle - \langle \rho_a(x) \rangle \langle \rho_b(y) \rangle = \rho_a(x) \delta_{ab} \delta(x,y) + \rho_a(x) \rho_b(y) h_{ab}(x,y) , \\ \Gamma_{ab}^{(2)}(x,y) &= \frac{\delta^2 \Gamma_m[\boldsymbol{\rho}, \mathbf{h}]}{\delta \rho_a(x) \delta \rho_b(y)} = \frac{1}{\rho_a(x)} \delta_{ab} \delta(x,y) - c_{ab}(x,y) , \end{aligned} \quad (4.35)$$

where  $c_{ab}$  is the generalization to mixtures of the direct correlation function. We have the replicated version of the OZ relation in Eq. (2.175), i.e. that:

$$\sum_c \int_z \Gamma_{ac}^{(2)}(x,z) G_{cb}(z,y) = \delta_{ab} \delta(x,y) , \quad (4.36)$$

or equivalently:

$$h_{ab}(x,y) = c_{ab}(x,y) - \sum_c \int_z h_{ac}(x,z) \rho_c(z) c_{cb}(z,y) . \quad (4.37)$$

### 4.2.1 Replica symmetric ansatz and calculation of the complexity

The replicated Morita-Hiroike functional in Eq. (4.34) must be extremalized with respect to the pair correlation  $h_{ab}$ , which gives a self consistent equation on  $h_{ab}$ , making use of the replicated version of Eq.(2.180) [77]:

$$w_{ab}(x,y) = \ln(1 + h_{ab}(x,y)) - h_{ab}(x,y) + c_{ab}(x,y) + \frac{2}{\rho_a(x) \rho_b(y)} \frac{\delta}{\delta h_{ab}(x,y)} \{2\text{PI diagrams}\} , \quad (4.38)$$

We already see that the form of pair potential that we have chosen implies an asymmetry between  $h_{ab}$  with  $a \neq b$  and  $h_{aa}$ . Otherwise, we will suppose that all replicas play the same role, and we define for the following:

$$\begin{cases} h(x, y) \equiv h_{aa}(x, y), \\ \tilde{h}(x, y) \equiv h_{ab}(x, y) \quad \text{with } a \neq b. \end{cases} \quad (4.39)$$

This is equivalent to a 1RSB structure in the context of mean-field disordered spin glasses [126], although we merely assumed replica symmetry. We called the  $aa$  correlation function  $h$ , since we anticipate that in the ergodic phase,  $\tilde{h} = 0$  and thus  $h_{aa}$  is the liquid correlation function. For the density fields  $\rho_a(x)$ , the chemical potentials are not supposed to be asymmetric, and we suppose that as a result  $\rho_a(x) = \rho \quad \forall a$ .

With the expression of the double Legendre transform and the 1RSB ansatz, performing our program is quite easy starting from this set of equations:

- The thermodynamic limit has been taken, since Mayer diagrams, apart from a trivial volume dependence, will depend only on  $\rho = N/V$ , so that  $N$  and  $V$  can safely be sent to infinity ;
- Letting the couplings go to zero is trivially done by setting  $w_{ab}$  to zero for  $a \neq b$  in Eq.(4.38) before evaluation of  $h_{ab}$  ;
- The equivalence between replicas assumed in Eq.(4.39) will render the free energy analytic in  $m$ , since the summations over replica indices will make the appearance of  $m$  explicit, and the free-energy will then only depend on  $m$ ,  $h$  and  $\tilde{h}$ . For example we can perform the summations over the replica indices in Eq.(4.37) to get:

$$\begin{cases} c(x, y) = h(x, y) - \rho \int_z h(x, z)c(z, y) - (m-1)\rho \int_z \tilde{h}(x, z)\tilde{c}(z, y) \\ \tilde{c}(x, y) = \tilde{h}(x, y) - \int_z \tilde{h}(x, z)c(z, y) - \rho \int_z h(x, z)\tilde{c}(z, y) - (m-2)\rho \int_z \tilde{h}(x, z)\tilde{c}(z, y) \end{cases} \quad (4.40)$$

- We can take the limit  $m = 1$  that we are interested in:

$$\begin{cases} c(x, y) = h(x, y) - \rho \int_z h(x, z)c(z, y) \\ \tilde{c}(x, y) = \tilde{h}(x, y) - \int_z \tilde{h}(x, z)c(z, y) - \rho \int_z h(x, z)\tilde{c}(z, y) + \rho \int_z \tilde{h}(x, z)\tilde{c}(z, y) \end{cases} \quad (4.41)$$

- The replicated free-energy is calculated in the end by inserting  $h$  and  $\tilde{h}$  that result from Eq.(4.38) and Eq.(4.41) back into Eq.(4.34).

The first natural thing approximation to do is to neglect altogether the 2PI diagrams in the full expression of the free-energy. This was done by Mézard and Parisi [121], and we review their results here, in the light of our analogy between the static order parameter  $\tilde{h}$  and the dynamical one  $f(k)$  provided by Eq.(4.23).

### 4.2.2 Replicated Hyper-Netted-Chain approximation

Now if we neglect the 2PI diagrams, Eq.(4.38) gives two self consistent equations on  $h$  and  $\tilde{h}$ :

$$\begin{cases} \ln(1 + h(x, y)) &= w(x, y) + h(x, y) - c(x, y) \\ \ln(1 + \tilde{h}(x, y)) &= \tilde{h}(x, y) - \tilde{c}(x, y) \end{cases} \quad (4.42)$$

These equations must be supplemented with the replicated Ornstein-Zernike equations evaluated at  $m = 1$  Eq.(4.41), that read in Fourier space:

$$\begin{cases} c(k) = h(k) - \rho h(k)c(k), \\ \tilde{c}(k) = \tilde{h}(k) - \rho h(k)\tilde{c}(k) - \rho \tilde{h}(k)c(k) + \rho \tilde{h}(k)\tilde{c}(k). \end{cases} \quad (4.43)$$

We see that the functions  $h$  and  $c$  do not depend on  $\tilde{h}$  and  $\tilde{c}$ , as expected since they must coincide with the corresponding liquid quantities when  $\tilde{h} = \tilde{c} = 0$ . They are given by the HNC equations, that have been already discussed in chapter 2.

The functions  $\tilde{h}$  and  $\tilde{c}$  satisfy a similar set of equations, that also involve  $h$  and  $c$ :

$$\begin{cases} \tilde{c}(x, y) = \tilde{h}(x, y) - \ln(1 + \tilde{h}(x, y)) \\ \tilde{c}(k) = \tilde{h}(k) - \rho h(k)\tilde{c}(k) - \rho \tilde{h}(k)c(k) + \rho \tilde{h}(k)\tilde{c}(k). \end{cases} \quad (4.44)$$

We can rewrite the second of these equations as:

$$\tilde{c}(k) = \frac{(1 - \rho c(k))\tilde{h}(k)}{1 + \rho h(k) - \rho \tilde{h}(k)}, \quad (4.45)$$

and use the definition of the structure factor Eq.(2.130), the Ornstein-Zernike equation Eq.(2.175) and the link between  $h_{ab}$  for  $a \neq b$  with the non-ergodicity factor Eq.(4.23) to obtain:

$$\tilde{c}(k) = \frac{1}{\rho S(k)} \frac{f(k)}{1 - f(k)}. \quad (4.46)$$

Since  $\tilde{c}$  and  $\tilde{h}$  are both related to  $f$ , we see that Eq.(4.43) is a self-consistent equation for the non-ergodicity parameter.

One may wonder if there is any resemblance between such result and the Mode-Coupling one. To make an explicit bridge between the two, we expand the logarithm term in powers of  $f$ , to get, to lowest order:

$$\frac{f(k)}{1 - f(k)} = \frac{S(k)}{2\rho} \int_q S(q)S(k - q)f(q)f(k - q), \quad (4.47)$$

which has the very same structure as the long-time limit of the Mode-Coupling equation Eq.(1.11), except that the kernel is missing here. For the sake of comparison, we note that we can rewrite the MCT equation as:

$$\begin{aligned} \frac{f(k)}{1 - f(k)} &= \frac{\rho S(k)}{2} \int_q \mathcal{M}(k, q)S(q)S(k - q)f(q)f(k - q), \\ \mathcal{M}(k, q) &= \left[ \frac{k \cdot q}{k^2} \Gamma_{liq}^{(2)}(q) + \frac{k \cdot (k - q)}{k^2} \Gamma_{liq}^{(2)}(k - q) + \rho \Gamma_{liq}^{(3)}(q, k - q) \right]^2. \end{aligned} \quad (4.48)$$

Note here the presence of the three-body direct correlation function of the liquid, even though it is usually neglected, since it has been shown to be negligible with respect to the other, two-body term [10], except for special cases [9]. We see that Mode-Coupling only keeps  $\mathcal{O}(f^2)$  terms, whereas even a simple approximation like HNC retains an infinite number of those. However the HNC kernel to second order is trivial, and reminiscent of the result obtained by [3] by a dynamical field-theory calculation. The result of such equation is that  $f(k) = 1$  for all densities, a result that must be rejected when compared to the trivial solution  $f(k) = 0$ . In contrast, if one keeps the full  $\ln$  term, we obtain the following self-consistent equation:

$$\frac{f(k)}{1-f(k)} = \rho S(k) \mathcal{FT} \left\{ \frac{(S \otimes f)(r)}{\rho} - \ln \left( 1 + \frac{(S \otimes f)(r)}{\rho} \right) \right\}, \quad (4.49)$$

where  $\otimes$  means convolution in real space, and  $\mathcal{FT}\{g(r)\}$  is the Fourier transform of  $g(r)$ .

We solved this equation, combined with the HNC approximation for the liquid part, for the hard-sphere pair potential:

$$w(r) = \begin{cases} -\infty & \text{if } r < \sigma \\ 0 & \text{otherwise} \end{cases}, \quad (4.50)$$

which is the  $T \rightarrow 0$  limit of the harmonic spheres potential Eq.(1.20).

Similarly to the liquid HNC equations, the numerical scheme we used was the following:

- Start from a guess on  $\tilde{c}(k)$ ;
- Deduce the corresponding  $f(k)$  with Eq.(4.46);
- Inverse Fourier transform to obtain  $f(r)$ ;
- Plug into Eq.(4.49) to get a new estimate of  $f(k)$ ;
- Deduce the corresponding  $\tilde{c}(k)$ ;
- Iterate this procedure until  $\tilde{c}(k)$  does not change anymore between two steps.

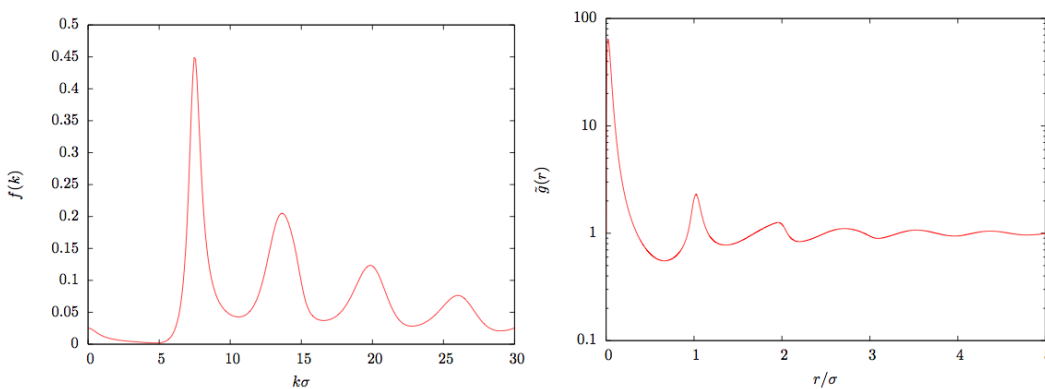


Figure 4.1: Left: Non-ergodicity factor computed from Eq.(4.49) for hard-spheres in 3 dimensions, computed at the transition. Right: Corresponding  $\tilde{g}$  function in real space.

Upon solving the RHNC equation, we, *without assuming it*, the existence of a dynamical transition [121]: for hard spheres, for densities lower than  $\rho_d \approx 1.14$ , the solution to Eq. (4.49) is always

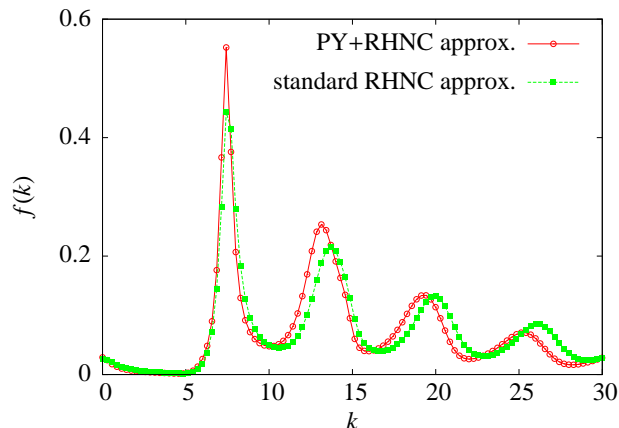


Figure 4.2: Non-ergodicity factor as a function of the wave vector at packing fraction 0.6, for the standard replicated HNC calculation, and from the combination of PY approximation for the diagonal part and RHNC for the off-diagonal correlation.

$f(k) = 0$ , i.e. a liquid phase, whereas  $f(k)$  discontinuously jumps to a non zero value for  $\rho \geq \rho_d$ , indicating the glass transition. This results is quite good, because the dynamical transition for three-dimensional hard spheres is estimated to be around  $\rho_d \approx 1.08$ . Note that Mode-Coupling Theory instead strongly underestimates the transition [72].

As described in Chapter 2, the HNC equation was solved by gradually increasing the density and inserting the previous value for  $c(k)$  in the next step. Here we can not do that since for all densities smaller than  $\rho_d$ ,  $\tilde{c}(k)$  sticks to 0. At each density we thus started with a Gaussian guess for  $\tilde{c}(k)$  until a first non-zero value of the function is spontaneously generated. To stabilize the value of the critical density, we decrease the density and iterate again the scheme by using this obtained  $f(k)$  as a starting point, until the solution spontaneously disappears. The obtained non-ergodicity factor is shown in Fig. 4.1.

The qualitative behavior is generally good: the non-ergodicity factor has a strong peak around  $k = 2\pi/\sigma$  and oscillates in phase with  $S(k)$  while gradually, decreasing to zero at large  $k$ . However, the obtained structure factor is too small to be realistic:  $f(k)$  is quite far from the numerical results (see [170, 72]) which are instead well captured by the Mode-Coupling theory.

We will demonstrate that the order parameter  $h_{ab}$  with  $a \neq b$  can be used as an organizing device for the theory in order to gradually incorporate higher-order correlations of the liquid into the replica result. Of course, we see in Fig 4.1 that the order parameter is not a small quantity, and thus an expansion in powers of  $h_{ab}$  is not a priori justified. Note however that RHNC already re-sums an infinite number of diagrams containing arbitrary numbers of  $h_{ab}$  links, which maybe explains its ability to predict a transition towards a non-small value of the order parameter. Our purpose here is to build from RHNC and incorporate more diagrams, and we will see that even keeping the lowest order correction modifies sensibly the results obtained. Furthermore this lowest order correction allows for the calculation of the two-mode term in the equation for the non-ergodicity parameter.

### 4.2.3 Improvement over the liquid quantities

A first natural question to ask is the role of the liquid HNC approximation that was plugged into the resolution of the self-consistent equation on the non-ergodicity parameter. We have seen that in the  $m = 1$  limit, the liquid quantities decouple from the inter-replica correlations. This allows us to use

any liquid theory approximation to evaluate liquid quantities that appear in our equations. Formally, this is justified by writing the Gibbs free-energy  $\Gamma_m$  in Eq. (4.34) as:

$$\Gamma_m[\boldsymbol{\rho}, \mathbf{h}] = \Gamma_m^{HNC}[\boldsymbol{\rho}, \mathbf{h}] + \Gamma_{liq}^{2PI}[\boldsymbol{\rho}, \mathbf{h}] + \Gamma_{glass}^{2PI}[\boldsymbol{\rho}, \mathbf{h}] , \quad (4.51)$$

where  $\Gamma_{liq}^{2PI}$  is the sum of all 2PI diagrams that do not contain any  $h_{ab}, a \neq b$  links. We can now use the variational principles, which will give the full liquid correlation function for the  $a = b$  components. For a given approximation of  $\Gamma_{glass}^{2PI}$ , we will obtain a self consistent equation for the  $a \neq b$  components. Neglecting altogether  $\Gamma_{glass}^{2PI}$ , we recover the set of equations Eqs.(4.44), in which  $c$  and  $h$  are now the full liquid correlation functions. Of course, inside the glass phase, the liquid quantities cannot be obtained numerically or experimentally, so that such a full re-summation is useless. Instead, we need to have an approximation that can be extrapolated from the liquid phase. For example we can choose the PY approximation for the liquid quantities. Choosing to work at a packing fraction (defined as  $\varphi = \pi\rho/6$ )  $\varphi = 0.6$ , which is expected to be above the dynamical transition, we solved the RHNC equation for the off-diagonal part, Eq. (4.44) with the PY direct correlation function as an input for the diagonal part, and found that this brings about a little improvement over standard RHNC results. It is known that the PY approximation gives a less important underestimation of the peak of  $S(k)$ , which is the main ingredient that leads to the glass transition. In standard RHNC as in the PY version of it, we find a transition from a liquid state at  $\varphi < \varphi_d$  to a glass state at  $\varphi \geq \varphi_d$ , where the self-consistent equation on  $\tilde{h}$  admits a non-zero solution. The value of the critical density is shifted downwards from  $\varphi_c \approx 0.599$  to 0.591 by the use of PY approximation, which is an improvement, even if modest. We show the resulting non-ergodicity factor in the two sets of approximations in Fig. 4.2. Even though use of the PY approximation gives a slightly larger non ergodicity factor, the result is still very small when compared to simulation and experimental data, where  $f$  is much closer to 1 at small wave vectors. We conclude that the source of the problem in the static approach is not the diagonal part of the liquid. We should therefore seek for a way of improving the equation for the off-diagonal correlation, Eq. (4.44).

#### 4.2.4 Systematic expansion in powers of the order-parameter

In order to make further progress, we must incorporate some ‘‘glassy’’ 2PI diagrams (that contain  $h_{ab}, a \neq b$  links) into the free-energy. In the following, we will denote such links by  $\tilde{h}$  links for simplicity, but the reasonings we perform are valid also in more general ansätze than the replica symmetric one. We expand  $\Gamma_{glass}^{2PI}$  in powers of  $\tilde{h}$ :

$$\Gamma_{glass}^{2PI}[\boldsymbol{\rho}, \mathbf{h}] = \sum_{n=1}^{\infty} \text{Tr}' \frac{1}{n!} \left. \frac{\delta^n \Gamma_{glass}^{2PI}[\boldsymbol{\rho}, \mathbf{h}]}{\delta h_{a_1 b_1}(x_1, y_1) \cdots \delta h_{a_n b_n}(x_n, y_n)} \right|_{\tilde{h}=0} h_{a_1 b_1}(x_1, y_1) \cdots h_{a_n b_n}(x_n, y_n) , \quad (4.52)$$

where the prime on the trace means that we must choose  $a_i \neq b_i \forall i$ , and we have started the expansion at first order since the full functional must vanish in the liquid phase, where  $\Gamma_{glass}^{2PI} = 0$  by construction.

Since the diagrams are 2PI, it is easy to see that they must contain at least three of these  $\tilde{h}$  links. Indeed, a  $\tilde{h}$  link joins two nodes that have different replica indices, say  $a$  and  $b$ . All the nodes connected to the  $a$  node by a path of  $h$  links must also have replica index  $a$ , and the same applies to the  $b$  node. Thus all  $\tilde{h}$  links are nodal links: they separate the diagram into two parts, each of which has a different replica index. If a 2PI diagram would contain one or two  $\tilde{h}$  links, then differentiating once or twice with respect to  $\tilde{h}$  would cut the diagram into two parts, which is in contradiction with the fact that the diagram is 2PI. Thus we proved that all 2PI diagrams contain either zero, or three,

or more  $\tilde{h}$  links (this was already found in [26, Appendix A3], and our order parameter expansion is thus the “weak glass” expansion described in this reference).

Thus the lowest order correction to the free-energy in an expansion in powers of  $\tilde{h}$  is a cubic one. When the free-energy is differentiated with respect to  $\tilde{h}$  in order to obtain the equation for the non-ergodicity parameter, this cubic correction will give contributions at order  $\mathcal{O}(\tilde{h}^2)$  to the missing kernel of Eq.(4.49). To make contact with the long-time limit of the MCT equation Eq.(1.11), we thus have to re-sum all  $\mathcal{O}(\tilde{h}^3)$  2PI diagrams.

Let us look at the diagrammatic structure of the  $\mathcal{O}(\tilde{h}^3)$  diagrams of the free-energy. A diagram that contains three  $\tilde{h}$  links can have at most six parts composed of  $h$  links and  $\rho$  nodes that all have the same replica index. But since the diagram is a free-energy contribution, it must be 1PI, as explained in Chapter 2, i.e. it cannot be cut into two parts by cutting a line. The only 1PI possibilities to order  $\tilde{h}^3$  are the diagrams depicted in Fig. 4.3.

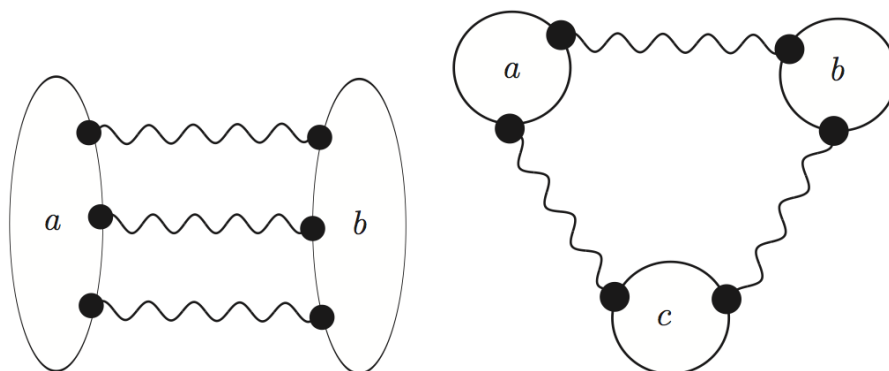


Figure 4.3: Diagrams that contribute to the free-energy at order  $\tilde{h}^3$ . A wiggly line joining two replica indices  $a$  and  $b$  is a  $h_{ab}$  function, a black dot attached to a zone with replica index  $a$  is an integration point weighted by a density factor  $\rho_a$ .

Note that the ring diagram in Fig. 4.3 is already contained in the re-summation performed by the HNC approximation since it is 1PI but not 2PI. Thus we only have to calculate the diagram on the left to get the contribution that corrects the HNC result in Eq.(4.49). It is important to understand that there are two distinct re-summations involved in this calculation: first a re-summation of all the diagrams that are not 2PI (the RHNC approximation), then a further re-summation of the diagrams that contain exactly three  $\tilde{h}$  links (the lowest order correction in  $\tilde{h}$  to RHNC). In practice, we will calculate the sum of all  $\mathcal{O}(f^3)$  diagrams. This sum contains diagrams that are not 2PI, and thus will pick a contribution coming from the RHNC approximation, and diagrams that are 2PI, that will give the desired lowest order contribution.

### 4.3 Expansion at third order

Formally, we have to calculate the third derivative of the free-energy with respect to  $h_{ab}$  with  $a \neq b$ , and evaluate this derivative at zero  $\tilde{h}$ , to discard all the diagrams that are of higher order in  $\tilde{h}$  than  $\tilde{h}^3$ . In the following we will need to distinguish the derivatives with respect to the density and with respect to the correlation functions, as well as derivatives with respect to chemical potentials and with

respect to pair potentials. We define:

$$\begin{aligned}\Gamma_a^{(1,0)}(x_1) &= \frac{\delta \Gamma_m[\boldsymbol{\rho}, \mathbf{h}]}{\delta \rho_a(x_1)}, \\ \Gamma_{ab}^{(0,1)}(x_1, y_1) &= \frac{\delta \Gamma_m[\boldsymbol{\rho}, \mathbf{h}]}{\delta h_{ab}(x_1, y_1)}, \\ \Gamma_{a,cd}^{(1,1)}(x_1; x_2, y_2) &= \frac{\delta^2 \Gamma_m[\boldsymbol{\rho}, \mathbf{h}]}{\delta \rho_a(x_1) \delta h_{cd}(x_2, y_2)},\end{aligned}\tag{4.53}$$

and so on. We will also need to define derivatives of  $\ln Z_m$  with respect to the chemical potentials and pair potentials:

$$\begin{aligned}W_a^{(1,0)}(x_1) &= \left. \frac{\delta \ln Z_m[\boldsymbol{\nu}, \mathbf{w}]}{\delta \nu_a(x_1)} \right|_{\boldsymbol{\nu}^*, \mathbf{w}^*}, \\ W_{ab}^{(0,1)}(x_1, y_1) &= \left. \frac{\delta \ln Z_m[\boldsymbol{\nu}, \mathbf{w}]}{\delta w_{ab}(x_1, y_1)} \right|_{\boldsymbol{\nu}^*, \mathbf{w}^*}, \\ W_{a,cd}^{(1,1)}(x_1; x_2, y_2) &= \left. \frac{\delta^2 \ln Z_m[\boldsymbol{\nu}, \mathbf{w}]}{\delta \nu_a(x_1) \delta w_{cd}(x_2, y_2)} \right|_{\boldsymbol{\nu}^*, \mathbf{w}^*},\end{aligned}\tag{4.54}$$

and so on. Because of our analysis, we see that the  $n = 1$  and  $n = 2$  terms in Eq. (4.52) are necessary zero. We want to calculate the first non-zero term in this expansion, the third-order term. In practice, we found it easier to calculate the third derivative of the total free energy, and subtract from it the third order term of the RHNC free-energy, i.e. we will calculate, with the above notations:

$$\Gamma_{ab,cd,ef}^{(0,3)}(x_1, y_1; x_2, y_2; x_3, y_3) = \frac{\delta^3 \left[ \Gamma_m^{HNC}[\boldsymbol{\rho}, \mathbf{h}] + \Gamma_{glass}^{2PI}[\boldsymbol{\rho}, \mathbf{h}] \right]}{\delta h_{ab}(x_1, y_1) \delta h_{cd}(x_2, y_2) \delta h_{ef}(x_3, y_3)},\tag{4.55}$$

with  $a \neq b$ ,  $c \neq d$  and  $e \neq f$ . The third order term of the RHNC free-energy will be simply calculated from Eq. (4.34). The third derivative we seek can be related to cumulants of the density and the second derivative  $\Gamma^{(0,2)}$  by exploiting the properties of the double Legendre transform.

Considering, for simplicity, a discretized version of our theory, we have that  $\boldsymbol{\rho}$  is an  $m \times M$  matrix, where  $M$  is the number of points of the underlying lattice, and  $\boldsymbol{\rho}^{(2)} \equiv \{\rho_{ab}^{(2)}\}_{a,b}$  is an  $m \times m \times M \times M$  object, and the same applies to  $\boldsymbol{\nu}$  and  $\mathbf{w}$ . We can write the two pairs  $\boldsymbol{\rho}, \boldsymbol{\rho}^{(2)}$  and  $\boldsymbol{\nu}, \mathbf{w}$  in the form of two vectors:

$$\Psi \equiv \left( \boldsymbol{\rho}, \boldsymbol{\rho}^{(2)}/2 \right),\tag{4.56}$$

$$\Phi \equiv (\boldsymbol{\nu}, \mathbf{w}),\tag{4.57}$$

with the convention that if  $i > mM$  an index  $i$  must be understood as a group of two space coordinates  $(x_i, y_i)$  and two replica indices  $(a_i, b_i)$ , but if  $i \leq mM$ , it must be understood as one space coordinate and one replica index. The double Legendre transform  $\Gamma_m$  can then be written as:

$$\left\{ \begin{array}{l} \Gamma_m[\Psi] = \text{Tr} \Phi_1^* \Psi_1 - \ln Z_m[\Phi^*], \\ \text{with } \Phi^* \text{ such that } \left. \frac{\delta \ln Z_m[\Phi]}{\delta \Phi_1} \right|_{\Phi^*} = \Psi_1. \end{array} \right.\tag{4.58}$$

With these notations, we can make direct use of Eq.(2.69) which gives us:

$$\frac{\delta^3 \Gamma_m[\Psi]}{\delta \Psi_1 \delta \Psi_2 \delta \Psi_3} = -\text{Tr} \left( \frac{\delta^2 \Gamma_m[\Psi]}{\delta \Psi_1 \delta \Psi_{1'}} \frac{\delta^2 \Gamma_m[\Psi]}{\delta \Psi_2 \delta \Psi_{2'}} \frac{\delta^2 \Gamma_m[\Psi]}{\delta \Psi_3 \delta \Psi_{3'}} \frac{\delta^3 \ln Z_m[\Phi]}{\delta \Phi_1 \delta \Phi_{2'} \delta \Phi_{3'}} \right)_{\Phi^*}.\tag{4.59}$$



We are interested in the continuum space limit of this expression, evaluated in the liquid, and with 1, 2 and 3 that are all greater than  $mM$ . Then we get, after replacing derivatives with respect to  $\rho^{(2)}$  with derivatives with respect to  $h$ :

$$\begin{aligned}
& \Gamma_{ab,cd,ef}^{(0,3)}(x_1, y_1; x_2, y_2; x_3, y_3) = \\
& - \Gamma_{ab,a'}^{(1,1)}(x_1, y_1; x'_1) \Gamma_{cd,c'}^{(1,1)}(x_2, y_2; x'_2) \Gamma_{ef,e'}^{(1,1)}(x_3, y_3; x'_3) W_{a',c',e'}^{(3,0)}(x'_1; x'_2; x'_3) \\
& - \frac{2}{\rho^2} \Gamma_{ab,a'b'}^{(0,2)}(x_1, y_1; x'_2, x'_3) \Gamma_{cd,c'}^{(1,1)}(x_2, y_2; x'_2) \Gamma_{ef,e'}^{(1,1)}(x_3, y_3; x'_3) W_{a'b',c',e'}^{(2,1)}(x'_1, y'_1; x'_2; x'_3) \\
& - \text{two permutations } \{(a, b); (x_1, y_1)\} \leftrightarrow \{(c, d); (x_2, y_2)\} \leftrightarrow \{(e, f); (x_3, y_3)\} \\
& - \frac{4}{\rho^4} \Gamma_{ab,a'}^{(1,1)}(x_1, y_1; x'_1) \Gamma_{cd,c'd'}^{(0,2)}(x_2, y_2; x'_2, y'_2) \Gamma_{ef,e'f'}^{(0,2)}(x_3, y_3; x'_3, y'_3) W_{a',c'd',e'f'}^{(1,2)}(x'_1; x'_2, y'_2; x'_3, y'_3) \\
& - \text{two permutations } \{(a, b); (x_1, y_1)\} \leftrightarrow \{(c, d); (x_2, y_2)\} \leftrightarrow \{(e, f); (x_3, y_3)\} \\
& - \frac{8}{\rho^6} \Gamma_{ab,a'b'}^{(0,2)}(x_1, y_1; x'_1, y'_1) \Gamma_{cd,c'd'}^{(0,2)}(x_2, y_2; x'_2, y'_2) \Gamma_{ef,e'f'}^{(0,2)}(x_3, y_3; x'_3, y'_3) W_{a'b',c'd',e'f'}^{(0,3)}(x'_1, y'_1; x'_2, y'_2; x'_3, y'_3).
\end{aligned} \tag{4.60}$$

Implicit summation and integration over repeated indices and variables, is assumed for compactness.

We note that this expression is correct independantly of the value of  $m$ , the replica ansatz chosen, and the value of the fields  $\rho$  and  $\mathbf{h}$  chosen. However three simplifications will occur: we are performing a Taylor expansion in powers of  $h_{ab}$ , with  $a \neq b$ , so that the indices  $a, b, c, d, e$  and  $f$  in Eq. (4.60) must be chosen so that  $a \neq b$ ,  $c \neq d$  and  $e \neq f$ . Secondly we must evaluate the derivatives at zero off-diagonal correlation ( $\tilde{h} \rightarrow 0$  in the RS ansatz). Finally we are interested only in the dynamical transition point, which is described by the  $m \rightarrow 1$  limit. These three features will greatly simplify the calculation.

There are two types of objects that we need to compute in order to use this relation: cumulants of the microscopic densities that are generated by the differentiation of  $\ln Z_m$  with respect to  $\nu_a$  and  $w_{ab}$ , and second derivatives of  $\Gamma_m$  with respect to  $\rho_a$  and  $h_{ab}$ . In the end, we want to evaluate these objects in the liquid phase where  $\tilde{h}$  is equal to zero. But we know that the free energy can be written as the HNC free energy plus 2PI contributions, that are  $\mathcal{O}(\tilde{h}^3)$ , i.e. contain more than three  $\tilde{h}$  links. Thus when taking one or two derivatives of the 2PI diagrams with respect to  $\tilde{h}$ , they still will contain at least one  $\tilde{h}$  link, and will all cancel out when evaluated at zero  $\tilde{h}$ . This proves that Eq. (4.60) when evaluated in the liquid phase can be computed by replacing the  $\Gamma_m$  functionals in the r.h.s. by  $\Gamma_m^{\text{HNC}}$ .

Thus the needed derivatives of  $\Gamma_m$  can be computed starting from Eq. (2.179) by dropping the 2PI diagrams. The only difficult term is the sum of ring diagrams. We have seen that the derivative of the sum of chain diagrams with respect to a link is  $h - c$ . Thus we have that:

$$\frac{\delta \Gamma_m^{\text{HNC}}[\rho, \mathbf{h}]}{\delta h_{ab}(x_1, y_1)} = \frac{1}{2} \rho_a(x_1) \rho_b(y_1) \left( \ln(1 + h_{ab}(x_1, y_1)) - h_{ab}(x_1, y_1) + c_{ab}(x_1, y_1) \right). \tag{4.61}$$

In order to perform a second derivative with respect to  $h$ , one must resort to the expression of  $c$  as a function of  $h$  and  $\rho$  in Eq. (4.37). We can expand it perturbatively to find the equivalent of Eq. (2.176) to multicomponent systems:

$$c_{ab}(x, y) = h_{ab}(x, y) + \sum_{n=1}^{\infty} (-1)^n h_{aa_1}(x, x_1) \rho_{a_1}(x_1) \cdots \rho_{a_n}(x_n) h_{a_nb}(x_n, y), \tag{4.62}$$

We easily find upon differentiation:

$$\begin{aligned} \frac{\delta c_{ab}(x_1, y_1)}{\delta h_{cd}(x_2, y_2)} &= \rho_c(x_2)\rho_d(y_2) \left( \frac{1}{\rho_a(x_1)} \delta_{ac} \delta(x_1, x_2) - c_{ac}(x_1, x_2) \right) \left( \frac{1}{\rho_b(y_1)} \delta_{bd} \delta(y_1, y_2) - c_{bd}(y_1, y_2) \right), \\ &= \rho_c(x_2)\rho_d(y_2) \Gamma_{ac}^{(2)}(x_1, x_2) \Gamma_{bd}^{(2)}(y_1, y_2). \end{aligned} \quad (4.63)$$

In principle, this expression should be symmetrized with respect to a change of indices, but here everything will be traced in the end of the calculation, thus we can keep working with non-symmetrized quantities. We obtain as a consequence:

$$\begin{aligned} \frac{\delta^2 \Gamma_m^{HNC}[\boldsymbol{\rho}, \mathbf{h}]}{\delta h_{ab}(x_1, y_1) \delta h_{cd}(x_2, y_2)} &= \frac{1}{2} \rho_a(x_1) \rho_b(y_1) \left( \frac{1}{1 + h_{ab}(x_1, y_1)} - 1 \right) \delta_{ab, cd}(x_1, y_1; x_2, y_2) \\ &+ \frac{1}{2} \rho_a(x_1) \rho_b(y_1) \rho_c(x_2) \rho_d(y_2) \Gamma_{ac}^{(2)}(x_1, x_2) \Gamma_{bd}^{(2)}(y_1, y_2). \end{aligned} \quad (4.64)$$

And finally taking the limit  $\tilde{h} \rightarrow 0$  with  $a \neq b$  (a limit we denote by  $\bullet|_{liq}$  in the following) we get:

$$\begin{aligned} \Gamma_{ab, cd}^{(0,2)}(x_1, y_1; x_2, y_2) |_{liq} &= \frac{1}{2} \rho^4 \delta_{ac} \delta_{bd} \Gamma_{liq}^{(2)}(x_1, x_2) \Gamma_{liq}^{(2)}(y_1, y_2), \\ &\equiv \frac{1}{2} \rho^4 \delta_{ac} \delta_{bd} \Gamma_{HNC}^{(0,2)}(x_1, x_2; y_1, y_2). \end{aligned} \quad (4.65)$$

The other needed derivative is  $\Gamma^{(1,1)}$ , which is calculated from Eq. (4.61) by noting that differentiating  $c$  with respect to the density, at  $h$  fixed, simply gives a product of  $c$  functions:

$$\frac{\delta c_{ab}(x_1, y_1)}{\delta \rho_c(x_2)} = -c_{ac}(x_1, x_2) c_{bc}(y_1, x_2). \quad (4.66)$$

Now recall that derivatives with respect to density must be done at  $\rho^{(2)}$  fixed instead, so we use the chain rule:

$$\left. \frac{\delta c_{ab}(x_1, y_1)}{\delta \rho_c(x_2)} \right|_{\rho^{(2)} \text{ cte}} = \left. \frac{\delta c_{ab}(x_1, y_1)}{\delta \rho_c(x_2)} \right|_{h \text{ cte}} + \sum_{e,f} \int_{u,v} \left. \frac{\delta h_{ef}(u, v)}{\delta \rho_c(x_2)} \right|_{\rho^{(2)} \text{ cte}} \left. \frac{\delta c_{ab}(x_1, y_1)}{\delta h_{ef}(u, v)} \right|_{\rho \text{ cte}}, \quad (4.67)$$

to obtain the final result:

$$\left. \frac{\delta^2 \Gamma_m^{HNC}[\boldsymbol{\rho}, \mathbf{h}]}{\delta h_{ab}(x_1, y_1) \delta \rho_c(x_2)} \right|_{liq} = -\frac{1}{2S(k=0)} \left[ \delta_{ac} \Gamma_{liq}^{(2)}(y_1, x_2) + \delta_{bc} \Gamma_{liq}^{(2)}(x_1, x_2) \right], \quad (4.68)$$

where  $S(k)$  is the structure factor of the liquid.

If we drop the space indexes, we can now perform the trace over replica indexes in Eq. (4.60), since all derivatives are delta functions with respect to replica indices. We obtain:

$$\begin{aligned} \Gamma_{ab, cd, ef}^{(0,3)} &= -\rho^6 \Gamma_{HNC}^{(0,2)} \otimes \Gamma_{HNC}^{(0,2)} \otimes \Gamma_{HNC}^{(0,2)} \otimes W_{ab, cd, ef}^{(0,3)} \\ &+ \frac{\rho^4}{2S(0)} \Gamma_{liq}^{(2)} \otimes \Gamma_{HNC}^{(0,2)} \otimes \Gamma_{HNC}^{(0,2)} \otimes W_{ab, cd, e}^{(1,2)} \\ &+ \{2 \text{ perms.}\} \\ &- \frac{\rho^2}{2S(0)} \Gamma_{liq}^{(2)} \otimes \Gamma_{liq}^{(2)} \otimes \Gamma_{HNC}^{(0,2)} \otimes W_{ab, c, e}^{(2,1)} \\ &- \{2 \text{ perms.}\} \\ &+ \frac{1}{8S(0)} \Gamma_{liq}^{(2)} \otimes \Gamma_{liq}^{(2)} \otimes \Gamma_{liq}^{(2)} \otimes W_{a, c, e}^{(3,0)}. \end{aligned} \quad (4.69)$$

where  $\otimes$  means space convolution with respect to two spatial indexes.

Finally, we only have left the task to compute the derivatives of the logarithm of the partition function with respect to pair potentials or chemical potentials. These terms are cumulants of microscopic one- or two-point densities, that are easily computed within the RS framework that we use here, as we explain in the following.

### 4.3.1 Replica symmetric structure of the theory

We have denoted by  $\langle \bullet \rangle$  the equilibrium average for the replicated system. Once again, in the limit  $w_{ab} \rightarrow 0$  for  $a \neq b$ , all replicas fall in the same state but are otherwise uncorrelated inside the state. Finally, we want to evaluate all our averages in the liquid phase. This leads to the following rule to compute the average  $\langle \bullet \rangle$ : one should

- factorize the averages  $\langle \bullet \rangle$  when they involve different replicas, and
- remove the replica indexes.
- replace  $\langle \bullet \rangle = \langle \bullet \rangle_{liq}$

For instance, for any spatial argument, and for  $a \neq b$ , we have that following the prescription above

$$\langle \hat{\rho}_a \hat{\rho}_b \rangle = \langle \hat{\rho}_a \rangle \langle \hat{\rho}_b \rangle = \langle \hat{\rho} \rangle_{liq} \langle \hat{\rho} \rangle_{liq} = \rho^2 . \quad (4.70)$$

Similarly, assuming that different letters denote different values of the indexes:

$$\begin{aligned} \langle \hat{\rho}_a \hat{\rho}_a \hat{\rho}_b \rangle &= \langle \hat{\rho}_a \hat{\rho}_a \rangle \langle \hat{\rho}_b \rangle = \langle \hat{\rho} \hat{\rho} \rangle_{liq} \langle \hat{\rho} \rangle_{liq} = \rho(G_{liq} + \rho^2) , \\ \langle \hat{\rho}_{ab}^{(2)} \hat{\rho}_{ac}^{(2)} \rangle &= \langle \hat{\rho}_a \hat{\rho}_b \hat{\rho}_a \hat{\rho}_c \rangle = \langle \hat{\rho}_a \hat{\rho}_a \rangle \langle \hat{\rho}_b \rangle \langle \hat{\rho}_c \rangle = \langle \hat{\rho} \rangle_{liq} \langle \hat{\rho} \rangle_{liq} \langle \hat{\rho} \hat{\rho} \rangle_{liq} = \rho^2 (G_{liq} + \rho^2) . \end{aligned} \quad (4.71)$$

We will thus obtain quantities that do not depend on replica indices anymore, allowing to sum over these indices, and finally take the  $m \rightarrow 1$  limit. The free-energy will have an overall factor  $m(m-1)$ , and thus we will consider the free energy divided by  $m(m-1)$ . Indeed, recalling that we will calculate a free-energy correction of the form:

$$\begin{aligned} \delta\Gamma_m[\boldsymbol{\rho}, \mathbf{h}] &\equiv \frac{1}{3!} \sum_{a \neq b} \sum_{c \neq d} \sum_{e \neq f} \int_{x_1, y_1, \dots, x_3, y_3} \Gamma_{ab,cd,ef}^{(0,3)}(x_1, y_1; x_2, y_2; x_3, y_3) h_{ab}(x_1, y_1) h_{cd}(x_2, y_2) h_{ef}(x_3, y_3) \\ &= \frac{1}{3!} \int_{x_1, \dots, y_3} \left( \sum_{a \neq b, c \neq d, e \neq f} \Gamma_{ab,cd,ef}^{(0,3)}(x_1, y_1; x_2, y_2; x_3, y_3) \right) \tilde{h}(x_1, y_1) \tilde{h}(x_2, y_2) \tilde{h}(x_3, y_3) \end{aligned} \quad (4.72)$$

Now it is in order to remember that we will want to evaluate everything at  $m = 1$  at the end of the calculation. Everything will be proportional to  $m - 1$ , thus we will first remove this factor before evaluating. Afterwards, all terms that contain an additional factor  $m - 1$  will disappear. Now when we look at Eq.(4.69), we see that there are terms in which replica indices do not appear explicitly, for example in the term containing  $W_{a,c,e}^{(3,0)}$ ,  $b, d$  and  $f$  do not appear. They are only constrained to be different from their conjugate indices  $a, c$  and  $e$  respectively, thus when summing over all values of these indices, we will obtain three factors  $m - 1$ , and the term will cancel in the  $m \rightarrow 1$  limit. This observation allow us to discard all terms but those containing  $W^{(0,3)}$  in the limit  $m \rightarrow 1$ .

### 4.3.2 Final calculation

Before turning to the explicit evaluation of  $W^{(0,3)}$ , it is useful to remark that, within the RS structure that we have, we can parametrize its replica dependence in a simple way.

Take a matrix that depends on two pairs of replica indexes  $M_{ab,cd}$ , with  $a \neq b$  and  $c \neq d$  (we do not explicit the space indexes). Examination of the different possibilities for  $a, b, c$  and  $d$  shows that we have only three genuinely different possibilities:

$$M_{ab,cd} = \begin{cases} M_{ab,ab} , \\ M_{ab,ac} , \\ M_{ab,cd} . \end{cases} \quad (4.73)$$

This is a consequence both of the RS ansatz and of the symmetry of the functions with respect to permutations of indexes (and their associated space indexes). This can be summarized in:

$$M_{ab,cd} = M_1 \frac{\delta_{ac}\delta_{bd} + \delta_{ad}\delta_{bc}}{2} + M_2 \frac{\delta_{ac} + \delta_{ad} + \delta_{bc} + \delta_{bd}}{4} + M_3 , \quad (4.74)$$

where  $M_1, M_2$  and  $M_3$  are related to the above terms by:

$$\begin{cases} M_1 = 2 [M_{ab,ab} - 2M_{ab,ac} + M_{ab,cd}] , \\ M_2 = 4 [M_{ab,ac} - M_{ab,cd}] , \\ M_3 = M_{ab,cd} . \end{cases} \quad (4.75)$$

The quantity that we are interested in is a matrix that depends on three pairs of indexes. In this case there are 8 topologically different possibilities [164]:

$$W_{ab,cd,ef}^{(0,3)} = \begin{cases} W_1 = W_{ab,bc,ca} , \\ W_2 = W_{ab,ab,ab} , \\ W_3 = W_{ab,ab,ac} , \\ W_4 = W_{ab,ab,cd} , \\ W_5 = W_{ab,ac,bd} , \\ W_6 = W_{ab,ac,ad} , \\ W_7 = W_{ab,ac,de} , \\ W_8 = W_{ab,cd,ef} . \end{cases} \quad (4.76)$$

A relation like Eq. (4.74) is again possible, but cumbersome, and we do not write it explicitly because

we do not need it. By using the prescription for calculating averages of one and two-point densities described above, we can easily compute the  $W_i$ . We obtain:

$$W_1 = \frac{1}{8} \left[ \begin{array}{l} G_{liq}(x_1, x_2)G_{liq}(y_1, x_3)G_{liq}(y_2, y_3) \\ + \rho^2 (G_{liq}(x_1, x_2)G_{liq}(y_1, x_3) + G_{liq}(x_1, x_2)G_{liq}(y_2, y_3) + G_{liq}(y_1, x_3)G_{liq}(y_2, y_3)) \end{array} \right] , \quad (4.77)$$

$$W_2 = \frac{1}{8} \left[ \begin{array}{l} W_{liq}^{(3)}(x_1, x_2, x_3)W_{liq}^{(3)}(y_1, y_2, y_3) \\ + \rho W_{liq}^{(3)}(x_1, x_2, x_3) (\rho^2 + G_{liq}(y_1, y_2) + G_{liq}(y_1, y_3) + G_{liq}(y_2, y_3)) \\ + \rho W_{liq}^{(3)}(y_1, y_2, y_3) (\rho^2 + G_{liq}(x_1, x_2) + G_{liq}(x_1, x_3) + G_{liq}(x_2, x_3)) \\ + \rho^2 (G_{liq}(x_1, x_2)G_{liq}(y_1, y_3) + G_{liq}(x_1, x_2)G_{liq}(y_2, y_3) + G_{liq}(x_1, x_3)G_{liq}(y_1, y_2)) \\ + \rho^2 (G_{liq}(x_1, x_3)G_{liq}(y_2, y_3) + G_{liq}(x_2, x_3)G_{liq}(y_1, y_2) + G_{liq}(x_2, x_3)G_{liq}(y_1, y_3)) \end{array} \right] , \quad (4.78)$$

$$W_3 = \frac{1}{8} \left[ \rho^3 W_{liq}^{(3)}(x_1, x_2, x_3) + \rho G_{liq}(y_1, y_2) \left( W^{(3)}(x_1, x_2, x_3) + \rho G_{liq}(x_1, x_3) + \rho G_{liq}(x_2, x_3) \right) \right], \quad (4.79)$$

$$W_5 = \frac{1}{8} \rho^3 W_{liq}^{(3)}(x_1, x_2, x_3), \quad (4.80)$$

$$W_6 = \frac{1}{8} \rho^2 G_{liq}(x_1, x_2) G_{liq}(y_1, x_3), \quad (4.81)$$

and we find  $W_4 = W_7 = W_8 = 0$ . The factors  $1/8$  come from the fact that a derivative of  $\ln Z_m$  with respect to  $w$  gives  $\hat{\rho}^{(2)}/2$  and not  $\hat{\rho}^{(2)}$ . Of course, the choice of spatial indexes is arbitrary, and one can make any permutation, as long as it respects the symmetry of the functions. We can now perform the trace over replica indexes in Eq. (4.72), which will give an expression analytic in  $m$ . We omit the space indices in the following, but they are recovered by considering all permutations of the space indices written in Eqs. (4.77–4.81). The number of terms are obtained by considering the number of possible ways to choose a particular arrangement of replica indices among  $m$  indices. For example to construct a term contributing to  $W_2$ , one must first pick a value of  $a$  ( $m$  possibilities), then a different value of  $b$  ( $m-1$  possibilities) which shows that the trace of  $W_2$  let appear  $m(m-1)$  identical terms (with the exact same space indices structure). In addition to this multiplicity, because of the invariance by permutation of indices (together with their corresponding space indices), we have that:

$$W_{ab,ab,ab}^{(0,3)} = W_{ab,ba,ab}^{(0,3)} = W_{ab,ab,ba}^{(0,3)} = W_{ab,ba,ba}^{(0,3)}, \quad (4.82)$$

and this will give four terms that have the same replica structure, but permutations of space indices. The multiplicity of  $W_2$  is thus  $4m(m-1)$ . Performing the same counting on all cubic masses, we obtain:

$$\frac{1}{m(m-1)} \sum_{a \neq b, c \neq d, e \neq f} W_{ab,cd,ef}^{(0,3)} = 4W_2 + (m-2)[8W_1 + 24W_3] + (m-2)(m-3)[8W_5 + 24W_6] + \mathcal{O}(m-1). \quad (4.83)$$

After taking the  $m \rightarrow 1$  limit, we obtain:

$$\begin{aligned} \lim_{m \rightarrow 1} \frac{1}{m(m-1)} \sum_{a \neq b} \sum_{c \neq d} \sum_{e \neq f} W_{ab,cd,ef}^{(0,3)} &= 4W_2 - 8W_1 - 24W_3 + 16W_5 + 48W_6 \\ &= \frac{1}{2} W_{liq}^{(3)}(x_1, x_2, x_3) W_{liq}^{(3)}(y_1, y_2, y_3) - G_{liq}(x_1, x_2) G_{liq}(y_1, x_3) G_{liq}(y_2, y_3). \end{aligned} \quad (4.84)$$

Finally we can perform the convolution with the derivatives of the HNC free energy in Eq. (4.72), and by making repeated use of the second- and third-order OZ equations we obtain:

$$\lim_{m \rightarrow 1} \frac{\delta \Gamma_m[\boldsymbol{\rho}, \mathbf{h}]}{m(m-1)} = -\frac{\rho^6}{6} \int_{x_1, \dots, y_3} V(x_1, \dots, y_3) \tilde{h}(x_1, y_1) \tilde{h}(x_2, y_2) \tilde{h}(x_3, y_3), \quad (4.85)$$

$$V(x_1, \dots, y_3) = \frac{1}{2} \Gamma_{liq}^{(3)}(x_1, x_2, x_3) \Gamma_{liq}^{(3)}(y_1, y_2, y_3) - \Gamma_{liq}^{(2)}(x_1, x_2) \Gamma_{liq}^{(2)}(y_1, x_3) \Gamma_{liq}^{(2)}(y_2, y_3). \quad (4.86)$$

This third order correction includes the RHNC term, which is recovered by setting  $c_{liq}^{(3)} = 0$  [82], but which we can also recover by directly differentiating Eq. (4.65). In any case we find:

$$V(x_1, \dots, y_3) = V^{HNC}(x_1, \dots, y_3) + V^{2PI}(x_1, \dots, y_3), \quad (4.87)$$

where we defined:

$$V^{HNC}(x_1, \dots, y_3) = -\Gamma_{liq}^{(2)}(x_1, x_2) \Gamma_{liq}^{(2)}(y_1, x_3) \Gamma_{liq}^{(2)}(y_2, y_3) + \frac{1}{2\rho^4} \delta(x_1, x_2) \delta(x_1, x_3) \delta(y_1, y_2) \delta(y_1, y_3), \quad (4.88)$$

which is the contribution coming from  $\Gamma_m^{HNC}$ , and

$$V^{2PI}(x_1, \dots, y_3) = \frac{1}{2} c_{liq}^{(3)}(x_1, x_2, x_3) c_{liq}^{(3)}(y_1, y_2, y_3) + \frac{1}{2\rho^2} \delta(x_1, x_2) \delta(x_1, x_3) c_{liq}^{(3)}(y_1, y_2, y_3), \quad (4.89)$$

which is the sought for contribution coming from  $\Gamma_m^{2PI}$ . We obtain finally:

$$\begin{aligned} \frac{\Gamma_m[\boldsymbol{\rho}, \mathbf{h}]}{m(m-1)} \Big|_{m=1} &= \frac{\Gamma_m^{HNC}[\boldsymbol{\rho}, \mathbf{h}]}{m(m-1)} \Big|_{m=1} - \frac{\rho^4}{6} \int_{x_1, x_2, x_3, y} c_{liq}^{(3)}(x_1, x_2, x_3) \tilde{h}(x_1, y) \tilde{h}(x_2, y) \tilde{h}(x_3, y) \\ &\quad - \frac{\rho^6}{12} \int_{x_1, \dots, y_3} c_{liq}^{(3)}(x_1, x_2, x_3) c_{liq}^{(3)}(y_1, y_2, y_3) \tilde{h}(x_1, y_1) \tilde{h}(x_2, y_2) \tilde{h}(x_3, y_3). \end{aligned} \quad (4.90)$$

This is the desired result: the next order term in the order-parameter expansion beyond the RHNC approximation. From this approximation of the free-energy, we can make use of the variational principle to obtain a closed equation on  $\tilde{h}$ . For a translationally invariant system we get:

$$\begin{aligned} \tilde{c}(r) = \tilde{h}(r) - \ln[1 + \tilde{h}(r)] &+ \frac{\rho^4}{2} \int_{r_1 \dots r_4} c_{liq}^{(3)}(r, r_1, r_3) c_{liq}^{(3)}(0, r_2, r_4) \tilde{h}(r_1, r_2) \tilde{h}(r_3, r_4) \\ &+ \frac{\rho^2}{2} \int_{r_1, r_2} c_{liq}^{(3)}(r, r_1, r_2) \tilde{h}(r_1) \tilde{h}(r_2) + \frac{\rho^2}{2} \int_{r_1, r_2} c_{liq}^{(3)}(0, r_1, r_2) \tilde{h}(r - r_1) \tilde{h}(r - r_2). \end{aligned} \quad (4.91)$$

which provides the first correction to Eq. (4.44). Using translational invariance as well as the invariance under permutation of the three variables of  $c^{(3)}$ , we get:

$$\begin{aligned} c_{liq}^{(3)}(r_1, r_2, r_3) &= c_{liq}^{(3)}(r_1 - r_2; r_1 - r_3) \equiv c_{liq}^{(3)}(r; s), \\ \text{with } r = r_1 - r_2 \quad s &= r_1 - r_3, \\ c_{liq}^{(3)}(r; s) &= c_{liq}^{(3)}(s, r) = c_{liq}^{(3)}(-r; s - r). \end{aligned} \quad (4.92)$$

Defining the double fourier transform of  $c_{liq}^{(3)}$  as:

$$c_{liq}^{(3)}(k, q) = \int_{r, s} e^{-ikr} e^{-iqs} c_{liq}^{(3)}(r, s), \quad (4.93)$$

we obtain two invariance principles:

$$c_{liq}^{(3)}(k, q) = c_{liq}^{(3)}(q, k) = c_{liq}^{(3)}(-k - q, q). \quad (4.94)$$

Performing a Fourier transformation on our equation we get

$$\begin{aligned} \tilde{c}(k) = \mathcal{F}(\tilde{h} - \ln[1 + \tilde{h}]) &(k) + \frac{\rho^4}{2} \int_q c_{liq}^{(3)}(-k, q) c_{liq}^{(3)}(k, -q) \tilde{h}(q) \tilde{h}(k - q) \\ &+ \frac{\rho^2}{2} \int_q c_{liq}^{(3)}(q, k - q) \tilde{h}(q) \tilde{h}(k - q) + \frac{\rho^2}{2} \int_q c_{liq}^{(3)}(-q, -k + q) \tilde{h}(q) \tilde{h}(k - q), \end{aligned} \quad (4.95)$$

which using the invariances in Eq. (4.94) is simplified to:

$$\tilde{c}(k) = \mathcal{F}(\tilde{h} - \ln[1 + \tilde{h}]) (k) + \frac{1}{2} \int_q \left( \left[ 1 + \rho^2 c_{liq}^{(3)}(q, k - q) \right]^2 - 1 \right) \tilde{h}(q) \tilde{h}(k - q). \quad (4.96)$$

Before turning to a numerical resolution of this equation, we can again make the naive expansion of the HNC term in powers of  $\tilde{h}$ , and keep only the lowest order term, to obtain:

$$\frac{f(k)}{1 - f(k)} = \frac{S(k)}{2\rho} \int_q \rho^4 \Gamma_{liq}^{(3)}(k, -q)^2 S(q) S(k - q) f(q) f(k - q). \quad (4.97)$$

This recovers exactly the three-body term in the MCT kernel Eq. (1.10). This result is highly surprising because it is the outcome of a purely static calculation, while the MCT kernel arises from a dynamical calculation.

### 4.3.3 Three-body correlations and numerical solving

We thus have obtained a closed equation of the order-parameter, that necessitates as an input the two- and three-body direct correlation functions of the liquid. We already quoted that we decided here to work within the PY approximation for the two-point functions. It is known [77] that the PY approximation [141], which amounts to treat the fluid in a mean-field approximation, but under the exact constraint that the pair correlation function should vanish for distances smaller than 1 [63], is particularly efficient for hard spheres. Furthermore, we dispose of an analytic expression for the two-body direct correlation function in that approximation [171, 165]. However, the three-body direct correlation function still needs to be approximated. Computing the third-order direct correlation function is in itself a hard problem of liquid theory. The best approximation available was shown by numerical works [24] to be the HNC3 approximation developed by Attard [8]. However, this approximation is very computationally demanding, and because our purpose here is merely to demonstrate the importance of higher-order terms in the expansion in powers of the order parameter, we do not aim at quantitative efficiency, and wish to find a simpler approximation scheme.

### 4.3.4 Denton & Ashcroft approximation

A good compromise between simplicity and efficiency for evaluating the third-order direct correlation function [23] is the Denton-Ashcroft approximation [56]. This approximation gives an analytic form that necessitates as an input only the second-order direct correlation function, for which we can use the PY result. Within their approximation,  $c_{liq}^{(3)}$  is given by:

$$c_{DA}^{(3)}(k, q) = \frac{1}{c_{liq}^{(2)}(0)} \left[ c_{liq}^{(2)}(k) \partial_\rho c_{liq}^{(2)}(q) + c_{liq}^{(2)}(q) \partial_\rho c_{liq}^{(2)}(k) \right] - \frac{\partial_\rho c_{liq}^{(2)}(0)}{\left( c_{liq}^{(2)}(0) \right)^2} c_{liq}^{(2)}(k) c_{liq}^{(2)}(q). \quad (4.98)$$

Within this approximation, angular dependance is neglected. We can recover it by symmetrizing the expression:

$$c_{DAS}^{(3)}(k, q) = \frac{1}{3} \left[ c_{DA}^{(3)}(k, q) + c_{DA}^{(3)}(k, |k+q|) + c_{DA}^{(3)}(q, |k+q|) \right]. \quad (4.99)$$

As stated before, we use as an input the Percus-Yevick direct correlation function, that reads (in units of the hard-sphere diameter):

$$c_{PY}^{(2)}(r) = \begin{cases} -a - 6 \varphi b r - \frac{1}{2} \varphi a r^3 & r \leq 1, \\ 0 & r > 1. \end{cases} \quad (4.100)$$

where  $\varphi$  is the packing fraction,  $a = (1 + 2\varphi)^2 / (1 - \varphi)^4$  and  $b = -(1 + \varphi/2)^2 / (1 - \varphi)^4$ . The corresponding Fourier transforms, and derivatives with respect to density are simply computed analytically. Using this approximation for  $c_{liq}^{(3)}$ , and writing the integrals in bipolar coordinates by using the isotropy of the liquid, we obtain the following set of equations:

$$\begin{cases} \tilde{c}(k) &= F(k) + H(k), \\ F(r) &= \tilde{h}(r) - \ln \left( 1 + \tilde{h}(r) \right), \\ H(k) &= \frac{\rho S(k)}{8\pi^2 k} \int_0^\infty du \int_{|k-u|}^{k+u} dv u v \tilde{h}(u) \tilde{h}(v) \left( \left[ 1 + \rho^2 \tilde{c}_{DAS}^{(3)}(u, v; k) \right]^2 - 1 \right), \end{cases} \quad (4.101)$$

where we have defined

$$\hat{c}_{DAS}^{(3)}(u, v; k) = \frac{1}{3} \left[ c_{DA}^{(3)}(k, u) + c_{DA}^{(3)}(k, v) + c_{DA}^{(3)}(u, v) \right]. \quad (4.102)$$

Equations (4.98) – (4.102) now completely specify our approximation. We present in the following a preliminary numerical resolution in order to demonstrate the importance of the correction  $H$ .

### 4.3.5 Numerical resolution methodology

The usual calculation for HNC alone is more stable if we write the iteration procedure in terms of  $\tilde{c}$  and  $\tilde{\chi} = \tilde{h} - \tilde{c}$ , which would give in our case:

$$\tilde{c}(r) = e^{\tilde{\chi}(r)+H(r)} - 1 - \tilde{\chi}(r), \quad (4.103)$$

or the same equation with  $H = 0$  in the case of RHNC. We first solve the RHNC equation Eq. (4.101) with  $H = 0$ , by using PY approximation for the two-point functions. Once a stable solution of the RHNC equations has been found we introduce the three-body correction  $H$ , and solve by the very same Picard iterative scheme that is used for solving HNC and RHNC. Explicitly, the resolution will give:

- Start from the value of  $k\tilde{c}(k)$ , obtained with the previous iteration, or from the old HNC value if first iteration
- Use Eq. (4.37) to deduce the value of  $k\tilde{h}(k)$  and  $k\tilde{\chi}(k)$
- Use  $k\tilde{h}(k)$  to evaluate  $kH(k)$
- Inverse Fourier transform  $k\tilde{\chi}(k)$  and  $kH(k)$  to obtain  $r\tilde{\chi}(r)$  and  $rH(r)$
- Use it to evaluate the new  $r\tilde{c}(r)$  with Eq. (4.103)
- Fourier transform  $r\tilde{c}(r)$  to obtain  $k\tilde{c}(k)$
- Mix it with the old  $k\tilde{c}(k)$  to avoid rapid changes
- Repeat these steps until  $k\tilde{c}(k)$  has converged

We used a grid of  $2^{10}$  equally spaced points on a box of size 11, and a mixing parameter 0.01. We note that evaluation of the correcting term  $H$  in Eq. (4.101) has a computational cost of order of the square number of points on the grid, significantly slowing down the resolution of the equation, since to avoid instabilities,  $\tilde{c}$  is made to evolve very slowly by the mixing procedure.

### 4.3.6 Results and discussion

We solved our improved equation (4.101) for several packing fractions starting from  $\varphi = 0.6$ , and decreasing it until the non-trivial solution for  $\tilde{h}$  disappeared. We found that the inclusion of the three-body terms, even when using a crude approximation such as the symmetrized Denton & Ashcroft approximation, leads to a strong shift of the dynamical transition point from  $\varphi_d = 0.591897$  to  $\varphi_d = 0.555860$ , which is closer to the predicted MCT transition but farther from the numerically estimated transition. It is hard to guess what would be the evolution of  $\varphi_d$  when additional corrections are added.



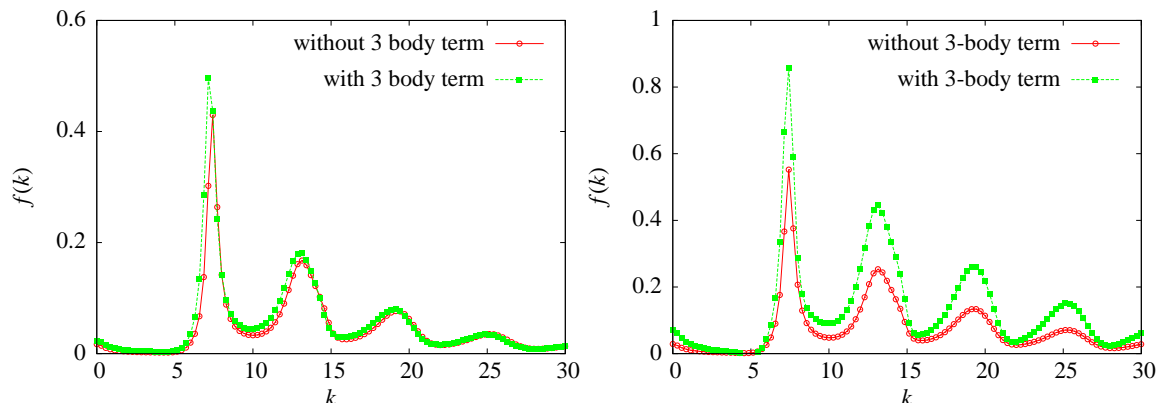


Figure 4.4: Left: Non-ergodicity factor as a function of the wave vector very close to the critical point  $\varphi = \varphi_d$ , for the PY + HNC calculation, and with inclusion of the three body term. Right: Non-ergodicity factor as a function of the wave vector at fixed packing fraction 0.6, for the PY + RHNC calculation, and with inclusion of the three body term.

The resulting non-ergodicity factors at the transition are depicted in the left panel of Fig. 4.4. The inclusion of the three body term has significantly enhanced the first peak of  $f(k)$  upon inclusion of our correction. These preliminary results must be treated with caution, because it was found [66] that the numerical solving of the RHNC equation is sensitive to the discretization used, and very large grids with a very large number of points must be used in order to obtain stable results. This situation is expected to be the same with the presence of the 3 body term, but the  $\mathcal{O}(N^2)$  scaling of the numerical resolution in our case prevented us from performing a stability analysis. The qualitative picture is nevertheless not expected to be modified by these considerations.

In the right panel of Fig. 4.4 we show the results inside the glass phase, at a fixed packing fraction  $\varphi = 0.6$ , with and without inclusion of the three-body term. In this case the effect of including the 3-body term is much bigger and goes in the right direction of increasing  $f(k)$  at small  $k$  (although still not enough at very small  $k$  below the first peak).

### 4.3.7 Higher orders

Our calculation provides the *exact* free-energy and correlation function at order  $\tilde{h}^2$ . This feature allows us to put into correspondence the MCT kernel, which is also  $\mathcal{O}(f^2)$ , with the replica result. We have seen that the MCT kernel in Eq. (1.10) contains exactly the three-body contribution we obtain with replica theory, which is already a quite surprising result, given the differences that exist between the two approaches. However, it shows that the two-body terms contained in the MCT kernel are thus impossible to obtain within a static framework. The peculiar wave-vector dependance of these terms arise from the calculation of forces, inherent in dynamical theories, but absent in static ones. One could however wonder whether these two-body terms could arise in a dynamical calculation because of the factorization of a dynamical four-point vertex function, that would be forced to be expressed as a  $\mathcal{O}(f^2)$  function. Indeed, the main approximation involved in Mode-Coupling theories is the factorization of a four-point function, and since MCT breaks down at high dimensions, it is possible that in the process, “glassy” correlations are factorized along with “liquid” ones, forcefully introducing these new  $\mathcal{O}(f^2)$  terms. This is nevertheless highly speculative, and no satisfying dynamical theory exists yet, that would be able to investigate these considerations (note however two formulations in

[159] and [117] that may have this potential).

An interesting feature of our calculation is that, once the theory is set up, we can already uncover the next terms with a diagrammatical visualization of the expansion. To go further, we can now wonder what is the term  $\mathcal{O}(\tilde{h}^4)$  in the free-energy (that would correspond to a  $\mathcal{O}(f^3)$  term for the correlation function). The requirement that we must have 2PI diagrams is quite strong, and it is easy to convince one-self that the only possible diagram that we can construct is shown in Figure 4.5. The four-point functions that are connected by  $\tilde{h}$  lines are made of 1PI diagrams, and we will thus obtain a new contribution to the free-energy that contains the 4-point vertex functions of the liquid:

$$\text{const} \times \int_{r_1, \dots, r_8} \Gamma_{liq}^{(4)}(r_1, \dots, r_7) \Gamma_{liq}^{(4)}(r_2, \dots, r_8) \times \tilde{h}(r_1, r_2) \cdots \tilde{h}(r_7, r_8). \quad (4.104)$$

Interestingly, we don't even have to work out the precise diagrammatics behind this procedure, since RHNC gives a contribution in every diagram, and at all orders in  $\tilde{h}$ , so that we can use RHNC to fix the prefactor of each diagram we compute.

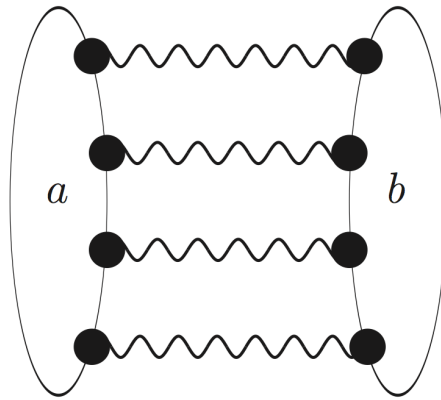


Figure 4.5: Diagrams that contribute to the free-energy at order  $\tilde{h}^4$ . A wiggly line joining two replica indices  $a$  and  $b$  is a  $h_{ab}$ , with  $a \neq b$  function, a black dot attached to a zone with replica index  $a$  is an integration point weighted by a density factor  $\rho_a$ .

Computing the  $n$ -th order direct correlation function is still a difficult problem, but with approximations such as the Denton-Ashcroft approximation, that are issued from density functional theory, we can deduce from the approximation for  $c^{(3)}$  the corresponding approximation for  $c^{(n)}$  by successive differentiation with respect to density. The last difficulty is that an  $\mathcal{O}(f^n)$  kernel will require the numerical evaluation of an  $n$ -dimensional integral, that have a computational cost of order  $\mathcal{O}(N^n)$ .

In order to visualize the increasing difficulty of going to the next orders, we show in Figure 4.6 the possible diagrams at order  $\tilde{h}^5$ . We see that new, intricate terms arise, and that in general, the  $\mathcal{O}(\tilde{h}^n)$  contribution will contain all vertex functions of the liquid of orders ranging from 3 to  $n$ .

## 4.4 Conclusion and discussion

Our analysis shows that the 2PI corrections to the RHNC free energy are quantitatively relevant at the dynamical transition, and must be properly taken into account in order to obtain an accurate static description of the transition. It seems then that only by doing this properly we will be able to make a clear connection between dynamical and static theories of the dynamical transition of glasses. In this respect our results are the following:

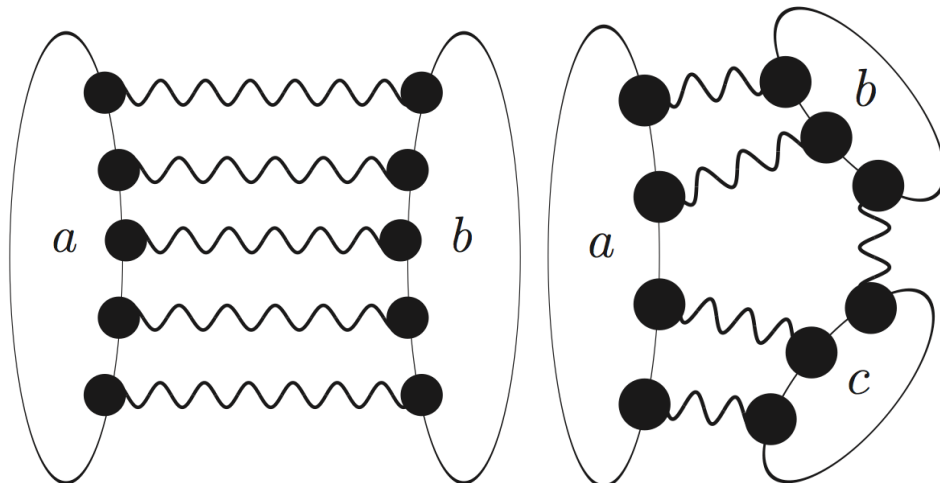


Figure 4.6: Diagrams that contribute to the free-energy at order  $\tilde{h}^5$ . A wiggly line joining two replica indices  $a$  and  $b$  is a  $h_{ab}$ , with  $a \neq b$  function, a black dot attached to a zone with replica index  $a$  is an integration point weighted by a density factor  $\rho_a$ .

- At the level of the RHNC approximation, the equation for  $f(k)$  can be developed in powers of  $f(k)$ . The result is Eq. (4.47), which corresponds to the Mode-Coupling equation with a kernel equal to 1. The latter is also the result of a zero-th order field theory calculation as reported in [3].
- The first correction to the RHNC approximation provides an additional contribution to the kernel which happens to correspond exactly to the three-body term of the Mode-Coupling kernel.
- The next corrections will give terms proportional to  $f^3$  in the right hand side of Eq. (4.47), hence no additional contributions to the Mode-Coupling kernel can be generated by these terms. We are forced to conclude that there is no way of generating the terms of the Mode-Coupling kernel proportional to  $c_{liq}(k)$  by means of a static computation.
- We have shown the way to compute higher-order terms, although we expect the numerical resolution of the corresponding approximations to be hard.

It would be therefore very important to perform a similar calculation (namely, a systematic expansion in powers of  $f(k)$ ) also on the dynamical side. This would allow for a systematic comparison of the results. One would then obtain a proper theory for the ergodicity breaking that occurs at  $\varphi_d$ , free of the ambiguities of MCT, and systematically improvable. Work has been done in this direction in the last years [3, 91, 4, 85], but the situation is still unsatisfactory.

On the static side, the first task to be performed is to reconcile the small cage expansion and the 2PI approach that we use in this work in order to have a unified static theory. The way to do this is indicated by the shape of the pair correlation function between two different replicas at the transition, depicted in Fig. 4.7. We see that  $\tilde{g}$  develops a strong peak at  $r = 0$ , that dominates the rest of its features. This peak simply reflects the fact that, in the glass phase, two replicas tend to be very close from each other. In the small cage expansion, this idea is reflected in the introduction of a cage size parameter  $A$ , which serves as a expansion parameter. In our case a direct introduction of the cage size  $A$  would be more difficult, because it would amount to parametrize the pair correlation

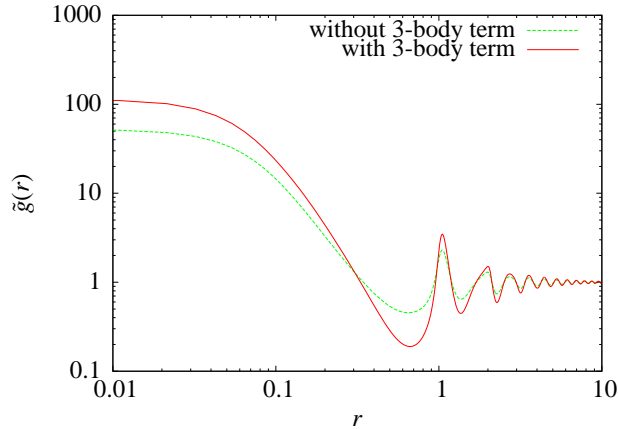


Figure 4.7: Inter-replica pair correlation function  $\tilde{g}(r)$  at packing fraction  $\varphi = 0.6$ , with and without three-body correction.

function by the cage size, which is difficult to do without specifying a given shape of cages. In the high dimensional limit, the cage can safely be approximated by a Gaussian as far as the free energy is concerned [103], but this is not expected to hold in our low dimensional case [39].

It is interesting to note that we have observed, as in Fig. 4.7 that the inclusion of the three-body term systematically increases the spatial separation between the first, glassy, peak of  $\tilde{g}(r)$  and the subsequent, liquid peaks. A clear separation between these contributions allows for an unambiguous definition of the molecules introduced in order to perform small-cage expansions [123, 138], and is clearly a sign that reconciling RHNC with small-cage expansions may not be out of reach.

The large contribution coming from the peak at  $r = 0$  in  $\tilde{g}$  shows that the diagrams that contribute the most to the free-energy are the most connected ones [138]. It should be possible to put these diagrams in correspondence with the diagrams re-summed in the small cage expansions of [123] and [138] in order to make progress. Our work has set up the tools necessary to perform such resummations and we believe this is the natural line of work to follow in the future.

## Chapter 5

# Jamming transition

In this chapter we present the results obtained when applying the ideas of replica theory as presented in Chapter 4 to the vicinity of the jamming point, with the goal to assess whether the jamming transition is the zero-temperature mechanism that controls the glass transition at finite temperature. We study harmonic spheres at very large volume fractions, around 0.64, and at very low or zero temperature, in order to study the jamming phase diagram of Fig. 1.5. It is found that for these very dense states, at very low temperature, replica theory can be cast into a computationally efficient approximation scheme, allowing us to argue, within a given set of approximations, that the jamming transition is a phenomenon conceptually different from the glass transition, in the line of the calculations on mean-field models of [100] and [110] and hard spheres [138], and numerical experiments on harmonic spheres [22, 21].

We predict, without assuming it, the existence of a jamming transition, solely from microscopic calculations, and successfully reproduce a large set of observed characteristics of the Jamming transition.

### 5.1 Mean-field hypothesis

Based on previous works cited above, we have in mind the schematic phase diagram reported in Fig. 5.1. In this picture, that we will derive in the following, the liquid undergoes an ideal glass transition at the Kauzmann temperature  $T_K(\varphi)$  (note that in the following, we will mostly use the volume fraction  $\varphi = \pi\rho\sigma^3/6$  instead of the density, because it is more suited to the study of hard-spheres and jamming).

The line  $T_K(\varphi)$  vanishes at a volume fraction  $\varphi_K$  which also corresponds to the ideal glass transition for hard spheres [138]. The point  $\varphi_K$  is *not the jamming transition*: the ground state energy and pressure remain zero across  $\varphi_K$ . Above  $\varphi_K$ , the system enters, at zero temperature, a *hard sphere glassy state*. In this state, particles vibrate near well-defined (but random) positions, and the system is not jammed yet [138]. Jamming occurs when the glass reaches its close packing density, which we shall call “glass close packing” (GCP), following [138]. We *identify the jamming transition with  $\varphi_{GCP}$* . Note that at this point this is only an assumption, although a reasonable one, and quantitative arguments will be derived in the following.

The main theoretical difficulty in the study of the jamming transition at  $\varphi_{GCP}$  is that it occurs deep inside the glass phase. Therefore, we first need to develop an accurate theoretical description of the glass phase. As discussed in detail in [19], previous theories of the glass phase fail (see Fig. 5.1).

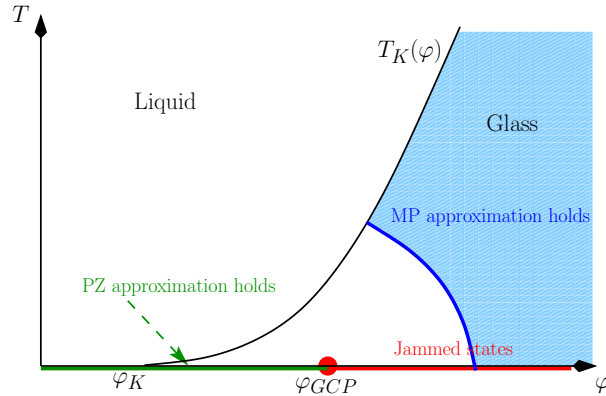


Figure 5.1: A schematic phase diagram for the glassy states of the model defined by Eq. (1.20) showing both the glass transition line at  $T_K(\varphi)$  and the jamming point at  $T = 0$  and  $\varphi = \varphi_{GCP}$ . The Parisi-Zamponi (PZ) approach only holds at  $T = 0$  and  $\varphi < \varphi_{GCP}$ , while the Mézard-Parisi (MP) approach holds for large enough densities and temperatures. We developed a method to fill the gap between the PZ and MP analytical schemes to explore the vicinity of the jamming transition.

The Mézard-Parisi approach (denoted by MP in the following) [121, 122] holds only at high enough temperature or density, where a simple harmonic approximation for vibrations in the glass holds. The Parisi-Zamponi approach (denoted by PZ) [138] holds only in the hard sphere region,  $T = 0$  and  $\varphi < \varphi_{GCP}$ . The central theoretical achievement that we describe here is an approximation scheme that can naturally interpolate between those of MP and PZ and is correct in the entire vicinity of the jamming transition, thus allowing us to fully explore the phase diagram of Fig. 5.1, and in particular the region of low temperature,  $T \ll T_K(\varphi)$  and  $\varphi \sim \varphi_{GCP}$ . We theoretically obtain from a first principle calculation a large number of the observed behaviors of harmonic spheres in numerical experiments [134, 135, 59, 152, 178], and predict new results for the correlation functions of this system around the jamming transition.

Our approach is very different from, but complementary to, recent theoretical works on jamming. The aim of our work is to show, directly from the Hamiltonian, that the jamming transition exists, and determine from first principles its location and properties. Other approaches assume the existence of jammed states and try to obtain geometrical informations on them [43, 156], or develop a scaling picture of the jamming transition by showing that the transition is characterized by a diverging correlation length [175].

Before proceeding further, it is worth noting that even though the mean-field picture on which we will base our calculations is expected to be tempered, in finite dimensional models by nucleation processes [108, 36], we expect that the local and static properties that we intend to compute (such as the number of contacts, energy of a packing, etc.) will not be affected by these processes in the very low temperature and high density regime near the jamming transition.

For this reason, in this work we follow Mézard and Parisi [121, 122] and directly apply the mean-field concepts described above to three dimensional glass-formers.

### 5.1.1 Thermodynamics of the glass phase

In Chapter 4, we used the replica trick to detect the emergence of a non-zero complexity, signaling the appearance of an exponential number of metastable states, responsible for the slowing down of the

dynamics. However, the idea of replicating the system can be pushed further, in order to compute the thermodynamics of the glass phase, as was shown by Monasson [126].

Returning to Eq.(4.13), the ideal glass transition is reached at the Kauzmann temperature  $T_K(\varphi)$ , defined by the point where the saddle point of Eq.(4.13) for which the complexity vanishes:

$$\left\{ \begin{array}{l} \frac{\partial \Sigma(f)}{\partial f} \Big|_{f^*(T_K, \varphi)} = \frac{1}{T_K(\varphi)}, \\ \Sigma(f^*(T_K(\varphi), \varphi)) = \Sigma(f_{min}) = 0. \end{array} \right. \quad (5.1)$$

In the following we will work directly with the entropy of the system, i.e. the logarithm of its partition function. It can be read off from the free-energy by multiplying by  $-\beta$ . We will call this object the “free-entropy”:

$$\mathcal{S} = -\beta F = \lim_{N \rightarrow \infty} \frac{1}{N} \ln Z \quad (5.2)$$

The free-entropy has a simple expression for  $T < T_K(\varphi)$ , where the complexity sticks to zero:

$$\mathcal{S}_{\text{glass}}(T, \varphi) = -\beta f_{\min}(T, \varphi). \quad (5.3)$$

We have shown in Chapter 4 that introducing  $m$  replicas coupled together allows for an explicit computation of the complexity. After introducing  $m$  replicas, Eq.(4.13) was modified to obtain Eq.(4.25), which contained an  $m$  dependance that allows for the computation of  $\Sigma$ . We rewrite here this equation in terms of the quantity  $\mathcal{S}$ :

$$\left\{ \begin{array}{l} \mathcal{S}(m; T, \varphi) = \Sigma(f^*(m; T, \varphi)) - m\beta f^*(m; T, \varphi), \\ \frac{\partial \Sigma}{\partial f}(f^*(m; T, \varphi)) = \frac{m}{T}, \\ \Sigma(f^*(m; T, \varphi)) = -m^2 \frac{\partial}{\partial m} \left( \frac{\mathcal{S}(m; T, \varphi)}{m} \right). \end{array} \right. \quad (5.4)$$

Eq.(5.3) shows that for  $T < T_K$  the free energy of the glass is equal to  $f_{\min}(T)$ , the point where  $\Sigma(f) = 0$ . Note also that this value of  $f$  depends only on the free-energy landscape, which is the same for all replicas, and it is thus independent of  $m$ . Inside the glass phase, if there are several copies, the free-energy will simply be equal to  $m f_{\min}(T)$ .

The parameter  $m$  allows, without changing the temperature or density, to modify the value of  $f^*$  the saddle point in Eq.(5.4), i.e. to displace the Kauzmann temperature artificially. If we choose  $m^*$  it so that  $f^*(m^*; T, \varphi) = f_{\min}(T, \varphi)$ , the complexity will be zero when evaluated at this free-energy, and the expression of the free-entropy will simply become:

$$\mathcal{S}(m^*; T, \varphi) = -m^* \beta f_{\min}(T, \varphi), \quad (5.5)$$

and, recalling Eq.(5.3), the free-entropy of the glass will be obtained by dividing by  $m^*$ :

$$\mathcal{S}_{\text{glass}}(T, \varphi) = \frac{\mathcal{S}(m^*; T, \varphi)}{m^*} \quad \text{if } T < T_K. \quad (5.6)$$

Still,  $m^*$  is an unknown, but we remark that it is made to constrain that  $f^* = f_{\min}$ . Since we expect the complexity to be a monotonic function of  $f$ , this is equivalent to say that  $m^*$  is made up so that

$\Sigma(f^*) = \Sigma(f_{min}) = 0$ . Thus  $m^*$  is calculated as the value of  $m$  that cancels the complexity. But the complexity can be calculated as the derivative of  $\mathcal{S}/m$  as shown in Eq.(5.4). Thus  $m^*$  is so that:

$$\left. \frac{\partial}{\partial m} \left( \frac{\mathcal{S}(m; T, \varphi)}{m} \right) \right|_{m^*} = 0, \quad (5.7)$$

and thus is the value of  $m$  that minimizes  $\mathcal{S}/m$ , which finally gives:

$$\mathcal{S}_{glass}(T, \varphi) = \min_m \frac{\mathcal{S}(m; T, \varphi)}{m}. \quad (5.8)$$

Now we see that, in order to compute the thermodynamics inside the ideal glass phase, one must be able to calculate the free entropy of a replicated liquid, and extremize it with respect to the number of copies.

### 5.1.2 The small cage expansion

Computing the free-energy and complexity of the glass amounts to computing the free entropy of an  $m$ -time replicated liquid. One can use a replicated version of standard liquid theory approximations such as the replicated Hyper-Netted-Chain (HNC) [121, 33] presented in Chapter 4, but we have seen that these approximations break down deep in the glass phase [138]. One can also follow Mézard and Parisi (MP) [122, 123] and start at high density, then perform cage expansions: at high densities the copies stay close to the originals, forming molecules of size  $A$ . One can then expand the replicated free entropy with respect to this parameter  $A$ . To do this, one has to switch from a liquid of copies from a liquid of molecules, as described below.

#### Mézard-Parisi approach

We will denote by  $x_i^a$  the  $d$ -dimensional position of particle  $i$  of replica  $a$ , and collect all replica indices in  $m \times d$  dimensional vectors, defining:

$$\bar{x} \equiv \{x^1, \dots, x^m\}. \quad (5.9)$$

We define the partition function of the replicated liquid:

$$Z_m[z] = \sum_{N=0}^{\infty} \frac{1}{N!} \int d\bar{x}_1 \dots d\bar{x}_N \prod_{i < j} \prod_{a=1}^m e^{w(x_i^a - x_j^a)} \prod_{i=1}^N z(\bar{x}_i), \quad (5.10)$$

where we have defined:

$$d\bar{x} \equiv d^d x^1 \dots d^d x^m. \quad (5.11)$$

Note that a  $(N!)^{m-1}$  factor has been absorbed in all the possible relabelings of the molecules.  $z$  a generalized activity for the replicated liquid. If we take  $z$  independant of the replica indices, we obtain a set of  $m$  uncoupled copies, that all have the same chemical potential. We can make  $z$  depend on the replica positions to constrain the replicas to be close. For example the small cage expansion of Mézard and Parisi [122] is obtained by choosing:

$$z^{\text{MP}}(\bar{x}) = z \exp \left( -\frac{\varepsilon}{m} \sum_{a < b} [x^a - x^b]^2 \right). \quad (5.12)$$



This corresponds to setting a quadratic attraction of intensity  $\varepsilon$  between the copies. We define the usual Mayer function plus its molecular counterpart:

$$\begin{aligned} f(x, y) &\equiv e^{w(x, y)} - 1, \\ \bar{f}(\bar{x}, \bar{y}) &\equiv e^{w(x^1, y^1)} \dots e^{w(x^m, y^m)} - 1 = \left( \prod_{a=1}^m e^{w(x^a, y^a)} \right) - 1. \end{aligned} \quad (5.13)$$

and in the hard sphere case  $f$  is a Heaviside function. For harmonic spheres,  $f$  looks like a smoothed Heaviside function. We rewrite the partition function as:

$$Z_m[z, \bar{f}] = \sum_{N=0}^{\infty} \frac{1}{N!} \int d\bar{x}_1 \dots d\bar{x}_N \prod_{i < j} \left( 1 + \bar{f}(\bar{x}_i, \bar{x}_j) \right) \prod_{i=1}^N z(\bar{x}_i), \quad (5.14)$$

The MP small cage expansion chooses the above particular form of activity, then Legendre transform the free-energy with respect to the intensity of the coupling to obtain a functional of the parameter coupled to the coupling intensity, the cage size. Indeed

$$\frac{\partial \ln Z_m[z^{\text{MP}}]}{\partial \varepsilon} = \left\langle -\frac{1}{m} \sum_{i=1}^N \sum_{a < b} (x_i^a - x_i^b)^2 \right\rangle. \quad (5.15)$$

By replica symmetry, and homogeneity, we have that:

$$\sum_{i=1}^N \sum_{a < b} (x_i^a - x_i^b)^2 = \frac{m(m-1)}{2} \langle (x_i^a - x_i^b)^2 \rangle \quad (5.16)$$

which is directly related to the cage size, as defined in a replica scheme:

$$A \equiv \frac{1}{2d} \langle (x_i^a - x_i^b)^2 \rangle, \quad (5.17)$$

which is, in a dynamical point of view, the height of the long-time plateau in the mean-square displacement. Finally we see that:

$$\frac{\partial \ln Z_m[z^{\text{MP}}]}{\partial \varepsilon} = -(m-1)dA, \quad (5.18)$$

which shows that  $\varepsilon$  and  $A$  are indeed a pair of coupled variables through a Legendre transformation.

The small cage expansion amounts to Legendre transforming the free-energy, to obtain a functional of the cage size, then expanding in powers of  $A$  this functional. In practice this is done via a large  $\varepsilon$  expansion before Legendre transforming.

This scheme is not suited to the pair potentials that lead to a jamming transition, since they must contain a singularity, preventing one to follow the original strategy of Mézard and Parisi. In practice this leads to a singular expansion in powers of  $A$  [138].

### Molecular formulation

To correctly treat the replicated hard sphere system, Parisi and Zamponi (PZ) [138] developed an effective potential approximation, which amounts to performing an expansion in powers of  $\sqrt{A}$  instead of  $A$ . We explain in the following the extension of the effective potential approximation to finite temperature harmonic spheres. By construction, we will see that we are bound to recover both high density MP results and zero temperature PZ results in a unified treatment.

The strategy adopted by Paris and Zamponi was to perform a Legendre transform with respect to the full activity  $z(\bar{x})$ . As described in Chapter 2, one then obtains the free energy as a functional of the single molecule density and the interaction potential.

We can see that  $z$  is coupled to the density of molecules by a direct computation:

$$\begin{aligned}
\frac{\delta \ln Z_m}{\delta z(\bar{x})} &= \frac{1}{Z_m} \sum_{N=0}^{\infty} \frac{1}{N!} \int \prod_{i=1}^N d\bar{x}_i \prod_{i<j} \left(1 + \bar{f}(\bar{x}_i, \bar{x}_j)\right) \frac{\delta}{\delta z(\bar{x})} \left( \prod_{i=1}^N z(\bar{x}_i) \right), \\
&= \sum_{j=1}^N \frac{1}{Z_m} \sum_{N=0}^{\infty} \frac{1}{N!} \int \prod_{i=1}^N d\bar{x}_i \prod_{i<j} \left(1 + \bar{f}(\bar{x}_i, \bar{x}_j)\right) \delta(\bar{x} - \bar{x}_i) \prod_{\substack{i=1 \\ i \neq j}}^N z(\bar{x}_i), \\
&= \sum_{j=1}^N \frac{1}{Z_m} \sum_{N=0}^{\infty} \frac{1}{N!} \int \prod_{i=1}^N d\bar{x}_i \prod_{i<j} \left(1 + \bar{f}(\bar{x}_i, \bar{x}_j)\right) \delta(\bar{x} - \bar{x}_i) \frac{1}{z(\bar{x}_j)} \prod_{i=1}^N z(\bar{x}_i), \\
&= \frac{1}{z(\bar{x})} \sum_{j=1}^N \frac{1}{Z_m} \sum_{N=0}^{\infty} \frac{1}{N!} \int \prod_{i=1}^N d\bar{x}_i \prod_{i<j} \left(1 + \bar{f}(\bar{x}_i, \bar{x}_j)\right) \delta(\bar{x} - \bar{x}_i) \prod_{i=1}^N z(\bar{x}_i), \\
&= \frac{1}{z(\bar{x})} \left\langle \sum_{i=1}^N \delta(\bar{x} - \bar{x}_i) \right\rangle.
\end{aligned} \tag{5.19}$$

Defining:

$$\rho(\bar{x}) \equiv \left\langle \sum_{i=1}^N \delta(\bar{x} - \bar{x}_i) \right\rangle, \tag{5.20}$$

we obtain:

$$\frac{\delta \ln Z_m}{\delta \ln z(\bar{x})} = \rho(\bar{x}). \tag{5.21}$$

We emphasize again that this is not the same object than the replicated density define in the previous chapter. The precise diagrammatic relation between the expansions performed in this chapter and thos performed in the previous chapter are still to be established.

We perform now the Legendre transform of  $\ln Z$  with respect to the molecular activity:

$$\left\{ \begin{array}{l} \mathcal{S}[\rho] = \ln Z_m [\ln z^*[\rho]] - \int d\bar{x} \rho(\bar{x}) \ln z^*[\rho](\bar{x}), \\ z^*[\rho] \text{ such that } \left. \frac{\delta \ln Z_m}{\delta \ln z(\bar{x})} \right|_{z^*} = \rho(\bar{x}). \end{array} \right. \tag{5.22}$$

Here we have omitted the thermodynamic limit, we will take it later to ease the notations.

### Ideal gaz case

As usual in liquid theory one must start with the ideal gaz case. In the ideal gaz, we have:

$$\begin{aligned}
Z_m^{IG}[z] &= \sum_{N=0}^{\infty} \frac{1}{N!} \int d\bar{x}_1 \cdots d\bar{x}_N \prod_{i=1}^N z(\bar{x}_i) \\
&= \sum_{N=0}^{\infty} \frac{1}{N!} \left( \int d\bar{x} z(\bar{x}) \right)^N \\
&= \exp \left( \int d\bar{x} z(\bar{x}) \right).
\end{aligned} \tag{5.23}$$

This allows the explicit Legendre transformation:

$$\frac{\delta \ln Z_m^{IG}}{\delta \ln z(\bar{x})} = e^{\ln z(\bar{x})}, \tag{5.24}$$

which shows that:

$$z^*[\rho](\bar{x}) = \rho(\bar{x}) , \quad (5.25)$$

and thus we get directly as expected:

$$\mathcal{S}^{IG}[\rho] = \int d\bar{x} \rho(\bar{x}) [1 - \ln \rho(\bar{x})] . \quad (5.26)$$

By using Mayer diagrammatics, we will thus obtain that our replicated entropy is expressed as the sum of this ideal gaz contribution, plus diagrams with  $\rho(\bar{x})$  nodes and  $\bar{f}$  links.

$$\mathcal{S}[\rho] = \mathcal{S}^{IG}[\rho] + \bullet\text{---}\bullet + \begin{array}{c} \bullet \\ / \quad \backslash \\ \bullet \quad \bullet \end{array} + \begin{array}{c} \bullet \quad \bullet \\ | \quad | \\ \bullet \quad \bullet \end{array} + \dots \quad (5.27)$$

### Gaussian ansatz for the molecule density

We can not extremize the free-energy in the full space of  $\mathbb{R}^m$  functions, and we must find a simplifying assumption. Since  $\varepsilon$  and  $A$  are coupled parameters, we will suppose that  $\rho$  keeps the original Gaussian form of the MP choice of activity, but with  $\varepsilon$  replaced by  $1/A$ :

$$\rho^G(\bar{x}) = \text{Cte} \exp \left( -\frac{1}{2mA} \sum_{a<b} (x^a - x^b)^2 \right) . \quad (5.28)$$

This is a strong assumption: we suppose that the cage seen by a particle is well approximated by a Gaussian. We rewrite this as:

$$\exp \left( -\frac{1}{2mA} \sum_{a<b} (x^a - x^b)^2 \right) = \exp \left( -\frac{1}{2A} \sum_a (x^a)^2 \right) \exp \left( \frac{1}{2} \left( \frac{1}{A} \sum_a x^a \right) \frac{A}{m} \left( \frac{1}{A} \sum_a x^a \right) \right) \quad (5.29)$$

We can represent the second exponential by an integral under a Gaussian weight of variance  $A/m$  by noting that:

$$\exp \left( \frac{1}{2} \left( \frac{1}{A} \sum_a x^a \right) \frac{A}{m} \left( \frac{1}{A} \sum_a x^a \right) \right) = \frac{1}{(2\pi A/m)^{d/2}} \int dX \exp \left( -\frac{1}{2} \frac{X^2}{A/m} + X \frac{1}{A} \sum_a x^a \right) . \quad (5.30)$$

We obtain:

$$\rho^G(\bar{x}) = \text{Cte} \frac{m^{d/2}}{(2\pi A)^{d/2}} \int dX \exp \left( -\frac{1}{2A} \sum_a (X - x^a)^2 \right) . \quad (5.31)$$

The molecule density must be normalized to  $N$  the number of molecules, thus we can fix the prefactor by calculating the normalization:

$$N = \int d\bar{x} \rho^G(\bar{x}) = \text{Cte} \frac{m^{d/2}}{(2\pi A)^{d/2}} \int dX \left[ (2\pi A)^{d/2} \right]^m \quad (5.32)$$

And thus:

$$\text{Cte} = \frac{N}{V} \frac{m^{-d/2}}{(2\pi A)^{(m-1)d/2}} , \quad (5.33)$$

and we get the final Gaussian ansatz for the molecule density [138]:

$$\rho^G(\bar{x}) = \rho \int dX \prod_{a=1}^m \gamma_A(X - x^a) , \quad (5.34)$$

where  $\gamma_A$  is a normalized and centered Gaussian of variance  $A$ :

$$\gamma_A(x) = \frac{1}{(2\pi A)^{d/2}} \exp \left( -\frac{x^2}{2A} \right) . \quad (5.35)$$

These functions will tend to delta functions in the jamming limit, where the cage size is expected to go to zero, and we will make a repeated use of them.

### Ideal gaz contribution in the Gaussian ansatz

We can now evaluate the functional  $\mathcal{S}$  at this particular value of the molecule density. First we note that:

$$\ln \rho^G(\bar{x}) = \ln \rho - \frac{d}{2} \ln m - \frac{(m-1)d}{2} \ln(2\pi A) - \frac{1}{2mA} \sum_{a<b} (x^a - x^b)^2 . \quad (5.36)$$

We can now compute:

$$\begin{aligned} \int d\bar{x} \rho(\bar{x}) \ln \rho(\bar{x}) &= \rho \int_{X, \bar{x}} \left( \prod_{a=1}^m \gamma_A(X - x^a) \right) \left[ \ln \left( \frac{\rho}{m^{d/2} (2\pi A)^{(m-1)d/2}} \right) - \frac{1}{2mA} \sum_{a<b} (x^a - x^b)^2 \right] \\ &= \rho V \left[ \ln \rho - \frac{d}{2} \ln m - \frac{(m-1)d}{2} \ln(2\pi A) - \frac{d}{2} (m-1) \right] , \end{aligned} \quad (5.37)$$

and finally:

$$\begin{aligned} \mathcal{S}^{IG}[\rho^G] &= \rho V \left[ 1 - \ln \rho \right] + \mathcal{S}_{\text{harm}}(m, A) , \\ \mathcal{S}_{\text{harm}}(m, A) &= \rho V \left[ \frac{d}{2} \left( 1 - m + \ln m \right) + \frac{(m-1)d}{2} \ln(2\pi A) \right] . \end{aligned} \quad (5.38)$$

### Reorganizing the Mayer expansion

Now we want to express the free-energy of the replicated liquid as the free-energy of an effective liquid. The strategy to do so is to average over the positions of  $m-1$  replicas, and keep only one replica, say replica 1, as reference. This procedure will give rise to effective interactions, two-body ones, but also many-body interactions. We have seen that the free-entropy is given by the ideal gaz result plus the sum of all connected and irreducible Mayer diagrams, which carry  $\rho(\bar{x})$  nodes and  $\bar{f}(\bar{x}, \bar{y})$  links. How will the small cage expansion affect the diagrams? At lowest order, the Gaussian ansatz for the density will give delta functions, and thus all replicas will be at the same integration point. Thus we have that:

$$\bar{f}(\bar{x}, \bar{y}) \xrightarrow{A \rightarrow 0^+} e^{mw(x^1, y^1)} - 1 = f_1^{(m)}(x^1, y^1) , \quad (5.39)$$

where we have defined:

$$f_1^{(m)}(x, y) \equiv e^{mw(x, y)} - 1 . \quad (5.40)$$

This is the Mayer function of a liquid interacting via a potential  $w$ , but at temperature  $T/m$ . Thus we expect the lowest order result to give an effective liquid interacting via the original potential, at temperature  $T/m$ , as was already found in [122]. Note that here we have chosen a given replica as a reference, but we could also have chosen the center of mass of the molecule as a reference. In our translationally invariant case, this has no consequence, but simplifies the calculations. If translational invariance does not hold, an expansion around the center of mass is required.

What we can thus do is to separate the integrations on the  $x_i^1$  from those on the others replicas, and to decompose the total Mayer function in two contributions:

$$\bar{f} = f_1^{(m)} + \left[ \bar{f} - f_1^{(m)} \right] . \quad (5.41)$$

Each node is integrated upon, with weight  $\rho^G$ , and we separate this into:

$$\int d\bar{x} \rho^G(\bar{x}) \left( \bullet \right) = \int \rho dx^1 \int \mathcal{D}\mathbf{x} \left( \bullet \right) , \quad (5.42)$$

where we have defined the measure  $\mathcal{D}\mathbf{x}$  as:

$$\mathcal{D}\mathbf{x} \equiv \frac{\rho^G(\bar{x})}{\rho} dx^2 \cdots dx^m . \quad (5.43)$$

And we have trivially that  $\int \mathcal{D}\mathbf{x} = 1$ .

Now consider one diagram of the free-entropy, and make the replacement of the links described above. This amounts to take the same diagram, but with links that can be either  $f_1^{(m)}$  or  $\bar{f} - f_1^{(m)}$ :

$$\begin{aligned} \mathcal{S}[\rho^G] = \mathcal{S}^{IG}[\rho^G] &+ \text{---} + \text{=---} + \text{---} + \text{---} + \text{---} + \text{---} \\ &+ \text{---} + \text{---} + \text{---} + \text{---} + \text{---} + \dots \end{aligned} \quad (5.44)$$

The double lines are  $\bar{f} - f_1^{(m)}$  links, while the normal lines are  $f_1^{(m)}$  links.

We can classify these diagrams by the number of  $\bar{f} - f_1^{(m)}$  links they contain, since they are a small quantity. At lowest order, we get a sum of diagrams with only  $f_1^{(m)}$  links. All integrations over the replicas other than replica 1 give 1 because of our choice of measure. Adding to these diagrams the result from the ideal gaz, we recover as anticipated the free-entropy of a liquid interacting via a potential  $mw$ , plus the harmonic part described earlier:

$$\mathcal{S}[\rho^G, w] \xrightarrow{A \rightarrow 0^+} \mathcal{S}_{liq}[\rho, mw] + \mathcal{S}_{\text{harm}} . \quad (5.45)$$

### Expansion at first order

At order 1 in the numbers of  $\bar{f} - f_1^{(m)}$  links, we obtain the sum of all diagrams of the free-entropy  $\mathcal{S}[\rho, mw]$ , where one has replaced one of the  $f_1^{(m)}$  links by a  $\bar{f} - f_1^{(m)}$  link. Thus we get:

$$\begin{aligned} \mathcal{S}[\rho^G, w] &= \mathcal{S}_{liq}[\rho, mw] + \mathcal{S}_{\text{harm}} + \mathcal{S}^{(2)} + \mathcal{O}((\bar{f} - f_1^{(m)})^2) , \\ \mathcal{S}^{(2)} &= \text{=---} + \text{---} + \text{---} + \dots \end{aligned} \quad (5.46)$$

We can write  $\mathcal{S}^{(2)}$  as an integral:

$$\begin{aligned} \mathcal{S}^{(2)} &= \int d\bar{x}d\bar{y} \rho^G(\bar{x}) \rho^G(\bar{y}) \left[ \bar{f}(\bar{x}, \bar{y}) - f_1^{(m)}(x^1, y^1) \right] F(x^1, y^1) , \\ F(x, y) &= \text{---} + \text{---} + \text{---} + \dots \end{aligned} \quad (5.47)$$

The links of the diagrams are  $f_1^{(m)}$ , and the white labeled nodes don't carry any weight. This sum of diagrams is obviously equal to the derivative of  $\mathcal{S}[\rho, mw]$  with respect to  $f_1^{(m)}$  divided by  $\rho^2$ . But we know that:

$$\left( 1 + f_1^{(m)}(x, y) \right) \frac{\delta \mathcal{S}[\rho, mw]}{\delta f_1^{(m)}(x, y)} = \frac{1}{2} \rho^{(2)}(T/m; x, y) . \quad (5.48)$$

Thus we find:

$$F(x, y) = \frac{1}{\rho^2} \frac{1}{2} \rho^{(2)}(T/m; x, y) e^{-mw(x, y)} \quad (5.49)$$

And we obtain the final result:

$$\begin{aligned} \mathcal{S}[\rho^G, w] &= \mathcal{S}_{liq}[\rho, mw] + \mathcal{S}_{harm} + \frac{\rho^2}{2} \int_{x,y} g(T/m; x, y) Q(x, y) , \\ Q(x, y) &= e^{(1-m)w(x,y)} \int dX dY \gamma_A(X-x) \gamma_A(Y-y) \int \left( \prod_{a=2}^m dx^a \gamma_A(X-x^a) \right) \left( \prod_{a=2}^m dy^a \gamma_A(Y-y^a) \right) \\ &\quad \left[ \prod_{a=2}^m e^{w(x^a, y^a)} - e^{(m-1)w(x,y)} \right] . \end{aligned} \quad (5.50)$$

We can simplify a bit the expression of  $Q$ :

$$\begin{aligned} 1 + Q(x, y) &= e^{(1-m)w(x-y)} \int dX dY \gamma_A(X-x) \gamma_A(Y-y) q(X-Y)^{m-1} , \\ q(x, y) &= \int dudv \gamma_A(x-u) \gamma_A(y-v) e^{w(u-v)} . \end{aligned} \quad (5.51)$$

Using translational invariance we can rewrite all this as:

$$\begin{aligned} \mathcal{S}[\rho^G, w] &= \mathcal{S}_{liq}[\rho, mw] + \mathcal{S}_{harm}(m, A) + \frac{\rho^2 V}{2} \int_r g(T/m; r) Q(T, m, A; r) , \\ Q(T, m, A; r) &= e^{(1-m)w(r)} \int_{r'} \gamma_{2A}(r-r') q(A, T; r')^{m-1} - 1 , \\ q(A, T; r) &= \int_{r'} \gamma_A(r-r') e^{w(r')} , \end{aligned} \quad (5.52)$$

where we have made explicit the dependances on temperature,  $m$  and  $A$ . To come back to the initial free-entropy, one has to do the inverse Legendre transform, and thus find the optimal Gaussian density, which amounts to finding the optimal cage size  $A^*$ .

Due to the Gaussian *ansatz*, and the quadratic form of the harmonic potential Eq.(1.20), the function  $q$  has a tractable expression [20], that depends on both parameters  $A$  and  $m$ :

$$\begin{aligned} q(A, T; r) &= \frac{1}{2} \left( 2 + \operatorname{erf} \left[ \frac{r-1}{2\sqrt{A}} \right] - \operatorname{erf} \left[ \frac{r+1}{2\sqrt{A}} \right] \right) + \frac{4A^{3/2}\beta}{(1+4A\beta)\sqrt{\pi}r} \left( e^{-\frac{(r-1)^2}{4A}} - e^{-\frac{(r+1)^2}{4A}} \right) \\ &\quad + e^{-\frac{(r-1)^2\beta}{1+4A\beta}} \frac{r+4A\beta}{2r(1+4A\beta)^{3/2}} \left( \operatorname{erf} \left[ \frac{r+4A\beta}{2\sqrt{A(1+4A\beta)}} \right] + \operatorname{erf} \left[ \frac{1-r}{2\sqrt{A(1+4A\beta)}} \right] \right) \\ &\quad - e^{-\frac{(r+1)^2\beta}{1+4A\beta}} \frac{r-4A\beta}{2r(1+4A\beta)^{3/2}} \left( \operatorname{erf} \left[ \frac{r-4A\beta}{2\sqrt{A(1+4A\beta)}} \right] - \operatorname{erf} \left[ \frac{1+r}{2\sqrt{A(1+4A\beta)}} \right] \right) \end{aligned} \quad (5.53)$$

We can see easily that the Mézard-Parisi approximation scheme is recovered if we suppose that the potential  $w(r)$  is differentiable in  $r = 1$ . Indeed coming back to the expression of  $q$  we have:

$$q(A, T; r) = \int d^3 r' \gamma_{2A}(r') e^{w(r-r')} \underset{A \rightarrow 0}{\sim} e^{w(r)} \left[ 1 + A \Delta_r w(r) + A [\nabla_r w(r)]^2 + \mathcal{O}(A^2) \right] . \quad (5.54)$$

Plugging this into the expression of the free-energy we get the first-order correction:

$$G(m, A; T) = -3A(m-1) \int_0^\infty dr r^2 \Delta_r w(r) g(T/m; r) , \quad (5.55)$$

which reproduces the MP result when introduced in the expression of the free-entropy.

### Formulation in terms of two-body effective potential

Parisi and Zamponi [138] have shown that the molecular liquid could be expressed as an effective liquid, albeit with modified interaction: the two-body potential  $w$  is replaced by an effective potential  $w_{\text{eff}}$ , and higher-order interaction potentials also arise. Here we neglect the higher-order potentials. They are expected to be negligible at high dimensions but not necessarily in finite dimensions. However taking them into account makes the calculation much harder, already at next order.

The calculation is schematically represented in Fig. 5.2. The two body effective potential  $w_{\text{eff}}$  is

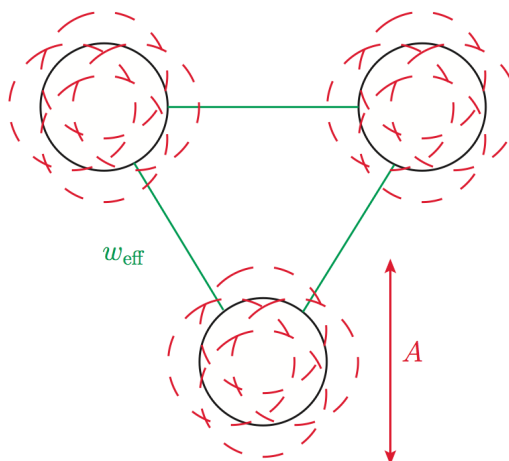


Figure 5.2: A schematic representation of the effective potential approximation. Each particle in the original liquid is replicated  $m$  times (dashed spheres). Assuming that the replicated particles form a molecule of average cage size  $A$ , in the partition sum, we trace out the degrees of freedom of  $(m - 1)$  copies of the liquid to obtain an effective one-component liquid (black spheres) interacting with an effective pair potential  $w_{\text{eff}}$  (green lines).

defined as:

$$e^{w_{\text{eff}}(x,y)} = e^{w(x,y)} \left\langle \prod_{a=2}^m e^{w(x^a,y^a)} \right\rangle_{x,y}, \quad (5.56)$$

where the average is over the molecule probability density, at fixed  $x^1 = x$  and  $y^1 = y$ :

$$\langle \bullet \rangle_{x,y} = \int d\bar{x}d\bar{y} (\bullet) \delta(x^1 - \bar{x})\delta(y^1 - \bar{y}) \frac{\rho^G(\bar{x})\rho^G(\bar{y})}{\rho^2}. \quad (5.57)$$

It is easy to check that in the  $A \rightarrow 0$  limit, this effective potential reduces to  $e^{mw}$ , and that we get:

$$e^{w_{\text{eff}}(x,y)} = e^{mw(x,y)} \left[ 1 + Q(x,y) \right]. \quad (5.58)$$

In three dimensions, this can be rewritten, for future use, as:

$$e^{w_{\text{eff}}(r)} = e^{w(r)} \frac{1}{r\sqrt{4\pi A}} \int_0^\infty du u \left[ e^{-\frac{(r-u)^2}{4A}} - e^{-\frac{(r+u)^2}{4A}} \right] q(A,T;r)^{m-1}. \quad (5.59)$$

Equation (5.52) allows for a full calculation of the replicated free entropy, and allows us to recover both the MP small cage expansion in powers of  $A$  at high density, and the PZ expansion in powers of  $\sqrt{A}$  at zero temperature, as we will show below. In the following, we do not discuss the details of the calculations, that are extensively described in [20]. Again we emphasize that, due to the Gaussian

approximation that we make for the density, and the quadratic form of the potential, the detailed calculations only involve Gaussian integrals. Numerical minimizations must also be performed, for example to compute the optimal number of replicas  $m^*$ , or the optimal cage size.

### 5.1.3 Low temperature liquid theory approximation

Our purpose in interpolating between zero and finite temperature was to be able to probe the vicinity of the jamming point in the  $(\varphi, T)$  phase diagram, thus we are interested mainly in the low temperature behavior of the glass. We can exploit this by making an approximation that will allow us to push the analytical calculation much further. Defining the cavity distribution function  $y$  by  $g(r) = e^{w(r)}y(r)$  [77], we make the approximation of taking the cavity function of the liquid as a constant and equal to its  $T = 0, r = 1$  value, which we call  $y_{liq}^{HS}(\varphi)$ . As  $T$  goes to zero, we see that the exponential factor converges towards a step function around  $r = 1$ , so that in all integrals that are cut at  $r = 1$  by the pair potential, we can safely evaluate  $y$  at its  $r = 1$  value. Expanding  $y$  in powers of  $T$ , it is easy to convince oneself that the temperature dependence leads to subleading contributions in the integrals. Thus we suppose:

$$g(T/m; r) \sim e^{mw(r)} y_{liq}^{HS}(\varphi), \quad (5.60)$$

which simplifies further the expression of the free-entropy. We have made explicit the dependance of  $y$  on the packing fraction.

The last quantities that we need to compute are the free entropy  $\mathcal{S}_{liq}$  and the pair correlation function  $g_{liq}(r)$  of the liquid. Given the pair correlation function, which represents the probability of finding a particle at distance  $r$  from a particle fixed at the origin, we can express the internal energy  $U$  as:

$$U(T, \varphi) = 12\varphi \int_0^\infty dr r^2 g(T, \varphi; r) v(r). \quad (5.61)$$

Plugging the low temperature approximation Eq. (5.60) for the liquid into this, we obtain:

$$U_{liq}(T, \varphi) \underset{T \rightarrow 0}{\sim} 12\varphi y_{liq}^{HS}(\varphi) \int_0^1 dr r^2 (1-r)^2 e^{-\beta(1-r)^2}. \quad (5.62)$$

Making use of the standard identity  $U(T) = \frac{\partial(F/T)}{\partial(1/T)}$ , we can derive the low temperature approximation for the free entropy of the liquid:

$$\mathcal{S}_{liq}(T, \varphi) \underset{T \rightarrow 0}{\sim} \mathcal{S}_{liq}^{HS}(\varphi) + 6\varphi y_{liq}^{HS}(\varphi) \left[ \frac{\sqrt{\pi}}{2} \sqrt{T} (2+T) \operatorname{erf}\left(\frac{1}{\sqrt{T}}\right) + T (e^{-1/T} - 2) \right], \quad (5.63)$$

where  $y_{liq}^{HS}(\varphi)$  and  $\mathcal{S}_{liq}^{HS}(\varphi)$  are short-hand notations for  $y_{liq}(T = 0, \varphi; r = 1)$  and  $\mathcal{S}_{liq}(T = 0, \varphi)$ .

At this level of approximation, it is clear that the only input that is needed from liquid theory is the equation of state of the hard sphere liquid. From any given equation of state one can easily deduce the hard sphere free entropy  $\mathcal{S}_{liq}^{HS}$  and cavity function  $y_{liq}^{HS}$ . The most reasonable choice would be to use the phenomenological Carnahan-Starling (CS) equation of state, as in [138], that provides the best fit to the hard sphere pressure.

We instead used the Hyper-Netted Chain approximation described in the end of Chapter 2. Although HNC is known to be less accurate for the hard sphere system, using HNC allows us to also compare our results to the ones obtained from the MP approach valid at large density and finite temperatures. The HNC approximation overestimates  $y_{liq}^{HS}$  by 20% in the relevant range of volume



fraction  $\varphi \sim 0.64$ . This has the effect of reducing the glass transition density obtained from the theory, from the value  $\varphi_K = 0.62$  obtained from CS [138] to  $\varphi_K = 0.58$  obtained with HNC.

Therefore the reader should keep in mind that the glass densities reported in the following are lower than the correct ones. In any case, here we are more interested in the low-temperature scaling in the glass phase than to the actual value of the glass transition density. We also checked that the scaling results are insensitive to the precise choice of the equation of state of the hard sphere liquid.

With all these approximations, the free-entropy simplifies further into

$$\begin{aligned} \mathcal{S}(m, A; T, \varphi) &= \mathcal{S}_{liq}(T/m, \varphi) + \mathcal{S}_{harm}(m, A) + 4\varphi y_{liq}^{HS}(\varphi) G(m, A; T) , \\ G(m, A; T, \varphi) &= 3 \int_0^\infty dr r^2 \left[ q(A, T; r)^m - e^{mw(r)} \right] . \end{aligned} \quad (5.64)$$

Optimization over  $A$  gives a self-consistent equation for the optimal cage radius  $A^*(m; T, \varphi)$  that reads:

$$\begin{aligned} J(m, A^*(m; T, \varphi); T) &= \frac{9}{4\pi\rho y_{liq}^{HS}(\varphi)} , \\ J(m, A; T) &\equiv \frac{A}{1-m} \frac{\partial G(m, A; T)}{\partial A} = \frac{3mA}{1-m} \int_0^\infty dr r^2 q(A, T; r)^{m-1} \frac{\partial q(A, T; r)}{\partial A} . \end{aligned} \quad (5.65)$$

## 5.2 Thermodynamics of the glass

### 5.2.1 Complexity and phase diagram

As discussed above, the glass transition is signaled by the point where the saddle point in Eq. (4.13) reaches the minimum  $f_{min}$  at which the complexity  $\Sigma(f)$  vanishes. In the replica formalism, the equilibrium complexity  $\Sigma(f^*)$  in Eq. (5.1) corresponds to the complexity in Eq. (4.25) evaluated at  $m = 1$ . We call this quantity the ‘‘equilibrium’’ complexity of the liquid  $\Sigma_{eq}(T, \varphi)$ . The latter is easily computed by expanding the equations around  $m = 1$ :

$$\begin{aligned} \Sigma_{eq}(T, \varphi) &= \mathcal{S}_{liq}(T, \varphi) - \frac{3}{2} \ln \left( 2\pi A^*(m=1; T, \varphi) \right) - 3 - 12\varphi y_{liq}^{HS}(\varphi) H \left( m=1, A^*(m=1; T, \varphi); T \right) , \\ H(m, A; T) &\equiv \frac{1}{m} \frac{\partial G(m, A; T)}{\partial m} = \frac{1}{m} \int_0^\infty dr r^2 q(A, T; r)^m \ln q(A, T; r) + \frac{1}{m} \int_0^\infty dr r^2 w(r) e^{mw(r)} . \end{aligned} \quad (5.66)$$

For  $\varphi \geq \varphi_K$ , the complexity vanishes at a temperature  $T_K(\varphi)$ , called the Kauzmann temperature, that increases with the density. These results are summarized in the left frame of Fig. 5.3, where we show the complexity as a function of temperature for several volume fractions around  $\varphi_K$ . In the inset we show the zero temperature limit of the complexity  $\Sigma_{eq}^{HS}$  as a function of the density, that vanishes at  $\varphi_K$ .

From the complexity we deduce the phase diagram shown in the right frame of Fig. 5.3. In this figure we report  $T_K(\varphi)$ , as obtained in the framework of the effective potential approximation, and we compare it with the result obtained from the Mézard-Parisi small cage expansion [19]. In the effective potential case we find that the Kauzmann temperature goes to zero at  $\varphi_K \approx 0.5769$ , quadratically with the temperature. On the other hand, the result from the small cage expansion is a finite  $T_K(\varphi)$  which jumps to zero abruptly at a value of  $\varphi$  which is unrelated to hard sphere results. This is due to fact that the small cage expansion is valid only in the region indicated in Fig. 5.1. On the other hand, our effective potential computation becomes inaccurate when the temperature is too high because of

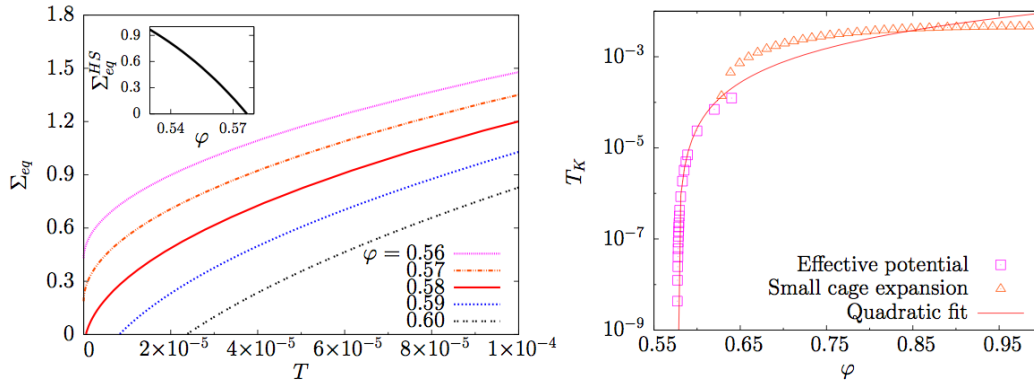


Figure 5.3: Left: Equilibrium complexity against temperature for several volume fractions around  $\varphi_K$ , calculated within the effective potential approximation. Inset: complexity of hard spheres, obtained as the  $T \rightarrow 0$  limit of the complexity  $\Sigma_{eq}$ , plotted against the volume fraction. Right: Kauzmann temperature against volume fraction, within the the effective potential approach developed in this work (open squares). The quadratic fit (red line) gives an estimated Kauzmann transition for hard spheres at  $\varphi_K = 0.576898$ . The small cage Mézard-Parisi approach breaks down at low temperatures and low densities [123].

the approximation in Eq. (5.60). Still we obtain a reasonable matching of the two approximation schemes for intermediate densities around  $\varphi = 0.64$ . It would be easy, in principle, to reconcile the two approximations at all volume fractions, including the crossover regime, by avoiding the low temperature approximation made in Eq. (5.60), but these computations would require a much heavier numerical treatment.

## 5.2.2 Relaxation time and glass fragility

The calculation of the liquid complexity, apart from signaling the glass transition, can be related to the relaxation time and fragility of the glass as described in the introduction, through Eq.(1.17) and its mean-field counterpart Eq.(1.19).

In Refs. [21, 22], Berthier and Witten showed that, for harmonic spheres, compressing the system leads to a very sensible increase of the fragility. Using our results for the complexity, we are able to qualitatively check whether replica theory can reproduce this feature. Indeed, thanks to Eq. (1.19), the fragility can be extracted equivalently from the relaxation time or from the complexity. Since the fragility is usually evaluated at the conventionally defined laboratory glass transition, we arbitrarily define the glass transition temperature  $T_g(\varphi)$  as the temperature at which the equilibrium complexity is equal to one,  $\Sigma(T_g(\varphi), \varphi) = 1$ , which is a typical value of the configurational entropy at the glass transition in most numerical simulations and experiments (its precise value is immaterial for our purposes). Using these values of  $T_g$  and  $\Sigma_g = 1$ , we can construct an Angell plot similar to Fig. 5.4 of the introduction, but for the complexity. In Fig. 5.4 we show the inverse of the complexity, linked to the logarithm of the relaxation time by Eq. (1.17), plotted against  $T_g/T$ , for several densities. The fragility is the slope of the curves in  $T_g/T = 1$  [112]. One can clearly see that increasing the density drastically increases the fragility of the glass-former.

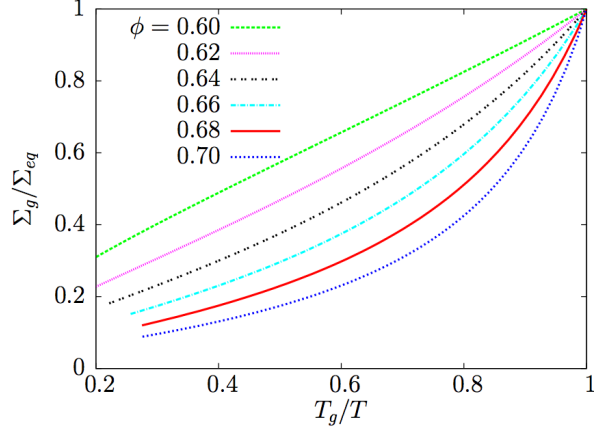


Figure 5.4: A thermodynamic Angell plot of  $\Sigma_g/\Sigma_{eq}$ , with  $\Sigma_g = 1$  as a definition of the glass transition, plotted against  $T_g/T$ , for different volume fractions. The thermodynamic fragility is predicted to increase rapidly with volume fraction, in agreement with numerical simulations [21].

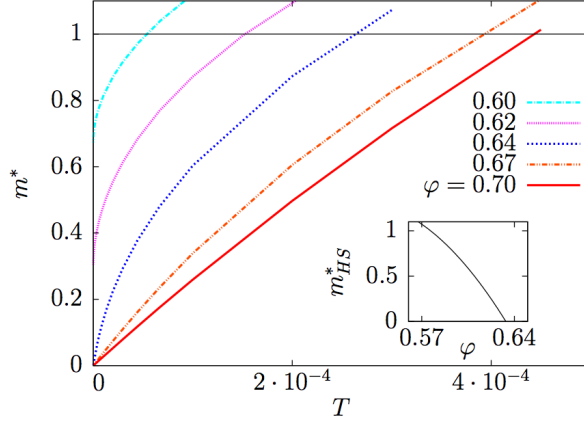


Figure 5.5: Optimal number of replicas  $m^*$  as a function of  $T$ , for several volume fractions. The inset shows the  $T \rightarrow 0$  limit of  $m^*$  as a function of the volume fraction.

### 5.2.3 Free-energy of the glass

We now turn to the calculation of the free entropy of the glass,  $\mathcal{S}_{glass}$ . We have seen that in order to compute  $\mathcal{S}_{glass}(T, \varphi)$ , one needs to optimize the replicated free entropy  $\mathcal{S}(m, A; T, \varphi)/m$  with respect to  $A$  first (in order to perform the inverse Legendre transform), then with respect to  $m$ , via Eq. (5.8). Calling  $A^*(T, \varphi)$  and  $m^*(T, \varphi)$  the optimal values of  $A$  and  $m$ , we obtain:

$$\mathcal{S}_{glass}(T, \varphi) = \frac{\mathcal{S}(m^*(T, \varphi), A^*(T, \varphi); T, \varphi)}{m^*(T, \varphi)}. \quad (5.67)$$

Starting from Eq. (5.67), we can deduce all quantities of interest, for instance the pressure and energy of the glass and its specific heat.

We start from the general thermodynamic relations  $U = -d\mathcal{S}/d\beta$  and  $p = \beta P/\rho = -\varphi d\mathcal{S}/d\varphi$ , where  $p$  is the so-called “reduced pressure” or “compressibility factor”. We have that the free-energy of the glass is  $\mathcal{S}(m^*, A^*; T, \varphi)/m^*$ , where  $m^*$  and  $A^*$  are determined by optimization of  $\mathcal{S}(m, A; T, \varphi)/m$ . Therefore, we do not need to take explicit derivatives with respect to  $m$  and  $A$ , and we can directly

compute the derivatives with respect to density and temperature to obtain explicit expressions for the energy and the pressure [20].

The pressure is thus obtained simply as:

$$\begin{aligned} p_{glass}(T, \varphi) &= -\frac{\varphi}{m^*} \frac{\partial \mathcal{S}(m^*, A^*; T, \varphi)}{\partial \varphi} \\ &= \frac{1}{m^*} p_{liq}(T/m^*, \varphi) - \frac{4\varphi}{m^*} \left[ y_{liq}^{HS}(\varphi) + \varphi \frac{dy_{liq}^{HS}(\varphi)}{d\varphi} \right] G(m^*, A^*; T) . \end{aligned} \quad (5.68)$$

The energy is obtained as:

$$U_{glass}(T, \varphi) = -\frac{1}{m^*} \frac{\partial \mathcal{S}(m^*, A^*; T, \varphi)}{\partial \beta} = -12\varphi y_{liq}^{HS}(\varphi) \int_0^\infty dr r^2 q(A^*, T; r)^{m^*-1} \frac{\partial q(A^*, T; r)}{\partial \beta} . \quad (5.69)$$

As expected, we can check that this can be rewritten as:

$$-\beta U_{glass}(T, \varphi) = 12\varphi y_{liq}^{HS}(\varphi) \int_0^\infty dr r^2 w(r) e^{w_{\text{eff}}(r)} . \quad (5.70)$$

An important quantity for the following is the optimal number of replicas  $m^*$ . In Fig. 5.5, we show its behavior as a function of the temperature, for different volume fractions. We see that the  $T \rightarrow 0$  limit of  $m^*(T, \varphi)$  converges when  $\varphi$  is not too large to a finite value, which we call  $m_{HS}^*(\varphi)$ , and which is shown in the inset. The replica parameter of hard spheres vanishes at a density  $\varphi_{GCP}$ , the glass close packing. This point is the equivalent, in our mean-field picture, of the jamming point of harmonic spheres. The behavior of the cage radius  $A^*$  is similar to that of  $m^*$ .

Since our goal is to study the vicinity of the jamming point, we have to take into account that the optimal number of replicas, as well as the optimal cage size, vanish at jamming.

From the knowledge of  $m^*$  and  $A^*$ , we can deduce the energy and specific heat of the glass. We show in Fig. 5.6 the temperature evolution of the specific heat for three densities, one below  $\varphi_{GCP}$ , one very close to it, and one above. Upon crossing the ideal glass transition, the specific heat undergoes a finite jump. We find that the amplitude of this jump increases continuously with  $\varphi$  from  $\varphi_K$ . A qualitatively similar result was obtained in numerical simulations [21], where the jump of specific heat was studied at the numerical glass transition temperature. The behavior of the specific heat correlates well with the evolution of the thermodynamic fragility discussed in Fig. 5.4. Finally, we note that the  $T \rightarrow 0$  limit of the specific heat jumps discontinuously from 0 to 3/2 at  $\varphi_{GCP}$ , which reveals that the ground state properties of the glass phase abruptly change at the jamming transition, as we now study in more detail.

### 5.3 Jamming point of harmonic spheres

We now turn to the study of the region of the phase diagram deep in the glass phase, inside the line  $T_K(\varphi)$  and close to the jamming point  $\varphi_{GCP}$ , see Fig. 5.1. In this region,  $m^*(T, \varphi)$  is very small, as we discussed in the last section (see Fig. 5.5). In principle, one could just compute  $m^*(T, \varphi)$  and then take the limit  $T \rightarrow 0$  and  $\varphi \rightarrow \varphi_{GCP}$  (“jamming limit”). However, both numerically and analytically, it is much more convenient to exchange the optimization with respect to  $m$  and  $A$  with the jamming limit, take the latter first, and then optimize the free energy. This is because, in the jamming limit, many of the integrals that appear in the free energy simplify considerably. However, the scaling of  $m$  and  $A$  in the jamming limit is different depending on the order of the limits, which emphasizes the asymmetry that exists between both sides of the jamming point. In this section we discuss how to exchange the jamming limit with the optimization procedure.

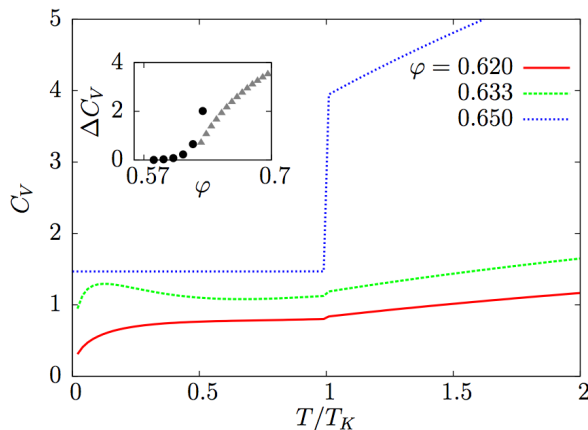


Figure 5.6: Specific heat  $C_V$  of the system plotted against  $T/T_K$ , for several volume fractions. The curves for  $\varphi = 0.620, 0.633$  are obtained with the effective potential method. The curve for  $\varphi = 0.650$  is obtained with the Mézard-Parisi small cage expansion [123], since at this density  $T_K(\varphi)$  is too high and the effective potential method is not reliable. Inset: Specific heat jump at  $T_K$ ; the black dots are obtained with the effective potential approximation, the gray triangles are obtained with the Mézard-Parisi small cage expansion.

### 5.3.1 Zero temperature, below close packing

We consider first the limit  $T \rightarrow 0$  for fixed  $\varphi < \varphi_{GCP}$ . In this case, we are bound to recover the results of [138] for hard spheres. We reproduce here these results, in order to fix the notations and for the sake of completeness. This is easily seen by considering the  $T \rightarrow 0$  limit of the expression of the function  $q$ :

$$q(A, T; r) \xrightarrow{T \rightarrow 0} q(A; r) = \frac{1}{2} \left( 2 + \operatorname{erf} \left[ \frac{r-1}{2\sqrt{A}} \right] - \operatorname{erf} \left[ \frac{r+1}{2\sqrt{A}} \right] \right) + \sqrt{\frac{A}{\pi}} \frac{1}{r} \left( e^{-\frac{(r-1)^2}{4A}} - e^{-\frac{(r+1)^2}{4A}} \right), \quad (5.71)$$

which recovers the result found in Parisi and Zamponi for the hard-sphere case. We expect the optimal number of replicas  $m^*(T, \varphi)$  and cage radius  $A^*(T, \varphi)$  to tend to finite values  $m_{HS}^*(\varphi)$  and  $A_{HS}^*(\varphi)$  when  $T \rightarrow 0$ . Therefore, to recover hard spheres results, one has to take the limit  $T \rightarrow 0$  at fixed  $A$  and  $m$ , and optimize the resulting free entropy over  $A$  and  $m$ .

The corresponding expression for the replicated free entropy coincides with that of [138] and reads:

$$\begin{aligned} \mathcal{S}(m, A; T, \varphi) &\xrightarrow{T \rightarrow 0} \mathcal{S}(m, A; \varphi) = \mathcal{S}_{\text{harm}}(m, A) + \mathcal{S}_{\text{liq}}^{HS}(\varphi) + 4\varphi y_{\text{liq}}^{HS}(\varphi) G(m, A), \\ G(m, A) &= 3 \int_0^\infty dr r^2 \left[ q(A; r)^m - \theta(r-1) \right]. \end{aligned} \quad (5.72)$$

We numerically solved the optimization equations; the result for  $m_{HS}^*(\varphi)$  is plotted in the inset of Fig. 5.5. Approaching  $\varphi_{GCP}$  by the left,  $m_{HS}^*$  goes to zero linearly:

$$m_{HS}^* \underset{\varphi \rightarrow \varphi_{GCP}}{\propto} (\varphi_{GCP} - \varphi), \quad (5.73)$$

From the inset of Fig. 5.5 we find the value of the glass close packing to be:

$$\varphi_{GCP} = 0.633353, \quad (5.74)$$

recovering the result of [138].

We also find that  $A_{HS}^*$  also goes to zero with  $m$  as  $\alpha m$ . Thus the close packing limit for hard spheres can be computed by taking first the limit  $T \rightarrow 0$ , and then  $m \rightarrow 0$  with  $A = \alpha m$ . Optimization on  $A$  will now become an optimization on  $\alpha$ . The  $q$  function, when  $A = \alpha m$  and  $m \rightarrow 0$  has for limits:

$$q(m\alpha; r) \xrightarrow{m \rightarrow 0} \begin{cases} 0 & r < 1, \\ 1 & r \geq 1 \end{cases}, \quad (5.75)$$

Going to next order by resorting to the asymptotic expansion of the error function, and neglecting subleading terms, we obtain:

$$q(m\alpha; r) \underset{m \rightarrow 0}{\sim} \theta(r-1) + \sqrt{\frac{A}{\pi}} e^{-\frac{(r-1)^2}{4A}} \left[ \frac{1}{r} + \frac{1}{1-r} R \left( \frac{|1-r|}{\sqrt{A}} \right) \right]. \quad (5.76)$$

From this we can obtain the expansion of  $G$  in powers of  $m$ :

$$\begin{aligned} G(m, \alpha m) &\underset{m \rightarrow 0}{\sim} m^{m/2} G_0^{HS}(\alpha) (1 + R_1 m + R_2 m^2 + \dots) + S_1 m^2 + S_2 m^{5/2} + \dots, \\ G_0^{HS}(\alpha) &= 3 \int_0^1 dr r^2 e^{-\frac{(r-1)^2}{4A}}. \end{aligned} \quad (5.77)$$

The first part comes from the  $r < 1$  part of the integral, and the other, subdominant one comes from the  $r > 1$  part of the integral. Finally the free-entropy can be expressed only with analytic terms:

$$\begin{aligned} \mathcal{S}_0^{HS}(\alpha; \varphi) &\equiv \lim_{m \rightarrow 0} \mathcal{S}(m, A = \alpha m; \varphi) = -\frac{3}{2} \left[ \ln(2\pi\alpha) + 1 \right] + \mathcal{S}_{liq}^{HS}(\varphi) + 4\varphi y_{liq}^{HS}(\varphi) G_0^{HS}(\alpha), \\ G_0^{HS}(\alpha) &= 3 \left[ \sqrt{\pi\alpha} (1 + 2\alpha) \operatorname{erf} \left( \frac{1}{2\sqrt{\alpha}} \right) + 2\alpha e^{-\frac{1}{4\alpha}} - 4\alpha \right]. \end{aligned} \quad (5.78)$$

The optimization over  $\alpha$  gives a self consistent equation for the optimal value  $\alpha_{HS}^*$ :

$$\begin{aligned} J_0^{HS}(\alpha_{HS}^*(\varphi)) &= \frac{3}{8\varphi y_{liq}^{HS}(\varphi)}, \\ J_0^{HS}(\alpha) &= \alpha \frac{dG_0^{HS}(\alpha)}{d\alpha}. \end{aligned} \quad (5.79)$$

To find the complexity, we must go to the leading order in the small  $m$  expansion (since we need to take a derivative with respect to  $m$ ). This reads:

$$\mathcal{S}(m, \alpha m; \varphi) = \mathcal{S}_0^{HS}(\alpha; \varphi) + \frac{1}{2} \left[ 3 + 4\varphi y_{liq}^{HS}(\varphi) G_0^{HS}(\alpha) \right] m \ln m + \mathcal{O}(m, (m \ln m)^2). \quad (5.80)$$

We compute the complexity as:

$$\begin{aligned} \Sigma(m, \alpha; \varphi) &= -m^2 \frac{d}{dm} \left[ \mathcal{S}(m, \alpha m; \varphi) / m \right] \\ &= \mathcal{S}_0^{HS}(\alpha; \varphi) - \frac{m}{2} \left[ 3 + 4\varphi y_{liq}^{HS}(\varphi) G_0^{HS}(\alpha) \right]. \end{aligned} \quad (5.81)$$

Taking the  $m \rightarrow 0$  limit, and evaluating this at the optimal value of  $\alpha$ , we get the complexity of hard spheres at  $m = 0$ :

$$\Sigma_0^{HS}(\varphi) = \mathcal{S}_0^{HS}(\alpha_{HS}^*(\varphi); \varphi). \quad (5.82)$$

This complexity vanishes linearly at  $\varphi_{GCP}$ , signaling the jamming transition. The optimal value of  $\alpha$  is found to be very small at the transition, which will prove to be convenient in the following:

$$\alpha_{HS}^*(\varphi_{GCP}) = 9.72187 \times 10^{-5}. \quad (5.83)$$

We can also obtain the leading term of the optimal number of replicas from Eq. (5.81) by noting that  $m^*$  is defined as  $\Sigma(m^*) = 0$  leading to:

$$m_{HS}^*(\varphi) = \frac{2\Sigma_0^{HS}(\varphi)}{3 + 4\varphi y_{liq}^{HS}(\varphi) G_0^{HS}(\alpha_{HS}^*(\varphi))} . \quad (5.84)$$

The value of the cavity function of hard spheres at  $GCP$  is found to be:

$$y_{liq}^{HS}(\varphi_{GCP}) = 23.6238 , \quad (5.85)$$

and the value of  $G_0^{HS}$  at the transition is:

$$G_0^{HS}(\alpha_{HS}^*(\varphi_{GCP})) = 0.0170908 . \quad (5.86)$$

Gathering all this we can find the linear behavior of  $m_{HS}^*$  near the transition:

$$m_{HS}^*(\varphi) \underset{\varphi \rightarrow \varphi_{GCP}}{\sim} \tilde{\mu}(\varphi_{GCP} - \varphi) , \quad (5.87)$$

$$\tilde{\mu} = 20.7487 .$$

We can also get the scaling of the reduced pressure for  $\varphi \rightarrow \varphi_{GCP}^-$  by using the expression of the pressure given in Eq. (5.68):

$$p_{glass} \underset{\varphi \rightarrow \varphi_{GCP}}{\sim} \frac{3.03430 \varphi_{GCP}}{\varphi_{GCP} - \varphi} . \quad (5.88)$$

The prefactor is only 1% different from the correct value which is the space dimension  $d = 3$ , predicted by free volume theory [149] and by the small cage expansion of Ref. [138].

The pressure of the glass is thus found to diverge at the glass close packing point, which is consistent with our postulate that the glass close packing is indeed identified, in our mean-field picture, with the jamming transition.

To sum up, we have detected the glass close packing point, at a density consistent with the numerically observed values. Upon approaching this point from lower densities at zero temperature, harmonic spheres behave like hard-spheres, that are in an ideal glassy state, whose reduced pressure is found to diverge at the glass close packing point. By studying this point for higher densities, we will confirm that this point is a critical jamming point, as defined in the numerical simulations [135].

### 5.3.2 Zero temperature, above close packing

For  $\varphi > \varphi_{GCP}$ , the harmonic spheres have a finite energy at  $T = 0$ , due to overlaps. Then, because of the repulsion the spheres are jammed, and  $A^*$  vanishes at  $T = 0$ . It turns out from the numerical calculation of  $m^*$  and  $A^*$ , both in the small cage expansion [123] and in the potential approximation (see the previous section) that the optimal number of replicas  $m^*$  tends to zero when  $T \rightarrow 0$ . One finds that  $m = T/\tau$  and  $A = m\alpha$  with constants  $\alpha$  and  $\tau$ . Therefore for  $\varphi > \varphi_{GCP}$  one has to take the  $T \rightarrow 0$  limit with  $\alpha = A/m$  and  $\tau = T/m$  kept constant. Optimization over  $m$  and  $A$  is replaced by an optimization over  $\alpha$  and  $\tau$ .

The replicated free entropy simplifies considerably in this limit. We first observe that the  $G$  function becomes in the double limit  $A = \alpha m$  and  $T = m\tau$ :

$$G(m, \alpha m; m \tau) \underset{m \rightarrow 0}{\sim} G_0(\alpha, \tau) = G_0^{HS} \left( \alpha + \frac{\tau}{4} \right) - G_0^{HS} \left( \frac{\tau}{4} \right) . \quad (5.89)$$

The free-entropy thus becomes:

$$\mathcal{S}(m, \alpha; m; \tau, \varphi) \xrightarrow{m \rightarrow 0} \mathcal{S}_0(\alpha, \tau; \varphi) = -\frac{3}{2} \left[ \ln(2\pi\alpha) + 1 \right] + \mathcal{S}_{liq}(\tau, \varphi) + 4\varphi y_{liq}^{HS}(\varphi) G_0(\alpha, \tau) . \quad (5.90)$$

Optimization over  $A$  is again replaced by an optimization over  $\alpha$  by a very similar self-consistent equation than in the HS case:

$$\begin{aligned} J_0^{HS}(\alpha^*(\tau, \varphi)) &= \frac{3}{8\varphi y_{liq}^{HS}(\varphi)} , \\ J_0^{HS}(\alpha) &= \alpha \frac{dG_0(\alpha, \tau)}{d\alpha} . \end{aligned} \quad (5.91)$$

Taking the  $\tau \rightarrow 0$  limit, we see that we recover the hard-sphere results. Thus the jamming limit from above ( $\varphi > \varphi_{GCP}$ ) corresponds to sending  $\tau$  to zero in the previous equations. Expanding the equations around  $\tau = 0$  allows the derivation of the scaling behavior of the thermodynamic quantities above the jamming point [20].

Expanding the free-entropy we find:

$$\begin{aligned} \mathcal{S}_0(\alpha^*(\tau, \varphi), \tau; \varphi) &= \mathcal{S}_0^{HS}(\alpha; \varphi) + \tau \mathcal{S}_1(\alpha, \varphi) + \mathcal{O}(\tau^2) , \\ \mathcal{S}_1(\alpha, \varphi) &= \varphi y_{liq}^{HS}(\varphi) \left[ \frac{1}{\alpha} J_0^{HS}(\alpha) - 6 \right] . \end{aligned} \quad (5.92)$$

Evaluating this at the optimal value of  $\alpha$ , we get at lowest order in  $\tau$ :

$$\mathcal{S}_0(\tau, \varphi) \equiv \mathcal{S}_0(\alpha^*(\tau, \varphi), \tau; \varphi) = \mathcal{S}_0^{HS}(\alpha_{HS}^*(\varphi); \varphi) + \tau \mathcal{S}_1(\alpha_{HS}^*(\varphi), \varphi) + \mathcal{O}(\tau^2) . \quad (5.93)$$

From this we can deduce the complexity and energy of the states by coming back to the reasonings that lead to the expression of the complexity deduced from the replicated free-energy. We know that:

$$\mathcal{S}(m; T, \varphi) = \Sigma(f^*(m; T, \varphi)) - m\beta f^*(m; T, \varphi) . \quad (5.94)$$

But in the  $T \rightarrow 0$  limit, the free energy of the states is just their internal energy  $e$ , thus in the limit where  $T = m\tau$  we get:

$$\mathcal{S}(m = T/\tau; T, \varphi) \xrightarrow{T \rightarrow 0} \mathcal{S}_0(\tau, \varphi) = \Sigma_0(e^*) - e^*/\tau . \quad (5.95)$$

From the same reasoning than in Eq. (5.4) we get that:

$$\left\{ \begin{array}{l} \Sigma_0(\tau, \varphi) = \frac{\partial [\tau \mathcal{S}_0(\tau, \varphi)]}{\partial \tau} , \\ e(\tau, \varphi) = \tau^2 \frac{\partial \mathcal{S}_0(\tau, \varphi)}{\partial \tau} . \end{array} \right. \quad (5.96)$$

These relations give us the parametric equation determining the complexity and the energy of the states:

$$\left\{ \begin{array}{l} \Sigma_0(\tau, \varphi) = \Sigma_0^{HS}(\varphi) + \tau \mathcal{S}_1(\varphi) , \\ e(\tau, \varphi) = \tau^2 \mathcal{S}_1(\varphi) . \end{array} \right. \quad (5.97)$$

This allows to obtain the behavior of the complexity as a function of the energy:

$$\Sigma_0(e, \varphi) = \Sigma_0^{HS}(\varphi) + 2\sqrt{e\mathcal{S}_1(\varphi)} . \quad (5.98)$$



Since  $\mathcal{S}_1$  is finite at  $\varphi_{GCP}$  and  $\Sigma_0^{HS}$  vanishes linearly, we obtain a quadratic dependance to the ground state energy on  $\varphi - \varphi_{GCP}$ . We find:

$$\begin{aligned}\Sigma_0^{HS}(\varphi) &= 62.9577(\varphi_{GCP} - \varphi) , \\ \mathcal{S}_1(\varphi_{GCP}) &= 3767.51 ,\end{aligned}\tag{5.99}$$

Using these values we find the scaling of the optimal effective temperature  $\tau^*$  to scale as:

$$\begin{aligned}\tau^*(\varphi) &\underset{\varphi \rightarrow \varphi_{GCP}}{\sim} \tilde{\tau}(\varphi - \varphi_{GCP}) , \\ \tilde{\tau} &= 0.00835535 ,\end{aligned}\tag{5.100}$$

and the energy of the ground state as:

$$e_{GS}(\varphi) \underset{\varphi \rightarrow \varphi_{GCP}}{\sim} 0.263017(\varphi - \varphi_{GCP})^2 .\tag{5.101}$$

By a similar procedure, the pressure evaluated at  $\varphi_{GCP}$  gives the following scaling:

$$P_{glass}(T = 0, \varphi) \underset{\varphi \rightarrow \varphi_{GCP}}{\sim} 0.403001(\varphi - \varphi_{GCP}) .\tag{5.102}$$

Clearly the same scaling could have been obtained from the exact relation  $P_{glass}(T = 0, \varphi) = \frac{6\varphi^2}{\pi} \frac{de_{GS}}{d\varphi}$ .

We numerically obtain the behavior of the complexity as a function of the energy of the packing, and this is reported in Fig. 5.7.

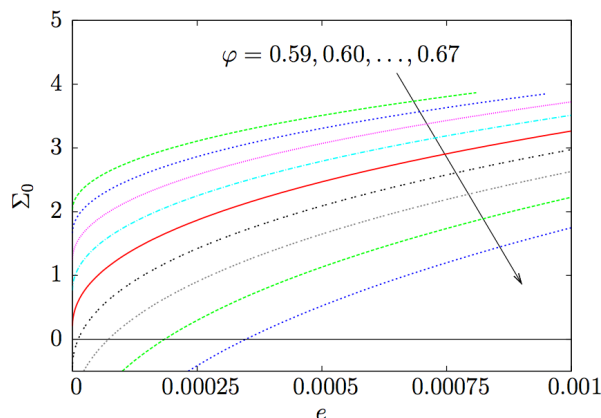


Figure 5.7: Complexity of the energy minima  $\Sigma_0(e, \varphi)$  as a function of energy for several densities.

In this section we have thus derived the scaling laws (5.101) and (5.102) first observed numerically above the jamming transition at zero temperature [135], which indicate that solidity emerges continuously at the jamming density. These results also confirm the postulated correspondence between the jamming transition observed numerically and the glass close packing density defined within our theoretical approach.

### 5.3.3 Scaling around jamming

We have shown in Secs. 5.3.1 and 5.3.2 that all the thermodynamic quantities are singular at  $\varphi_{GCP}$  and  $T = 0$ ; for instance  $m^*$  is finite below  $\varphi_{GCP}$  while it vanishes proportionally to  $T$  above  $\varphi_{GCP}$ .

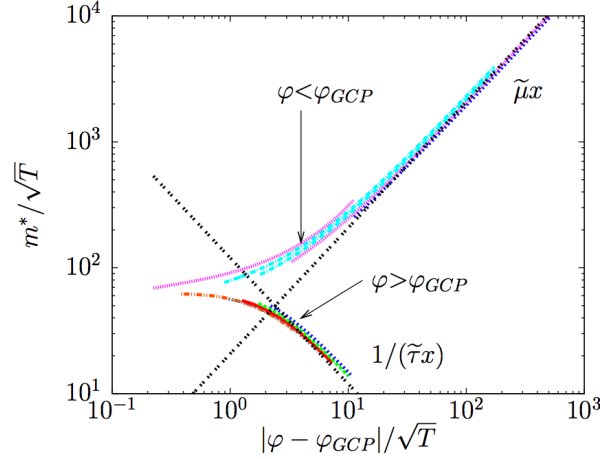


Figure 5.8: Scaling of  $m^*(T, \varphi)/\sqrt{T}$  as a function of the rescaled temperature  $|\varphi - \varphi_{GCP}|/\sqrt{T}$  for  $\varphi = 0.58, 0.59, \dots, 0.70$ . The asymptotic forms corresponding to Eq. (5.104) are also reported.

The reduced pressure is also finite below  $\varphi_{GCP}$ , while it diverges at  $\varphi_{GCP}$  and is formally infinite above  $\varphi_{GCP}$ . Both the energy and the pressure vanish below  $\varphi_{GCP}$  while they are finite above  $\varphi_{GCP}$ .

From this observation, and since all quantities are analytic at finite  $T$ , it follows that all these quantities must satisfy scaling relations if  $T$  is small enough and  $\varphi$  is close enough to  $\varphi_{GCP}$  [136]. We discuss explicitly the case of  $m^*$  for which we assume a scaling relation of the form

$$m^*(T, \varphi) = T^\gamma \tilde{m}_\pm \left( \frac{|\varphi - \varphi_{GCP}|}{T^\nu} \right), \quad (5.103)$$

where the two scaling functions correspond to the two sides of the transition. In the hard sphere limit  $T \rightarrow 0$  and  $\varphi < \varphi_{GCP}$ , to recover Eq. (5.73) we need  $\tilde{m}_-(x \rightarrow \infty) = \tilde{\mu}x$ , where  $\tilde{\mu}$  is a constant, and  $\gamma = \nu$ . For  $\varphi > \varphi_{GCP}$  instead,  $m^* = T/\tau^*(\varphi)$  and to recover Eq. (5.101) we need  $\tilde{m}_+(x \rightarrow \infty) = 1/(\tilde{\tau}x)$ , where  $\tilde{\tau}$  is a constant, and  $\gamma = \nu = 1/2$ . Finally, we are led to the scaling

$$\begin{cases} m^*(T, \varphi) = \sqrt{T} \tilde{m}_\pm \left( \frac{|\varphi - \varphi_{GCP}|}{\sqrt{T}} \right), \\ \tilde{m}_-(x \rightarrow \infty) = \tilde{\mu}x, \\ \tilde{m}_+(x \rightarrow \infty) = \frac{1}{\tilde{\tau}x}. \end{cases} \quad (5.104)$$

This scaling is successfully tested in Fig. 5.8.

Qualitatively similar scaling forms (with different exponents) apply to thermodynamic quantities such as the energy, the pressure, or the complexity. Although we do not show the corresponding scaling plots explicitly, the energy and the pressure are plotted and compared with numerical data in the following (Fig. 5.10). Note finally that a scaling plot for the complexity is related, in the spirit of the Adam-Gibbs relation in Eq. (1.17), to the scaling plot of the numerically measured relaxation time reported in Ref. [22].

## 5.4 The pair correlation function

The pair correlation function is a key quantity that gives a lot of insight into the structure of dense fluids or packings. In this section we derive an expression for the correlation function of the glass and use it to discuss the scaling of the contact peak of  $g(r)$  close to the jamming transition.

### 5.4.1 General expression of the correlation function of the glass

It has been shown in [138, Eqs.(67)-(68)] that one can compute the correlation function of the glass starting from the replicated free energy. This is done by adding a small perturbation  $u(r)$  to the potential of replica 1 and taking the derivative of the free energy with respect to  $u(r)$  and finally setting  $u$  to zero. The glass correlation function is then calculated as:

$$g_{glass}(r) = \frac{2}{\rho} \frac{\delta \mathcal{S}}{\delta u(r)} \Big|_{u=0}. \quad (5.105)$$

We start from Eq. (5.52) and we use approximation (5.60). Since the perturbation acts only on replica 1, we have

$$\mathcal{S}(m, A; T, \varphi) = \mathcal{S}_{harm}(m, A) + \mathcal{S}_{liq} \left[ \varphi, e^{mw(r)+u(r)} \right] + \frac{3\varphi}{\pi} y_{liq}^{HS}(\varphi) \int d^3r e^{mw(r)+u(r)} Q(r), \quad (5.106)$$

and  $Q(r)$  depends only on the potentials of replicas 2 to  $m$ , so it is independent of  $u$ . Taking the derivative with respect to  $u(r)$  we have, using again Eq. (5.60):

$$\begin{aligned} g_{glass}(r) &= g_{liq}(T/m, \varphi; r) + y_{liq}^{HS}(\varphi) e^{mw(r)} Q(r) \\ &= y_{liq}^{HS}(\varphi) e^{mw(r)} [1 + Q(r)] \\ &= y_{liq}^{HS}(\varphi) e^{w_{eff}(r)}. \end{aligned} \quad (5.107)$$

Therefore the correlation function of the glass is directly related to the effective potential within the low temperature approximation we used to compute the thermodynamics of the system. Of course, an improved expression for this correlation could be obtained by using the HNC approximation to describe the effective liquid. In that case,  $g_{glass}(r)$  would be the HNC correlation of the effective liquid. Still, the much simpler expression (5.107) is enough to capture the scaling of  $g_{glass}(r)$  around jamming, at least close to the first peak. In the rest of this section we discuss the scaling form that is obtained starting from Eq. (5.107).

A very interesting quantity related to  $g(r)$  is the number of contacts, defined as the number overlaps per particle. Within our low temperature approximation it is given by:

$$z(T, \varphi) = 24\varphi \int_0^1 dr r^2 g_{glass}(r) = 24\varphi y_{liq}^{HS}(\varphi) \int_0^1 dr r^2 e^{w_{eff}(r)}. \quad (5.108)$$

This expression simplifies into:

$$z(T, \varphi) = 24\varphi y_{liq}^{HS}(\varphi) \int_0^\infty du u^2 q(A, T; u)^{m-1} \hat{q}(A, T; u), \quad (5.109)$$

where  $\hat{q}$  is the part of the function  $q$  that vanishes in the  $T = 0$  limit:

$$\begin{aligned} \hat{q}(A, T; r) &= q(A, T; r) - \lim_{T \rightarrow 0} q(A, T; r), \\ &= -\sqrt{\frac{A}{\pi}} \frac{1}{r(1+4A\beta)} \left( e^{-\frac{(r-1)^2}{4A}} - e^{-\frac{(r+1)^2}{4A}} \right) \\ &\quad + e^{-\frac{(r-1)^2\beta}{1+4A\beta}} \frac{r+4A\beta}{2r(1+4A\beta)^{3/2}} \left( \operatorname{erf} \left[ \frac{r+4A\beta}{2\sqrt{A(1+4A\beta)}} \right] + \operatorname{erf} \left[ \frac{1-r}{2\sqrt{A(1+4A\beta)}} \right] \right) \\ &\quad - e^{-\frac{(r+1)^2\beta}{1+4A\beta}} \frac{r-4A\beta}{2r(1+4A\beta)^{3/2}} \left( \operatorname{erf} \left[ \frac{r-4A\beta}{2\sqrt{A(1+4A\beta)}} \right] - \operatorname{erf} \left[ \frac{1+r}{2\sqrt{A(1+4A\beta)}} \right] \right). \end{aligned} \quad (5.110)$$

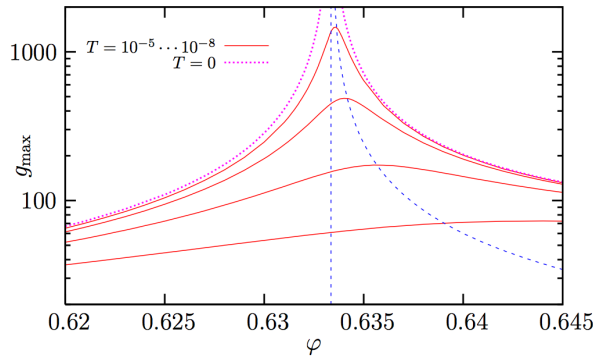


Figure 5.9: Evolution of the maximum of the glass pair correlation function with  $T$  and  $\varphi$ . While  $g_{max}$  diverges on both sides of the transition at  $T = 0$  as  $g_{max} \sim |\varphi - \varphi_{GCP}|^{-1}$ , this divergence becomes a smooth maximum at finite  $T$  near the transition, whose position shifts with temperature. This behavior compares very well with numerical [178, 59, 152] and experimental observations [178, 42].

Similarly the energy of the glass can be computed as:

$$U_{glass}(T, \varphi) = 12\varphi y_{liq}^{HS}(\varphi) \int_0^\infty du u^2 q(A, T; u)^{m-1} \left( -\frac{\partial \tilde{q}(A, T; u)}{\partial \beta} \right). \quad (5.111)$$

The starting point of the analysis of the correlation function of the glass are Eq. (5.107) and the expression of the effective potential.

### 5.4.2 Scaling of the peak of the pair correlation at finite temperature

Here we discuss the effect of thermal fluctuations on the maximum of  $g_{glass}(r)$  near the the  $T = 0$  jamming transition at  $\varphi_{GCP}$ . This situation was studied numerically and experimentally in Refs. [178, 84]. We focus on the scaling of this maximum in a region of small  $T$  and for  $\varphi \sim \varphi_{GCP}$ . In Fig. 5.9 we show the behavior of the maximum of  $g_{glass}(r)$ , which we call  $g_{max}$ , as a function of the density, for temperatures ranging from  $10^{-5}$  to 0. This figure demonstrates that we are able to derive analytically all behaviors reported in Refs. [178, 42, 59, 152]. Namely, the density at which the pair correlation function reaches its maximum shifts towards higher values when the temperature departs from 0 and increases as  $\sqrt{T}$ , while the maximum  $g_{max}$  diverges as  $|\varphi - \varphi_{GCP}|^{-1}$  on both sides of the transition.

As discussed in the previous section, the zero temperature limit is very different for  $\varphi < \varphi_{GCP}$  or  $\varphi > \varphi_{GCP}$ . Thus we now discuss these two limits separately.

### 5.4.3 Zero temperature below jamming: hard spheres

As explained above, we send  $T \rightarrow 0$  before taking the jamming limit  $m \rightarrow 0$  and  $A = \alpha m$ . By studying the behavior of the effective potential in this limit (starting from the asymptotic behavior of  $q$ ), we find that it diverges at  $r = 1^+$ :

$$e^{w_{\text{eff}}(r)} = \frac{1}{m} \Delta_\alpha \left( \frac{r-1}{m\sqrt{4\alpha}} \right), \quad (5.112)$$

where the scaling function  $\Delta$  is given by:

$$\Delta_\alpha(\lambda) = 2 \int_0^{1/\sqrt{4\alpha}} dx x (1 - x\sqrt{4\alpha})^2 e^{-2\lambda x - x^2}. \quad (5.113)$$

For  $\varphi \rightarrow \varphi_{GCP}^-$  we found that  $m \sim \tilde{\mu}(\varphi_{GCP} - \varphi)$  and the optimal cage size  $A^* = \alpha^* m$  with a finite  $\alpha^* = \alpha^*(\varphi_{GCP})$ , we thus find the following scaling for the pair correlation function:

$$\begin{cases} g_{glass}(r)(\varphi_{GCP} - \varphi) = f\left[\frac{r-1}{\varphi_{GCP} - \varphi}\right], \\ f(\lambda) = \frac{y_{liq}^{HS}(\varphi)}{\tilde{\mu}} \Delta_{\alpha^*} \left[ \frac{\lambda}{\tilde{\mu}\sqrt{4\alpha^*}} \right], \end{cases} \quad (5.114)$$

The height of the peak scales as:

$$g_{glass}(r=1^+, \varphi \rightarrow \varphi_{GCP}) \sim \frac{1.09922}{\varphi_{GCP} - \varphi}, \quad (5.115)$$

and its width as  $\varphi_{GCP} - \varphi$ .

The number of contacts is the integral of the peak at  $r=1^+$  which is given by

$$\begin{aligned} z &\sim 24\varphi \int_{peak} dr g_{glass}(r) \\ &\sim 24\varphi y_{liq}^{HS}(\varphi) \sqrt{4\alpha^*} \int_0^\infty d\lambda \Delta_{\alpha^*}(\lambda) \end{aligned} \quad (5.116)$$

Using the actual values derived in the previous section, we get  $z = 6.13720$  for  $\varphi = \varphi_{GCP}$ , which is slightly above the expected  $z = 2d = 6$ .

Note that it has been shown in [138] that within a systematic expansion in  $\sqrt{\alpha}$ , one gets  $z = 2d$  at first order. Here instead, in order to match with the soft sphere computation, we are using an approximation scheme which is not a consistent expansion in  $\sqrt{\alpha}$ . This could explain the fact that  $z \neq 2d$ . It would be interesting to have a full computation of the next term in the small  $\alpha$  expansion to check whether the equality  $z = 2d$  survives at this order. Unfortunately this seems to be a quite hard task.

#### 5.4.4 Zero temperature above jamming

For  $\varphi > \varphi_{GCP}$ , the appropriate limit is to send  $T \rightarrow 0$  with  $m = T/\tau$  and  $A = \alpha m$ . We obtain for the effective potential the following leading behavior:

$$e^{w_{eff}(r)} = \theta(r-1) + \theta(1-r)\theta\left(r - \frac{4\alpha}{\tau+4\alpha}\right) \frac{(1+4\alpha/\tau)[1+(r-1)(1+4\alpha/\tau)]^2}{r^2} e^{-\frac{\tau+4\alpha}{\tau^2}(r-1)^2}. \quad (5.117)$$

Close to  $\varphi_{GCP}$  this function develops a delta peak close to  $r=1$  with height  $(\varphi - \varphi_{GCP})^{-1}$  and width  $\varphi - \varphi_{GCP}$ , in the same way than in the hard-sphere case. The main difference we observe with the hard sphere limit is that, despite the fact that both cases give rise to a delta function at  $r=1$ , the mechanism is different since for hard spheres the support is concentrated on  $r=1^+$  while for soft spheres it is concentrated on  $r=1^-$ . Another interesting observation is that the theory predicts that  $g_{glass}(r)$  should vanish exactly for  $r < \frac{4\alpha}{\tau+4\alpha}$ ; this means that no pair of spheres can have an overlap larger than  $\frac{\tau}{\tau+4\alpha}$ . Indeed in the limit  $\tau \rightarrow 0$  we recover the  $GCP$  at which no overlaps are present. Unfortunately, a direct numerical test of this prediction is impossible: this is because when  $1-r = \frac{\tau}{\tau+4\alpha}$ , the exponential term in Eq. (5.117) is equal to  $\exp(-1/(\tau+4\alpha))$ . Since both  $\tau$  and  $\alpha$  are already extremely small (of the order of  $10^{-3}$  at best),  $g_{glass}(r)$  is extremely small in the region where we predict it to vanish, and numerically the signal to noise ratio becomes too large.

Again in the limit  $\varphi \rightarrow \varphi_{GCP}^+$  we obtain the scaling forms

$$\begin{cases} g_{glass}(r)(\varphi - \varphi_{GCP}) = f\left[\frac{1-r}{\varphi - \varphi_{GCP}}\right], \\ f(\lambda) = \frac{y_{liq}^{HS}(\varphi)4\alpha^*}{\tilde{\tau}} \left(1 - \frac{4\alpha^*\lambda}{\tilde{\tau}}\right)^2 e^{-\frac{4\alpha^*\lambda^2}{\tilde{\tau}^2}}, \end{cases} \quad (5.118)$$

The number of contacts is easily obtained from Eq. (5.108) and Eq. (5.117) and we found:

$$z(T=0, \varphi) = z(T=0, \varphi_{GCP}) + C(\varphi - \varphi_{GCP}), \quad (5.119)$$

where  $z(T=0, \varphi_{GCP})$  is 6.13720, the same value than in the hard-sphere case. This result is at odds with the numerical finding of a square root behavior [59, 152]. We comment further on this discrepancy, in Sec. 5.6.

Note that this value of  $z(T=0, \varphi_{GCP})$  is identical to the one obtained on the hard sphere side (as it can be easily proven analytically), despite the fact that the two definitions of  $z$  are not equivalent. In the soft sphere case we defined  $z$  as the number of overlaps. On the hard sphere side, this number is strictly zero, therefore we defined  $z$  as the integral of the delta peak at  $r = 1^+$ .

## 5.5 Comparison with numerical data

In this section, we compare the prediction of the theory with numerical data, in particular to test the scaling in temperature and in  $\delta\varphi = \varphi - \varphi_{GCP}$  around the glass close packing point.

### 5.5.1 Details of the numerical procedure

We investigated a system of  $N = 8000$  identical harmonic spheres. The system was prepared using the standard procedure of Ref. [134]. We started from a random configuration at high density; we then minimized the energy, and then reduced slowly the density, at each step minimizing the energy again, until a jammed configuration of zero energy and volume fraction  $\varphi_j$  was found. This jammed configuration corresponds, according to the mean-field interpretation of [138], to the  $T = 0, p \rightarrow \infty$  limit of a given hard sphere glass, or equivalently to the  $T \rightarrow 0, P \rightarrow 0$  limit of a corresponding soft sphere glass. Starting from that configuration, we prepared configurations at different  $T$  and  $\varphi$  by using molecular dynamics simulations as in Ref. [22] to equilibrate the system inside the glass state selected by the initial jammed configuration. Since we always used very small  $T$  and  $\varphi \sim \varphi_j$ , the system is not able to escape from that glass state, so it always remains in the vicinity of the original jammed configuration. This is a crucial requirement to numerically obtain scaling behavior near  $\varphi_j$  as microscopic rearrangements would directly affect the location of  $\varphi_j$  in the simulations [40]. We tested the absence of such an effect in our simulations by repeating the energy minimization starting from some equilibrated configurations at different  $T$  and  $\varphi$ , and checking that we always found the same value of  $\varphi_j$  (within numerical errors). For the particular series of run described below, we estimated  $\varphi_j = 0.643152 \pm 0.000020$  by fitting the zero temperature energy using  $e(\varphi) \propto (\varphi - \varphi_j)^2$ .

### 5.5.2 Difficulties in the comparison with the theory

When comparing the theory with the numerical data, we face two difficulties. First of all, the value of  $\varphi_j$  depends on the numerical protocol and on its particular realization we used, and therefore

cannot be directly compared with  $\varphi_{GCP}$ . Note that  $\varphi_{GCP}$  should represent an upper bound for  $\varphi_j$ , whatever the protocol, but the value  $\varphi_{GCP} = 0.633353$  we report seems to contradict this statement. The reason is simply that our theoretical computations are based on the HNC equation of state for liquid hard spheres, which (as discussed above), underestimates the value of  $\varphi_{GCP}$ : a better result is obtained using the Carnahan-Starling equation of state, which gives  $\varphi_{GCP} = 0.683$ , consistently with the value of  $\varphi_j$  found above [138]. To avoid confusion, here we stick to the use of the HNC equation of state; the theoretical calculations can be easily repeated for any other equation of state, and the scaling around  $\varphi_{GCP}$  is unaffected by this choice. Once again we stress that the absolute values of density reported here should always be taken with this caveat in mind. Since we are interested here mainly in the relative distance to jamming, which is  $\varphi - \varphi_j$  for the numerical data, and  $\varphi - \varphi_{GCP}$  for the theory, the absolute values of density are not crucial for our purposes.

The second difficulty is the following. For hard spheres, the theory predicts that the reduced pressure diverges as  $p_{glass}^{HS} \sim 3\varphi_{GCP}/(\varphi_{GCP} - \varphi)$ , while  $y_{glass}^{HS}(\varphi) \sim 1.1/(\varphi_{GCP} - \varphi)$  for  $\varphi \rightarrow \varphi_{GCP}^-$ . As one can easily check, these scalings imply that the theory violates the exact thermodynamic relation  $p_{glass}^{HS} = 1 + 4\varphi y_{glass}^{HS}(\varphi)$ , as already noticed in [138]. In particular, the divergence of  $p_{glass}^{HS}$  is correct, while the coefficient of the divergence of  $y_{glass}^{HS}(\varphi)$  is overestimated by a factor of  $\sim 1.46562$ . We will comment on the origin of this problem in Sec. 5.6. This error affects the prefactors in the scalings of  $g_{glass}(r)$  and of  $z$  around  $\varphi_{GCP}$ . To correct for this error, we rescaled the  $\delta\varphi$  of the numerical data in such a way that the coefficient of the divergence of  $y_{glass}^{HS}$  is the same as the theoretical one.

To summarize, when comparing numerical data with the theory, we consider  $\delta\varphi = \varphi - \varphi_{GCP}$  for the theory, and  $\delta\varphi = 1.46562(\varphi - \varphi_j)$  for the numerical data such that the values of  $y_{glass}^{HS}(\delta\varphi)$  for theory and simulations are exactly the same close to  $\delta\varphi = 0$ . Note that this adjustment is based solely on the analysis of the hard sphere side of the jamming transition ( $\delta\varphi < 0$ ), but we find that it allows to describe the full scaling also for positive  $\delta\varphi$ .

If the reader is uncomfortable with the above reasonings, another way of thinking is that we need to adjust two free parameters (the position of the transition and the amplitude of the rescaling of  $\delta\varphi$ ) to obtain the best comparison of theory and numerical simulations. While the location is  $\varphi_j$  was always adjusted in previous work [59, 152, 134, 166], we need to adjust also one prefactor as we seek to compare theoretical predictions to simulations in absolute values, and not only at the level of leading diverging contributions.

### 5.5.3 Energy, pressure, average coordination

We start our discussion by the simplest observables. In Fig. 5.10 we plot the average energy  $U_{glass}(T, \varphi)$  and the inverse reduced pressure  $1/p_{glass}(T, \varphi)$  as functions of  $\delta\varphi$  for several temperatures. The agreement between theory and numerical data, with the rescaling of  $\delta\varphi$  discussed above, is nearly perfect. The scaling around jamming is clearly visible in the figures. For instance,  $U_{glass}(T, \varphi)$  tends to a finite value for  $\delta\varphi > 0$ , while for  $\delta\varphi < 0$  it goes to zero as a power law, since in this case the system becomes a hard sphere glass. Similarly, the reduced pressure is finite for  $\delta\varphi < 0$ , while it diverges proportionally to  $\beta$  for  $\delta\varphi > 0$ , since in this case the pressure is finite at zero temperature. At finite temperature, the curves interpolate between the two regimes. Scaling functions similarly to the ones shown in Fig. 5.8 for  $m^*$  can easily be constructed.

In Fig. 5.11 we report the average coordination number  $z(T, \varphi)$ , as a function of  $\delta\varphi$  for several temperatures. At  $T = 0$ , the average coordination jumps from 0 to 6 (for numerical data) or to 6.13720 (for the theory). For  $\delta\varphi > 0$ , the average coordination grows linearly in  $\delta\varphi$  for the theory, while it grows as  $\delta\varphi^{1/2}$  for the numerical data. Therefore, the theory fails to capture the correct evolution of

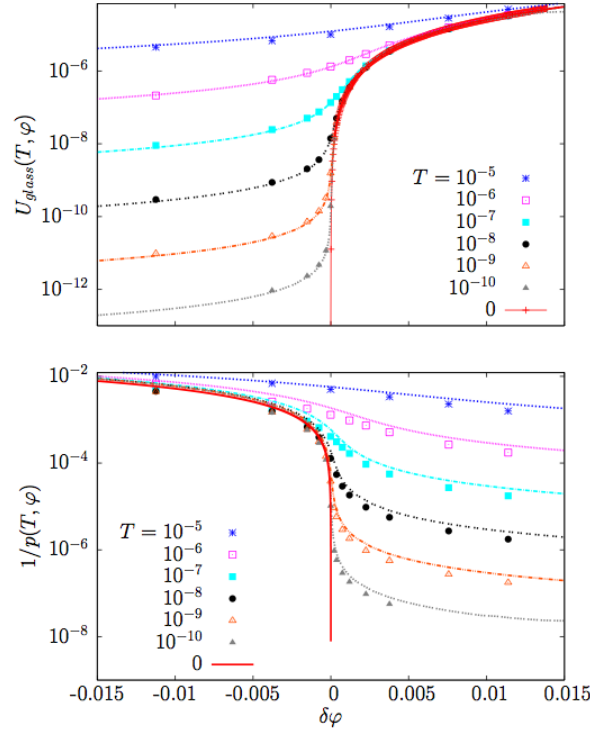


Figure 5.10: Energy  $U_{glass}(T, \varphi)$  (top panel) and inverse reduced pressure  $1/p_{glass}(T, \varphi)$  (bottom panel) as functions of distance from jamming  $\delta\varphi$ , for several temperatures. We define  $\delta\varphi = \varphi - \varphi_{GCP}$  for the theory, and  $\delta\varphi = 1.46562(\varphi - \varphi_j)$  for the numerical data.

this structural property at  $\delta\varphi > 0$  and  $T = 0$ .

A more detailed description of what happens is obtained by looking to the data at finite  $T$ . When temperatures become too large, e.g. at  $T = 10^{-5}$ , the theory eventually fails because of the low- $T$  approximation we made on the liquid theory in Eq. (5.60). For any fixed temperature  $T \leq 10^{-6}$ , we observe that the theory describes perfectly the numerical data for  $\delta\varphi < 0$  and also for positive  $\delta\varphi$  up to some crossover value  $\delta\varphi_h(T)$ . Around  $\delta\varphi_h(T)$  the theory starts deviating from the numerical data. The data in Fig. 5.11 suggest that  $\delta\varphi_h(T)$  is an increasing function of  $T$ , i.e. that for higher temperatures the theory performs better, if the temperature is low enough that approximation (5.60) makes sense. Indeed, we expect that for  $\delta\varphi_h(T) \rightarrow 0$  for  $T \rightarrow 0$ , since at  $T = 0$  the theory fails to capture the behavior of the contact number at  $\delta\varphi > 0$ . We will come back to this point below.

#### 5.5.4 Correlation function

We now report data for the scaling of the contact peak of  $g_{glass}(r)$  near jamming. We first consider a fixed  $\delta\varphi < 0$ , and change the temperature. In Fig. 5.12 we report data for  $\delta\varphi = -0.00078$  for several temperatures. In this regime the theory works very well down to  $T = 0$ ; this is expected since we know that the theory works at  $T = 0$  for hard spheres [138].

Next, we consider a fixed  $\delta\varphi > 0$  and plot  $g_{glass}(r)$  for several temperatures. This is done in Fig. 5.13 for four different values of  $\delta\varphi$ . Here, we observe that, like for the average coordination (Fig. 5.11), the theory works very well at moderately large  $T$ . However, on lowering  $T$ , at some point we observe that the numerical  $g_{glass}(r)$  saturates to a limiting curve which has a maximum at



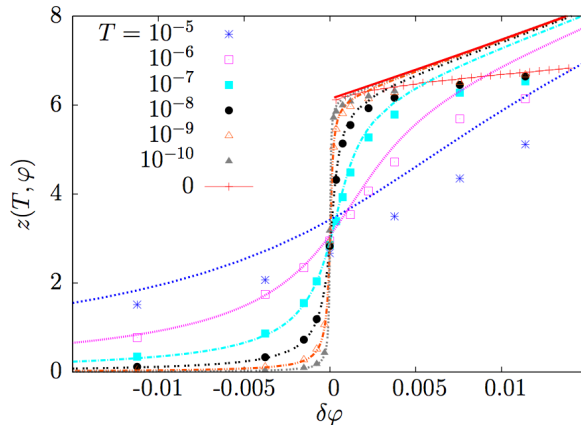


Figure 5.11: Average number of contacts  $z$  as a function of distance from jamming  $\delta\varphi$ , for several temperatures. We define  $\delta\varphi = \varphi - \varphi_{GCP}$  for the theory, and  $\delta\varphi = 1.46562(\varphi - \varphi_j)$  for the numerical data.

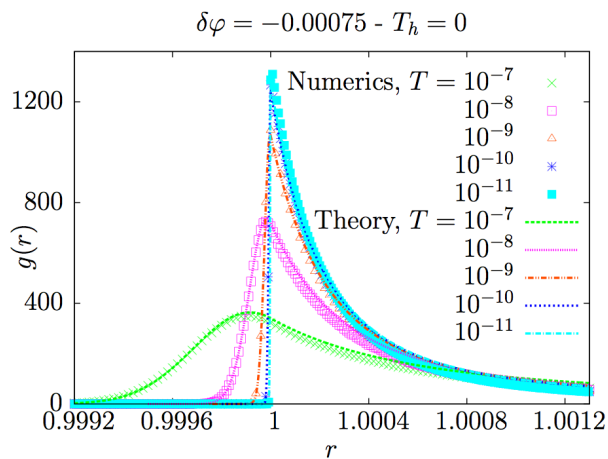


Figure 5.12: Pair correlation  $g_{glass}(r)$  just below jamming predicted by theory (full lines) and measured in numerical simulations (symbols). Here  $\delta\varphi = -0.00075$ .

$r < 1$ . By contrast, the theoretical curves slowly evolve towards the  $T = 0$  theoretical limit, which is a half-Gaussian centered in  $r = 1$ , with its  $r > 1$  part removed.

Therefore, below a certain temperature  $T_h(\delta\varphi)$  (the inverse of the function  $\delta\varphi_h(T)$  mentioned above), a deviation between theory and numerical data is observed close to the maximum of  $g_{glass}(r)$ . Clearly, the deviation between data and theory is a smooth crossover, so determining  $T_h(\delta\varphi)$  is not easy. Here we choose the following procedure. The numerical data accumulate on a master curve as  $T \rightarrow 0$ . Therefore we define  $T_h(\delta\varphi)$  as the value of temperature at which the theoretical curve best fits the  $T \rightarrow 0$  numerical curve. As an example, in the upper left panel of Fig. 5.13, we see that the theoretical curve for  $T = 10^{-10}$  fits very well the numerical curves for both  $T = 10^{-10}, 10^{-11}$ , while the  $T = 10^{-11}$  theoretical curve is quite different. We fix  $T_h = 10^{-10}$  for this value of  $\delta\varphi$ . Clearly the ambiguity on the precise numerical value of  $T_h$  is rather large. Despite this, we are able to qualitatively confirm that  $T_h(\delta\varphi)$  is an increasing function of  $\delta\varphi$ , as already suggested in the previous section. The function  $T_h(\delta\varphi)$  determined from the pair correlation functions is reported in Fig. 5.14. It emerges continuously from zero above  $\varphi_{GCP}$ . A comparison with the temperature scale given by the glass

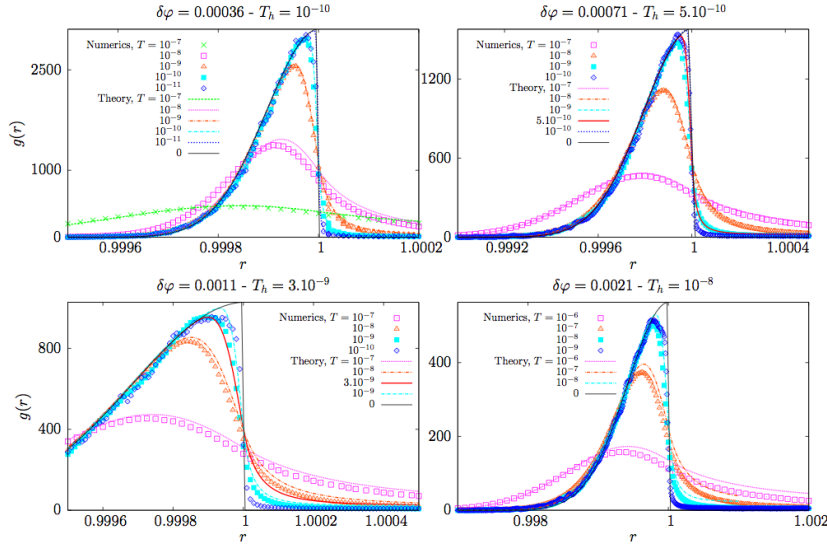


Figure 5.13: Pair correlations  $g_{glass}(r)$  above jamming predicted by theory (full lines) and measured in numerical simulations (symbols). The agreement is very good for  $T > T_h(\delta\varphi)$ , the values of  $T_h(\delta\varphi)$  are reported above the figures. Below  $T_h(\varphi)$ , the numerical curves do not evolve anymore, while the theoretical curves continue to evolve towards the  $T = 0$  theoretical limit.

temperature shows that it is orders of magnitude smaller than  $T_K$ . Thus it is only in the small regime of  $T < T_h$  and  $\varphi > \varphi_{GCP}$  that our the effective potential approach misses some important physics, as we discuss below in Sec. 5.5.5.

Finally, in Fig. 5.15 we show that  $g_{glass}(r)$ , at  $T = 0$ , follows the scaling relations predicted by the theory, Eqs. (5.114) and (5.118), for  $|\delta\varphi| \rightarrow 0$ , with different scaling functions on the two sides of the transition. While the scaling is perfect for  $\delta\varphi < 0$  [138], for  $\delta\varphi > 0$  there is a small deviation around the maximum as already discussed, which is however very small in the scaling regime for  $\delta\varphi \rightarrow 0$ .

### 5.5.5 Discussion

The main discrepancy between the theory and numerical data is in the region  $\delta\varphi > 0$  and very small temperature  $T < T_h(\delta\varphi)$ . Here, the average coordination scaling  $z \propto \delta\varphi^{1/2}$  at  $T = 0$  is not obtained. Furthermore, the shape of the peak of  $g_{glass}(r)$  is only partially captured by the theory. We tentatively attribute these discrepancies to the particular nature of the vibrational modes at  $T = 0$  and  $\delta\varphi > 0$ . It has been shown that in this regime the low-frequency spectrum is dominated by spatially correlated vibrational modes. These modes cannot be described by our approach, in which vibrations are assumed to be Gaussian and only two-body correlations are taken into account. Therefore it is to be expected that the particular features of the jamming transition that are related to these correlated soft modes are not well reproduced by our theory.

On the hard sphere side, the soft modes induce a square-root divergence of the pair correlation function  $g_{glass}(r) \propto 1/\sqrt{r-1}$ . Yet, for  $\delta\varphi \rightarrow 0^-$ , this square root singularity is well separated from the contact peak [138]; therefore the shape of the scaling function for the contact peak is not affected by the soft modes and it is indeed correctly reproduced by the theory (see [138] and Fig. 5.15).

On the other side of the transition and for small  $\delta\varphi > 0$  both the contact peak and the square root singularity are shifted by  $\delta\varphi$ . In particular the square root contribution should become  $g_{glass}(r) \sim$

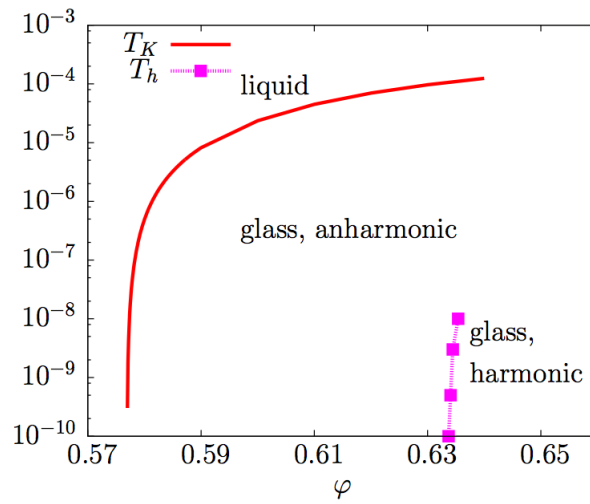


Figure 5.14: The crossover temperature  $T_h(\varphi)$ , as determined from Fig. 5.13, and compared with the Kauzmann temperature from Fig. 5.3.

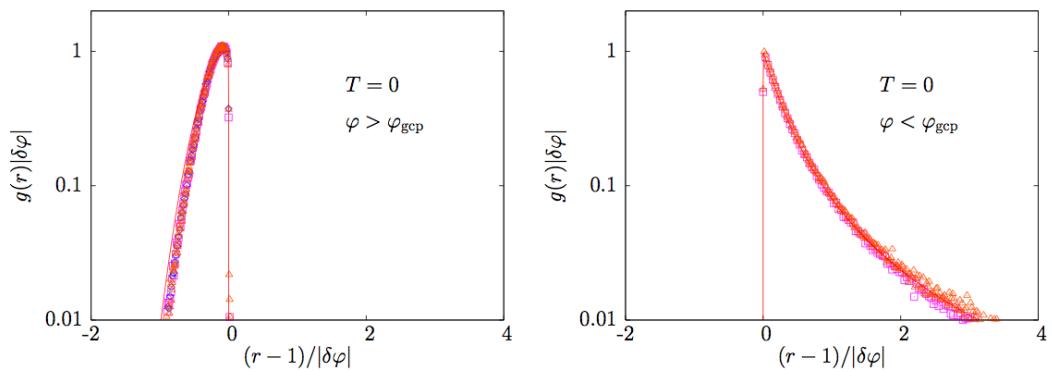


Figure 5.15: Scaling functions at  $T = 0$  above (left) and below (right) the jamming transition showing the convergence of the first peak near  $r = 1$  to a delta function with asymmetric scaling functions on both sides of the transition. To ease visualization, we show the evolution of  $g(r)/g_{max}$ , where  $g_{max}$  can be read from Fig. 5.9.

$1/\sqrt{r-1+a\delta\varphi}$ . Inserting this form of  $g_{glass}(r)$  into Eq. (5.108) yields the result that  $z = z_0 + c\delta\varphi^{1/2}$ , where  $z_0$  is the contribution of the contact peak. While  $z_0$  is clearly unaffected by the shift, the scaling of  $z$  with  $\delta\varphi$  directly stems from the square root singularity of the pair correlation function. Therefore, the scaling of  $z$  is dominated by the soft modes contribution, which might explain why it is not well captured by our theory.

On the other hand, inserting the same expression in the general formula for the internal energy, Eq. (5.61), one finds that  $e_{GS} \sim \tilde{e}\delta\varphi^2 + d\delta\varphi^{5/2}$ , the first term being the contribution of the contact peak, the second being the one of the square root singularity. Therefore, for the energy the contribution of the anomalous modes is subdominant, and for this reason we observe that the theory reproduces well the numerical data in this case. The anomalous correction  $\delta\varphi^{5/2}$  is of course not reproduced by the theory, that gives an expansion of  $e_{GS}$  in integer powers of  $\delta\varphi$ , but these are subdominant terms.

We also suspect that the shape of  $g_{glass}(r)$  near the peak is also influenced by a mixing of the contact peak with the square root singularity. While both contributions are well separated for  $\varphi < \varphi_j$ , this is not necessarily the case above jamming, which likely explains the small deviations observed in Figs. 5.13 and 5.15, but we could not find an empirical or scaling argument to disentangle both contributions.

Finally, it is interesting to remark that these deviations between theory and simulations are washed out by a finite temperature  $T > T_h(\delta\varphi)$ . We suspect that  $T_h(\delta\varphi)$  represents a temperature scale at which anharmonicity becomes relevant [176], and where the zero-temperature vibrational modes become irrelevant. Above this crossover temperature, vibrations are probably much less correlated and our approximations become correct. Interestingly, since  $T_h(\delta\varphi) \rightarrow 0$  for  $\delta\varphi \rightarrow 0^+$ , we conclude that the correlations at  $\delta\varphi = 0$  are extremely fragile, such that an arbitrary small temperature is able to destroy them and restore the agreement between theory and numerical data.

## 5.6 Conclusions

In this final section we summarize our results and we discuss some perspectives for future work.

### 5.6.1 Summary of results

Understanding the physical properties of dense packings of soft repulsive particles is a fully nonequilibrium problem, because the jamming transition occurs in the absence of thermal fluctuations deep inside a glassy phase where phase space is dominated by the existence of a large number of metastable states.

Nevertheless, we showed that it can successfully be addressed using equilibrium statistical mechanics tools. We have developed a mean-field replica theory of the jamming transition of soft repulsive spheres which satisfactorily derives, from first principles, the existence and location of a jamming transition. This transition, that happens only at  $T = 0$ , is exactly the same as the SAT/UNSAT transition of random constraint satisfaction problems [127, 120, 101]: it is the point where the Parisi parameter  $m^*$  that characterizes the 1RSB glass phase goes to zero, the reduced pressure of the hard sphere glass diverges, or, equivalently, its pressure and energy become finite. Within our approach, the jamming transition takes place deep into the glassy phase, and is thus a phenomenon which is physically distinct from the glass transition itself [110]. Finally, we have shown that the average coordination jumps from zero to  $\sim 6$  at the transition, and we derived scaling functions that describe well the contact peak of the pair correlation function.

Again, the absolute values of density reported in this study are affected by the fact that we used the HNC equation of state for the liquid [138], and thus quantitative agreement with simulations cannot be expected. Still, we found that the scaling around jamming is almost insensitive to the particular equation of state that is chosen for the liquid. We also investigated the region of small  $T$  around the jamming transition. We showed that the theory reproduces quite well the scaling numerical data with  $T$  and  $\delta\varphi$ , the distance from the jamming transition. On the hard spheres side of the transition ( $\delta\varphi < 0$ ) the theory works well down to  $T = 0$ . On the soft sphere side ( $\delta\varphi > 0$ ) we have identified a temperature  $T_h(\delta\varphi)$  below which, according to our interpretation, correlated vibrations that are neglected in our theory become relevant for some observables, and produce a series of interesting scalings that are not captured by our theory [175, 166, 105]. The most striking of these is the scaling of the number of contacts which our theory fails to reproduce.

### 5.6.2 Technical aspects

It is a major open problem to try and include in the theory a correct description of the divergent correlations in the vibrational modes that are relevant for  $\delta\varphi > 0$  and  $T < T_h(\delta\varphi)$ . Additionally, there are several more technical aspects on which the theory could be improved, even in the region where it works quite well.

Our theory falls within the general framework of the replica method, using the molecular liquid formulation of [122, 123]. However, to be able to describe the jamming transition, we had to develop a new approximation scheme, that is based on the effective potentials formulation of [138], and allows one to view the molecular liquid as a simple liquid with effective potentials involving an arbitrary number of particles. Our approximation scheme is based on the following steps:

1. As in [138], we neglect the three (and more)-body interactions, and retain the two-body effective potential only.
2. In addition, we observe that the effective potential is given by the original potential (rescaled by a factor  $m$ ) plus a small perturbation, therefore we use liquid perturbation theory to write the free energy of the replicated liquid as in Eq. (5.52).
3. Finally, we performed the low temperature approximation Eq. (5.60), in order to simplify the numerical calculations.

The last two approximations have been done mainly for practical reasons. However, we found that they are related to the first one. Indeed, if we get rid of approximation 3, we introduce an explicit dependence of  $y_{liq}$  on temperature, hence on  $\tau$  in the limit  $T \rightarrow 0$  and  $\delta\varphi > 0$ . It is easy to realize that this dependence affects the scaling close to jamming. An additional  $\sqrt{\tau}$  term appears in the small  $\tau$  expansion, which implies that  $\tau \propto \delta\varphi^2$  and  $e \propto \delta\varphi^3$ . An inspection of the small  $\tau$  expansion reveals that if  $y_{liq}$  does not depend on  $\tau$ , then a delicate cancellation happens to eliminate the  $\tau^{1/2}$  term and produce the correct scalings. The crucial observation is that the anomalous term contains the derivative of  $y_{liq}$  with respect to temperature, which is related to a three-body correlation function. Therefore we speculate that in a full treatment this term is cancelled by a term coming from the three body interaction potential. Therefore, getting rid of the third step of approximation might require taking into account three-body correlations as well.

This is of course an extremely interesting direction for future research, mainly because we suspect that getting rid of approximation 2 should allow us to eliminate the violation of the exact thermodynamic relation  $p_{glass}^{HS} = 1 + 4\varphi y_{glass}^{HS}(\varphi)$  that occurs in the theory and forces us to rescale  $\delta\varphi$  in order

to compare with numerical data. It is also possible that taking into account interactions involving several particles one could capture at least partially the long range correlations at jamming.

### 5.6.3 Some general directions for future work

Our approach is general enough to be systematically improved and generalized to various models (e.g. Hertzian potentials, or truncated Lennard-Jones potential). Moreover, recent work reported on a method to compute the shear modulus within the replica approach [177, 163]. This could allow us to add the external drive to the theory, and obtain a complete theoretical picture of the jamming transition in the three dimensional temperature, density, stress jamming phase diagram originally proposed by Liu and Nagel [104].

An important points that the theory fails to adress is the behavior of pair correlations over a broader range of distances. It was shown that pair correlation functions also exhibit singular behavior beyond the contact peak [59, 152], while the structure factor [60] and isothermal compressibility [18] also display intriguing anomalies at large scale. These anomalies are postulated to be related to the anomalous scaling of the number of contacts. Recent simulations at high dimensions [37] showed that all the previously mentioned anomalies are largely independant of the dimension The fact that these features are present in all dimensions would suggest that they can be also described by a mean-field computation like the one we performed.

A possibility would be that such anomalies at large scale are related to a complex organization of the free-energy minima that dominate the partition function at very low temperature. This would be reflected in an instability of our replica symmetric ansatz (in which free-energy minima are supposed to be isolated one from another), that would have to be replaced by a full-RSB ansatz.

Another difficulty of the theory comes from the fact that the cage in the glass phase was shown by recent simulations to be non-Gaussian [39], which invalidates, at least in principle, our Gaussian ansatz. The non-Gaussianity of the cage should be related to the long-range anomalies found at the transition, and thus taking properly these two points into account would require a theory that is able to compute the cage shape from first principles, and that is also able to cope with higher levels of replica symmetry breaking. Note that it has been found in [103] that in high-dimensions, the free-energy was not affected by the Gaussian ansatz for the cage, but this is not expected for our low-dimensional case.

## Chapter 6

# Conclusion and perspectives

In this thesis, we have focused on the theoretical study of the transitions towards an amorphous solid state: the glass transition and the jamming transition. Our general approach has been to focus on finite-dimensional realistic models of structural glasses, and to concentrate on the derivation, from the sole knowledge of the pair potential and the evolution equation of the system, of the transition from supercooled liquid to glass, or from non-jammed to jammed.

For practical reasons, when an explicit numerical calculation was needed, we specialized to the system of harmonic spheres, mainly because of its special importance in the field of the jamming transition. The harmonic spheres have bounded interaction strength and range, two properties that we exploited respectively in Chapter 3 and 5.

### 6.1 Dynamics near the glass transition

We first studied the dynamics of a system of harmonic spheres and developed a simple perturbative approach, that predicts the existence of a glass transition in a compact way, giving some hope to the extension of such theory to higher-orders. By using the strength of the interaction between particles of the system as an expansion parameter, we were able to recover, as the lowest order correction to the ideal gas dynamics, a closed equation on the non-ergodicity factor of the system that is very close to the one obtained within mode-coupling theory. However, the situation is still unsatisfactory, due to a  $U(1)$  symmetry that has been broken by hand in our formulation. However, the situation could be improved, and several proposals have been put forward in other areas of physics [97, 98]. The mathematical problem has now been formulated in a coherent way, and falls in the general class of the 2PI approximations of the free-energy of interacting bosons, which directly connects to hard condensed matter physics.

In retrospect, the use of the strength of the interaction as an expansion parameter sheds light on a set of numerical works by Ikeda and Miyazaki [81, 79, 80], who observed that mode-coupling predictions became good for the high density Gaussian-core model. This model indeed falls in the generic class of bounded repulsive potentials, which behave like ideal gases in the high density limit, i. e. the strength of the interaction can be taken as a small parameter in this case. Thus the statics become mean-field [106] at high density, and the dynamics start obeying closely the mode-coupling phenomenology.

Apart from that case, several theoretical approaches still need to be reconciled. Szamel formulated a diagrammatic formulation of the mode-coupling theory for Brownian dynamics [159], which could

provide another correct starting point for improvement of the theory. Independently, the approach of Kawasaki and Kim [92], which is based on the more traditional Martin-Siggia-Rose formalism, uses a loop expansion to derive the same result as mode-coupling theory. One advantage of Szamel's formulation over the latter is that it contains explicitly the high-order correlation functions of the equilibrium liquid, whereas these correlations must be uncovered by non-perturbative arguments in the case of standard field-theory. The task is straightforward for the two-point correlation function, but we expect it to be much harder in the case of higher-order correlation functions.

We are left with three distinct approaches, the three of them being satisfying in one respect: our approach provides an expansion parameter, the approach of Szamel takes properly into account the static properties of the system, and the one of Kawasaki and Kim respects properly all symmetries of the evolution equation. A dynamical approach that could unify these three approaches would be a major breakthrough in the field.

Once a satisfying first-principle derivation of the existence of a glass transition will be derived, it will be easy to deduce the corresponding expressions for the four-point functions that are currently used in numerical works or in experiments, and they will naturally become long range due to the sudden appearance of a non-zero value of the non-ergodicity parameter [160, 17, 16].

However, it has been argued early that the apparition of a non-zero ergodicity parameter is merely an artifact of numerical simulations and experiments, that are not able to wait for a sufficient time the equilibration of the system. In that case, a cross-over to dynamics that are controlled by the static landscape is expected to take place, which, in the replica interpretation at least, would eventually also lead to ergodicity breaking, but with a very different underlying mechanism.

Another possibility would be that a transition of dynamical nature indeed takes place, but is described by a more complicated (dynamical) order parameter. This possibility is supported by recent numerical simulations [119, 142] that uncovered a hidden dynamical transition associated with the glass transition. However, the matter of connecting this discovery with observed behaviors of the two- or four- point correlation functions, or to thermodynamic quantities is still elusive. Moreover the theoretical study of such transitions on realistic models is expected to be quite involved.

## 6.2 Statics vs. dynamics

Independently of dynamical calculations, we also considered the random-first-order transition theory, that focuses on the metastable states of the static free-energy landscape. This set of theoretical predictions are based on the assumption that the long-time dynamics of the system are dominated by the deep minima of the free-energy landscape. By resorting to the replica method, and liquid state theory, one is able to predict the appearance of a non-zero non-ergodicity parameter. The predictions coming from replica theory and mode-coupling theory for this quantity were already noticed to share a similar form [161, 138]. Szamel used this similarity to show that, in terms of replica theory, the mode-coupling result is obtained with a reasonable assumption of vanishing current between different metastable states, and further use of factorization approximations much like in the original mode-coupling derivation. We adopted another approach and asked, within the static replica theory, for a precise comparison between the dynamical and the static self-consistent equations for the non-ergodicity parameter. The dynamical equation limits itself to a two-mode approximation, so we performed the equivalent approximation in the static context. An immediate observation was that a term containing the three-body static correlation function is obtained in both approaches, but the dominant one, that contains two-body correlation, is absent from replica theory, and seems to emerge



from purely dynamical calculations.

This calculation allowed to correctly identify the class of diagrams that are relevant in the static computation, which can allow for a unified framework for replica theory computations. For example, one could make contact with the Mézard-Parisi [123] and Parisi-Zamponi [138] approximation schemes, or more generally with the effective potential approximation derived in Chapter 5, by making a Gaussian ansatz on the form of the off-diagonal correlation function, and perform cage expansions afterwards.

Once an approximation that is able to detect the glass transition (such as replicated HNC) has been found, the calculation that we performed also serves as a basis for setting up a Landau-like expansion around this approximation, by using the fact that the bifurcation mechanism with which the non-ergodicity appears gives rise to soft modes in the system.

In a broader perspective, the interplay between the metastable states (i.e. minima of the static free-energy), that are at the basis of the reasonings in replica theory, and dynamical quantities should be investigated. This is by definition impossible in the static context, and has to be investigated in a dynamical calculation. More precisely, one has to consider the low lying excited states of the evolution operator of the system, and try to put them in correspondence with the minima of the static free-energy, in the spirit of [27]. An analytical approach that would be able to address this question for realistic models of glasses is unfortunately for the moment out of reach. However, such a finding would be mandatory if it were found that no dynamical order parameter describes the glass transition properly, as suggested above.

Despite this intrinsic limitation of replica theory, it is an important task to push its predictions as far as possible in order to set the stage for a theory that would be able to incorporate both static and dynamical aspects of the glass transition.

### 6.3 Theory of the jamming transition

Finally, we have developed, based on replica theory, a microscopic theory for the jamming transition of harmonic spheres, able to quantitatively recover many observed scalings near the jamming transition. Of the three main questions discussed in this thesis, this is where the current theoretical tools give the most satisfying results. Indeed, the very high density at which the jamming transition takes place justifies most of the approximations performed by replica theory: the out-of-equilibrium procedures used to construct those states place the system directly in an ergodicity broken picture, where the system is trapped around one given local minima of the free-energy. The very high density justifies an expansion in the sizes of the cages seen by the particles, which also serves as an order parameter for the transition.

This successes allowed to clearly separate the glass transition, for which replica theory provides at worst an upper bound in terms of density, and the jamming transition, which occurs for densities even larger than this upper bound.

Despite these successes, we have seen that our theory is not able to capture the long-range correlations that appear precisely at the jamming transition. A non-linear mechanism that would allow for the appearance of system-wide correlations could be provided by the inclusion of three-body interactions. Another possibility, indicated by recent works in high dimensional systems [102], would be that these long-range anomalies are the product of a complex organisation of the metastable states near the jamming transition. Indeed, in our 1RSB ansatz, the metastable states are supposed to be isolated one from the other, and a more intricate organisation of these states could be captured by a

full-RSB ansatz.

Related to this issue is our assumption that the cage shape is Gaussian near the jamming transition. It was found in recent numerical simulations [39] that the cage is on the contrary non-Gaussian. Taking these two issues into account would require a theory that is able to derive the cage shape as well as cope with more complex ansätze for the replica symmetry. The only set-up that has this potential for the moment is the order-parameter expansion that we set up in Chapter 4, but more powerful resummations must be performed in order to establish a link with the effective potential approach that we used in Chapter 5.

# Bibliography

- [1] G. Adam and J. H. Gibbs. On the temperature dependence of cooperative relaxation properties in glass-forming liquids. *J. Chem. Phys.*, 43(1):139–146, july 1965. doi:10.1063/1.1696442.
- [2] A. Andreanov, G. Biroli, J.-P. Bouchaud, and A. Lefèvre. Field theories and exact stochastic equations for interacting particle systems. *Phys. Rev. E*, 74:030101, 2006. doi:10.1103/PhysRevE.74.030101.
- [3] A. Andreanov, G. Biroli, and A. Lefèvre. Dynamical field theory for glass-forming liquids, self-consistent resummations and time-reversal symmetry. *J. Stat. Mech.*, page P07008, 2006. doi:10.1088/1742-5468/2006/07/P07008.
- [4] A. Andreanov, J.-P. Bouchaud, and G. Biroli. Mode coupling as a landau theory of the glass transition. *Europhys. Lett.*, 88:16001, 2009. doi:10.1209/0295-5075/88/16001.
- [5] C. A. Angell. Structural instability and relaxation in liquid and glassy phases near the fragile liquid limit. *J. Non-Cryst. Solids*, 102:205–221, 1988. doi:10.1016/0022-3093(88)90133-0.
- [6] C. A. Angell. Formation of glasses from liquids and biopolymers. *Science*, 267(5206):1924–1935, 1995. doi:10.1126/science.267.5206.1924.
- [7] N. W. Ashcroft and N. D. Mermin. *Solid State Physics*. Holt Saunders, New York, 1976.
- [8] P. Attard. Integral equations and closure relations for the bridge function and for the triplet correlation function. *J. Chem. Phys.*, 93:7301, 1990.
- [9] A. Ayadim, P. Germain, and S. Amokrane. Mode-coupling theory for the glass transition: Test of the convolution approximation for short-range interactions. *Phys. Rev. E*, 84(6):061502, 2011. doi:10.1103/PhysRevE.84.061502.
- [10] J.-L. Barrat, W. Götze, and A. Latz. The liquid-glass transition of the hard-sphere system. *J. Phys.: Condens. Matter*, 1:7163–7170, 1989. doi:doi:10.1088/0953-8984/1/39/027.
- [11] R. J. Baxter. Direct correlation functions and their derivatives with respect to particle density. *J. Chem. Phys.*, 41:553, july 1964. doi:10.1063/1.1725907.
- [12] U. Bengtzelius, W. Götze, and A. Sjölander. Dynamics of supercooled liquids and the glass transition. *J. Phys. C: Solid State Phys.*, 17(33):5915–5934, november 1984. doi:doi:10.1088/0022-3719/17/33/005.
- [13] C. H. Bennett. Serially deposited amorphous aggregates of hard spheres. *J. Appl. Phys.*, 43:2727, 1972. doi:10.1063/1.1661585.

- [14] B. J. Berne and R. Pecora. *Dynamic Light Scattering*. Wiley, New York, 1976.
- [15] L. Berthier and G. Biroli. Theoretical perspective on the glass transition and amorphous materials. *Rev. Mod. Phys.*, 83(2):587, june 2011. doi:10.1103/RevModPhys.83.587.
- [16] L. Berthier, G. Biroli, J.-P. Bouchaud, W. Kob, K. Miyazaki, and D. R. Reichman. Spontaneous and induced dynamic correlations in glass formers. II. Model calculations and comparison to numerical simulations. *J. Chem. Phys.*, 126:184504, may 2007. doi:10.1063/1.2721555.
- [17] L. Berthier, G. Biroli, J.-P. Bouchaud, W. Kob, K. Miyazaki, and D. R. Reichman. Spontaneous and induced dynamic fluctuations in glass formers. I. General results and dependence on ensemble and dynamics. *J. Chem. Phys.*, 126:184503, may 2007. doi:10.1063/1.2721554.
- [18] L. Berthier, P. Chaudhuri, C. Coulais, O. Dauchot, and P. Sollich. Suppressed compressibility at large scale in jammed packings of size-disperse spheres. *Phys. Rev. Lett.*, 106:120601, 2011. doi:10.1103/PhysRevLett.106.120601.
- [19] L. Berthier, H. Jacquin, and F. Zamponi. Can the jamming transition be described using equilibrium statistical mechanics ? *J. Stat. Mech.*, page P01004, january 2011. doi:10.1088/1742-5468/2011/01/P01004.
- [20] L. Berthier, H. Jacquin, and F. Zamponi. Microscopic theory of the jamming transition of harmonic spheres. *Phys. Rev. E*, 84(5):051103, november 2011. doi:10.1103/PhysRevE.84.051103.
- [21] L. Berthier and T. A. Witten. Compressing nearly hard sphere fluids increases glass fragility. *Europhys. Lett.*, 86(1):10001, april 2009. doi:10.1209/0295-5075/86/10001.
- [22] L. Berthier and T. A. Witten. Glass transition of dense fluids of hard and compressible spheres. *Phys. Rev. E*, 80(2):021502, august 2009. doi:10.1103/PhysRevE.80.021502.
- [23] B. Bildstein and G. Kahl. Triplet correlation functions for hard spheres: Comparison of different approaches. *Phys. Rev. E*, 47(3):1712–1726, 1993.
- [24] B. Bildstein and G. Kahl. Triplet correlation functions for hard-spheres: Computer simulation results. *J. Chem. Phys.*, 100:5882, 1994.
- [25] K. Binder and W. Kob. *Glassy materials and disordered solids: An introduction to their statistical mechanics*. World Scientific, 2005.
- [26] G. Biroli and J.-P. Bouchaud. *Structural Glasses and Supercooled Liquids: Theory, Experiment, and Applications*, chapter The Random First-Order Transition Theory of Glasses: a critical assessment. John Wiley & Sons, Hoboken, New Jersey, 2009.
- [27] G. Biroli and R. Monasson. Relationship between long timescales and the static free-energy in the hopfield model. *J. Phys. A: Math. Gen.*, 31:L391–L396, march 1998. doi:10.1088/0305-4470/31/21/001.
- [28] P. Blasiak, A. Horzela, K. A. Penson, A. I. Solomon, and G. H. E. Duchamp. Combinatorics and boson normal ordering: A gentle introduction. *Am. J. Phys.*, 75(7):639–646, 2007. doi:10.1119/1.2723799.

- [29] J.-P. Bouchaud. The mode-coupling theory of supercooled liquids: Does it wear any clothes? <http://www.condmatjournalclub.org/?p=1022>, june 2010.
- [30] J.-P. Bouchaud and G. Biroli. On the Adam-Gibbs-Kirkpatrick-Thirumalai-Wolynes scenario for the viscosity increase in glasses. *J. Chem. Phys.*, 121:7347, july 2004. doi:[DOI:10.1063/1.1796231](https://doi.org/10.1063/1.1796231).
- [31] G. Brambilla, D. El Masri, M. Pierno, L. Berthier, L. Cipelletti, G. Petekidis, and A. B. Schofield. Probing the equilibrium dynamics of colloidal hard spheres above the mode-coupling glass transition. *Phys. Rev. Lett.*, 102(8):085703, february 2009. doi:[10.1103/PhysRevLett.102.085703](https://doi.org/10.1103/PhysRevLett.102.085703).
- [32] E. A. Calzetta and B.-L. B. Hu. *Non-Equilibrium quantum field theory*. Cambridge University Press, 2008.
- [33] M. Cardenas, S. Franz, and G. Parisi. Constrained Boltzmann-Gibbs measures and effective potential for glasses in hypernetted chain approximation and numerical simulations. *J. Chem. Phys.*, 110(3):1726–1734, january 1999. doi:[10.1063/1.478028](https://doi.org/10.1063/1.478028).
- [34] T. Castellani and A. Cavagna. Spin glass theory for pedestrians. *J. Stat. Mech.*, page P05012, may 2005. doi:[10.1088/1742-5468/2005/05/P05012](https://doi.org/10.1088/1742-5468/2005/05/P05012).
- [35] M. E. Cates and S. Ramaswamy. Do Current-Density nonlinearities cut off the glass transition? *Phys. Rev. Lett.*, 96(13):135701, 2006. doi:[10.1103/PhysRevLett.96.135701](https://doi.org/10.1103/PhysRevLett.96.135701).
- [36] A. Cavagna. Supercooled liquids for pedestrians. *Phys. Rep.*, 476(4-6):51–124, may 2009. doi:[10.1016/j.physrep.2009.03.003](https://doi.org/10.1016/j.physrep.2009.03.003).
- [37] P. Charbonneau, E. I. Corwin, G. Parisi, and F. Zamponi. Universal microstructure and mechanical stability of jammed packings. *Phys. Rev. Lett.*, 109(20):205501, 2012. doi:[10.1103/PhysRevLett.109.205501](https://doi.org/10.1103/PhysRevLett.109.205501).
- [38] P. Charbonneau, A. Ikeda, G. Parisi, and F. Zamponi. Glass transition and random close packing above three dimensions. *Phys. Rev. Lett.*, 107(18):185702, october 2011. doi:[10.1103/PhysRevLett.107.185702](https://doi.org/10.1103/PhysRevLett.107.185702).
- [39] P. Charbonneau, A. Ikeda, G. Parisi, and F. Zamponi. Dimensional study of the caging order parameter at the glass transition. *Proc. Nat. Acad. Sci.*, 109(35):13939–13943, August 2012. doi:[10.1073/pnas.1211825109](https://doi.org/10.1073/pnas.1211825109).
- [40] P. Chaudhuri, L. Berthier, and S. Sastry. Jamming transitions in amorphous packings of frictionless spheres occur over a continuous range of volume fractions. *Phys. Rev. Lett.*, 104(16):165701, april 2010. doi:[10.1103/PhysRevLett.104.165701](https://doi.org/10.1103/PhysRevLett.104.165701).
- [41] P. Chaudhuri, S. Karmakar, C. Dasgupta, H. R. Krishnamurthy, and A. K. Sood. Equilibrium glassy phase in a polydisperse hard-sphere system. *Phys. Rev. Lett.*, 95(24):248301, 2005. doi:[10.1103/PhysRevLett.95.248301](https://doi.org/10.1103/PhysRevLett.95.248301).
- [42] X. Cheng. Experimental study of the jamming transition at zero temperature. *Phys. Rev. E*, 81:031301, march 2010. doi:[10.1103/PhysRevE.81.031301](https://doi.org/10.1103/PhysRevE.81.031301).
- [43] M. Clusel, E. I. Corwin, A. O. N. Siemens, and J. Brujic. A 'granocentric' model for random packing of jammed emulsions. *Nature*, 460:611–615, july 2009. doi:[10.1038/nature08158](https://doi.org/10.1038/nature08158).

- [44] J. D. Cole. On a quasi-linear parabolic equation occurring in aerodynamics. *Quart. Appl. Math.*, 1951.
- [45] R. Colin, A. M. Alsayed, J.-C. Castaing, R. Goyal, L. Hough, and B. Abou. Spatially heterogeneous dynamics in a thermosensitive soft suspension before and after the glass transition. *Soft Matter*, 7:4504–4514, 2011. doi:10.1039/c0sm01184c.
- [46] J. H. Conway and N. J. A. Sloane. *Sphere Packings, Lattices and Groups*. Springer-Verlag, New York, 1993.
- [47] J. M. Cornwall, R. Jackiw, and E. Tomboulis. Effective action for composite operators. *Phys. Rev. D*, 10(8):2428–2445, 1974. doi:10.1103/PhysRevD.10.2428.
- [48] L. F. Cugliandolo and J. Kurchan. Analytical solution of the off-equilibrium dynamics of a long-range spin-glass model. *Phys. Rev. Lett.*, 71(1):173–176, july 1993. doi:10.1103/PhysRevLett.71.173.
- [49] S. P. Das and G. F. Mazenko. Fluctuating nonlinear hydrodynamics and the liquid-glass transition. *Phys. Rev. A*, 34(3):2265–2282, 1986. doi:10.1103/PhysRevA.34.2265.
- [50] C. Dasgupta and O. T. Valls. Free energy landscape of a dense hard-sphere system. *Phys. Rev. E*, 59(3):3123–3134, march 1999. doi:10.1103/PhysRevE.59.3123.
- [51] C. De Dominicis. Variational formulations of equilibrium statistical mechanics. *J. Math. Phys.*, 3(5):983–1002, 1962. doi:10.1063/1.1724313.
- [52] C. De Dominicis. Techniques de renormalisation de la théorie des champs et dynamique des phénomènes critique. *J. Phys. Colloques*, 37:C1–247–C1–253, 1976. doi:10.1051/jphyscol:1976138.
- [53] C. De Dominicis and P. C. Martin. Stationary entropy principle and renormalization in normal and superfluid system. i. algebraic formulation. *J. Math. Phys.*, 5(1):14–30, 1964. doi:10.1063/1.1704062.
- [54] C. De Dominicis and P. C. Martin. Stationary entropy principle and renormalization in normal and superfluid systems. ii. diagrammatic formulation. *J. Math. Phys.*, 5(1):31–59, 1964. doi:10.1063/1.1704064.
- [55] D. Dean. Langevin equation for the density of a system of interacting langevin processes. *J. Phys. A: Math. Gen.*, 29:613–617, 1996. doi:10.1088/0305-4470/29/24/001.
- [56] A. R. Denton and N. W. Ashcroft. High-order direct correlation functions of uniform classical liquids. *Phys. Rev. A*, 39(1):426–429, 1989. doi:10.1103/PhysRevA.39.426.
- [57] B. Derrida. Random-energy model: Limit of a family of disordered models. *Phys. Rev. Lett.*, 45(2):79–82, july 1980. doi:10.1103/PhysRevLett.45.79.
- [58] M. Doi. Second quantization representation for classical many- particle system. *J. Phys. A: Math. Gen.*, 9(9):1465, 1976. doi:10.1088/0305-4470/9/9/008.
- [59] A. Donev, S. Torquato, and F. H. Stillinger. Pair correlation function characteristics of nearly jammed disordered and ordered hard-sphere packings. *Phys. Rev. E*, 71(1):011105, january 2005. doi:10.1103/PhysRevE.71.011105.

- [60] A. Donev, S. Torquato, and F. H. Stillinger. Unexpected density fluctuations in jammed disordered sphere packings. *Phys. Rev. Lett.*, 95:090604, august 2005. doi:[10.1103/PhysRevLett.95.090604](https://doi.org/10.1103/PhysRevLett.95.090604).
- [61] D. J. Durian. Foam mechanics at the bubble scale. *Phys. Rev. Lett.*, 75:4780, december 1995. doi:[10.1103/PhysRevLett.75.4780](https://doi.org/10.1103/PhysRevLett.75.4780).
- [62] M. Dzero, J. Schmalian, and P. G. Wolynes. Replica theory for fluctuations of the activation barriers in glassy systems. *Phys. Rev. B*, 80:024204, july 2009. doi:[10.1103/PhysRevB.80.024204](https://doi.org/10.1103/PhysRevB.80.024204).
- [63] S. F. Edwards and M. Schwartz. Statistical mechanics in collective coordinates. *J. Stat. Phys.*, 110(3):497–502, 2003.
- [64] D. El Masri, G. Brambilla, M. Pierno, G. Petekidis, A. B. Schofield, L. Berthier, and L. Cipelletti. Dynamic light scattering measurements in the activated regime of dense colloidal hard spheres. *J. Stat. Mech.*, page P07015, july 2009. doi:[10.1088/1742-5468/2009/07/P07015](https://doi.org/10.1088/1742-5468/2009/07/P07015).
- [65] A. Fernandez-Nieves, H. Wyss, J. Mattsson, and D. A. Weitz, editors. *Microgel suspensions*. Wiley-VCH, 2011.
- [66] S. Franz, H. Jacquin, G. Parisi, P. Urbani, and F. Zamponi. Static replica approach to critical correlations in glassy systems. *J. Chem. Phys.*, 138(12):12A540, 2013. doi:[doi:10.1063/1.4776213](https://doi.org/10.1063/1.4776213).
- [67] G. H. Fredrickson and H. C. Andersen. Kinetic ising model of the glass transition. *Phys. Rev. Lett.*, 53(13):1244–1247, 1984. doi:[10.1103/PhysRevLett.53.1244](https://doi.org/10.1103/PhysRevLett.53.1244).
- [68] G. H. Fredrickson and H. C. Andersen. Facilitated kinetic ising models and the glass transition. *J. Chem. Phys.*, 83(11):5822–5831, 1985. doi:[10.1063/1.449662](https://doi.org/10.1063/1.449662).
- [69] J. H. Gibbs and E. A. Di Marzio. Nature of the glass transition and the glassy state. *J. Chem. Phys.*, 28(3):373–383, march 1958. doi:[10.1063/1.1744141](https://doi.org/10.1063/1.1744141).
- [70] D. L. Goodstein. *States of matter*. Prentice-Hall, Inc., Englewood Cliffs, New Jersey, 1975.
- [71] W. Götze. Properties of the glass instability treated within a mode coupling theory. *Z. Phys. B*, 60(2-4):195–203, 1985. doi:[10.1007/BF01304439](https://doi.org/10.1007/BF01304439).
- [72] W. Götze. Recent tests of the mode-coupling theory for glassy dynamics. *J. Phys.: Condens. Matter*, 11(10A):1–45, 1999. doi:[10.1088/0953-8984/11/10A/002](https://doi.org/10.1088/0953-8984/11/10A/002).
- [73] W. Götze and L. Sjögren.  $\alpha$ -relaxation near the liquid-glass transition. *J. Phys. C: Solid State Phys.*, 20:879–894, 1987. doi:[doi:10.1088/0022-3719/20/7/005](https://doi.org/10.1088/0022-3719/20/7/005).
- [74] W. Götze and L. Sjögren. The glass transition singularity. *Z. Phys. B*, 65(4):415–427, 1987. doi:[10.1007/BF01303763](https://doi.org/10.1007/BF01303763).
- [75] J. L. Green, K. Ito, K. Xu, and C. A. Angell. Fragility in liquids and polymers: new, simple quantifications and interpretations. *J. Phys. Chem. B*, 103(20):3991–3996, 1999. doi:[10.1021/jp983927i](https://doi.org/10.1021/jp983927i).

- [76] D. J. Gross and M. Mézard. The simplest spin glass. *Nucl. Phys. B*, 240(4):431–452, 1984. doi:10.1016/0550-3213(84)90237-2.
- [77] J. P. Hansen and I. R. McDonald. *Theory of simple liquids*. Academic Press, London, 1986.
- [78] E. Hopf. The partial differential equation  $u_t + uu_x = ixu_{xx}$ . *Comm. Pure Appl. Math.*, 3:201–230, 1950. doi:10.1002/cpa.3160030302.
- [79] A. Ikeda and K. Miyazaki. Glass transition of the monodisperse gaussian core model. *Phys. Rev. Lett.*, 106(1):015701, 2011. doi:10.1103/PhysRevLett.106.015701.
- [80] A. Ikeda and K. Miyazaki. Slow dynamics of the high density gaussian core model. *J. Chem. Phys.*, 135:054901, 2011. doi:10.1063/1.3615949.
- [81] A. Ikeda and K. Miyazaki. Thermodynamic and structural properties of the high density gaussian core model. *J. Chem. Phys.*, 135:024901, 2011. doi:10.1063/1.3609277.
- [82] H. Iyetomi. Hypernetted chain approximation, convolution approximation and perfect screening in coulombic many-particle system. *Progr. Theor. Phys.*, 71(3):427–437, 1984. doi:10.1143/PTP.71.427.
- [83] R. Jackiw. Functional evaluation of the effective potential. *Phys. Rev. D*, 9(6):1686–1701, 1974. doi:10.1103/PhysRevD.9.1686.
- [84] H. Jacquin and L. Berthier. Anomalous structural evolution of soft particles: Equilibrium liquid state theory. *Soft Matter*, 6:2970, april 2010. doi:10.1039/b926412d.
- [85] H. Jacquin and F. van Wijland. Field theoretic formulation of a mode-coupling equation for colloids. *Phys. Rev. Lett.*, 106:210602, 2011.
- [86] H. M. Jaeger, S. R. Nagel, and R. P. Behringer. Granular solids, liquids, and gases. *Rev. Mod. Phys.*, 68:1259, 1996. doi:10.1103/RevModPhys.68.1259.
- [87] H. K. Janssen. Field-theoretic method applied to critical dynamics. In Charles P. Enz, editor, *Dynamical Critical Phenomena and Related Topics*, volume 104, pages 25–47. Springer Berlin Heidelberg, Berlin, Heidelberg, 1979. doi:10.1007/3-540-09523-3\_2.
- [88] H. K. Janssen. *Topics in Modern Statistical Physics*, chapter On the renormalized field-theory of nonlinear critical relaxation. World Scientific, Singapore, 1992.
- [89] W. Kauzmann. The nature of the glassy state and the behavior of liquids at low temperatures. *Chem. Rev.*, 43(2):219–256, october 1948. doi:10.1021/cr60135a002.
- [90] K. Kawasaki. Stochastic model of slow dynamics in supercooled liquids and dense colloidal suspensions. *Physica A*, 208(1):35–64, 1994. doi:10.1016/0378-4371(94)90532-0.
- [91] B. Kim and K. Kawasaki. The mode coupling theory in the fdr-preserving field theory of interacting brownian particles. *J. Phys. A: Math. Gen.*, 40:F33–F42, 2007. doi:10.1088/1751-8113/40/1/F04.
- [92] B. Kim and K. Kawasaki. A fluctuation-dissipation relationship-preserving field theory for interacting brownian particles: one-loop theory and mode coupling theory. *J. Stat. Mech.*, page P02004, 2008. doi:10.1088/1742-5468/2008/02/P02004.



- [93] K. Kim and T. Munakata. Glass transition of hard sphere systems: Molecular dynamics and density functional theory. *Phys. Rev. E*, 68(2):021502, 2003. doi:[10.1103/PhysRevE.68.021502](https://doi.org/10.1103/PhysRevE.68.021502).
- [94] T. R. Kirkpatrick, D. Thirumalai, and P. G. Wolynes. Scaling concepts for the dynamics of viscous liquids near an ideal glassy state. *Phys. Rev. A*, 40(2):1045–1054, july 1989. doi:[10.1103/PhysRevA.40.1045](https://doi.org/10.1103/PhysRevA.40.1045).
- [95] T. R. Kirkpatrick and P. G. Wolynes. Connections between some kinetic and equilibrium theories of the glass transition. *Phys. Rev. A*, 35(7):3072–3080, april 1987. doi:[10.1103/PhysRevA.35.3072](https://doi.org/10.1103/PhysRevA.35.3072).
- [96] T. R. Kirkpatrick and P. G. Wolynes. Stable and metastable states in mean-field potts and structural glasses. *Phys. Rev. B*, 36(16):8552–8564, december 1987. doi:[10.1103/PhysRevB.36.8552](https://doi.org/10.1103/PhysRevB.36.8552).
- [97] T. Kita. Conserving gapless theory for weakly interacting bose gases. *J. Phys. Soc. Jpn*, 75(4):044603, 2006. doi:[10.1143/JPSJ.75.044603](https://doi.org/10.1143/JPSJ.75.044603).
- [98] T. Kita. Self-consistent perturbation expansion for bose-einstein condensates satisfying goldstone’s theorem and conservation laws. *Phys. Rev. B*, 80:214502, 2009. doi:[10.1103/PhysRevB.80.214502](https://doi.org/10.1103/PhysRevB.80.214502).
- [99] W. Kob and H. C. Andersen. Testing mode-coupling theory for a supercooled binary Lennard-Jones mixture. II. intermediate scattering function and dynamic susceptibility. *Phys. Rev. E*, 52(4):4134, 1995. doi:[10.1103/PhysRevE.52.4134](https://doi.org/10.1103/PhysRevE.52.4134).
- [100] F. Krzakała and J. Kurchan. Landscape analysis of constraint satisfaction problems. *Phys. Rev. E*, 76(2):021122, august 2007. doi:[10.1103/PhysRevE.76.021122](https://doi.org/10.1103/PhysRevE.76.021122).
- [101] F. Krzakała and L. Zdeborová. Potts glass on random graphs. *Europhys. Lett.*, 81(5):57005, march 2008. doi:[10.1209/0295-5075/81/57005](https://doi.org/10.1209/0295-5075/81/57005).
- [102] J. Kurchan, G. Parisi, P. Urbani, and F. Zamponi. Exact theory of dense amorphous hard spheres in high dimension. ii. the high density regime and the gardner transition. *J. Phys. Chem. B*, april 2013. doi:[10.1021/jp402235d](https://doi.org/10.1021/jp402235d).
- [103] J. Kurchan, G. Parisi, and F. Zamponi. Exact theory of dense amorphous hard spheres in high dimension i. the free energy. *J. Stat. Mech.*, 2012(10):P10012, 2012. doi:[10.1088/1742-5468/2012/10/P10012](https://doi.org/10.1088/1742-5468/2012/10/P10012).
- [104] A. J. Liu and S. R. Nagel. Jamming isn’t just cool anymore. *Nature*, 396:21, 1998. doi:[10.1038/23819](https://doi.org/10.1038/23819).
- [105] A. J. Liu, S. R. Nagel, W. van Saarloos, and M. Wyart. *Dynamical Heterogeneities in Glasses, Colloids, and Granular Media ed (Oxford: Oxford University Press) at press*. Oxford University Press, 2010.
- [106] A. A. Louis, P. G. Bolhuis, and J. P. Hansen. Mean-field fluid behavior of the gaussian core model. *Phys. Rev. E*, 62:7961–7972, december 2000. doi:[10.1103/PhysRevE.62.7961](https://doi.org/10.1103/PhysRevE.62.7961).
- [107] B. D. Lubachevsky and F. H. Stillinger. Geometric properties of random disk packings. *J. Stat. Phys.*, 60:561–583, march 1990. doi:[10.1007/BF01025983](https://doi.org/10.1007/BF01025983).

- [108] V. Lubchenko and P. G. Wolynes. Theory of structural glasses and supercooled liquids. *Annu. Rev. Phys. Chem.*, 58(1):235–266, may 2007. doi:10.1146/annurev.physchem.58.032806.104653.
- [109] J. M. Luttinger and J. C. Ward. Ground-state energy of a many-fermion system ii. *Phys. Rev.*, 118(5):1417–1427, 1960. doi:10.1103/PhysRev.118.1417.
- [110] R. Mari, F. Krzakała, and J. Kurchan. Jamming versus glass transitions. *Phys. Rev. Lett.*, 103(2):025701, july 2009. doi:10.1103/PhysRevLett.103.025701.
- [111] P. C. Martin, E. D. Siggia, and H. A. Rose. Statistical dynamics of classical systems. *Phys. Rev. A*, 8(1):423–437, 1973. doi:10.1103/PhysRevA.8.423.
- [112] L.-M. Martinez and C. A. Angell. A thermodynamic connection to the fragility of glass-forming liquids. *Nature*, 410:663–667, april 2001. doi:10.1038/35070517.
- [113] J. C. Maxwell. On the calculation of the equilibrium and stiffness of frames. *Philosophical Magazine Series 4*, 27(182):294–299, 1864. doi:10.1080/14786446408643668.
- [114] J. E. Mayer and E. W. Montroll. Molecular distribution. *J. Chem. Phys.*, 9(1):2–16, 1941. doi:10.1063/1.1750822.
- [115] J.E. Mayer and M. G. Mayer. *Statistical Mechanics*. Wiley, New York, 1940.
- [116] P. Mayer, K. Miyazaki, and D. R. Reichman. Cooperativity beyond caging: Generalized Mode-Coupling theory. *Phys. Rev. Lett.*, 97(9):095702, 2006. doi:10.1103/PhysRevLett.97.095702.
- [117] G. F. Mazenko. Smoluchovski dynamics and the ergodic-nonergodic transition. *Phys. Rev. E*, 83(4):041125, 2011.
- [118] E. Meeron. Nodal expansions. III. exact integral equations for particle correlation functions. *J. Math. Phys.*, 1(3):192–201, 1960. doi:10.1063/1.1703652.
- [119] M. Merolle, J. P. Garrahan, and D. Chandler. Space–time thermodynamics of the glass transition. *Proc. Nat. Acad. Sci.*, 102(31):10837–10840, 2005.
- [120] M. Mézard and A. Montanari. *Information, Physics, and Computation*. Oxford University Press, 2009.
- [121] M. Mézard and G. Parisi. A tentative replica study of the glass transition. *J. Phys. A: Math. Gen.*, 29(20):6515–6524, june 1996. doi:10.1088/0305-4470/29/20/009.
- [122] M. Mézard and G. Parisi. A first-principle computation of the thermodynamics of glasses. *J. Chem. Phys.*, 111(3):1076–1095, july 1999. doi:10.1063/1.479193.
- [123] M. Mézard and G. Parisi. Thermodynamics of glasses: A first principles computation. *Phys. Rev. Lett.*, 82(4):747–750, jan 1999. doi:10.1103/PhysRevLett.82.747.
- [124] M. Mézard, G. Parisi, and M. A. Virasoro. *Spin glass theory and beyond*. World Scientific, Singapore, 1987.
- [125] K. Miyazaki and D. R. Reichman. Mode-coupling theory and the fluctuation–dissipation theorem for nonlinear langevin equations with multiplicative noise. *J. Phys. A: Math. Gen.*, 38:L343–L355, 2005. doi:10.1088/0305-4470/38/20/L03.

- [126] R. Monasson. Structural glass transition and the entropy of the metastable states. *Phys. Rev. Lett.*, 75(15):2847–2850, oct 1995. doi:10.1103/PhysRevLett.75.2847.
- [127] R. Monasson. Introduction to phase transitions in random optimization problems. In J.P. Bouchaud, M. Mézard, and J. Dalibard, editors, *Complex Systems*, Les Houches, France, 2007. Elsevier.
- [128] H. Mori. Transport, collective motion, and brownian motion. *Progr. Theor. Phys.*, 33(3):423–455, 1965. doi:10.1143/PTP.33.423.
- [129] T. Morita. Theory of classical fluids: Hyper-netted chain approximation, ii. *Progr. Theor. Phys.*, 21(3):361–382, 1959. doi:10.1143/PTP.21.361.
- [130] T. Morita and K. Hiroike. Integral equation for pair distribution function. *Progr. Theor. Phys.*, 23:385–387, 1959. doi:10.1143/PTP.23.385.
- [131] T. Morita and K. Hiroike. A new approach to the theory of classical fluids. III. *Progr. Theor. Phys.*, 25:537–578, 1961. doi:10.1143/PTP.25.537.
- [132] J. W. Negele and H. Orland. *Quantum many-particle systems*. Westview Press, 1998.
- [133] T. H. Nishino and H. Hayakawa. Fluctuation-dissipation-relation-preserving field theory of the glass transition in terms of fluctuating hydrodynamics. *Phys. Rev. E*, 78(6):061502, 2008. doi:10.1103/PhysRevE.78.061502.
- [134] C. S. O’Hern, S. A. Langer, A. J. Liu, and S. R. Nagel. Random packings of frictionless particles. *Phys. Rev. Lett.*, 88(7):075507, january 2002. doi:10.1103/PhysRevLett.88.075507.
- [135] C. S. O’Hern, L. E. Silbert, A. J. Liu, and S. R. Nagel. Jamming at zero temperature and zero applied stress: The epitome of disorder. *Phys. Rev. E*, 68(1):011306, 2003. doi:10.1103/PhysRevE.68.011306.
- [136] P. Olsson and S. Teitel. Critical Scaling of Shear Viscosity at the Jamming Transition. *Phys. Rev. Lett.*, 99(17):178001, october 2007. doi:10.1103/PhysRevLett.99.178001.
- [137] L. S. Ornstein and F. Zernike. Accidental deviations of density and opalescence at the critical point of a single substance. *KNAW, Proceedings*, 17(II):793–806, 1914. Available from: <http://www.dwc.knaw.nl/biografie/pmknaw/?pagetype=publDetail&pId=PU00012727>.
- [138] G. Parisi and F. Zamponi. Mean-field theory of hard sphere glasses and jamming. *Rev. Mod. Phys.*, 82(1):789–845, march 2010. doi:10.1103/RevModPhys.82.789.
- [139] L. Peliti. Path integral approach to birth-death processes on a lattice. *J. Physique*, 46:1469–1483, 1985. doi:10.1051/jphys:019850046090146900.
- [140] J. K. Percus. Approximation methods in classical statistical mechanics. *Phys. Rev. Lett.*, 8(11):462–463, 1962. doi:10.1103/PhysRevLett.8.462.
- [141] J. K. Percus and G. J. Yevick. Analysis of classical statistical mechanics by means of collective coordinates. *Phys. Rev.*, 110(1):1, 1958.
- [142] E. Pitard, V. Lecomte, and F. van Wijland. Dynamic transition in an atomic glass former: A molecular-dynamics evidence. *Europhys. Lett.*, 96:56002, 2011.

- [143] M. Potthoff. Non-perturbative construction of the luttinger-ward functional. *Cond. Mat. Phys.*, 9(3):557–567, 2006.
- [144] T. V. Ramakrishnan and M. Yussouf. First-principles order-parameter theory of freezing. *Phys. Rev. B*, 19(5):2775–2794, march 1979. doi:10.1103/PhysRevB.19.2775.
- [145] F. Ritort and P. Sollich. Glassy dynamics of kinetically constrained models. *Adv. Phys.*, 52(4):219–342, 2003. doi:10.1080/0001873031000093582.
- [146] C. A. Rogers. *Packing and Covering*. Cambridge University Press, Cambridge, 1964.
- [147] G. S. Rushbrooke and H. I. Scoins. On the theory of fluids. *Proc. R. Soc. Lond. A*, 216:203–218, 1953. doi:10.1098/rspa.1953.0017.
- [148] E. E. Salpeter. On mayer’s theory of cluster expansions. *Ann. Phys.*, 5(3):183–223, 1958. doi:10.1016/0003-4916(58)90058-7.
- [149] Z. W. Salsburg and W. W. Wood. Equation of state of classical hard spheres at high density. *J. Chem. Phys.*, 37:798, 1962. doi:10.1063/1.1733163.
- [150] B. R. Saunders and B. Vincent. Microgel particules as model colloids : theory, properties and applications. *Advances in Colloid and Interface Science*, 80:1–25, 1999.
- [151] H. Senff and W. Richtering. Influence of cross-link density on rheological properties of temperature-sensitive microgel suspensions. *Colloid & Polym. Sci.*, 278(9):830–840, 2000. doi:10.1007/s003960000329.
- [152] L. E. Silbert, A. J. Liu, and S. R. Nagel. Structural signatures of the unjamming transition at zero temperature. *Phys. Rev. E*, 73(4):041304, april 2006. doi:10.1103/PhysRevE.73.041304.
- [153] Y. Singh. Density-functional theory of freezing and properties of the ordered phase. *Phys. Rep.*, 207(6):351–444, april 1991. doi:10.1016/0370-1573(91)90097-6.
- [154] Y. Singh, J. P. Stoessel, and P. G. Wolynes. Hard-sphere glass and the density-functional theory of aperiodic crystals. *Phys. Rev. Lett.*, 54(10):1059–1062, march 1985. doi:10.1103/PhysRevLett.54.1059.
- [155] L. Sjögren. Kinetic theory of current fluctuations in simple classical liquids. *Phys. Rev. A*, 22(6):2866–2882, 1980. doi:10.1103/PhysRevA.22.2866.
- [156] C. Song, P. Wang, and H. A. Makse. A phase diagram for jammed matter. *Nature*, 453(7195):629, may 2008. doi:10.1038/nature06981.
- [157] F. H. Stillinger, E. A. Di Marzio, and R. L. Kornegay. Systematic approach to explanation of the rigid disk phase transition. *J. Chem. Phys.*, 40(6):1564–1576, 1964. doi:10.1063/1.1725362.
- [158] G. Szamel. Is a “homogeneous” description of dynamic heterogeneities possible? *J. Chem. Phys.*, 121(8):3355–3358, 2004. doi:10.1063/1.1783873.
- [159] G. Szamel. Dynamics of interacting brownian particles: A diagrammatic formulation. *J. Chem. Phys.*, 127(8):084515, 2007. doi:10.1063/1.2759487.
- [160] G. Szamel. Divergent Four-Point dynamic density correlation function of a glassy suspension. *Phys. Rev. Lett.*, 101(20):205701, 2008. doi:10.1103/PhysRevLett.101.205701.

- [161] G. Szamel. Dynamic glass transition: Bridging the gap between mode-coupling theory and the replica approach. *Europhys. Lett.*, 91(5):56004, september 2010. doi:[10.1209/0295-5075/91/56004](https://doi.org/10.1209/0295-5075/91/56004).
- [162] G. Szamel and E. Flenner. Independence of the relaxation of a supercooled fluid from its microscopic dynamics: Need for yet another extension of the mode-coupling theory. *Europhys. Lett.*, 67(5):779–785, 2004. doi:[10.1209/ep1/i2004-10117-6](https://doi.org/10.1209/ep1/i2004-10117-6).
- [163] G. Szamel and E. Flenner. Emergence of Long-Range correlations and rigidity at the dynamic glass transition. *Phys. Rev. Lett.*, 107(10):105505, september 2011. doi:[10.1103/PhysRevLett.107.105505](https://doi.org/10.1103/PhysRevLett.107.105505).
- [164] T. Temesvári, C. De Dominicis, and I. R. Pimentel. Generic replica symmetric field-theory for short range ising spin glasses. *Eur. Phys. J. B*, 25(3):361–372, February 2002. doi:[10.1140/epjb/e20020041](https://doi.org/10.1140/epjb/e20020041).
- [165] E. Thiele. Equation of state for hard spheres. *J. Chem. Phys.*, 39(2):474–479, July 1963. doi:[doi:10.1063/1.1734272](https://doi.org/10.1063/1.1734272).
- [166] M. van Hecke. Jamming of soft particles: Geometry, mechanics, scaling and isostaticity. *J. Phys.: Condens. Matter*, 22(3):033101, december 2010. doi:[10.1088/0953-8984/22/3/033101](https://doi.org/10.1088/0953-8984/22/3/033101).
- [167] N. G. van Kampen. *Stochastic processes in physics and chemistry*. Elsevier Science & Technology Books, 2007.
- [168] J. M. J. van Leeuwen, J. Groeneveld, and J. de Boer. New method for the calculation of the pair correlation function. i. *Physica*, 25:792–808, 1959. doi:[10.1016/0031-8914\(59\)90004-7](https://doi.org/10.1016/0031-8914(59)90004-7).
- [169] W. van Megen, T. C. Mortensen, S. R. Williams, and J. Müller. Measurement of the self-intermediate scattering function of suspensions of hard spherical particles near the glass transition. *Phys. Rev. E*, 58(5):6073–6085, 1998. doi:[10.1103/PhysRevE.58.6073](https://doi.org/10.1103/PhysRevE.58.6073).
- [170] W. van Megen, S. M. Underwood, and P. N. Pusey. Nonergodicity parameters of colloidal glasses. *Phys. Rev. Lett.*, 67(12):1586–1589, 1991. doi:[10.1103/PhysRevLett.67.1586](https://doi.org/10.1103/PhysRevLett.67.1586).
- [171] M. S. Wertheim. Exact solution of the Percus-Yevick integral equation for hard spheres. *Phys. Rev. Lett.*, 10(8):321–323, april 1963. doi:[10.1103/PhysRevLett.10.321](https://doi.org/10.1103/PhysRevLett.10.321).
- [172] S. Whitelam, L. Berthier, and J. P. Garrahan. Dynamic criticality in Glass-Forming liquids. *Phys. Rev. Lett.*, 92(18):185705, 2004. doi:[10.1103/PhysRevLett.92.185705](https://doi.org/10.1103/PhysRevLett.92.185705).
- [173] S. Whitelam, L. Berthier, and J. P. Garrahan. Renormalization group study of a kinetically constrained model for strong glasses. *Phys. Rev. E*, 71(2):026128, 2005. doi:[10.1103/PhysRevE.71.026128](https://doi.org/10.1103/PhysRevE.71.026128).
- [174] G. C. Wick. The evaluation of the collision matrix. *Phys. Rev.*, 80(2):268–272, 1950. doi:[10.1103/PhysRev.80.268](https://doi.org/10.1103/PhysRev.80.268).
- [175] M. Wyart, L. E. Silbert, S. R. Nagel, and T. A. Witten. Effects of compression on the vibrational modes of marginally jammed solids. *Phys. Rev. E*, 72(5):051306, november 2005. doi:[10.1103/PhysRevE.72.051306](https://doi.org/10.1103/PhysRevE.72.051306).

- [176] N. Xu, V. Vitelli, A. J. Liu, and S. R. Nagel. Anharmonic and quasi-localized vibrations in jammed solids – modes for mechanical failure. *Europhys. Lett.*, 90:56001, 2010. doi:[10.1209/0295-5075/90/56001](https://doi.org/10.1209/0295-5075/90/56001).
- [177] H. Yoshino and M. Mézard. Emergence of rigidity at the structural glass transition: a first principle computation. *Phys. Rev. Lett.*, 105:015504, july 2010. doi:[10.1103/PhysRevLett.105.015504](https://doi.org/10.1103/PhysRevLett.105.015504).
- [178] Z. Zhang, N. Xu, D. T. N. Chen, P. Yunker, A. M. Alsayed, K. B. Aptowicz, P. Habdas, A. J. Liu, S. R. Nagel, and A. G. Yodh. Thermal vestige of the zero-temperature jamming transition. *Nature*, 459(7244):230, may 2009. doi:[10.1038/nature07998](https://doi.org/10.1038/nature07998).
- [179] J. Zinn-Justin. *Quantum Field Theory and Critical Phenomena*. Clarendon Press, Oxford, 1989.
- [180] R. Zwanzig. *Non-equilibrium statistical mechanics*. Oxford University Press, 2001.